Characterization of Textile Draping Behaviours for Composite Manufacturing Processes

by

Philippe Kanz

Thesis submitted to the University of Ottawa
in partial fulfillment of the requirements for the
M.A.Sc. Degree in Mechanical Engineering

Department of Mechanical Engineering
Faculty of Engineering
University of Ottawa

Abstract

The manufacture of composite components can be achieved using multiple processes. Once such process is the vacuum assisted resin transfer moulding method for manufacturing composite components. This process involves draping a fabric reinforcement over a mould, and then infusing the fabric reinforcement with resin under vacuum. The weight of the atmosphere pushes down on the fabric while the resin is curing, which increases the fibre volume fraction in the final part. The process is widely used in manufacturing composite components for aerospace applications, because it allows the manufacture of large and often complex parts. It also reduces tooling costs when compared to other composite manufacturing methods.

The process of draping the fabric onto the mould is of significant interest. Draping fabrics onto moulds forces them to deform into the shape of the mould, creating several difficulties related to fabric bending, fabric in-plane shearing, friction between layers of fabric, and spring back of fabrics once draped. Several testing methods are adapted from literature; others are created in this work in order to characterize the mechanical behaviour of fabrics. The mechanical parameters characterized through testing enable calculations of terms of draping energy. The energy required for draping a mould is associated with the difficulty of draping the fabric onto that mould. Drape energy calculations allow for direct comparisons of the draping performance of different fabrics and draping strategies.

Acknowledgements

For the project, I thank Dr. François Robitaille for his guidance in writing this thesis and the Hutchinson Research and Development team for supporting this project. Dr. Robitaille always believed I was capable of producing high quality work, and provided me with the opportunity of working with the industrial partner. The work conducted during my master's degree was extremely productive, and the team – at the time of writing this thesis, consisting of Fabian Basaldua-Robledo, Fabien Salles, Corentin Rannou, and Lionel Tapsoba – was very enjoyable to work with.

Since this thesis was written entirely during the COVID-19 global pandemic, I must thank my immediate family for supporting me throughout writing the thesis. I am also grateful for constant stimulating intellectual, scientific and often humorous discussions with my close friends Jean-Luc Bégin and Nicolas Galton during our walks and bike rides during the coronavirus lockdowns.

"Once you move a fridge down a tight set of stairs and back up again once you realize the exit isn't wide enough, you can pretty much do anything" – Philippe Kanz

Contents

List of Figures

List of Tables

Nomenclature

Greek letters		**Units**
α_f	Final fabric angle	*rad*
α_m	Bending angle	*rad*
β	Measurement of spring back	*mm*
γ	Shear angle	*rad*
ΔB_{Peirce}	Dispersion of bending stiffness	$\mu Nm^2/m$
ΔR_f	Dispersion of final radius of curvature	*m*
$\Delta SBE_{Bending}$	Variability bending spring back energy	*Nmm*
ΔSBE_{Shear}	Variability in-plane shear spring back energy	*Nmm*
$\Delta U_{Bending}$	Bending energy variability	μNm
ΔU_{shear}	Shear energy variability	*Nmm*
Δx	Extension of picture frame rig	*m*
$\Delta \alpha_f$	Dispersion of final fabric angle	*rad*
$\Delta \beta$	Dispersion of measurement of spring back	*mm*
Θ	Angle between warp and weft yarns	*rad*
K	Fabric curvature	m^{-1}
Φ	Yarn orientation	*rad*

Latin letters | | **Units**

B	Bending stiffness	$N{\cdot}m^2$
b	fabric width	m
B_{Peirce}	Bending stiffness, normalized by unit width	Nm^2/m
E	Elastic modulus	N/m^2
$F_{normalized}$	Normalized shear force	N/m
F_{shear}	Shear force	N
I	Moment of inertia	m^4
l	Beam length	m
L_{fabric}	Length of fabric	m
L_{frame}	Distance between two adjacent hinges	m
M	Fabric bending moment	Nm
R	Bending radius	m
R_0	Initial radius of curvature	m
Rf	Final radius of curvature	m
SBS	Base surface area	mm^2
SPF	Picture frame test area	mm^2
$U_{bending}$	Bending energy	μNm
U_{shear}	Shearing energy	Nmm
w	Linear weight density	N/m

Acronyms

ANOVA	Analysis of variance
C	Centre of base surface
DOE	Design of experiments
FRP	Fibre reinforced polymer
HSD	Honestly significant difference
KES	Kawabata evaluation system
MLE	Middle of longest edge
RUC	Repeating unit cell
SBE Bending	Bending spring back energy
SBE Shear	Shear spring back energy
SBR	Spring back ratio
SMR	Simulated mould radius
VARTM	Vacuum assisted resin transfer moulding

Chapter 1. Introduction

A composite is a material made from two or more materials. The combination provides a material with different properties than those of the two materials used for making the composite. Modern composites typically make use of carbon fibres, glass fibres, or aramid fibres for reinforcing a polymer. This category of composites is known as fibre reinforced polymers (FRP). Composite materials can have similar structural mechanical properties to metals, while being much lighter. A comparison of material properties of metals and composites appears in Table 1.1.

Table 1.1 – Comparison of material properties

Material	Elastic modulus	Ultimate tensile strength	Density
A92024 (Aluminium alloy) [1]	73.1 *GPa*	448 *MPa*	2.78 g/cm^3
E-Glass fibre-epoxy matrix, longitudinal direction (v_f = 0.60) [2]	45 *GPa*	1020 *MPa*	2.1 g/cm^3
AISI 4340 (Steel alloy) [3]	192 *GPa*	745 *MPa*	7.85 g/cm^3
High-modulus carbon fibre-epoxy matrix, longitudinal direction (v_f = 0.60) [2]	220 *GPa*	760 *MPa*	1.70 g/cm^3

Composite materials are extremely attractive for use in aircraft design, for the mass reductions that they enable. For example, 53 % of materials used in Airbus A350 are composites [4]. Composite components include the wings, centre wing box and keel beam, tall cone, skin panels, frames, stringers and doublers, and passenger and cargo doors [5].

1.1. Vacuum assisted resin transfer moulding

Many manufacturing processes can be used for fabricating an FRP composite component. Vacuum assisted resin transfer moulding (VARTM) is one such process. In VARTM, a dry and usually continuous reinforcement is positioned on a mould. Resin is injected under vacuum, and cured. The dry reinforcement used in VARTM is often a shaped stack of fabric layers made from carbon or glass fibres, known as a preform. A preform can be made from a single or from several layers of fabric. A preform can also consist of multiple pieces of dry reinforcement, known as patterns. The process of positioning the preform on the mould and of conforming the former to the latter's shape is known as draping. Figure 1.1 illustrates a typical VARTM set up used for manufacturing FRP composites.

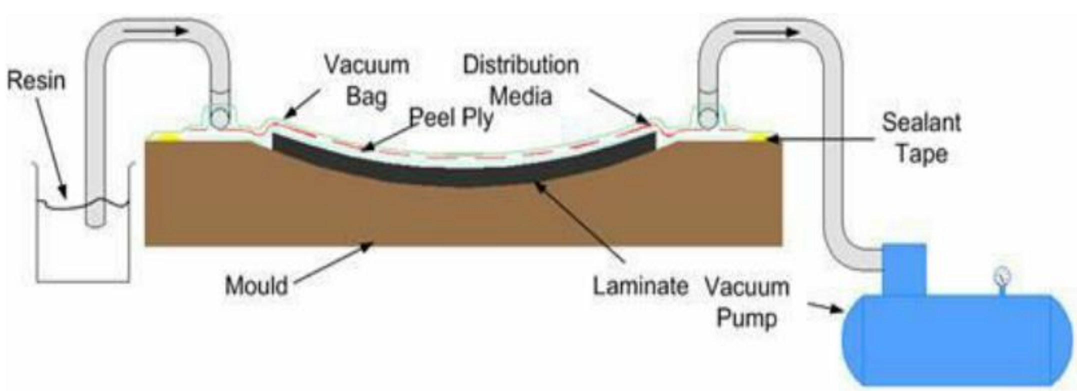

Figure 1.1 – Vacuum assisted resin transfer moulding [6]

VARTM offers many manufacturing advantages when compared with other composite manufacturing processes. Advantages of VARTM include a capability for manufacturing very large parts, and parts of complex geometry, combined with low tooling costs due to their usage of single-sided moulds subjected to low pressure levels.

These advantages make VARTM a very attractive manufacturing process for fabricating composite parts. However, there are many difficulties associated with VARTM manufacturing. Draping fabrics onto moulds of complicated geometry induces in-plane shear in these fabrics. Some fabrics are easy to drape onto moulds, while others cause great difficulties. Draping fabrics onto mould surfaces featuring small curvature radii often causes resin rich corners in the final parts. In-plane shearing of a fabric can cause wrinkles to appear on the surface of that fabric, leading to faulty composite parts. The permeability of the fabric may also decrease, impeding the flow of resin during injection or making preform saturation erratic and unpredictable. Multilayer stacks of some fabrics behave as one thick cohesive fabric would, while the layers within multilayer stacks of other fabrics slide and move relative to each other. Some fabrics are stable, while others are extremely unstable when cut or loaded at attachment points, for example. Finally, the behaviour of some fabrics is reproducible, while the behaviour of other fabrics is highly variable.

1.2. Industrial motivation

Software tools are available to support the engineering of the different operations in processes such as VARTM. Kinematic drape software uses a fisher-net algorithm for calculating in-plane shear angles in fabrics draped onto moulds [7]. Software can identify locations on moulds that will cause high shear angles, which are associated with fabric wrinkling and loss of permeability. However, they are very limited in practical, industrial use: they do not consider fabric architecture or the mechanical properties of fabrics when calculating shear angles, and they do not describe the difficulty of the draping process. Perhaps more importantly, they do not provide the user with instructions for how to best drape a fabric onto a mould; instead, they only evaluate scenarios that are entirely proposed by a human user.

As a result, the real difficulties associated with draping and the limitations of kinematic drape software make the manufacturing of preforms for composite components costly and time consuming, as it remains a largely trial-and-error procedure that can only be conducted by experts counting years of experience doing such work.

Industrial partner Hutchinson Aéronautique et Industrie, based in Montréal QC, manufactures composite components for the interior of commercial and private aircraft. The industry partner for this work manufactures a wide variety of complex composite components. In general, when a client requests the manufacture of a new composite component, the client sends a CAD drawing of the part to Hutchinson, and Hutchinson responds with a quote estimating the cost of manufacturing the part. A brief delay of a few days that must be upheld for securing the client. The quote must be as accurate as possible on part cost. As no software can predict efficiently the draping operation in VARTM, quotes are essentially produced by considering the manufacturing costs of previously manufactured parts similar to the new part, as a starting point. Further manual trial and error work is often conducted for refining the estimate and designing a preform and draping sequence that maximises part quality and minimizes manufacturing time. Trial and error work for designing the preforming process is highly time consuming and highly dependent on a limited number of experts. It reduces the competitiveness of the industry partner, and constitutes a major point of operational risk and uncertainty in the quotation process [8].

In order to reduce the time required for producing a quote for clients, and to increase the traceability and reproducibility of the process, Hutchinson and uOttawa created a first predictive tool for selecting the fabric to be used for draping the mould. The development of this first predictive tool is detailed in the Master's thesis of Sebastien Gagné [8]. The first predictive tool makes use of two databases for selecting the best fabric to drape onto a mould. The first database consists of mechanical characteristics of fabrics, and the second database consists of surfaces typically found on moulds used for manufacturing composite components.

In order to populate the database of fabric characteristics, a rapid characterization tool was developed for testing the in-plane shear, in-plane shear spring back, friction and stability of multiple fabrics as part of the first predictive tool developed by Gagné. Results from the rapid characterization tool consist in measurements of torque, with fabrics characterized by rankings on a scale from 1 to 10 where scores of 10 and 1 indicate excellent and marginal performance, respectively. Characterization of the bending behaviour was conducted by Gagné, draping a fabric onto a single curvature corner and measuring spring back. Results were then similarly ranked on a scale from 1 to 10. A summary of the characterization methods used by Gagné as part of his predictive tool appear in Figure 1.2.

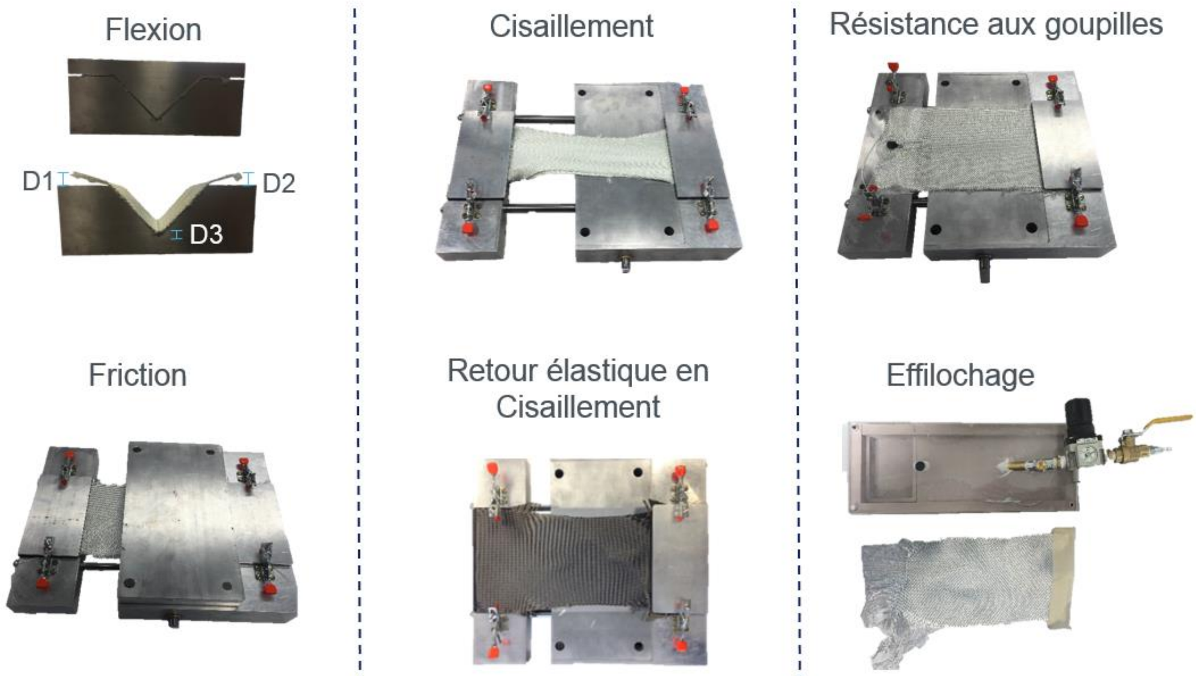

Figure 1.2 – Characterization test methods summary [8]

Gagné’s database of surface characteristics was built by decomposing industrial moulds into nine basic geometric features shown in Figure 1.3. Every basic mould feature was given a score from 1 to 10 in order to compare the extent of in-plane shear induced in the fabric by each basic mould feature, and another score from 1 to 10 compared the extent of fabric bending over the same basic geometric feature.

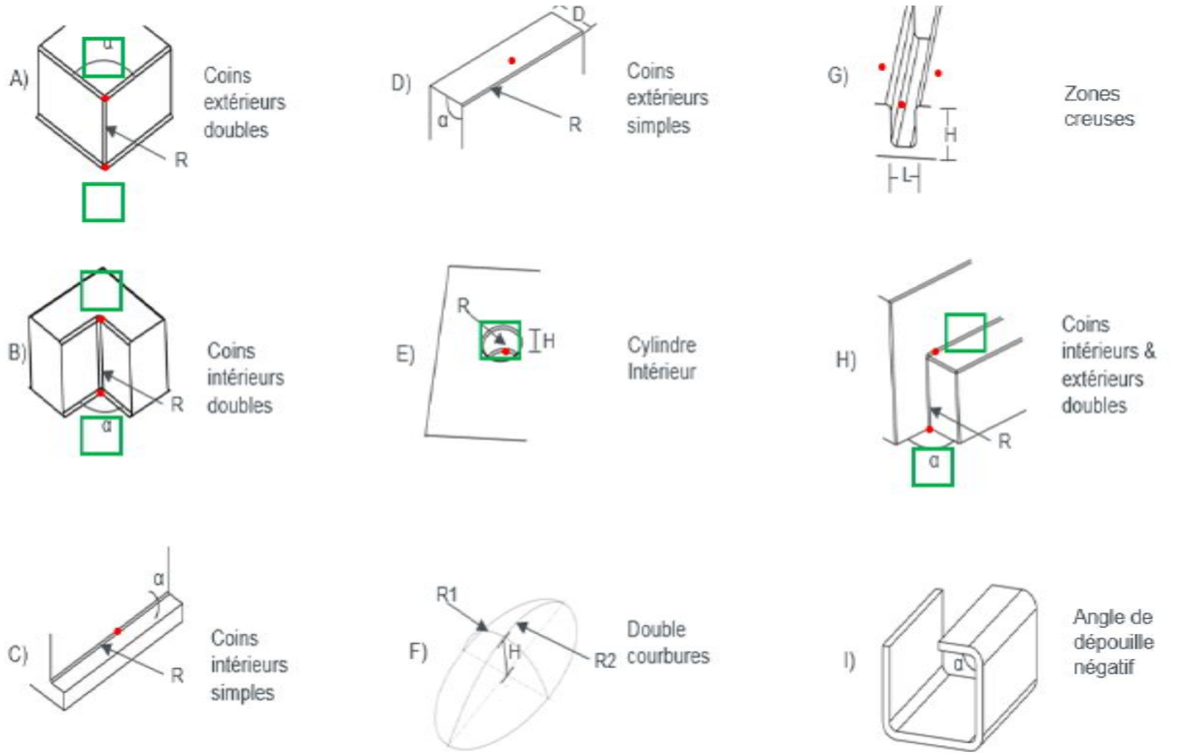

Figure 1.3 – Basic mould geometric features [8]

Scores given to each fabric characteristic and each basic mould feature were used in an algorithm selecting the best fabric to use for draping a given mould. The predictive tool developed by Gagné [8] was an excellent first attempt at creating a predictive tool for draping fabrics onto moulds, because it makes use of fabric characteristics and basic geometric features of the mould.

1.3. Project overview and objectives

The predictive tool developed by Gagné and reported in [8] is limited by several factors. Characterization of fabric behaviour during drape made use of rapid fabric characterization tools; therefore, fabric characteristics used in the predictive tool do not represent real fabric mechanical properties; furthermore, rankings from 1 to 10 have been deemed somewhat arbitrary. The evaluation of basic geometric mould features does not allow for direct measurement of shear angles in the fabric, and scores given for specific combination of mould features and mould dimensions have also been deemed somewhat arbitrary.

The work presented in this thesis constitutes part of the deliverables of a project aiming at developing a new predictive software tool that will assist industrial partner Hutchinson Aéronautique et Industrie with fabric and draping sequence selection for any given mould geometry, based on draping difficulties associated with the geometry of the mould and precise mechanical behaviour of the fabric. The software tool will ultimately provide a ply book describing an optimal draping sequence for a mould, along with estimates of manufacturing time and quality of the preform.

In order to achieve these goals, the project was broken down into three main components:

- A database of shear angles resulting from draping over redefined base geometries (Database A);
- A database of redefined fabric mechanical characteristics (Database B); and
- An algorithm that probes draping sequences and selects the best one using results in Databases A and B.

The new approach to the predictive tool improves upon Gagné's previous iteration of the predictive tool in several major areas: basic mould geometric features are replaced with systematic modelling formalism for all surfaces constituting any mould, accompanied by shear angle results in all cases. The database of scores representing fabric mechanical characteristics is replaced with a rigorous characterization and quantification of fabric mechanical properties. Finally, the predictive algorithm probes all possible preforming scenarios, whilst prioritising realistic drape sequences.

The creation and population of Database A is detailed in the master's thesis of Jacob Hoffer [9]. A five-parameter and a twelve-parameter conical frustums were developed for modelling all base surfaces found on industrial moulds. The five-parameter conical frustum shown in Figure 1.4 was used for building a variety of three and four-edged base surfaces shown in Figure 1.5. Some drape simulations were conducted on parameterized base surfaces. Taguchi analyses were used for creating linear functions interpolating shear angle values along all vertices of the base surface and at mid-points along base surface edges, based on the five-parameter conical frustum parameters. More work pertaining to database population remains to be done, for both the 5-parameter and 12-parameter frustums.

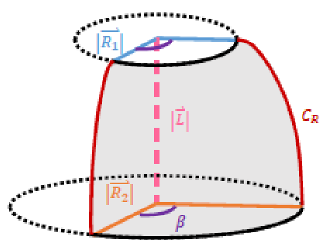

Figure 1.4 – Five-parameter conical frustum [9]

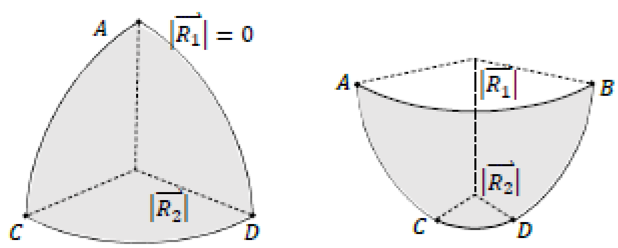

Figure 1.5 – Three and four-edge base surfaces [9]

The scope of this thesis is the database of fabric characteristics. One major aim was to develop characterization of fabric mechanical behaviour that is quantitative, rigorous and based on first principles analysis. Challenges in draping and their relations with measurable fabric characteristics were identified by interviewing composite manufacturing technicians at Hutchinson. Difficulties encountered by technicians during the draping process of VARTM relate to the following [10]:

1. Bending stiffness of fabric;
2. Bending spring back of fabrics once draped onto moulds;
3. In-plane shear behaviour of fabrics;
4. In-plane shear spring back of fabrics once draped onto moulds;
5. Friction between plies of multilayer fabrics as they are draped onto moulds;
6. Lack of stability of fabrics once pinned to moulds.

Two of the above fabric properties can be characterized using existing testing methods. The bending stiffness of fabrics was characterized using cantilever bend tests following a modified version of ASTM-F3260 Standard Test Method for Determining the Flexural Stiffness of Medical Textiles. The in-plane shear behaviour was characterized using picture-frame shear tests. Novel testing methods were developed and used for characterizing bending spring back, in-plane shear spring back, friction between plies of fabric and stability of fabrics.

Novel bending spring back tests developed as part of this thesis work consist of placing a fabric onto a simulated mould radius, applying a load to drape the fabric onto to the mould, and then releasing the applied load. Measurements of spring back were obtained for convex and concave corners, and for a variety of mould radii.

The picture-frame shear tests used for characterizing the in-plane shear behaviour of fabrics was modified in order to propose a novel characterization of in-plane shear spring back behaviour during the same test. In conventional picture-frame tests, shear load is plotted as a function of shear angle. In this thesis, picture-frame tests featured cyclical loading and un-loading; load was recorded during both phases of each test. The angle at which shear force reduced to zero was defined as the return angle, and was used for characterizing in-plane shear spring back of fabrics.

Friction tests were inspired by ASTM-D1894 Test Method for Static and Kinetic Coefficient of Friction of Plastic Film and Sheeting. The testing method used in this thesis uses a universal tensile tester for sliding a bloc over a surface covered in fabric reinforcement. The load recorded by the tensile tester was used for calculating the coefficient of friction of the selected fabrics.

Tests for pin stability of the fabric used a tensile tester for recording the load applied on a pin by the fabric, and fabric extension. Test results are defined as load at pin failure, and extension of the fabric at pin failure.

Finally, methods for calculating terms of draping energy based on characterization results are presented and used for calculating the energy required for draping one demonstrator mould, using three different draping strategies. The aim of the demonstrations is to identify the draping strategy requiring the least energy towards completing draping, as well as the draping strategy showing the least variability in outcome.

1.4. Chapter summary

This thesis consists of 7 chapters and 5 appendices. Chapter 1 introduces background information on composite materials and the vacuum assisted resin transfer moulding process, along with the industrial motivation for the project and an overview of work previously done.

Chapter 2 is a literature review covering fabric characterization methods. Draping issues related to fabric mechanical behaviour are summarized, followed by a brief overview of 2D fabric architecture. Fabric characterization methods are discussed including the Peirce bend test, Kawabata evaluation system for Fabrics, Kawabata conversion functions for subjective fabric comparison, in-plane shear testing methods, wrinkle recovery test, and friction tests for fabrics.

Chapter 3 summarizes the materials, the testing methods, and the statistical analyses used for characterizing the mechanical behaviour of fabrics. The technical specifications of three fabrics and a binder resin are presented, followed by testing procedures for bending, bending spring back, in-plane shear, inter-layer friction, and pin resistance characterization. Analysis of variance is used for comparing the performance of each fabric, and designs of experiments are used for building linear functions interpolating characterization results.

Chapter 4 presents characterization results for bending, spring back, in-plane shear, friction and pin resistance tests. This chapter includes statistical comparisons between each fabric for all characterization tests performed in this work. Linear interpolation function coefficients are listed for all fabric characteristics.

Chapter 5 presents methods for calculating the energy required for draping fabrics onto base surfaces, from characterization results and surface geometry. Average and dispersion statistics are used for estimating the average and variability of draping energy. Average drape energy is associated with drape time, while variability of drape energy is associated with reproducibility of the draping process.

Chapter 6 demonstrates the process for calculating the drape energy and the variability of the drape energy of fabrics over an industrial demonstrator, for different draping scenarios. The drape energy and variability calculations are used in conjunction with a tool that breaks down a mould into multiple base surfaces and an algorithm that lists potential drape sequences.

Chapter 7 summarizes contributions made for the industrial partner's project, and lists recommendations for future work in the characterization of fabric mechanical behaviour.

Chapter 2. Literature review

2.1. Introduction

In the garment industry, “drape” and “drapability” of fabrics refer to the property that allows a fabric to deform into eye-pleasing folds when acted upon by gravity [11]. In the context of this project, “drape” and “drapability” will refer to the forming of fabrics onto complex shapes in the context of vacuum assisted resin transfer moulding [10]. Many attempts have been made towards predicting the drapability of woven fabrics used in the garment industry. Most studies probed their bending and shear stiffness, which are two factors that are thought to affect the draping qualities of a fabric. These two characteristics are not sufficient to define the drape performance of a technical textile during preforming for the VARTM process: once technical textiles are conformed to mould surfaces, they generally spring back, both in bending and in shear. Spring back is difficult to quantify and it has received little to no attention in the scientific literature. However, it causes significant frustration and delay for the technicians manufacturing textile preforms for composite parts because it results in corners being rich in resin [10]. Fabric spring back also causes yarn in final parts to be poorly oriented and misaligned, which is problematic as the mechanical properties of composites depend on the yarn orientations with respect to loads applied on the part. Technical textiles also tend to be unstable – both carbon and glass fibre fabrics have a tendency to loose their yarns as they are manipulated by technicians [10]. The level of instability shown by different fabrics depends on fabric architecture and on friction between interlacing yarns. Plies in multilayered fabrics can also slide or rotate with respect to each other, which results in altered mechanical properties. The purpose of this chapter is to present the reader with background information on fabric architectures and existing methods for characterizing the mechanical parameters of fabrics that affect drape.

2.2. Fabric architecture

The yarns that constitute a fabric can be assembled and arranged in many different ways: they can be woven, knitted, non-woven, braided, or be arranged into netting or lace structures. Various types of structures are shown in Figure 2.1.

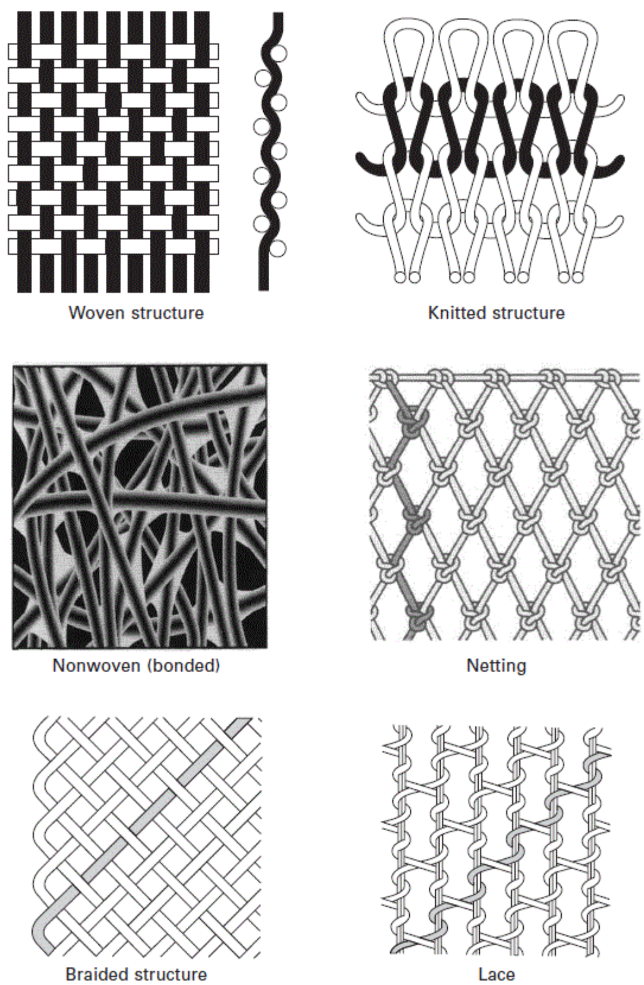

Figure 2.1 – Various fabric structures [12]

Most two dimensional woven structures consist of two sets of perpendicular yarns; such 2D weaves are knows as bidirectional. Yarns extending along the length of a bidirectional woven fabric are know as warp yarns, and perpendicular yarns extending along the width of the fabric are known as weft yarns. In woven fabrics, warp and weft yarns are interlaced in a repeating pattern which results in a coherent and stable structure [12]. Such patterns are defined by their smallest periodic unit, known as a repeating unit cell (RUC). There are many types of woven fabrics such as plain weaves, twill weaves and satin weaves as detailed below.

In any given fabric, yarn crossovers occur at every warp and weft intersection. In plain weave fabrics, the warp and weft yarns are interlaced at every crossover, as shown in Figure 2.2.

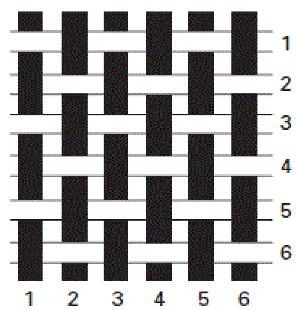

Figure 2.2 – Plain weave fabric (warp direction is vertical) [12]

In a twill weave fabric, the warp and weft yarns are repeatedly interlaced in both warp and weft directions in intervals of two or more crossovers. The twill weave pattern produces visible diagonal patterns along the surface of the fabric known as twill lines. Twill weaves are defined by their X/Y interlacing pattern, where X is the number of weft yarns passing under warp yarns and Y is the number of weft yarns passing over warp yarns, after these yarns have passed over an X weft yarn. A 1/3 twill fabric is shown in Figure 2.3, where the warp direction is vertical. The black squares indicate a warp yarn passing over a weft yarn, and the white squares indicate a weft yarn passing over a warp yarn. In other words, the black squares indicate the interlacing pattern.

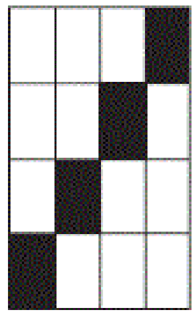

Figure 2.3 – 1/3 twill weave [12]

Satin weave fabrics are similar to twill weave fabrics: the warp and weft yarns are repeatedly interlaced in both warp and weft directions. However, in satin fabrics the weave pattern is modified in a way that eliminates twill lines. Satin fabrics are also defined by an X/Y sequence. The number of harnesses used in producing a satin fabric can also define satin terminology. An example of a 1/4 satin is shown in Figure 2.4. To produce this pattern, 5 harnesses were used, hence it is also known as a 5-harness satin (5HS satin). This pattern eliminates twill lines as it adds space between every warp and weft interlacing, as shown in Figure 2.4 where there are white spaces between every black square.

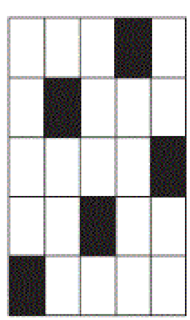

Figure 2.4 – 1/4 satin weave (5HS satin) [12]

2.3. Peirce bending tests

The earliest attempts to characterize the drape performance of fabrics were made by F. T. Peirce. Peirce noted that sensations of stiffness, softness and smoothness were often used for describing fabrics in the garment industry [13]. He introduced the concept of flexural rigidity to fabrics, and devised a test for quantifying this property The test involves a fabric bending under its own weight over an inclined plane of 41.5°. A cantilever bending rig used for the Peirce bending test is shown in Figure 2.5.

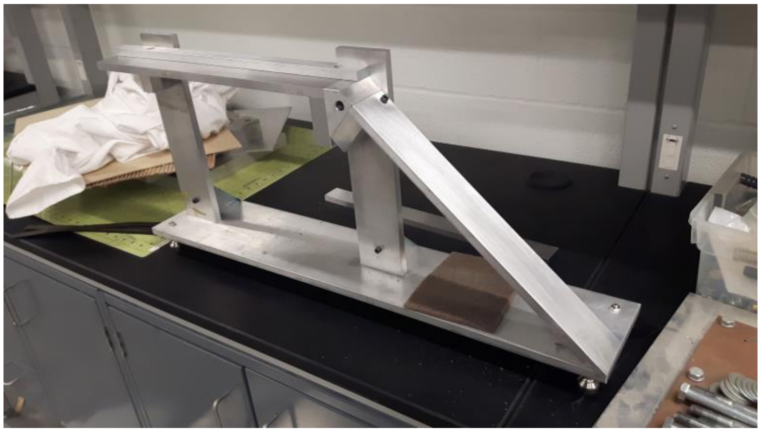

Figure 2.5 – Cantilever bending rig from University of Ottawa Composites Lab

Peirce assumed that a fabric may be modelled as a uniform linear elastic beam, i. e. a continuous material. Assuming that the relation between bending moment and curvature of a beam is linear, the bending rigidity is defined as follows:

$$M = \kappa B = \frac{1}{R} EI \tag{2.1}$$

where M is the bending moment (*Nm*), κ is the beam curvature (m^{-1}), B is the bending rigidity (Nm^2), R is the beam radius (*m*), E is the elastic modulus of the beam (N/m^2), and I is the moment of inertia of the beam (m^4).

The shape of a bent beam is described mathematically by a function representing the vertical displacement of the beam. The vertical displacement of the beam y (*m*) is a function of the horizontal position along the length of the beam x (*m*). According to the Euler-Bernouli beam theory, the curvature of the beam is given by $\kappa = y''$. Hence, the curvature of the beam is equal to the double derivative of the function representing vertical displacement along the length of the beam.

The bending moment M is readily derived based on the loading scenario shown in Figure 2.6.

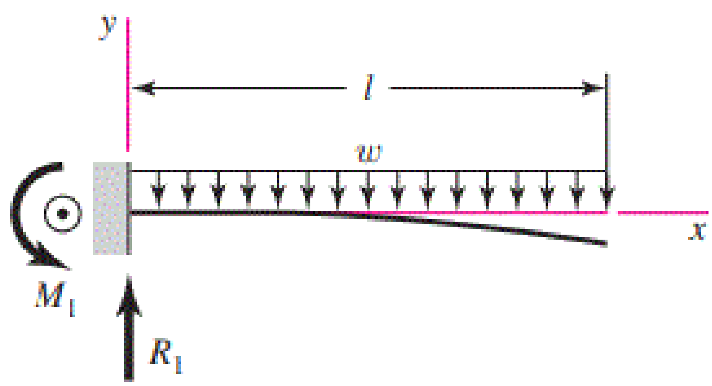

Figure 2.6 – Cantilever beam subjected to a uniform load [14]

The bending moment at any point throughout the length of the beam is given by

$$M = -\frac{w}{2}(l - x)^2 \tag{2.2}$$

where l is the beam length (*m*) and w is the beam weight per unit length (*N/m*).

Putting Equations (2.1) and (2.2) together,

$$M = By'' = -\frac{w}{2}(l - x)^2 \tag{2.3}$$

After isolating y'' and applying boundary conditions $y(0) = 0$ and $y'(0) = 0$, this equation reduces to

$$y(l) = \delta = -\frac{wl^4}{8B} \tag{2.4}$$

where δ is the vertical displacement at the end of the beam (*m*). From Figure 2.7, the angle between the inclined plane and the horizontal is given by

$$\tan\alpha = \frac{\delta}{l} \tag{2.5}$$

where α is the angle between the inclined plane and the horizontal axis (*rad*).

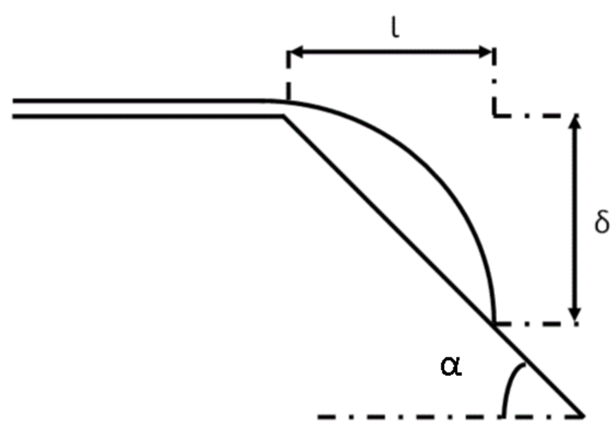

Figure 2.7 – Cantilever fabric overhanging a 41.5° inclined plane

Combining Equations (2.4) and (2.5) and re-arranging, an expression of the bending rigidity is obtained. The minus sign is removed, because it indicates a downward deflection. Assuming that the positive *y*-direction is downward, then

$$B = \frac{wl^3}{8\tan\alpha} \tag{2.6}$$

For large beam deflections, Peirce introduced a corrective term for large deformations equal to $\cos\left(\frac{\alpha}{2}\right)$. This corrective term is purely empirical [15]. Equation (2.6) becomes

$$B = \frac{wl^3}{8\tan\alpha}\cos\left(\frac{\alpha}{2}\right) \tag{2.7}$$

Standard commercial cantilever bending rigs have an inclined plane at 41.5°. At that angle $\frac{\cos\left(\frac{\alpha}{2}\right)}{\tan\alpha}$ is approximately equal to 1, and so Equation (2.7) becomes

$$B \approx \frac{wl^3}{8} \tag{2.8}$$

2.4. Kawabata evaluation system

Kawabata devised five different tests for evaluating the mechanical properties of garment fabrics [16]. The characterization methods are known as the Kawabata evaluation system (KES). The five tests use four rigs to characterize fabric mechanical properties. Using these rigs, it is possible to characterize 16 mechanical parameters related to mechanical behaviour of fabrics. Kawabata designed a tensile test, a bending test, an in-plane shearing test, a compression test, and a surface roughness and friction test. The tensile test and shear test use the same rig, and the remaining three tests each have their own rig, as shown in Figure 2.8.

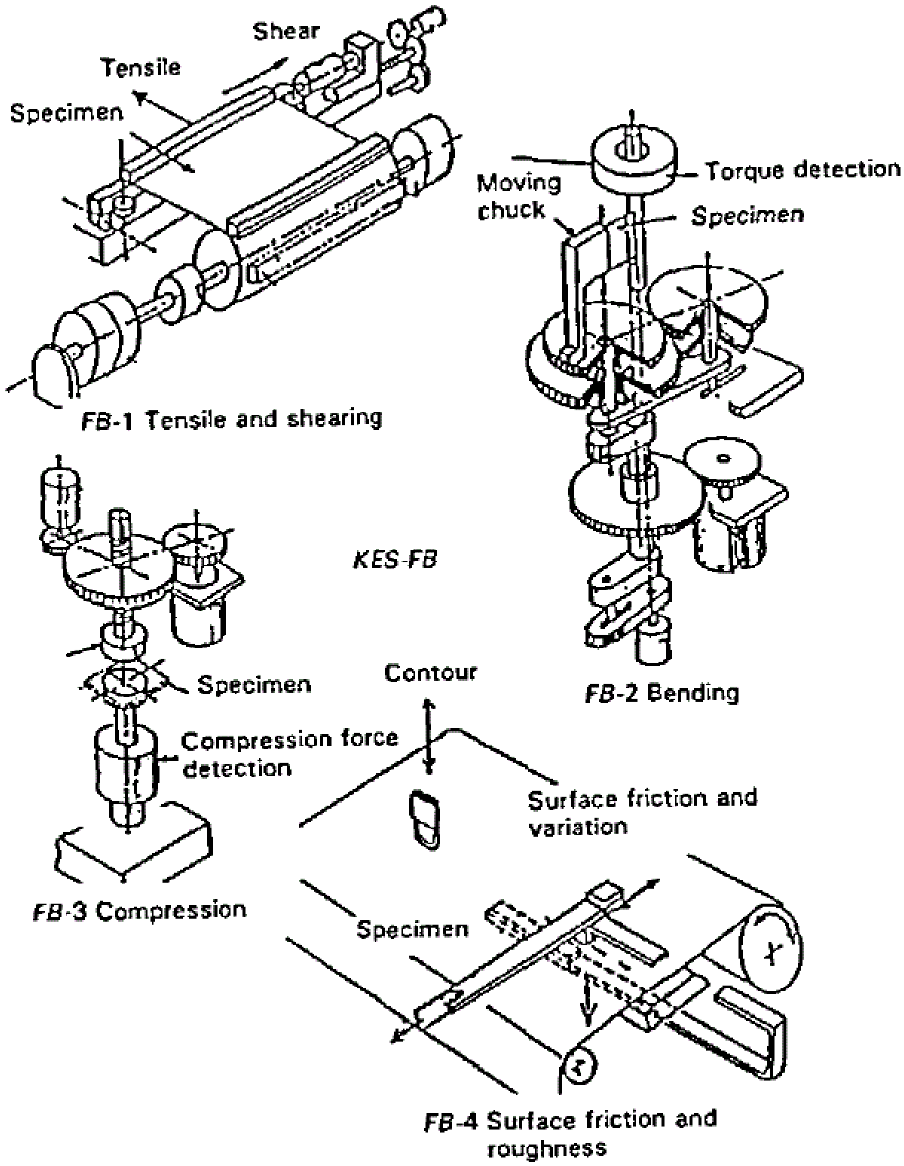

Figure 2.8 – Kawabata evaluation system [17]

The Kawabata tensile test consists of tensioning and releasing tension from a fabric sample fabric. Two sets of clamps are used for mounting the sample in the apparatus. The clamps are placed 5 *cm* apart, and the sample measures 20 *cm* × 20 *cm*. The tensile load is applied evenly between the two clamps, putting a 5 *cm* x 20 *cm* section of fabric under tension.

The Kawabata tensile test is shown in Figure 2.9 and Figure 2.10. The fabric sample is pulled from 0 $gf \cdot cm^{-1}$ of tension to 500 $gf \cdot cm^{-1}$ at a constant strain rate of 4×10^{-3} s^{-1}. Tension is released at the same strain rate. Load and extension are recorded throughout the whole test. Typical results from the Kawabata tensile test are shown on a force vs strain plot, Figure 2.11. Four mechanical parameters are obtained from the load-extension curves which result from the tensile test: the linearity of the load/extension curve *LT* (no units), the tensile energy *WT* ($gf \cdot cm/cm^2$), the tensile resilience *RT* (*%*) and the extensibility *EM* (no units). The linearity *LT* is the ratio of the tensile energy to the area of the triangle formed by points Q1, Q2 and Q3 on Figure 2.11. The tensile energy *WT* is the area under the loading curve (curve A). The tensile resilience *RT* is the ratio of the area under the unloading curve (curve B) to the area under the loading curve (curve A). The extensibility *EM* is the strain at 500 $gf \cdot cm^{-1}$. The machine used for this test is known as the KES-FB1 – Tensile-Shear Tester.

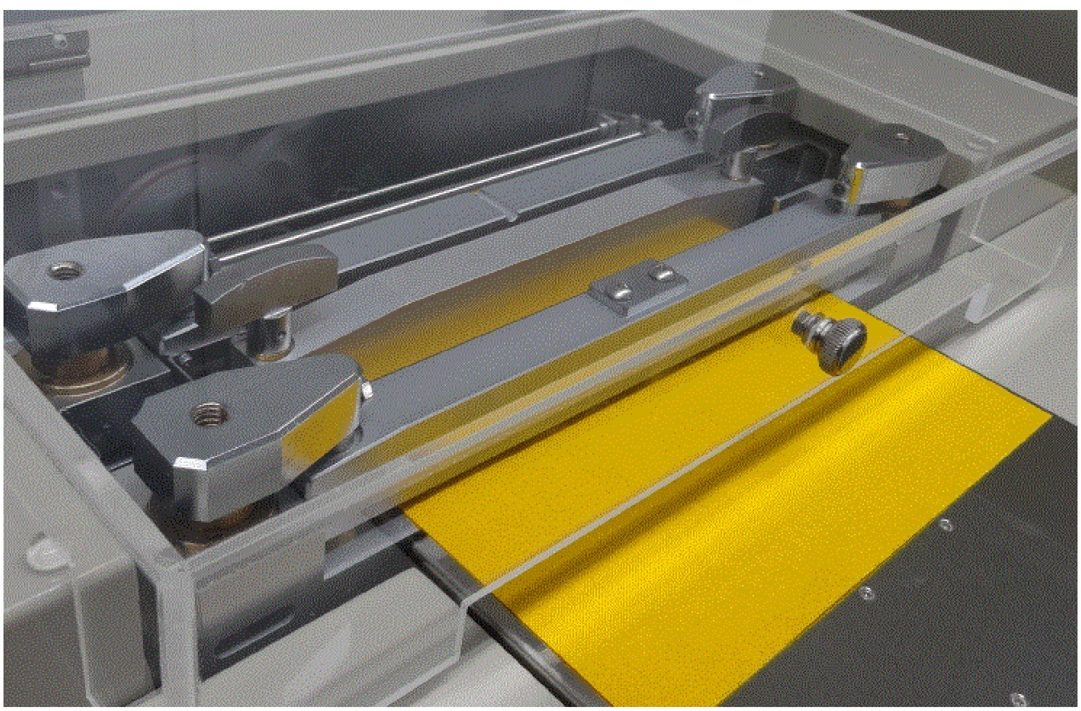

Figure 2.9 – KES-FB1 tensile test [18]

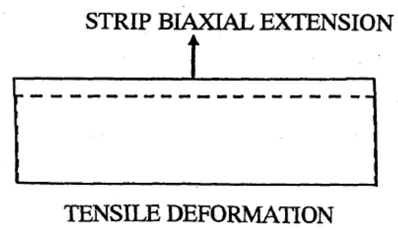

Figure 2.10 – KES tensile test deformation [16]

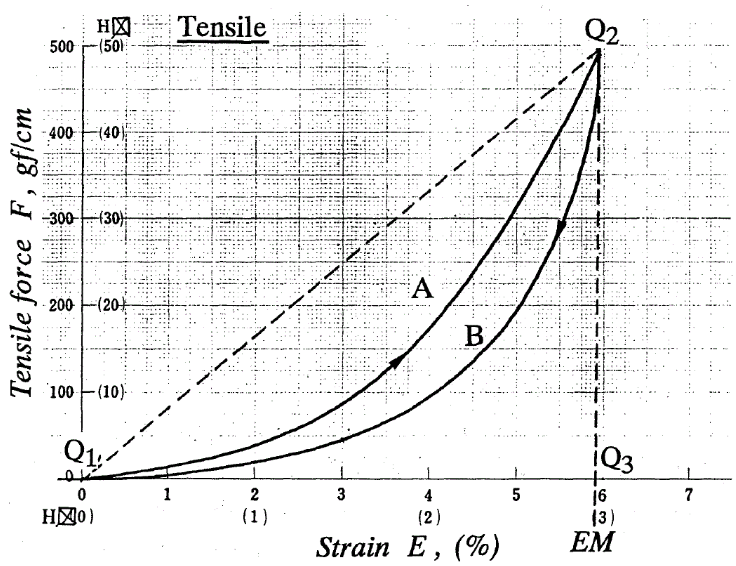

Figure 2.11 – KES tensile test curve [16]

The Kawabata bending test consists of bending a sample of fabric forwards and backwards (Figure 2.12). As with the Kawabata tensile test, two sets of clamps are used for mounting the sample in the apparatus. The clamps are positioned 1 *cm* apart, and the fabric sample measures 20 *cm* × 20 *cm*, which results in a 1 *cm* × 20 *cm* section of fabric being bent. The sample is bent at a constant curvature rate 5×10^{-3} $m^{-1}s^{-1}$. Once the fabric reaches a maximum curvature of 25×10^{-3} m^{-1}, the sample is returned to its initial state i.e. no curvature, and is then bent in the opposite direction. The curvature rate is the same while bending and straightening the samples, in both directions. The bending moment and curvature are recorded during the test, as the sample is bent and unbent. The fabric deformation mode is shown in Figure 2.13. Two mechanical parameters are obtained from the test: the bending rigidity B ($gf{\cdot}cm^2/cm$), and the bending moment hysteresis $2HB$ ($gf{\cdot}cm/cm$). It is noted that the bending moment is normalized by the width of sample in this bending test; therefore, units of bending rigidity are also normalized by unit width. The bending rigidity B is the slope of the curve between curvatures 0.5 and 1.5 cm^{-1}, and the bending hysteresis $2HB$ is measured at a curvature of 1 cm^{-1}, as shown in Figure 2.14. The machine used for the bending test is known as the KES-FB2 Bend Tester.

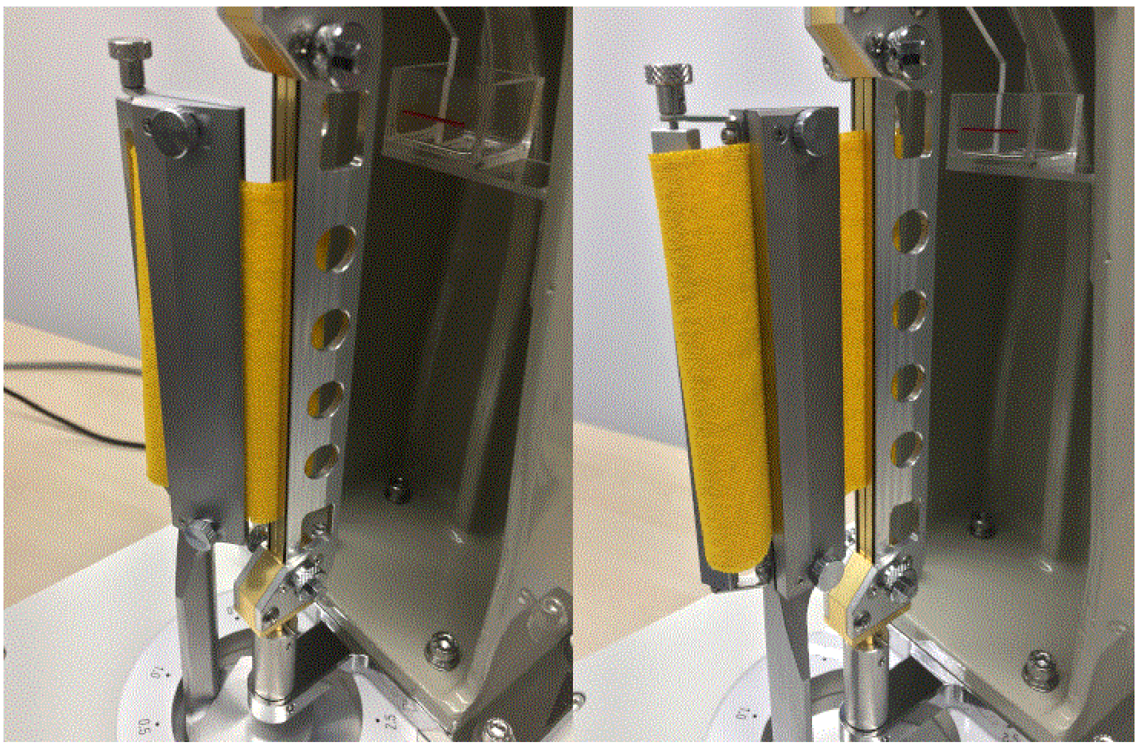

Figure 2.12 – KES-FB2 bending test [19]

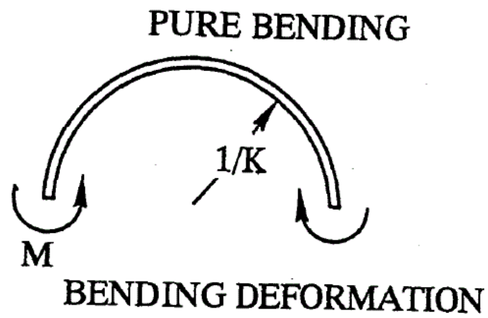

Figure 2.13 – KES bending test deformation [16]

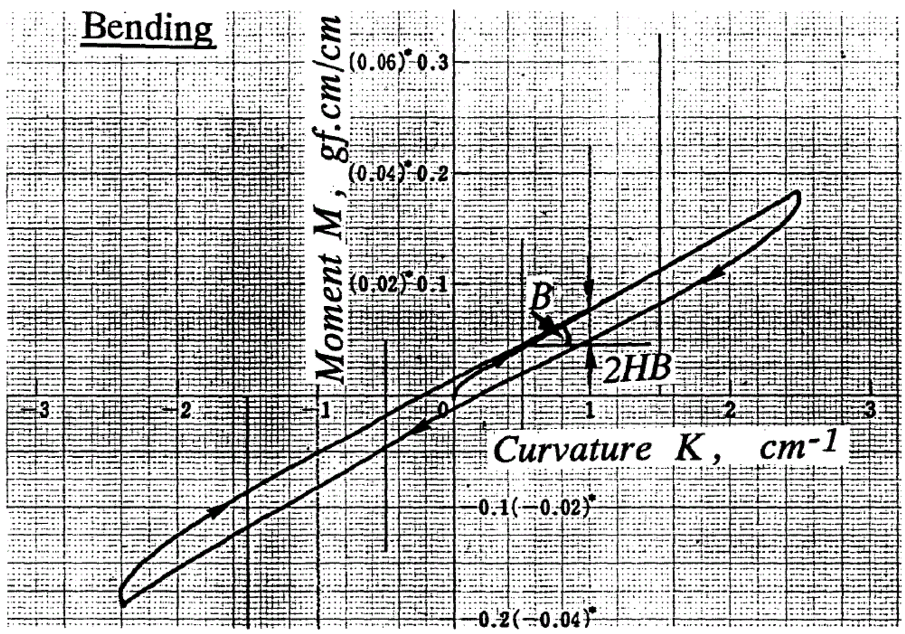

Figure 2.14 – KES bending test curve [16]

The Kawabata shear test consists of applying and releasing an in-plane shear load to fabric samples. This test uses the same apparatus, sample dimensions, and clamp placement as the Kawabata tensile test. A constant tension of 10 $gf{\cdot}cm^{-1}$ is applied to the sample, which is then sheared evenly between the clamps. The sample is sheared at a constant shear deformation rate of 1.46 $°s^{-1}$. Once the fabric reaches a shear angle of 8°, it is returned to its initial null shear strain state and then sheared in the opposite direction. The shear deformation rate is the same throughout the whole test. The deformation mode is shown in Figure 2.15. The shear force and shear angle are recorded during the test. The shear stiffness *G* ($gf \cdot cm^{-1}/°$) is the slope of the loading portion of the curve. The hysteresis of shear force *2HG* ($gf \cdot cm^{-1}$) is evaluated at a shear angle of 0.5°, and the hysteresis of shear force *2HG5* ($gf \cdot cm^{-1}$) is evaluated at a shear angle of 5°. These parameters are shown in Figure 2.16. The machine used for the shear test is known as the KES-FB1 – Tensile-Shear Tester.

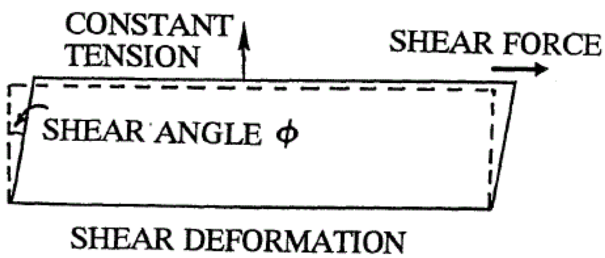

Figure 2.15 – KES shear test deformation [16]

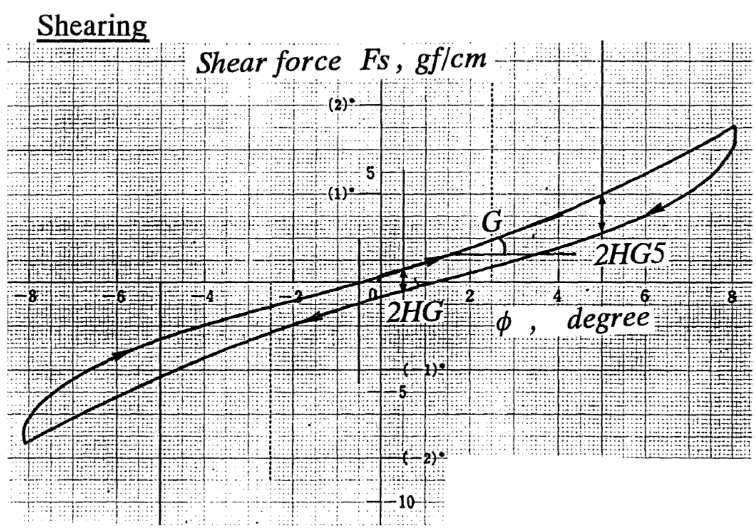

Figure 2.16 – KES shear test [16]

The Kawabata compression test consists of applying and releasing a compressive load normal to samples of fabric (Figure 2.17 and Figure 2.18). In this test, a 20 $cm \times 20\ cm$ sample of fabric is positioned on the testing apparatus. A small 2 cm^2 circular area is compressed to 50 gf/cm^2 in the direction of fabric thickness at a velocity of 20 $\mu m/s$ while the force and thickness are recorded. Once the maximum compression pressure is reached, the pressure is removed at the same velocity. Results of the test are plotted on a compressive pressure versus thickness plot. Four mechanical parameters are characterized: the linearity of compression LC (no units), the compressional energy WC ($gf{\cdot}cm/cm^{-2}$), the compressional resilience RC (%), and the thickness of the fabric T (mm) measured at 50 gf/cm^2 of compressive pressure. The linearity of compression LC is the ratio of compressional energy WC to the area of the triangle formed by points Q1, Q2 and Q3. The compressional energy WC is the area under the compression curve, shown in Figure 2.19. The compressional resilience RC is the ratio of the area under curve B to the compressional energy WC. The apparatus used for the compression test is known as the KES-FB3 Compression Tester.

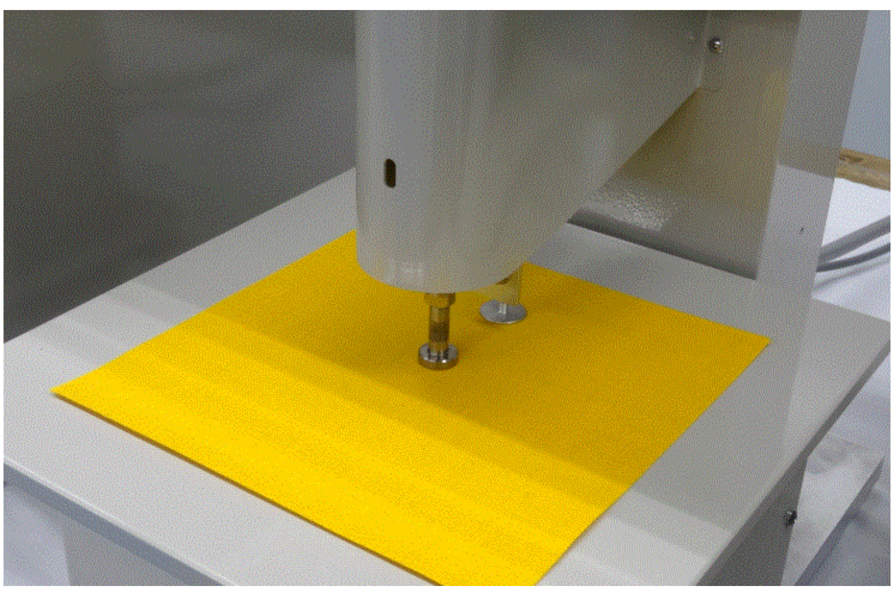

Figure 2.17 – KES compression test [20]

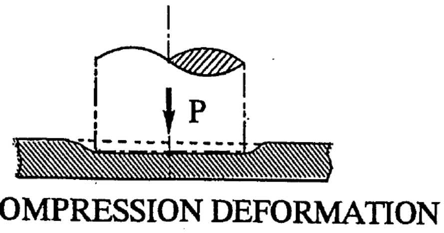

Figure 2.18 – KES compression deformation [16]

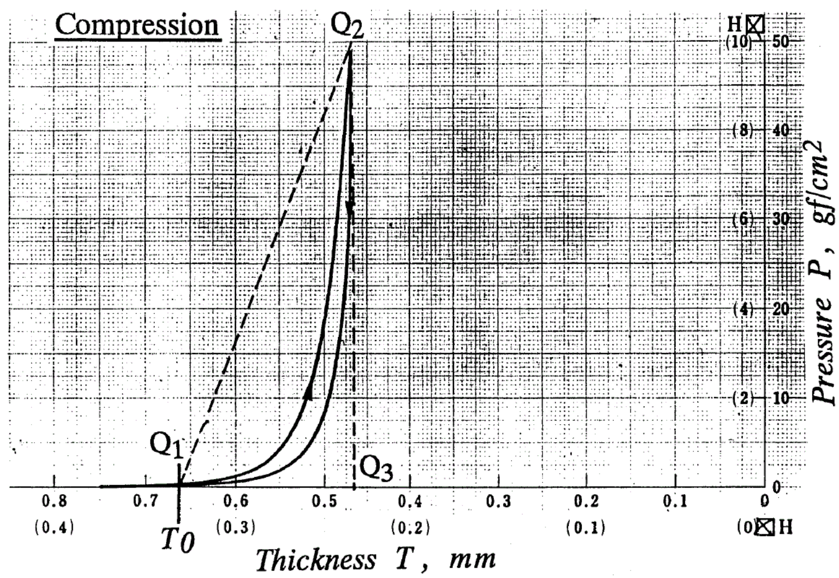

Figure 2.19 – KES compression test [16]

In the Kawabata surface test (Figure 2.20), sensors are used for measuring three mechanical parameters: the mean coefficient of friction *MIU* (no units), the mean deviation of the coefficient of friction (*MMD*) (no units), and the mean deviation of thickness *SMD* (μm). The frictional sensor consists of 10 parallel piano wires, each having a diameter of 0.5 *mm*, which are meant to simulate the human fingerprint. The sensor is pressed down on the fabric using a weight, to a force of 0.5 *N*. The sensor for the geometric smoothness consists of only 1 piano wire, to measure the geometry of the weave pattern. Sensors geometries are shown in Figure 2.21. The sensors are then swept across the surface of the fabric at a velocity of 1 *mm/s*. The coefficient of friction is the ratio of friction force to normal force. The mean coefficient of friction *MIU* is taken as the average coefficient of friction over a sweep of 2 *cm* (Figure 2.22), with values taken from the sensor that simulates the human fingerprint. The mean deviation of the coefficient of friction *MMD* is shown in Figure 2.23; it is the ratio of the hatched area over the sweep length. This parameter represents the frictional roughness. The mean deviation of thickness *SMD* is calculated using the same principle, but using data from the geometric roughness sensor. This parameter represents geometric roughness. The machine used for the surface tests is known as the KES-FB4 Surface Tester.

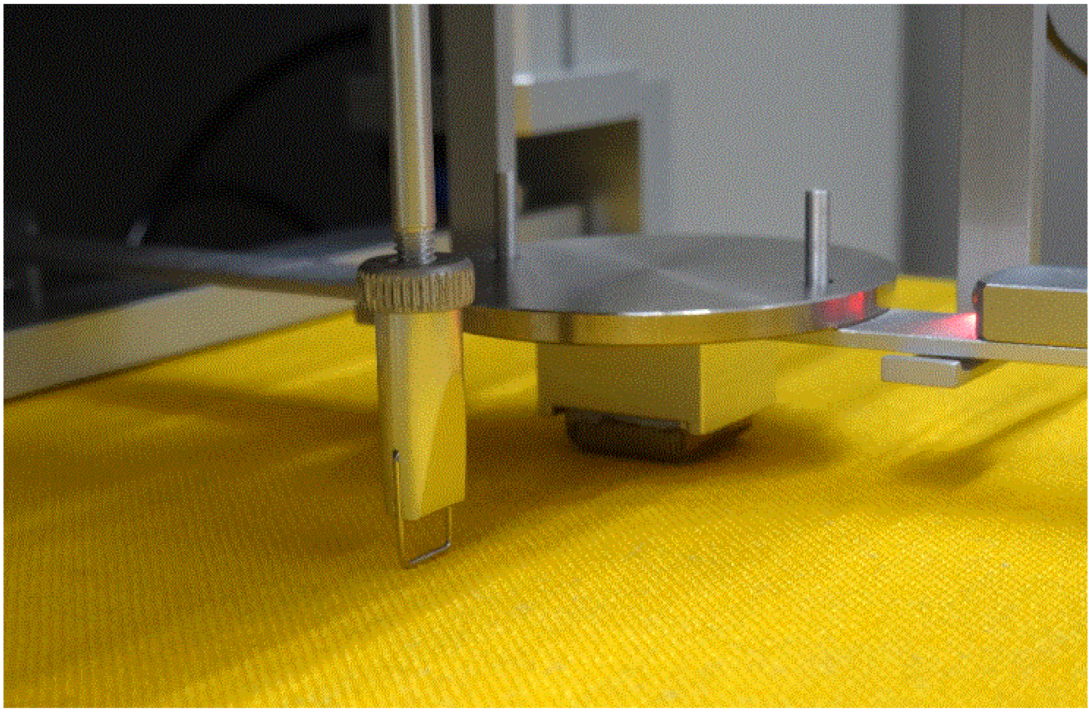

Figure 2.20 – KES surface test [21]

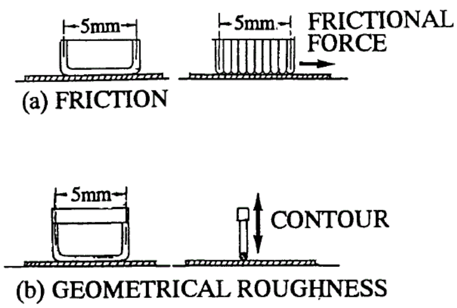

Figure 2.21 – KES surface tests sensors geometries [16]

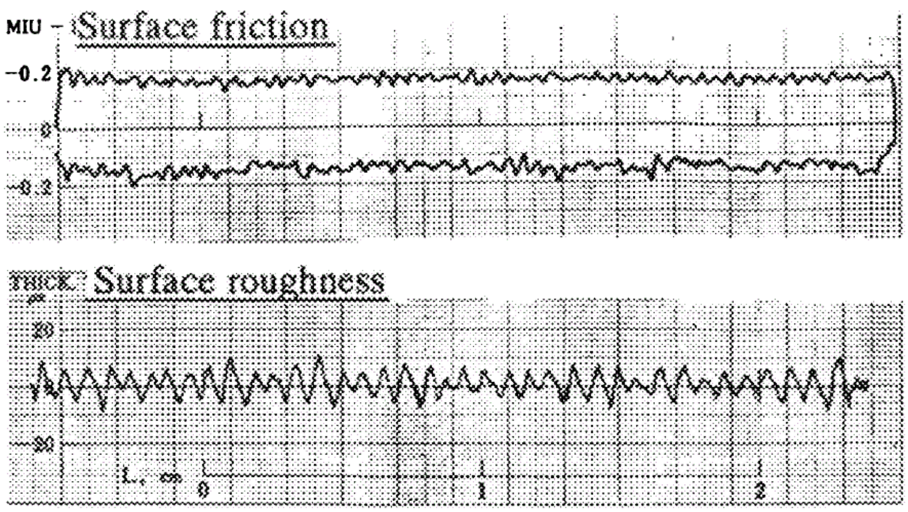

Figure 2.22 – KES surface test [16]

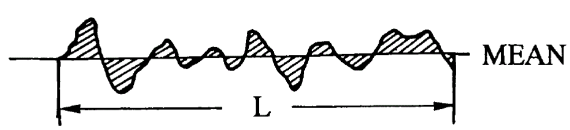

Figure 2.23 – Mean deviation [16]

While the Kawabata evaluation system is widely used in the garment textile industry, its use for characterizing composite preforms has been limited. Yu *et al.* [22] used the Kawabata evaluation system to characterize the mechanical behaviour of three carbon fibre fabrics: a plain weave, a 5 harness satin, and an angle-lock interweave fabric. Testing was conducted in three directions – along the warp yarns, along the weft yarns, and in the bias direction i.e. 45° with respect to the warp yarns. The tests brought interesting conclusions: hysteresis was seen in all tests, which means that the fabrics did not behave elastically. Fabric deformation was related to the loading rate and was time dependent. The fabrics' responses to imposed deformation was non-linear. Taking these factors into account, it can be said that mechanical parameters such as the bending stiffness taken as the slope between 0.5 $cm^{-1}$and 1.5 cm^{-1}, and the bending hysteresis taken at 1 cm^{-1} are defined somewhat arbitrarily. Other definitions may describe the behaviour of the fabric more accurately.

Lomov *et al.* [23] used the Kawabata evaluation system for testing the mechanical properties of three multiaxial multiply preforms. The fabrics tested are shown in Figure 2.24. Fabric B1 is a biaxial carbon fibre fabric with a [+45 / -45] ply orientation. Fabric B2 is also a biaxial carbon fibre fabric with a [0 / 90] ply orientation. Fabric Q is a quadriaxial carbon fabric with a [0 / -45 / 90 / +45] ply orientation.

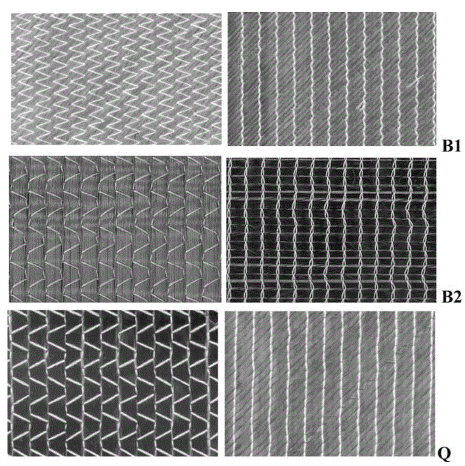

Figure 2.24 – Three fabrics studied by Lomov *et al.* [23]

The authors tested the multiply multiaxial fabrics in the machine direction (MD), the cross direction (CD) and the two bias directions +45° and -45° (BD +45, BD -45). These directions are shown in Figure 2.25.

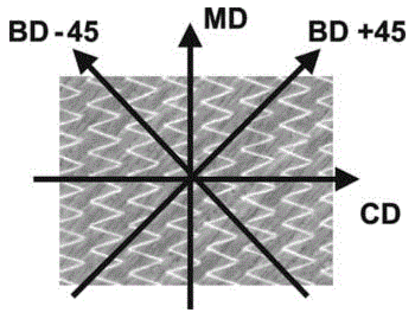

Figure 2.25 – Directions of fabric tests [23]

Several interesting conclusions were made with respect to the usefulness of the KES tests performed on fabric reinforcements for composite preforms:

- The bending test fully describes the bending behaviour of fabrics;
- The tension test requires a more reliable procedure, due to the fabrics slipping in the machine's grips;
- The shear test is useful for obtaining information on the initial shear behaviour of fabrics up to an angle of 8°, but should be used in conjunction with picture-frame tests to supply more information pertaining to the fabric's behaviour in high shear situations;
- The surface tests are useful for determining the coefficient of friction, but the surface roughness should only be used to rank the fabrics;
- The compression test is useful for determining the fabric's thickness and to characterize the fabric's behaviour under small compressional loads. This test should be supplemented

with compaction tests performed using universal testing frames for obtaining information for higher fabric compression loads.

2.5. Kawabata conversion functions

The Kawabata evaluation system for Fabrics was developed in order to characterize fabrics under low load conditions. When individual consumers characterize garment fabrics, they handle the fabrics and subjectively compare them. When consumers look at garment fabrics to evaluate them, appearance, comfort, and fitting to the human body's movements are key factors that affect the perceived quality of the fabric. Consumers do not evaluate the mechanical parameters obtained from the Kawabata evaluation system for Fabrics [24].

Kawabata studied the subjective evaluation of fabrics by examining the thought process used by expert evaluators to evaluate fabric performance. First, an expert evaluator touches the fabric with their hands, then they detect mechanical properties such as stiffness and surface properties again using their hands. After subjectively detecting the properties of the fabric, they come up with expressions that describe the properties that they detected. Finally, an overall rating is given to the fabric, based on each property that was evaluated. This process is shown in Figure 2.26.

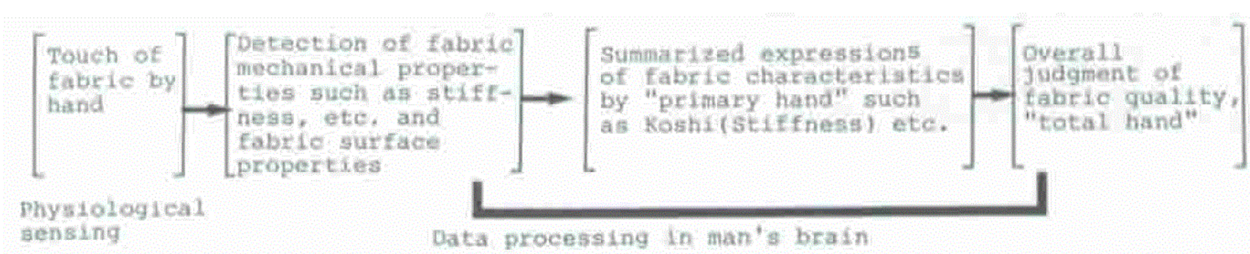

Figure 2.26 – Kawabata's subjective evaluation thought process [24]

Kawabata defined the expressions that describe the properties detected by the expert evaluators as "primary hands", and the overall evaluation of the fabric as the "total hand". Each "primary hand" depends on more than one mechanical parameter obtained from KES-F tests; each "primary hand" combines various parameters into one subjective description.

By discussing with expert evaluators in the garment textile industry, Kawabata defined three primary hands that describe subjective evaluations used by expert evaluators for men's winter suits, and four primary hands that describe the subjective evaluations used for men's summer suits. For winter suits, Koshi (stiffness) is defined as "a feeling related mainly to bending stiffness; a springy property promotes this feeling; a fabric having a compact weave density and made from springy and elastic yarn gives a high value". The Numeri (smoothness) is defined as "a mixed feeling coming from a combination of smooth, supple, and soft feelings; a fabric woven from a cashmere fibre gives a high value". Finally, the Fukurami (Fullness and Softness) is "a feeling coming from a combination of bulky, rich, and well formed impressions; a springy property in compression and thickness, accompanied by a warm feeling, is closely related with this property".

The primary hands used for men's summer suits are somewhat different. The Koshi (stiffness) is used and it has the same definition. The Shari (crispness) is "a feeling coming from a crisp and ridged fabric surface; this is found in highly woven fabrics made from a hard and strongly twisted yarn; this gives a cool feeling". The Hari (anti-drape stiffness) is "the opposite of limp conformability, whether the fabric is springy or not". The Fukurami (fullness and softness) is used again, and it is the same as for men's winter suits.

Kawabata determined that a score system of 0 to 10 was sufficient for evaluating the primary hands. A score of 0 meant that the fabric had no feeling associated with the primary hand being evaluated, while a score of 10 meant that the fabric had the strongest feeling. Kawabata also defined a scale from 0 to 5 to describe the usefulness of fabrics in manufacturing clothing. A score of 0 meant that the fabric was not useful, a score of 1 meant poor, 2 was fair, 3 was average, 4 was good, and 5 was excellent. The total hand is a function of the primary hands.

The Kawabata evaluation system for Fabrics was then used to objectively evaluate fabrics. Along with the subjective evaluation of the fabrics by expert evaluators, mechanical parameters were extracted from the Kawabata evaluation system for Fabrics. These parameters were then converted twice: once from the mechanical parameters to the primary hand scores, and then from the primary hand scores to the total hand value. The process is shown in Figure 2.27

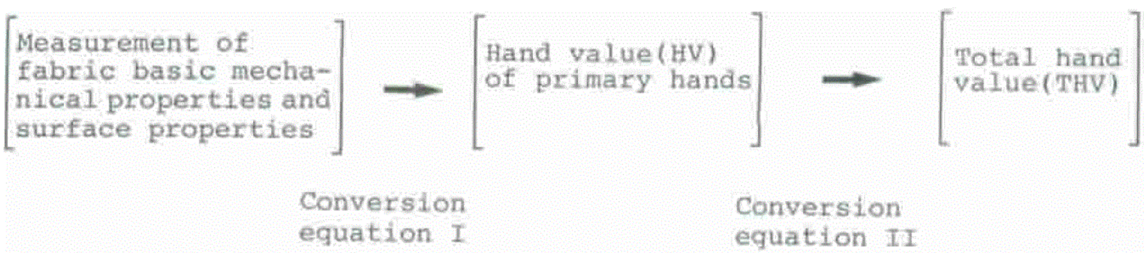

Figure 2.27 – Kawabata's objective evaluation process [24]

As each type of test resulted in multiple parameters being evaluated, all mechanical parameters were grouped within one of six blocs, based on the test from which they were extracted. The linearity of the force/extension curve (*LT*), tensile energy (*WT*), tensile resilience (*RT*), and extensibility (*EM*) form the tensile bloc. The bending rigidity (*B*) and hysteresis of bending moment (*2HB*) form the bending bloc. The shear stiffness (*G*), hysteresis of shear force at 0.5° (*2HG*), and hysteresis of shear force at 5° (*2HG5*) form the shearing block. The linearity of compression force/thickness curve (*LC*), compressive energy (*WC*), and compressive resilience (*RC*) form the compression bloc. The mean coefficient of friction (*MIU*), mean deviation of coefficient of friction (*MMD*), and mean deviation of thickness (*SMD*) form the surface bloc. Finally, the thickness (*T*) and weight per unit area (*W*) form the fabric construction bloc.

The conversion functions were built by conducting a stepwise block regression model between primary hand value scores given to fabrics by expert evaluators, and the mechanical parameters obtained from the Kawabata evaluation system for Fabrics. The result is a conversion function of the form:

$$Y_k = C_0 + \sum_{i=1}^{16} C_i x_i \tag{2.9}$$

where Y_k is the k^{th} primary hand value, C_0 and C_i are constants obtained from the regressions, and x_i is the deviation from the population mean normalized by the standard deviation, as shown below:

$$x_i = \frac{X_i - M_i}{\sigma_i} \tag{2.10}$$

In this equation, X_i is the i^{th} mechanical parameter for the fabric being evaluated, M_i is the average of the same i^{th} mechanical parameter evaluated for all fabrics, and σ_i is the standard deviation of the i^{th} mechanical parameter for all fabrics. There are 17 different constants for each primary hand. It is noted that both summer and winter suit conversion functions have their own sets of constants, even for the primary hands of Koshi (stiffness) and Fukurami (fullness and softness), which are used for describing both summer and winter fabrics.

The total hand value conversion function has the form

$$THV = C_0 + \sum_{k=1}^{n} \left(C_{k1} \frac{Y_k - M_{k1}}{\sigma_{k1}} + C_{k2} \frac{Y_k^2 - M_{k2}}{\sigma_{k2}} \right) \tag{2.11}$$

where C_0, C_{k1} and C_{k2} are fitted parameters, M_{k1} and σ_{k1} are the average and standard deviation of the primary hand Y_k for *n* fabrics, and M_{k2} and σ_{k2} are the average and standard deviation of primary hand squared Y_k^2 for n fabrics. These conversion equations were shown to have good predictive ability of the total hand values of fabrics.

2.6. In-plane shear testing methods

While the Kawabata evaluation system for Fabrics measures numerous mechanical parameters related to fabric deformation, draping of technical textile onto moulds is closely associated with their ability to shear in-plane, because shearing is the main deformation mode that is induced while the textile is being draped onto double-curvature surfaces [25]. The in-plane shearing of a fabric draped onto a hemisphere is shown in Figure 2.28. The Kawabata shear test (KES-FB1) characterises in-plane shear stiffness (*G*), hysteresis of shear force at 0.5° (*2HG*) and hysteresis of shear force at 5° (*2HG5*). The maximum shear angle reached during the test is 8°. Forming technical textiles onto complex moulds often induces much larger shear deformations, reducing the relevance of the Kawabata shear test.

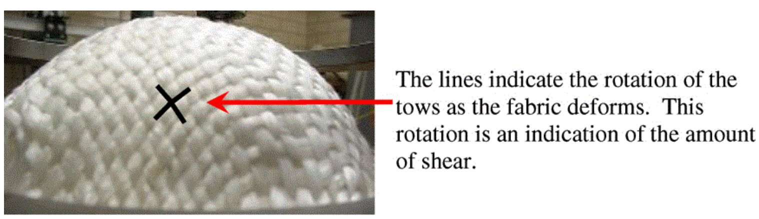

Figure 2.28 – Fabric shearing while being draped onto a hemisphere [26]

In-plane shearing of woven textile materials occurs in multiple stages. At the onset of shear, the warp and weft yarns rotate with respect to each other at their crossovers. The force required to shear the fabric during this stage is mainly caused by frictional torque at each warp and weft yarn crossover [18, 19]. The torque required to rotate the yarns at each crossover is given by

$$T_r = \mu_{cr} \times F_c \times R_{eff} \tag{2.12}$$

where μ_{cr} is the coefficient of friction at the crossover (no units), F_c is the normal force at the yarn crossover (N), and R_{eff} is the effective radius of rotation (m) [27]. A yarn crossover is shown in Figure 2.29 for a plain-weave fabric.

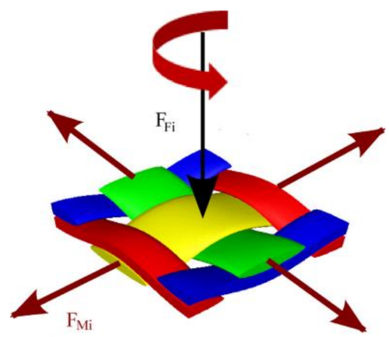

Figure 2.29 – Yarn crossover free body diagram [29]

As the textile is sheared, the warp and weft yarns start to compress each other laterally [28]. This compression increases the force required to shear the fabric. At higher shear angles, the lateral compression effect dominates the shear force. Eventually, wrinkles may appear while the fabric is sheared. The angle at which this occurs is known as the locking angle [19, 21]. The locking angle of technical textiles can inform the designer on the ability of that technical textile to conform to complex surfaces: as fabrics are formed onto moulds with complex geometries, shear is induced. A fabric that can be sheared further before reaching its locking angle can conform to a wider range of complex geometries without wrinkles appearing in the fabric.

It is possible to estimate the locking angle of a fabric based on the geometry of its yarns. By examining closely the weave pattern of a fabric, a RUC can be defined. One such RUC is shown in Figure 2.30 for a plain weave fabric. The smallest possible value of the locking angle is determined for a configuration where there is no gap between the warp (white) and the weft (black) yarns [30]. The geometric locking angle θ_l is a function of the yarn size and the length between two yarn crossovers, and can be expressed as follows:

$$\theta_l = \sin^{-1}\frac{t}{L} \tag{2.13}$$

where t is the yarn width (m) and L (m) is the length between two yarn crossovers.

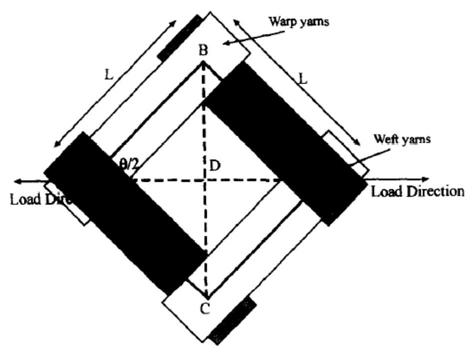

Figure 2.30 – Fabric repeating unit cell [30]

This geometric prediction of the locking angle is simplistic and generally not accurate; actual values of the locking angle deviate from this geometric prediction due to several factors including yarn friction, yarn slippage, tow width, and yarn lateral compaction [30].

2.6.1. In-plane picture-frame shear test

Locking angles are thus traditionally determined experimentally using a picture-frame test or a bias extension test. These tests isolate the in-plane shear behaviour of fabrics by inducing a state of pure in-plane shear, in the whole sample in the former case and in part of the sample in the latter case. The picture-frame apparatus consists of an articulated rig in the shape of a square frame as shown in Figure 2.31.

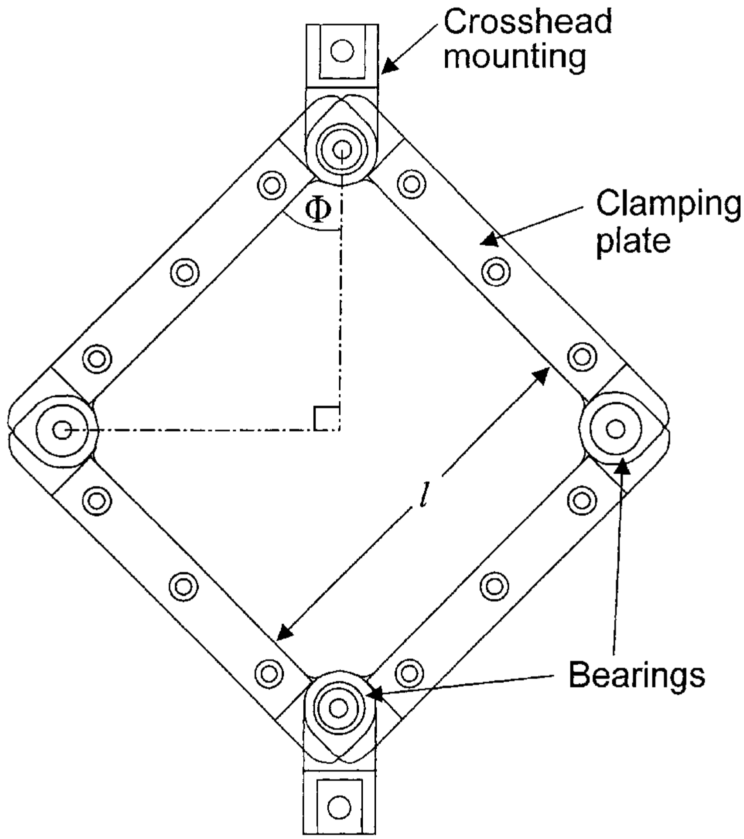

Figure 2.31 – Picture-frame shear testing rig [31]

The frame is hinged at all corners, allowing for the angle between two adjacent members on the frame to change as the two vertically opposed corners of the frame are pulled away from each other. Fabric are cut in cruciform samples. The flanges of the cross are clamped to the edges of the frame. As the frame is extended, the angle between the members of the frame changes, hence the angle between the warp and weft yarns also changes as shown in Figure 2.32. A tensile tester is used for measuring the force required to pull the frame, as well as the extension of the frame.

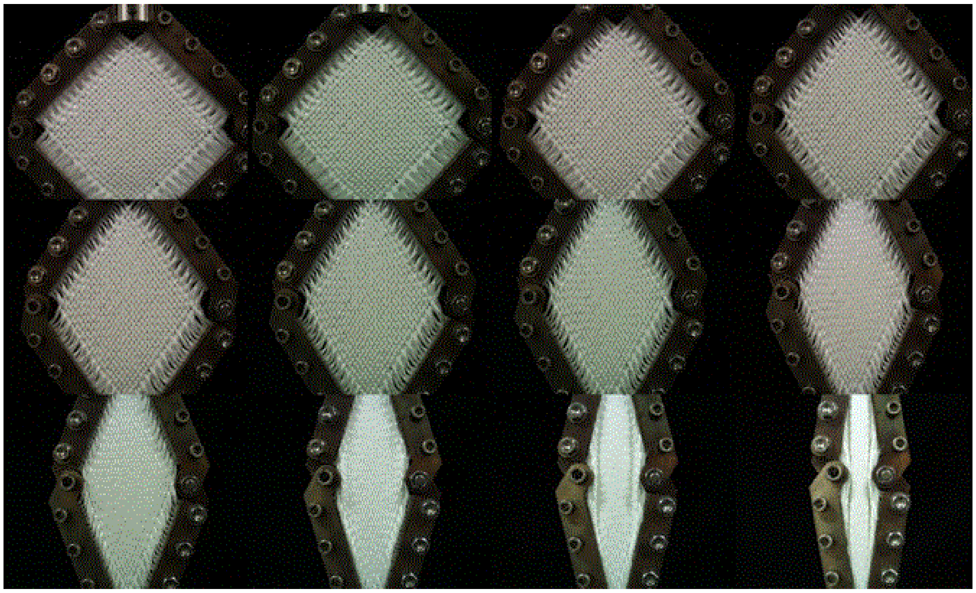

Figure 2.32 – Picture-frame shear test [26]

The shear angle of fabrics is given by

$$\gamma = 90° - \theta \tag{2.14}$$

where θ is the angle between the warp and weft yarns (°). In a picture-frame test, the warp and weft yarns are assumed parallel to the frame members throughout the entire test, therefore θ also represents the angle between two adjacent frame members. The angle between adjacent members on the picture-frame rig is given by

$$\theta = 2 \cdot \cos^{-1}\left(\frac{\sqrt{2}L_{frame} + \Delta x}{2L_{frame}}\right) \tag{2.15}$$

where L_{frame} is the distance between two adjacent hinges (m) and Δx is the extension of the rig (m) as measured by the tensile tester [26]. There are no current standards for picture-frame tests, which means that different picture-frame test rigs may accommodate fabric samples of different sizes. A larger sample means more yarn crossovers, requiring more force for shearing the fabric [32]. Furthermore, different researchers follow different procedures for sample preparation. The removal of yarns from the sample flanges that are parallel to the nearby frame member, and removal of yarns from the sample around its central square area illustrate two slightly different procedures followed in one study aiming at comparing the in-plane shear properties of the same fabrics in different laboratories, as shown in Figure 2.33.

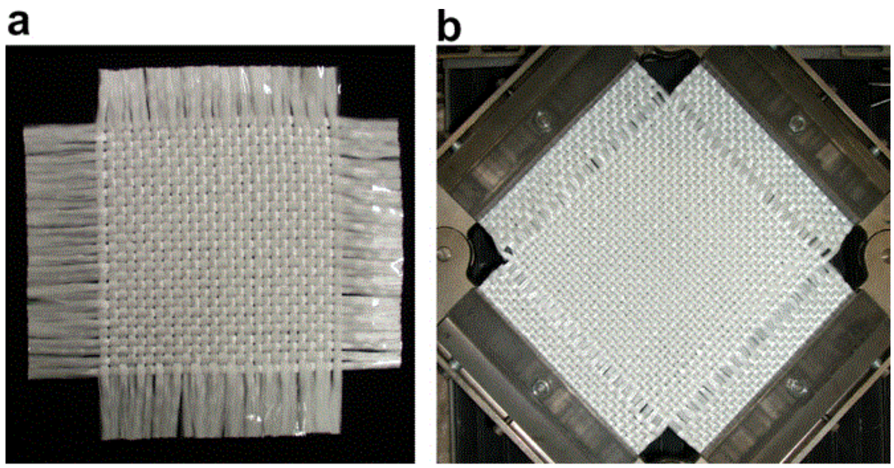

Figure 2.33 – Two different methods for preparing picture-frame test samples (a) Hong Kong University of Science and Technology, (b) University of Twente [26]

In this study, one participant sheared the fabric multiple times prior to testing, which resulted in less variability in picture-frame shear test results [26].

The shear-force required for deforming the fabric can be calculated as:

$$F_{shear} = \frac{F}{2\cos\theta} \tag{2.16}$$

where F_{shear} is the shear force (N) and F is the tensile force measured during the experiment (N). Since there is no standard test rig size, normalizing the shear force with respect to dimension of the frame and sample was proposed:

$$F_{norm} = \frac{F_{shear} L_{frame}}{{L_{fabric}}^2} \tag{2.17}$$

where L_{fabric}^2 is the area of sheared fabric during the shear test (m^2). This surface area is taken to be the central square area of the sample, shown in Figure 2.33. The units of the normalized shear force are N/m. Normalizing results obtained using different rig and sample sizes allows for results to be compared [26].

2.6.2. Bias-extension in-plane shear test

A bias-extension test can also be used for characterizing the in-plane shear properties of fabrics. In the bias-extension test, samples are cut in rectangles 45° from the warp and weft yarns. The samples are clamped and stretched using a universal testing frame. As the fabric is stretched, in-plane shear is induced in the central part of the sample. Achieving pure shear in that zone of the sample requires that the height to width ratio of the sample be greater than 2 [33]. If this condition is met three zones undergoing distinct behaviours appear as the sample is stretched, as shown in Figure 2.34 [34]. Pure shear only occurs in the middle zone of the sample (zone C).

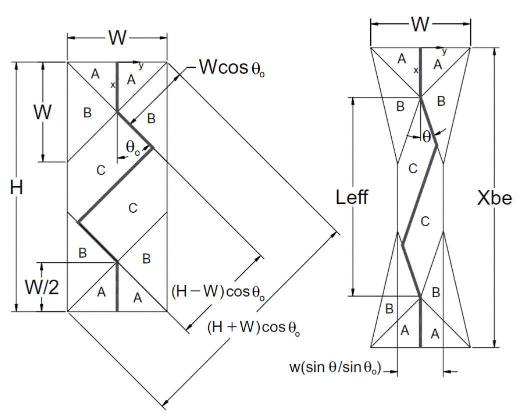

Figure 2.34 – Different regions of pure and combined shear [34]

In the bias extension test, the shear angle in zone C is calculated as:

$$\gamma = 90° - 2\cos^{-1}\left(\frac{(H-W)+\Delta x}{\sqrt{2}(H-W)}\right) \tag{2.18}$$

where H is the sample height (m) and W is the sample width (m), shown in Figure 2.34. The shear force in the bias-extension test is normalized as follows:

$$F_{norm}(\gamma) = \frac{1}{(2H-3W)\cos\gamma}\left(\left(\frac{H}{W}-1\right)\cdot F\cdot\left(\cos\frac{\gamma}{2}-\sin\frac{\gamma}{2}\right) - W\cdot F_{sh}\left(\frac{\gamma}{2}\right)\cdot\cos\frac{\gamma}{2}\right) \tag{2.19}$$

where F_{norm} is the normalized force having the same units as the normalized shear force for the picture-frame test (N/m). It is noted that the normalized shear force must be calculated using an iterative process as the shear force at γ is a function of the shear angle at angle $\gamma/2$ [26].

Both picture-frame shear tests and bias-extension tests produce curves of the shear force as a function of the shear angle. In some studies [35], a significant difference was observed between the normalized shear forces from bias-extension tests and picture-frame tests: the normalized shear force was generally much higher in picture-frame tests than in bias-extension tests. This large difference was eliminated by using a physical mechanism to remove the initial tension in the sample at the beginning of the picture-frame test [19, 26]. This is shown in Figure 2.35.

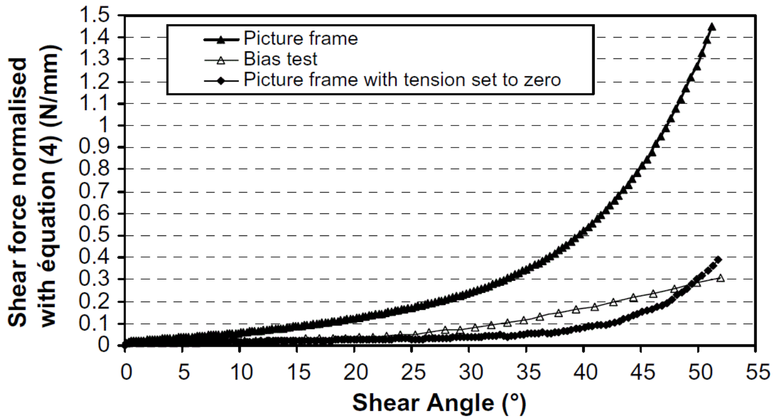

Figure 2.35 – Normalized shear force versus shear angle for bias-extension and picture frame tests [28]

It is important to note that some fabrics do not wrinkle upon shear [10], and therefore determining locking angles visually by finding the angle at which wrinkles occur is not always feasible. It is unclear why wrinkles do not appear on these fabrics. The locking angle may also be determined graphically by finding the inflection point on the shear force to shear angle curve, as shown in Figure 2.36 [33].

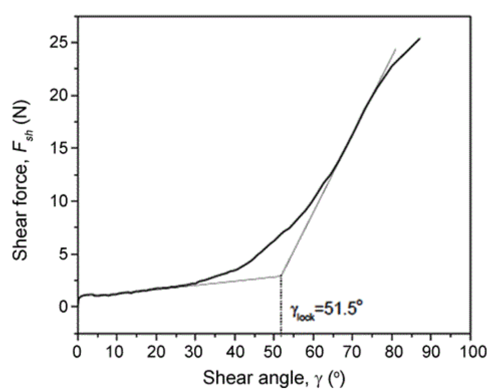

Figure 2.36 – Graphical definition of the locking angle [33]

2.7. Wrinkle recovery angle

As stated previously, technical reinforcements used in the manufacturing of composite parts show spring-back – once they are draped onto moulds, the fabric springs back [10]. A similar behaviour was studied by the textile industry: wrinkle recovery. Fabrics used for clothing should have a good resistance to creasing for the garment to be durable. Furthermore, consumers do not want fabrics that crease easily. Creasing recovery, or wrinkle recovery, is defined by the ability of a fabric to recover from being folded [36].

Standards ISO 2313 – Determination of the Recovery from Creasing of a Horizontally Folded Specimen of Fabric by Measuring the Angle of Recovery, and AATCC 66 – Wrinkle Recovery of Woven Fabrics: Recovery Angle were both developed in order to quantify the wrinkle recovery angle of fabrics. A common tool used for characterizing wrinkle recovery in woven fabrics is the Shirley Tester. In this test, a piece of fabric is folded. The fabric is then placed on a rig which allows the tester to measure the angle at which the fabric springs back. Figure 2.37 shows a typical wrinkle recovery testing rig, and Figure 2.38 shows the recovery angle of a fabric.

Figure 2.37 – Shirley crease recovery tester [37]

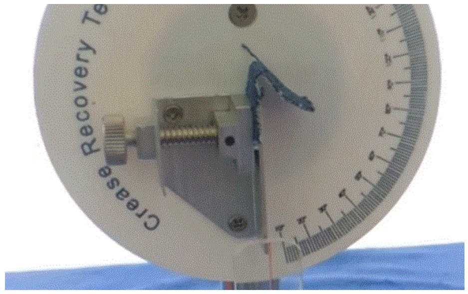

Figure 2.38 – Wrinkle recovery angle [37]

The deformation mode during creasing is bending. A rheological deformation model was proposed for describing the crease recovery behaviour, where the fabric is modelled as a linear elastic component parallel with a frictional constraint component [38].

Upon constructing the rheological model, the linear elastic component is linearly proportional to the bending rigidity, as shown below:

$$M = B\ k = \frac{B}{R} \tag{2.20}$$

The relation between the frictional constraint couple and curvature was assumed to be proportional to the square root of the bending curvature:

$$M_f = \frac{\mu_f}{\sqrt{R}} \tag{2.21}$$

where μ_f is the frictional constraint coefficient.

Using the energy method, it was shown that the crease recovery force can be expressed as:

$$F = \frac{\pi B}{4R^2} - \frac{1}{2}\pi\mu_f R_0 R_f^{-2.5} - \frac{1}{3}\pi\mu_f R_f^{-1.5} \tag{2.22}$$

where R_0 and R_f are the initial and final curvature radii of the fabric. Experiments showed that this model can predict wrinkle recovery properties of fabrics under low curvature bending conditions [38].

Wang et al. [39] designed a system that tests the dynamic wrinkle recovery angle. A weakness of the wrinkle recovery angle as defined in the AATCC 66 standard is that it measures an angle after a certain amount of time has passed, and measurements are taken by humans. The new system automates the process by using a video sequence acquisition system and a pneumatic presser. The machine uses compressed air for applying a constant force of 5 N to fold the fabric. The force is applied for 5 minutes. Once the force is removed, the recovery angle is measured optically, at different points in time. The system is shown in Figure 2.39.

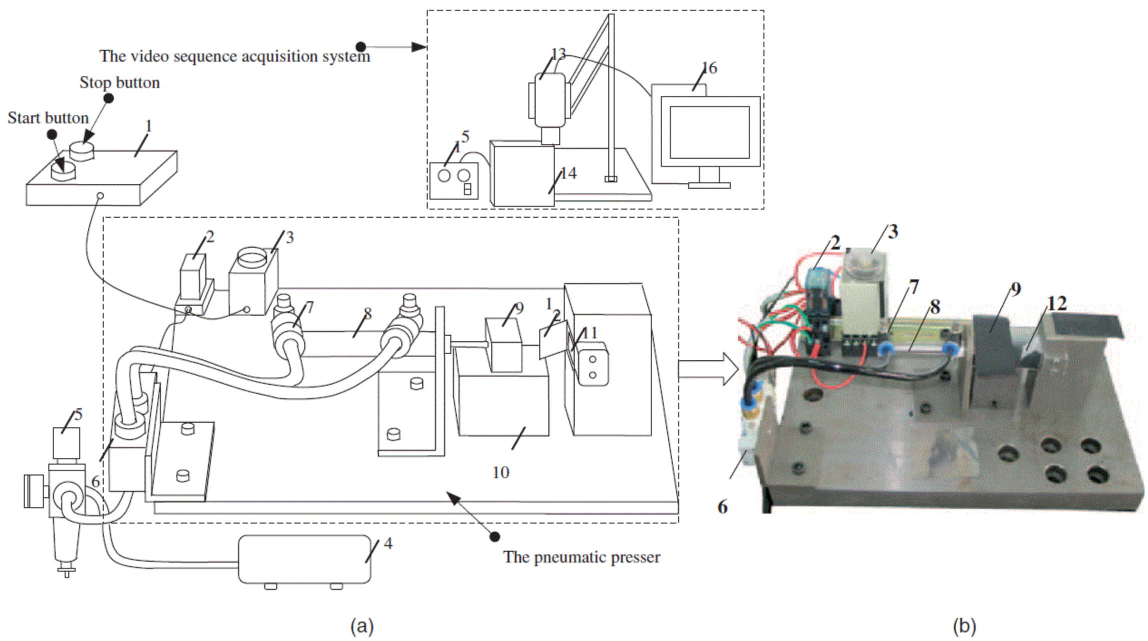

Figure 2.39 – Automatic wrinkle recovery tester [39]

In a subsequent study, Kawabata bending tests were performed on fabrics to obtain values of bending stiffness and bending hysteresis [36]. The Kawabata bending parameters were then correlated with the initial angular velocity and the final angle from the dynamic wrinkle recovery angle tests. The authors found that the bending stiffness and bending hysteresis correlated well with the initial angular velocity. They also found no clear link between the final angle, bending stiffness and bending hysteresis.

The AATCC and ISO standards specify that the wrinkle recovery angle should be measured along both warp and weft directions. This does not represent actual creasing behaviour of fabrics, as creases often are not aligned with the warp or the weft yarns of a fabric. Fridrichova tested creasing behaviour off the warp and weft directions, and proposed a crease recovery coefficient which takes into account the crease recovery from multiple directions [40]. Polar plots were created for showing the crease recovery angle as a function of the angle of the crease, as shown in Figure 2.40. The author found that different weave types had an influence on the wrinkle recovery angle.

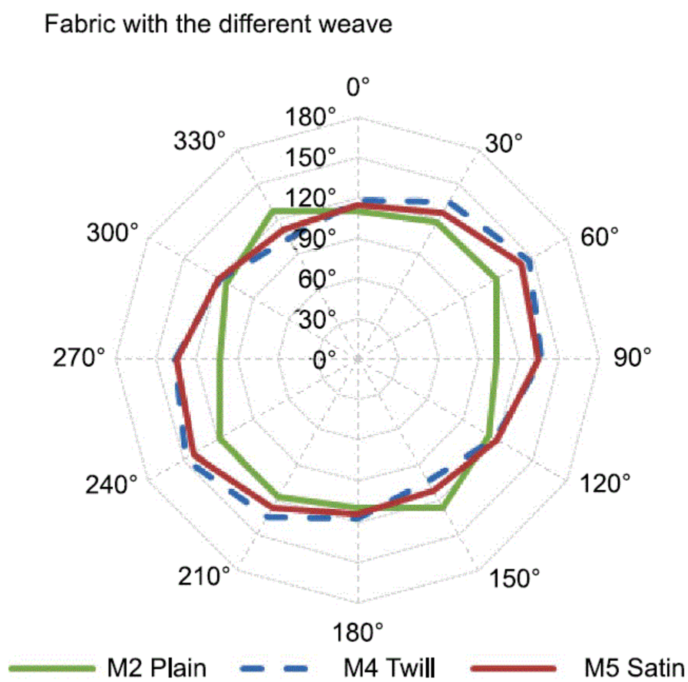

Figure 2.40 – Wrinkle return angle [40]

2.8. Friction tests

Friction between plies of fabric, and friction between the fabrics and the mould both play an important role while draping preforms onto moulds. Manufacturing technicians want to use fabrics stacks that behave as one fabric, i.e. individual plies do not slide or rotate with respect to each other while draping [10]. Various testing methods can be used for determining the frictional properties of a fabric. Ajayi [41] used a universal testing frame for pulling on a sled that slides across a fabric surface. The sled was pulled at a constant velocity. An inextensible pulling tow wound around a frictionless pulley and was secured to the crosshead of the universal testing frame to record the friction force. This method is based on standard ASTM D1894 - Standard Test Method for Static and Kinetic Coefficients of Friction of Plastic Film and Sheeting; the experimental set up is shown in Figure 2.41.

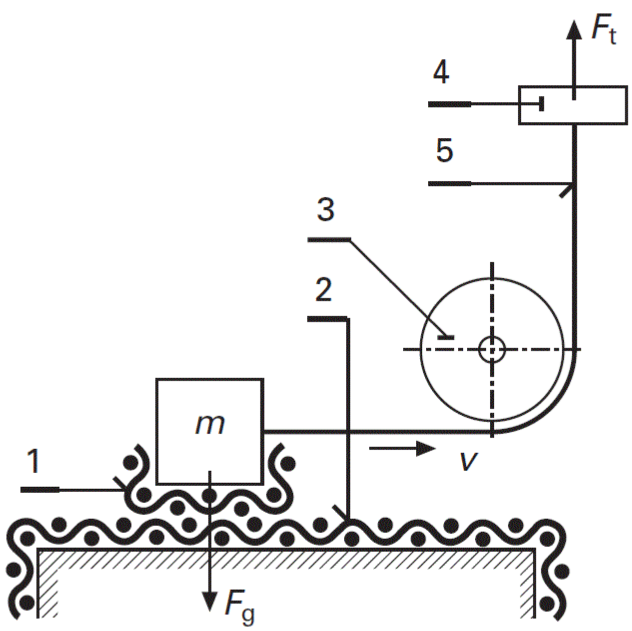

Figure 2.41 – Sled friction tests based on ASTM D1894 [42]

The coefficient of friction is defined as the ratio of the friction force F to the normal force N:

$$\mu = \frac{F}{N} \tag{2.23}$$

Stick-slip may be observed as the fabric slides across different surfaces. This phenomenon is due to periodic features on the surface of the textile – fabrics do not have a homogenous surface [42].

Ajayi [41] found that testing parameters affect results: increasing normal pressure decreased both the coefficient of friction and the extent of the stick-slip, possibly due to structural flattening of the fabric. Increasing the sliding velocity decreased stick-slip. Fabric structure also had an influence on stick-slip.

Another method for characterizing the frictional behaviour of fabrics consists in using an inclined plane, as shown in Figure 2.42. In this test, a fabric is secured to a block that rests on a horizontal plane. The plane is then slowly lifted until the block starts moving. This test allows the static coefficient of friction to be determined from the angle between the plane and the horizontal.

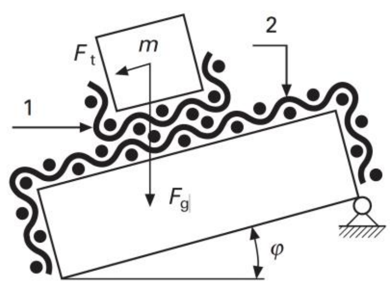

Figure 2.42 – Inclined plane friction test [42]

The inclined plane method forms the basis of the Shirley friction tester shown in Figure 2.43. The drawback of this method is that it only allows the tester to determine a static coefficient of friction.

Figure 2.43 – Shirley friction tester [43]

Chapter 3. Materials and methods

Hutchinson uses a number of certified reinforcement fabrics for making parts. Hutchinson routinely introduces additional fabrics, either certified or to be certified following a process independent from the work described in this thesis. In this work, four fabrics were selected for investigation, quantification and validation, including probing the repeatability of material behaviour. Two of these fabrics are currently used for producing composite parts for industrial clients (7500 style plain weave and 7781 style 8 harness satin), and one of them is actively considered for production (94932 style 4HS satin). The fourth fabric is the same 94932 style 4HS satin with binder applied to its surface [10].

3.1. Materials

3.1.1. Fabric 1 – 7500 style glass fibre plain weave

Fabric 1 is 7500 style plain weave glass fibre fabric made from EC9 134 x2 warp and weft yarns, Figure 3.1 [44]. Surface density specified by the manufacturer is 325 g/m^2. Specified warp and weft yarn thread counts are 6.3 yarns/*cm* and 5.5 yarns/*cm* respectively. Fabric thickness specified by the manufacturer is 0.28 *mm*. Testing of mechanical properties for Fabric 1 was conducted for both single layers and four-layer stacks.

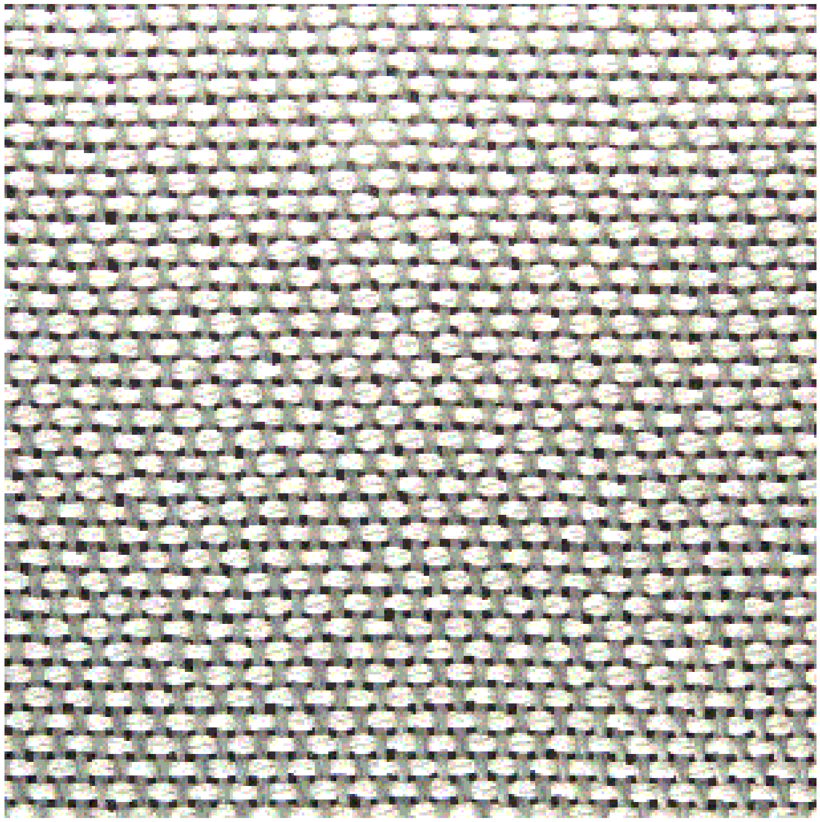

Figure 3.1 – 7500 style plain weave glass fibre fabric – Fabric 1

3.1.2. Fabric 2 – 7781 style glass fibre 8 harness satin

Fabric 2 is 7781 style 8HS satin weave glass fibre fabric made from EC6 66 warp and weft yarns [45]. The inside roll surface appears in Figure 3.2. Specified surface density is 303 g/m^2. Specified warp and weft yarn thread counts are 22.4 yarns/*cm* and 21.3 yarns/*cm* respectively. Specified fabric thickness is 0.23 *mm*. Testing of mechanical properties for Fabric 2 was conducted for both single layers and four-layer stacks.

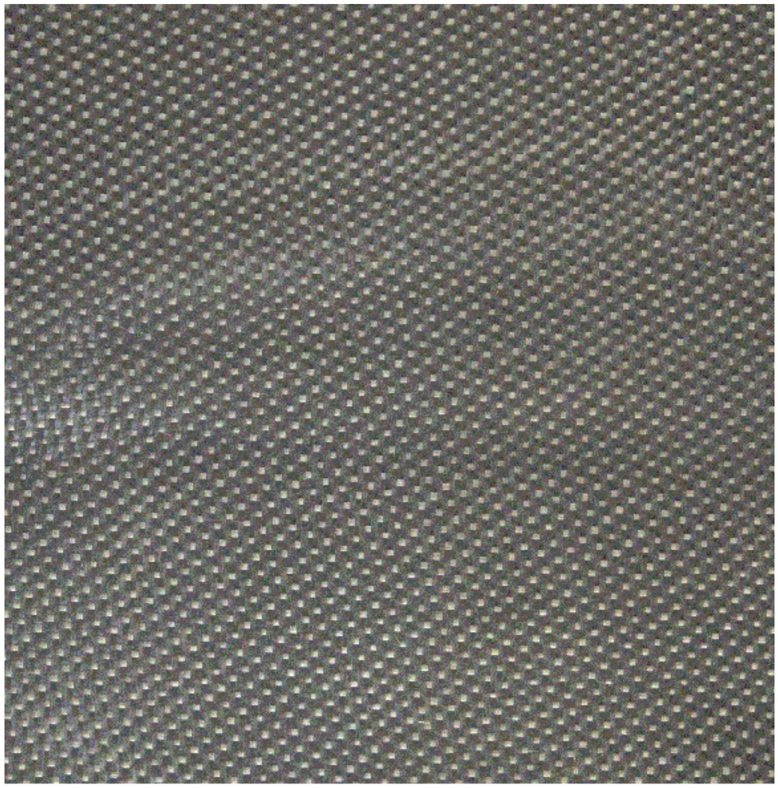

Figure 3.2 – 7781 style 8 harness satin glass fibre fabric – Fabric 2

3.1.3. Fabric 3 – 94932 style carbon fibre 4 harness satin

Fabric 3 is 94932 style 4HS satin weave carbon fibre fabric made from 3K 33MSI warp and weft yarns [46]. The inside roll surface appears in Figure 3.3. Surface density specified by the manufacturer is 196 g/m^2. Specified warp and weft yarn thread counts are 4.9 yarns/*cm* (12.5 yarns per inch). The manufacturer does not specify thickness for this fabric. Testing of mechanical properties for Fabric 3 was conducted for both single layers and three-layer stacks.

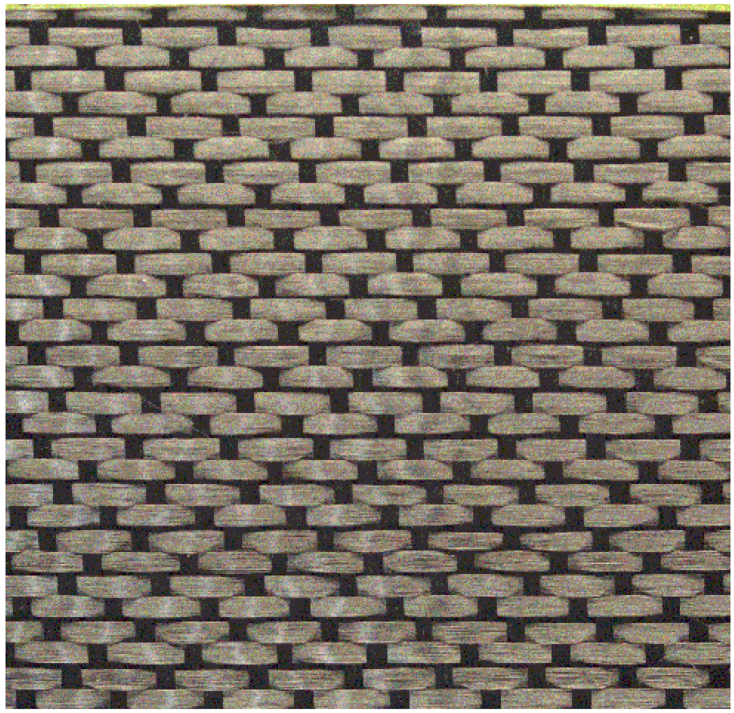

Figure 3.3 – 94932 style 4-harness carbon fibre fabric – Fabric 3

3.1.4. Fabric 4 – 94932 style carbon fibre 4 harness satin with binder

Fabric 4 is the same as Fabric 3 with powered binder applied to it. Applying binder to fabrics is known to alter their draping and preforming behaviour [10]. The binder used is PKHP-200 micronized powder, which is a sizing resin typically used for increasing adhesive strength between fibres and epoxy resins in composites [47]. Binder was deposited on Fabric 4 by gravity, before patterns were cut and while they were on the cutting table. The binder was deposited evenly using a vibrating apparatus developed by Hutchinson. The apparatus controls the quantity of binder applied to the fabric. The binder was then activated using a heating lamp. Once the binder was activated, the fabric was cut. Testing of mechanical properties for Fabric 4 was conducted for both single layers and three-layer stacks.

3.2. Methods

Technicians at Hutchinson face challenges upon handling and draping fabrics. These challenges can be linked with seven characteristics of the fabrics: 1) bending stiffness, 2) bending spring back, 3) in-plane shear stiffness, 4) in-plane shear spring back, 5) fabric-to-mould and fabric-to-fabric friction, and 6) resistance to holding pins. The following sections discuss tests typically conducted for characterizing fabrics in relation with each of these characteristics and challenges. Testing was generally conducted along three directions in the fabrics: along the warp direction, along the weft direction and along the bias direction, +/- 45° with respect to the warp yarns. Five repetitions were conducted per direction, for every single layer and multilayered stack.

3.2.1. Cantilever bending test

Two ASTM standards are available for characterizing the bending rigidity of fabrics: ASTM-D1388 Standard Test Method for Stiffness of Fabrics [48] and ASTM-F3260 Standard Test Method for Determining the Flexural Stiffness of Medical Textiles [49]. Both methods make use of a cantilevered bending rig where a fabric is bent under its own weight; however, the definition of bending rigidity is not the same in both standards.

In standard ASTM-D1388, the bending rigidity is calculated using

$$B = 1.421 \times 10^{-5} \times M \times \left(\frac{l}{2}\right)^3 \tag{3.1}$$

where M is the mass per unit area (g/m^2) and l is the length of overhanging fabric (mm). The overhanging length of fabric is measured in mm, units of constant 1.421 ×10^{-5} are m/s^2 and the bending stiffness units are $\mu J/m$, which makes little sense. Units for bending rigidity should be Nm^2 as derived in Section 2.3. Furthermore, the use of constant 1.421 ×10^{-5} is not explained, discussed or justified in the standard [50].

In standard ASTM-F3260, the bending rigidity is calculated using

$$B_{Peirce} = 9.81 \times 10^{-6} \times M \times \left(\frac{l}{2}\right)^3 \tag{3.2}$$

where constant 9.81 is the gravitational constant (m/s^2), and 10^{-6} is a unit conversion factor ($\frac{kg}{g}\frac{m^3}{mm^3}\frac{\mu m}{m}$).

It is noted that Equation (3.2) is almost identical to Equation (2.8), derived in Chapter 2. In this case the bending rigidity is normalized by the unit width of the sample, because the surface mass is used for calculating the bending rigidity rather than the linear mass. Henceforth, measurements of bending rigidity B normalized by unit width are labelled as bending stiffness B_{Peirce}.

The testing procedure defined in standard ASTM-F3260 was followed for quantifying the bending stiffness of the selected fabrics. The cantilever bending rig used for characterizing the selected fabrics is shown in Figure 3.4.

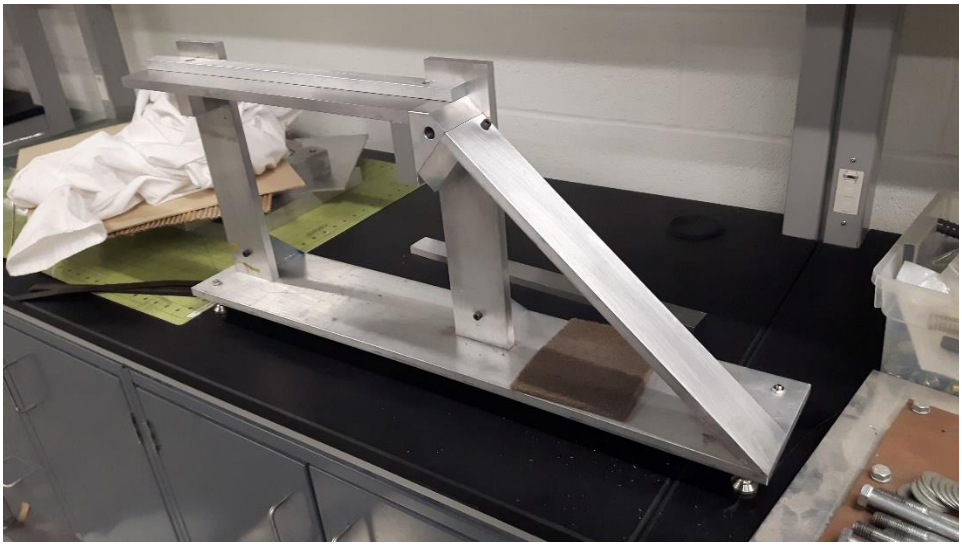

Figure 3.4 – Cantilever bending rig

The procedure is summarized as follows:

1. Cut samples to 25.40 *mm* × 457.20 *mm* (1 *in* × 18 *in*). ASTM-F3260 specifies cutting samples to 25.40 *mm* × 200.00 *mm* (1 *in* x 8 *in*). The range of stiffness of the fabrics tested was not known, therefore longer samples were used for alleviating issues if fabrics proved more stiff than typical fabrics targeted by the standard.
2. Weigh each sample using a balance with suitable reproducibility.
3. Place the sample on the rig, and place the slide on the sample.
4. Slide the fabric at approximately 120 *mm*/*min* until the edge of the sample touches the bend angle indicator.
5. Read and record overhang length to the nearest *mm*. If the specimen has a tendency to twist, take the reference point at the center of the leading edge.

6. Repeat steps 1 to 5 to test the face and back of both ends of each sample for a minimum of four readings per sample. Test the face and back at one end of sample before proceeding to test the face and back at the other end of sample.

Standard ASTM-F3260 specifies to report overhang length l (mm) for each of the 4 readings for each sample, bending stiffness B_{Peirce} ($\mu Nm^2/m$) for each of the four readings for each sample, average and standard deviation of overhanging fabric length l and bending stiffness B for each surface orientation (face and back) and each direction (warp and weft).

3.2.2. Bending spring back

A common difficulty occurring while draping a fabric onto a mould is the tendency of fabrics to spring back once draped. When a technician covers a draped mould with a vacuum bag, she/he has no way of determining whether a fabric remains properly conformed to the curved surfaces of the mould. Often it does not: the fabric shifts in the mould without the technician noticing, and the vacuum bag is positioned. This causes resin-rich corners in the cured part. Spring back can happen over both concave and convex mould surfaces.

There are currently no tests that characterize bending spring back in fabrics. Two new tests were developed as part of this work, for characterizing the tendency of a fabric to spring back over a mould. The first test consists in bending a fabric over a convex 90° corner. The second test consists in bending a fabric into a concave 90° corner. Each testing configuration was carried out over 5 different radii of 1.59 *mm* to 12.70 *mm* (1/16th *in*, 1/8th *in*, 1/4th *in*, 3/8th *in*, 1/2 *in*) as well as around a sharp edge. The rounded corners in Figure 3.5 and Figure 3.6 are referred to as convex and concave simulated mould radii (SMR) respectively.

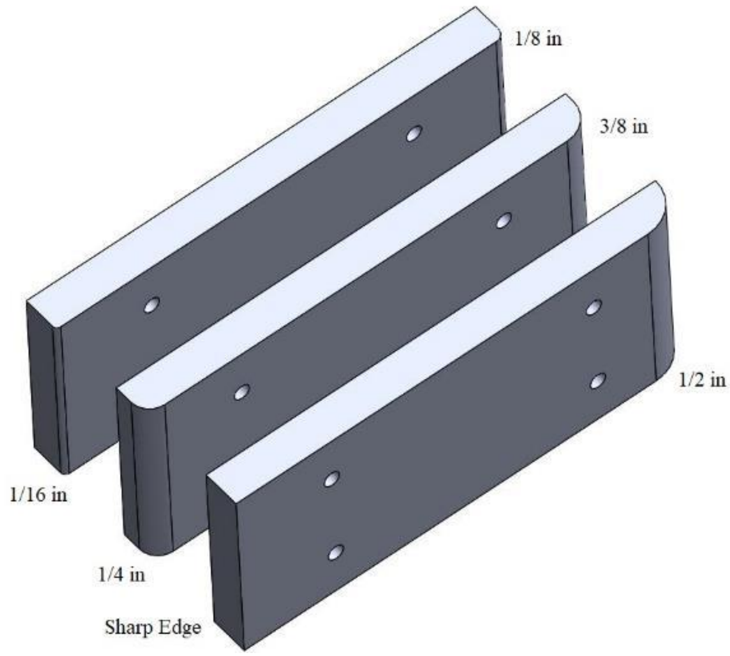

Figure 3.5 – Convex SMRs

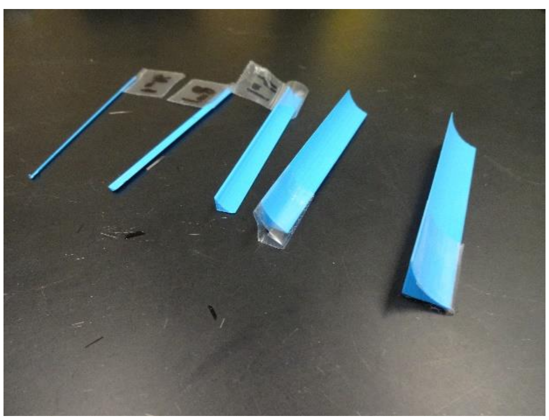

a)

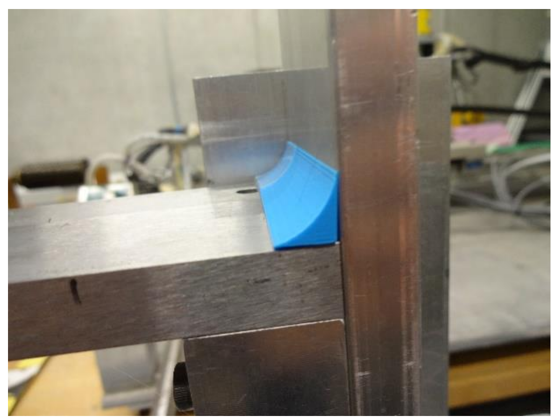

b)

Figure 3.6 – a) Concave SMRs; b) 12.70 *mm* (1/2 *in*) concave SMR positioned in corner of rig

Concave and convex SMRs are mounted on a reconfigured cantilever bending rig for characterizing spring back of the selected fabrics. The convex configuration appears in Figure 3.7 and the concave configuration appears in Figure 3.8.

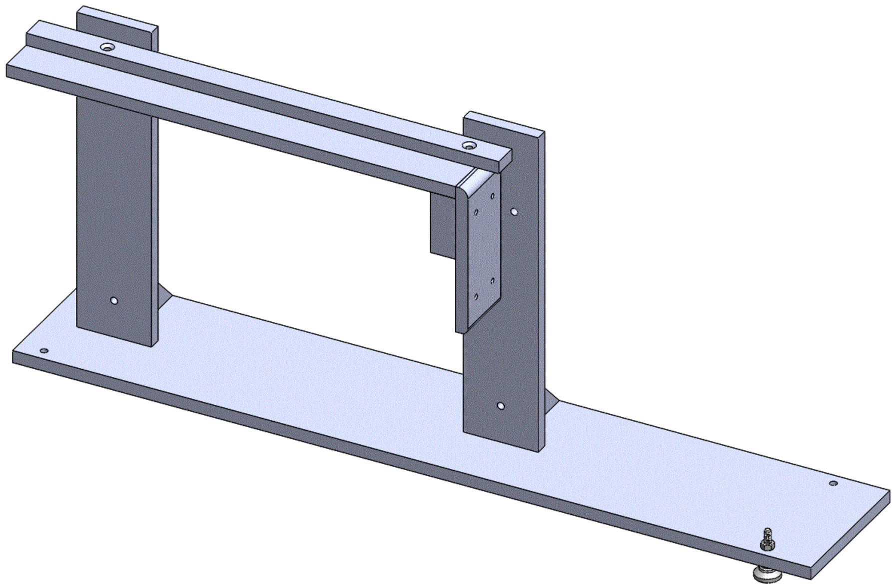

Figure 3.7 – Convex configuration of bending spring back rig

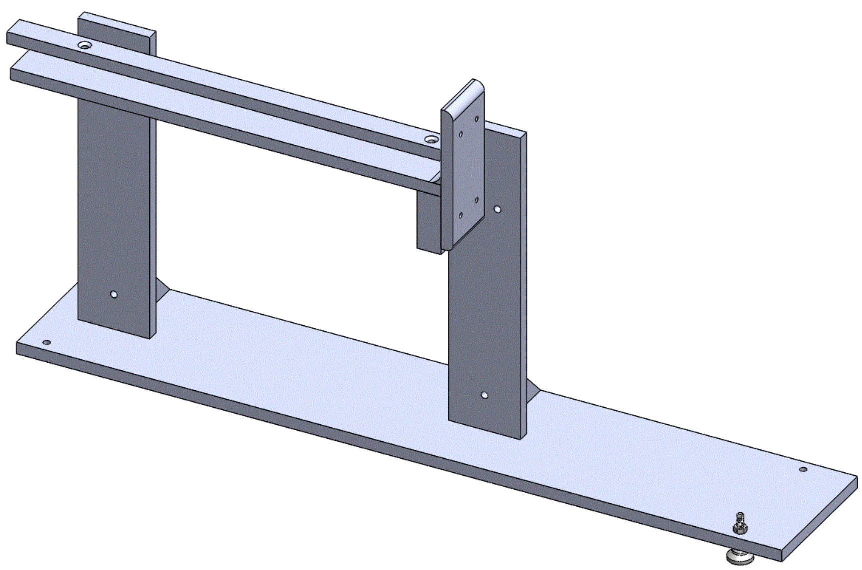

.

Figure 3.8 – Concave configuration of bending spring back rig

3.2.2.1. Convex spring back

The procedure used for characterizing bending spring back over a convex corner is summarized as follows:

1. Insert the desired convex SMR. Convex SMR radii varied from 0 *mm* (sharp edge), 1.59 *mm* (1/16th *in*), 3.18 *mm* (1/8th *in*), 6.35th *mm* (1/4th *in*), 9.52 *mm* (3/8th *in*) and 12.70 *mm* (1/2 *in*).
2. Position fabric on the rig. Slide fabric until it overhangs 10 *cm* from start of the curvature, shown in Figure 3.9.

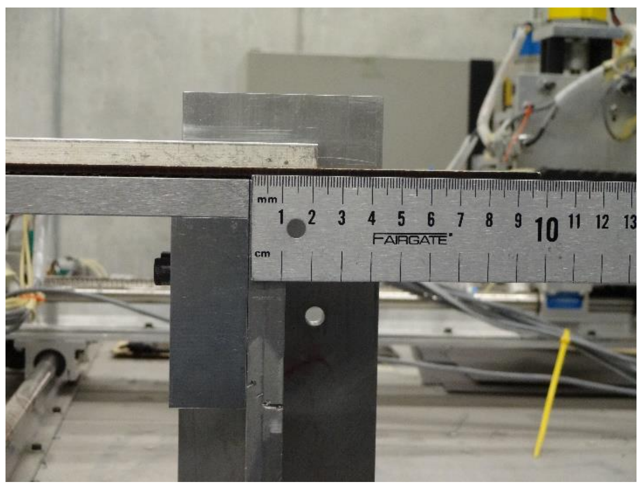

Figure 3.9 – 10 *cm* (4 *in*) of carbon fibre plain weave fabric overhanging from 12.70 *mm* (1/2 *in*) convex SMR

3. Measure horizontal distance between fabric and centre of SMR as shown in Figure 3.10. This configuration is referred to as the initial fabric position.

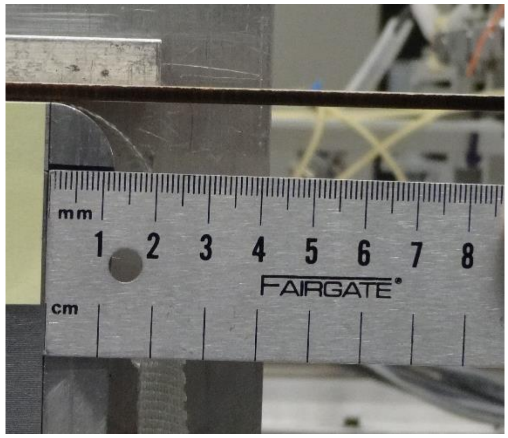

Figure 3.10 – Initial fabric position of glass fibre plain weave fabric around 12.7 *mm* (1/2 *in*) convex SMR

4. Position pressure plate on vertical surface of rig to conform fabric to vertical plane as shown in Figure 3.11. Apply light pressure for 15 seconds, ensuring that this light pressure is applied for the same amount of time for all samples.

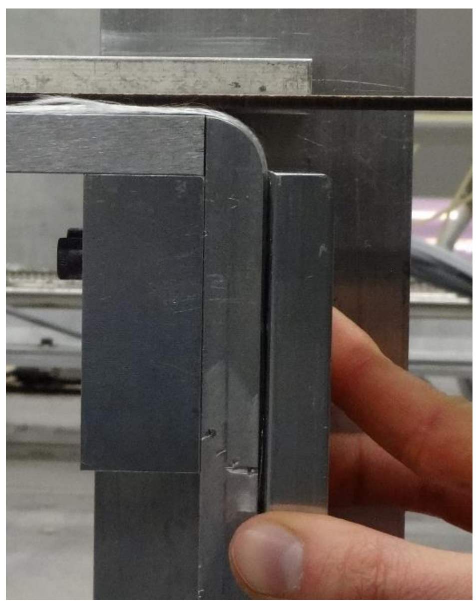

Figure 3.11 – Glass fibre plain weave fabric conformed to a 12.70 *mm* (1/2 *in*) convex SMR

5. Remove pressure and wait for 30 seconds, allowing fabric to spring back. Measure horizontal distance between fabric and centre of simulated mould radius as shown in Figure 3.12. This configuration is referred to as the final fabric shape.

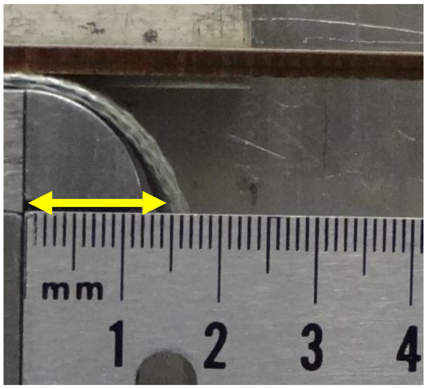

Figure 3.12 – Final fabric position of glass fibre plain weave fabric around 12.70 *mm* (1/2 *in*) convex SMR

6. Repeat steps 1 to 5 for both surfaces of fabric (front and back).

3.2.2.2. Concave spring back

The procedure used for characterizing bending spring back over a concave corner is summarized as follows:

1. Insert the desired concave SMR onto the rig. Concave SMR radii varied from 0 *mm* (sharp edge), 1.59 *mm* (1/16th *in*), 3.18 *mm* (1/8th *in*), 6.354 *mm* (1/4th *in*), 9.52 *mm* (3/8th *in*) and 12.70 *mm* (1/2 *in*). Concave SMRs are shown in Figure 3.6.
2. Position fabric on horizontal surface of rig, as shown in Figure 3.13.

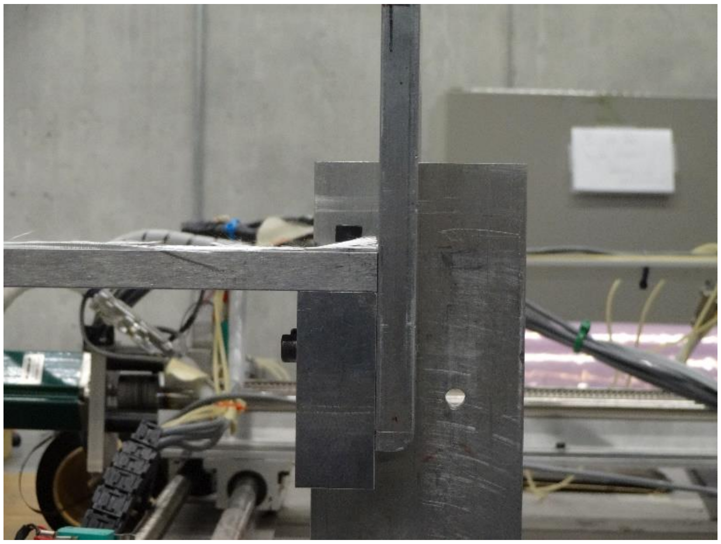

Figure 3.13 – Glass fibre plain weave fabric placed on rig – sharp edge

3. Gently lift the edge of the fabric (Figure 3.14a). Slide fabric 4 *cm* towards the vertical plane (Figure 3.14b). Once the fabric is in place, position fabric slide on fabric, 4 *cm* from the vertical plane.

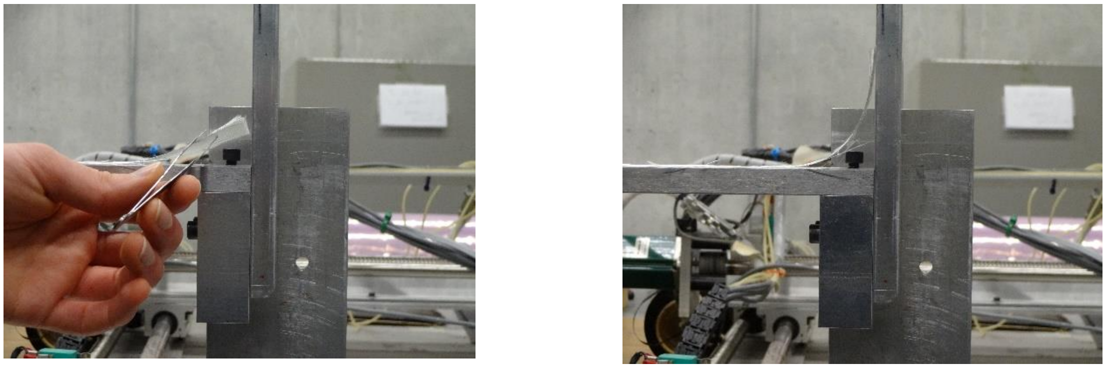

a) b)

Figure 3.14 – Glass fibre plain weave fabric slid 4 cm into rig corner - sharp edge

4. Measure vertical distance between horizontal and location where fabric touches vertical plane (Figure 3.15).

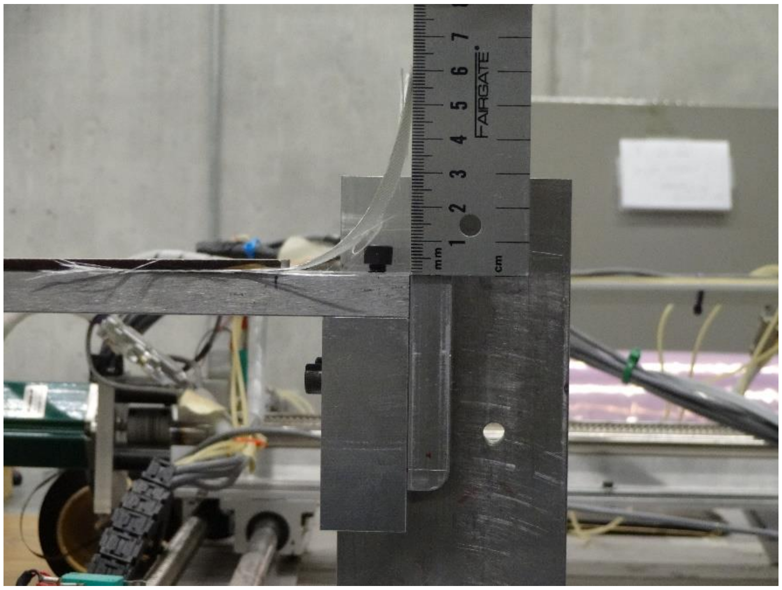

Figure 3.15 – Glass fibre plain weave fabric – slide positioned 4 cm from vertical plane (sharp edge)

5. Apply light pressure to conform fabric to SMR (Figure 3.16).

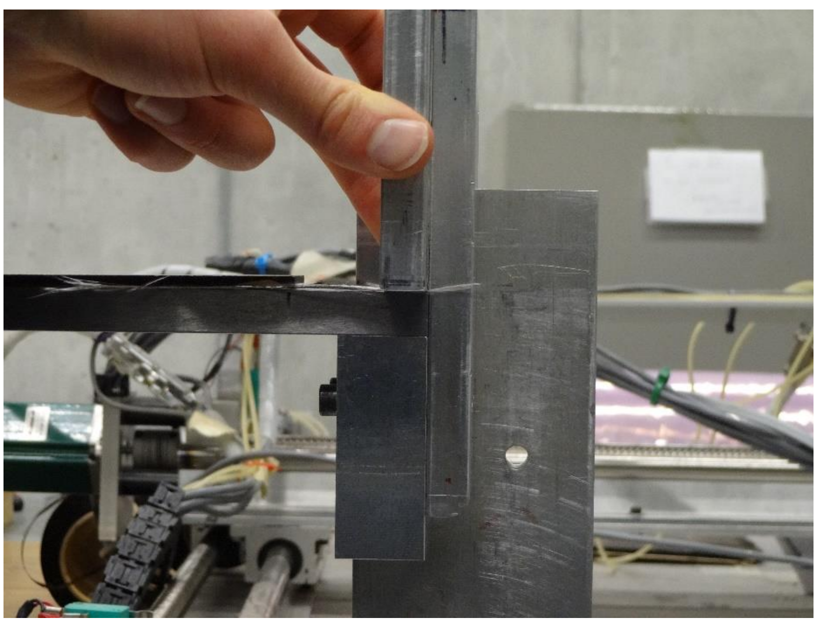

Figure 3.16 – Glass fibre plain weave fabric placed into corner (sharp edge)

6. Remove pressure and wait 15 seconds, allowing fabric to spring back. Measure vertical distance between horizontal and location where fabric touches vertical plane (Figure 3.17).

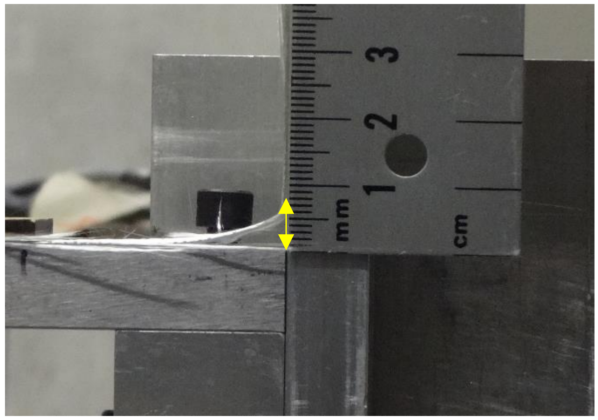

Figure 3.17 – Glass fibre plain weave fabric – final shape

7. Repeat steps 1 to 6 for both surfaces of fabric (front and back).

Measurements obtained from both convex and concave bending spring back tests are normalized with respect to the SMR to enable dimensionless comparisons of the spring back behaviour at different radii. The metric describing fabric spring back, labelled spring back ratio (SBR), is defined as:

$$SBR = \frac{\beta}{SMR} \tag{3.3}$$

where SMR is the simulated mould radius (*mm*) and β is the measurement of the final shape of the fabric (*mm*), shown in Figure 3.12 for convex corners and in Figure 3.17 for concave corners.

3.2.3. In-plane shear behaviour

The picture-frame rig used in this work for characterizing the in-plane shear behaviour of the selected fabrics is shown in Figure 3.18.

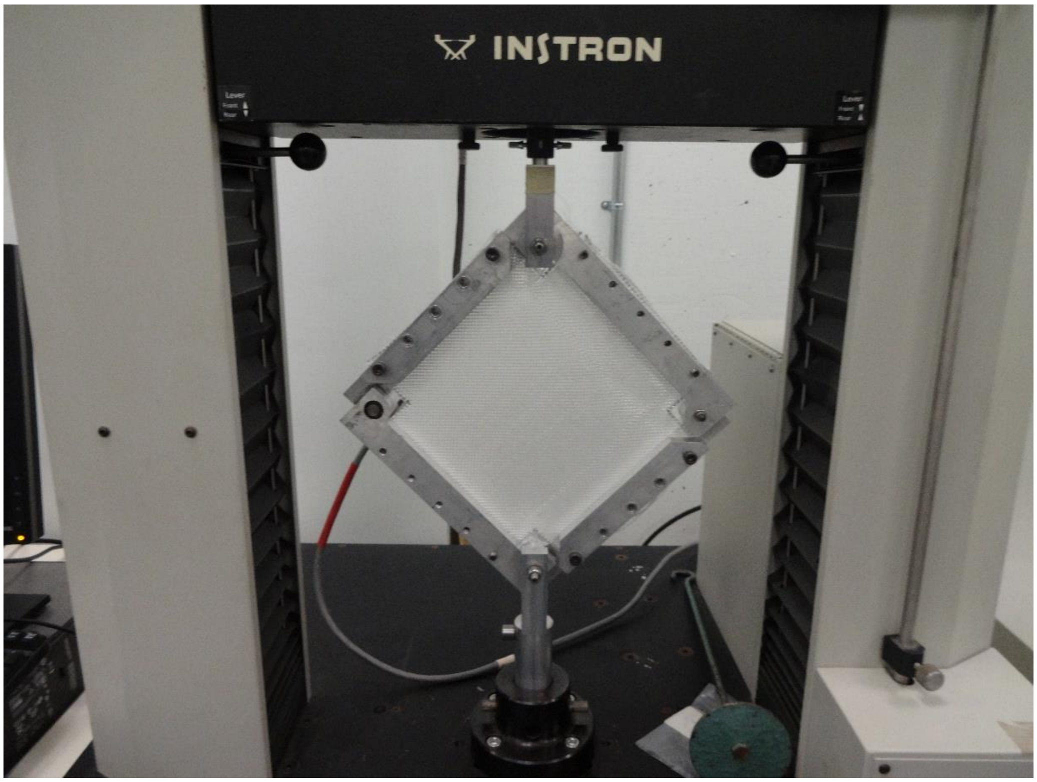

Figure 3.18 – Picture-frame testing rig used for characterizing the selected fabrics

The procedure used for characterizing the in-plane shear properties of fabrics is summarized as follows:

1. Cut samples of fabric to 228.60 *mm* × 228.60 *mm* (9 *in* × 9 *in*) squares.
2. Remove 44.45 *mm* × 44.45 *mm* (1.75 *in* × 1.75 *in*) square from each sample corner. This will result in a cruciform sample suitable for the picture-frame rig.
3. Using a laser-cut MDF pattern, align and punch 6.35 *mm* (0.25 *in*) diameter holes in sample, spaced 30 *mm* (1.18 *in*).

4. Align and clamp fabric sample on picture-frame.
5. Install 500 *N* load cell on tensile tester. Set crosshead extension rate to 60 *mm*/*min*, minimum extension to 0 *mm*, and maximum extension to 85 *mm* which corresponds to a maximum shear angle of 53°. Set tensile tester to cycle between extensions of 0 *mm* and 85 *mm*, five times.
6. Begin test while recording time, extension and load.
7. Plot normalized shear load, Equation (2.17), as a function of shear angle, Equation (2.14), for 5^{th} cycle of test.

As previously mentioned, there is no standard method for characterizing the in-plane shear behaviour of fabrics using a picture-frame test. The testing parameters listed above were selected to ensure reproducible results and simulate shear imposed on fabrics as they are draped onto moulds. The normalized shear load is not a linear function of the shear angle, which means that the slope of the graph cannot be used for characterizing in-plane shear stiffness. The normalized shear load may be used for comparing the relative difficulty to shear each fabric to any angle between 0° and 53°. The maximum normalized shear load will be used for comparing the selected fabrics in this work.

Fabrics subjected to large in-plane shear deformations may also exhibit spring back similar to bending spring back. This phenomenon is not documented in the scientific literature. Data generated from picture-frame tests were used for characterizing the shear angle at which shear force vanished during the return phase of the last cycle of tests, labelled as the return angle. The return angles of fabrics will be used for comparing in-plane shear spring back of different fabrics.

3.2.4. Friction

A friction test inspired by standard ASTM-D1894 Test Method for Static and Kinetic Coefficient of Friction of Plastic Film and Sheeting was developed for characterizing the coefficient of friction between layers of fabrics. Standard ASTM-D1894 involves sliding a block over a surface covered with a film in order to determine its coefficient of friction. In this work, the method was adapted for use with textile materials. A cable was used for connecting the block to the crosshead of a universal tensile testing machine and measure the force required for moving the block, as well as the displacement of the block. Figure 3.19 shows the apparatus used for conducting fabric friction tests.

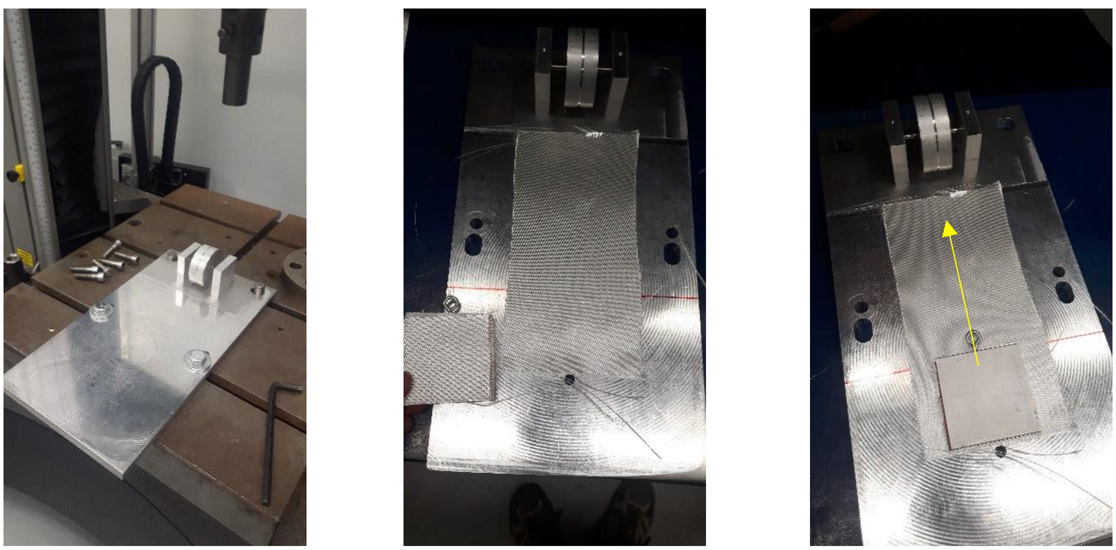

Figure 3.19 – ASTM-D1894 inspired friction test

The procedure used for characterizing friction between layers of fabric is summarized as follows:

1. Cut 63.50 *mm* × 63.50 *mm* (2.5 *in* × 2.5 *in*) square fabric samples. Mark the inside surface of the roll and the warp direction of the sample. These samples will be attached to the block.

2. Cut 101.60 *mm* × 215.90 *mm* (4 *in* × 8.5 *in*) rectangular fabric samples. Mark the inside surface of the roll and the warp direction of the sample. These samples will be attached to the surface.
3. Using two-sided tape, stick the square sample of fabric to the block. Ensure that the inside surface of the fabric is stuck to the block.
4. Using two-sided tape, stick the rectangle sample of fabric to the surface. Ensure that the inside surface of the fabric is facing up.
5. Install 10 *N* load cell in universal testing machine. Set crosshead extension rate to 120 *mm*/*min*, and maximum extension to 130 *mm*.
6. Attach steel music wire to load cell, thread wire through pulley, and attach music wire to block.
7. Align edge of block facing pulley with red markings. This allows for block to slide 130 *mm* during test.
8. Place 2 *lb* weight (907.18 *g*) on block, balance load cell and begin test.

The procedure for characterizing the friction between a fabric and aluminium is similar; however steps 2 and 4 are not necessary.

As mentioned in Section 2.8, increasing the pressure normal to the contact surface between fabrics decreases the coefficient of friction, and increasing the block sliding velocity decreases stick-slip [41]. Testing parameters were selected for maximizing repeatability of the results for the selected fabrics. The coefficient of friction between layers of fabric and between fabric and aluminium were calculated using Equation (2.23).

Technicians that drape multilayer preforms onto moulds often encounter layers of fabric that slide over small distances while being draped. Relative sliding of fabric layers in a multilayer preform causes defects in the final composite part. Therefore, technicians ensure that layers in a multilayer preform slide as little as possible while being draped onto moulds. The ideal behaviour is a stack of layers that stay together, hence the static coefficient of friction should be used for comparing fabrics. The stick-slip phenomenon observed when characterising friction increases the difficulty of characterising the static coefficient of friction.

Data generated from friction tests described above can be used for determining a mean coefficient of friction over small distances. The mean coefficient of friction over the first 5 mm displacement will be used for quantifying friction of one fabric sample. The first 5 *mm* displacement is taken as 5 *mm* from the first local maximum coefficient of friction, shown in Figure 3.20. The mean absolute deviation of the coefficient of friction over the first 5 *mm* displacement will be used for quantifying stick-slip of one sample.

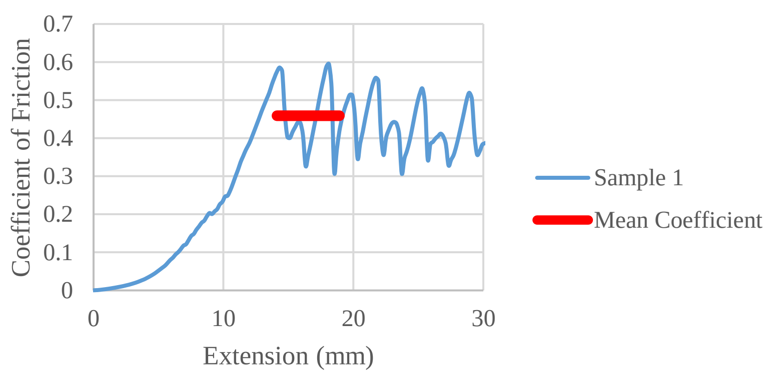

Figure 3.20 – Coefficient of friction of Fabric 1 – sample 1, warp direction

3.2.5. Pin stability

Upon draping, Hutchinson technicians use pins for securing textile preforms onto moulds as they are draped. Different types of fabrics respond differently to being pinned to a mould. A novel test is required for characterizing the stability of fabrics secured to moulds using pins.

The rig used for characterizing the frictional properties of fabrics was designed in order to also enable the characterization of pin loading stability. The procedure for characterizing pin stability is very similar to the procedure used for characterizing the frictional properties of fabrics. The procedure is summarized as follows:

1. Cut 63.50 *mm* × 127.00 *mm* (2.5 *in* × 5 *in*) rectangular fabric samples. Mark the warp direction of the fabric on the inside surface of the fabric roll.
2. Punch one hole 6.35 *mm* (0.25 *in*) in diameter along centreline of sample, at 25.40 *mm* (1 *in*) from a sample edge. The fabric test direction determines the location of the hole.
3. Using two-sided tape, attach fabric sample to block, ensuring that inside surface of fabric faces up. Ensure that hole is available for installing pin.
4. Install 10 *N* load cell in universal testing machine. Set crosshead extension rate to 120 *mm*/*min* and maximum extension to 80 *mm*.
5. Attach steel music wire to load cell, thread wire through pulley, and attach music wire to block.
6. Ensuring that there is no tension in wire, pin fabric to rig.
7. Balance load cell and begin test. Figure 3.21 shows pinned sample at beginning of test.

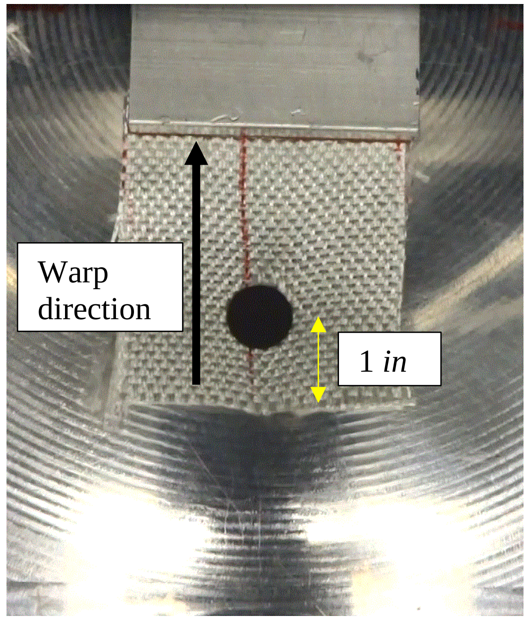

Figure 3.21 – Pin stability test

The above is a novel testing procedure. Testing parameters were selected in order to maximize testing results reproducibility. The end of the test was defined by any failure of the pin to hold the fabric in place on the rig. The load measured by the load cell at pin failure was recorded for characterizing the stability of the fabric.

3.3. Statistical analysis

Numerical results of all one-way analysis of variance (ANOVA) and design of experiments (DOE) are provided in Appendices A and B respectively. One-way ANOVAs were used for comparing the performance characteristics of each fabric. The α-level of each ANOVA was 0.1. DOEs were then used for constructing and structuring a usable database of fabric characteristics. The database leads to linear functions that allow interpolation between data points generated through testing.

This section details the format used for presenting analysis results. The response parameter used here is the surface mass of fabrics, measured prior to cantilever bending stiffness tests. All DOEs used in this work were limited to two level factors for simplifying result interpretation, interpolation and eventual expansion. In reality, some factors had multiple levels. Table 3.1 lists all input factors controlled in the experimental plans for each characterization test conducted in this work.

Table 3.1 – Factors analysed in this work

Factors	**Levels**	**Test**
Fabric	Fabric 1 Fabric 2 Fabric 3 Fabric 4	Bending stiffness Bending spring back In-plane shear Friction Pin resistance
Yarn orientations	0° (Warp) 45° (Bias) 90° (Weft)	Bending stiffness Bending spring back Friction Pin resistance
Number of Layers	Single layer Multilayer	Bending stiffness Bending spring back In-plane shear Friction Pin resistance
Mould Radius	0 *mm* 1.59 *mm* (1/16 *in*) 3.18 *mm* (1/8 *in*) 6.35 *mm* (1/4 *in*) 9.52 *mm* (3/8 *in*) 12.7 *mm* (1/2 *in*)	Concave bending spring back Convex bending spring back

Fabrics are listed as factors; however, each fabric is constructed using different fibre types, yarn dimensions, yarn spacings and weave patterns, which are not considered independently in the construction of linear functions. Prior to constructing the database of fabric characteristics, one-way ANOVAs were used for comparing the characteristics of single layer fabrics, the characteristics of multilayer fabrics, and the characteristics of single layer vs multilayer stacks of each fabric. Linear functions constructed in this work are unique to the tested fabrics; they consider the yarn orientation and the number of layers in the preform. The geometry of the mould is also considered in constructing the spring back interpolation functions.

DOEs in this work were limited to two level factors; however, there are three levels of yarn orientations – warp, bias and weft, two levels of numbers of layers – single and multilayers, and six levels of mould radius – 0 *mm*, 1.59 *mm*, 3.18 *mm*, 6.35 *mm*, 9.52 *mm* and 12.70 *mm*. In order to analyse results and produce linear interpolation functions when the controlled factors had more than two levels, additional DOE analyses were used for comparing the multiple levels of each factor, by comparing two adjacent levels at a time. Table 3.2 specifies the number of linear functions created for interpolation of SBR and their range of validity depending on the yarn orientation of the fabric and the mould radius. All functions listed also factor the number of layers used for creating the fabric.

Table 3.2 – Linear functions for SBR

	Interval of validity (*mm*)			
Yarn orientation interval of validity (°)	1.59 *mm* to 3.18 *mm*	3.18 *mm* to 6.35 *mm*	6.35 *mm* to 9.52 *mm*	9.52 *mm* to 12.70 *mm*
Warp (0°) to Bias (45°)	Function 1a	Function 2a	Function 3a	Function 4a
Bias (45°) to Weft (90°)	Function 1b	Function 2b	Function 3b	Function 4b

As each function is the result of a unique DOE, the effect of number of layers on the SBR of fabrics is calculated for each function. This effect may be different for each function.

The interpolation functions for the other characteristics do not feature the mould radius as an independent variable, therefore fewer linear functions are required for the interpolation of these characteristics, as shown in Table 3.3.

Table 3.3 – Linear functions for fabric characteristics

Yarn orientation interval of validity (°)	
Warp (0°) to Bias (45°)	Bias (45°) to Weft (90°)
Function 1a	Function 1b

3.3.1. Surface mass analysis

The primary purpose of this section is to illustrate the structure of results presented in Chapter 4. The surface mass data was collected along the warp, bias and weft direction for Fabrics 1 to 3, and along the warp and weft directions for Fabric 4 prior to conducting cantilever bending stiffness tests, as the bending stiffness of fabrics depends on the surface mass of the sample being tested. The surface masses of each sub-group tested appear in Figure 3.22. The first analyses are ANOVAs, used for comparing the surface masses of each fabric. The average surface mass of samples cut along the warp and weft directions was taken to represent the surface mass of each fabric. In every case, Tukey’s honestly significant difference (HSD) is used for making pairwise comparisons between the surface masses of the fabrics.

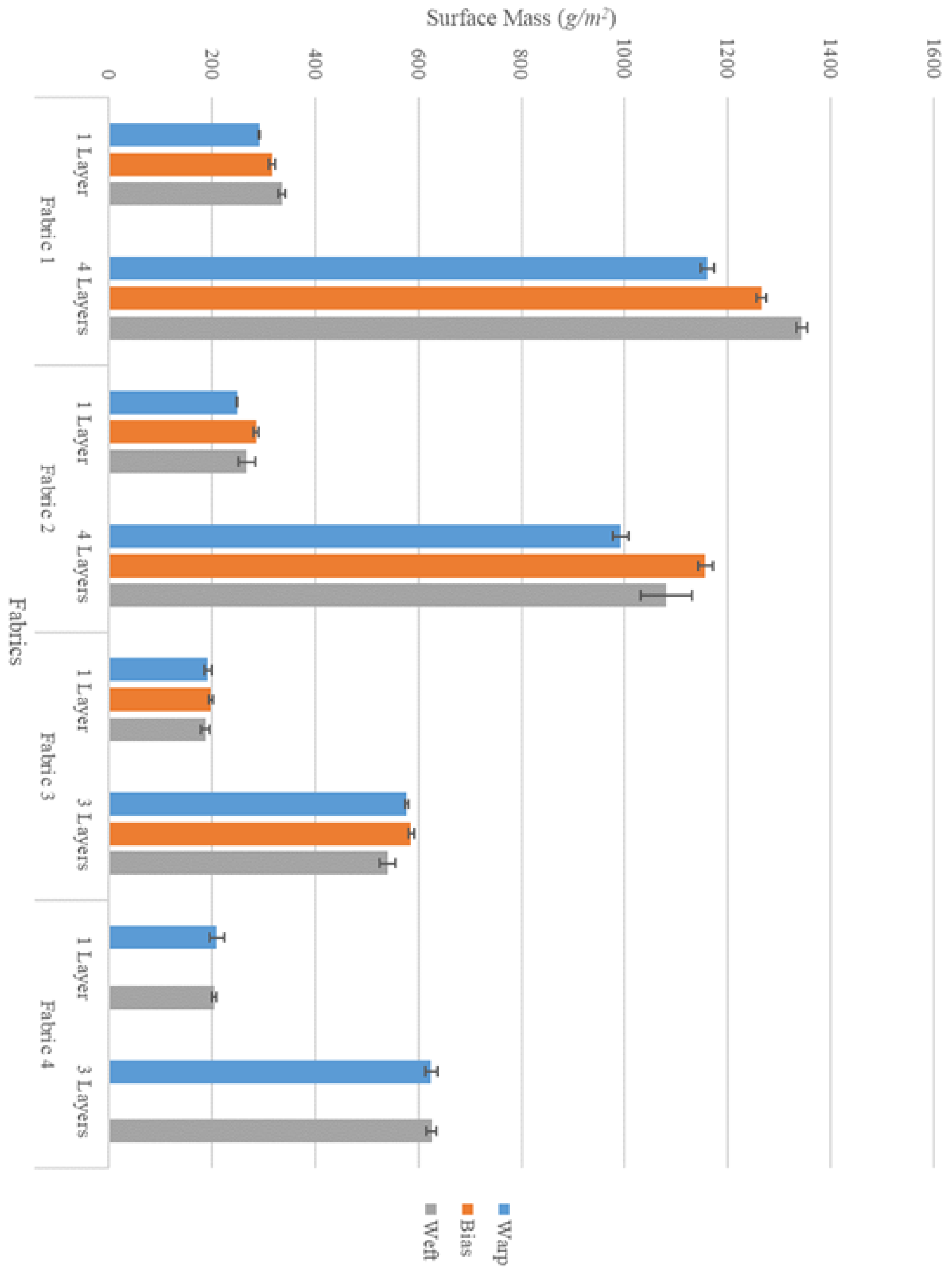

Figure 3.22 – Surface mass of fabrics

The first ANOVA compares the surface masses of single layer fabrics. The ANOVA table for this analysis is shown in Appendix B. The ANOVA resulted in a HSD value of 16 g/m^2. The average surface masses and HSD of single layer fabrics are shown in Figure 3.23. The surface masses of Fabrics 3 and 4 are not detectably different, as the surface masses are 16 g/m^2 apart. The surface masses of Fabrics 4, 2 and 1 are detectably different.

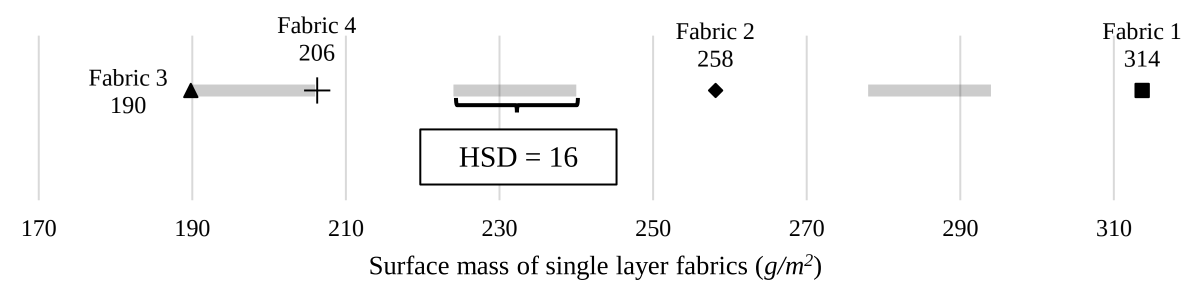

Figure 3.23 – Surface mass of single layer fabrics

The second ANOVA compares the surface masses of multilayer fabrics (Figure 3.24). The ANOVA resulted in a HSD value of 61 g/m^2. The surface masses of multilayer fabrics are all detectably different. It is noted that the difference between Fabrics 4 and 3 is 66 g/m^2, which is marginally greater than the HSD of 61 g/m^2.

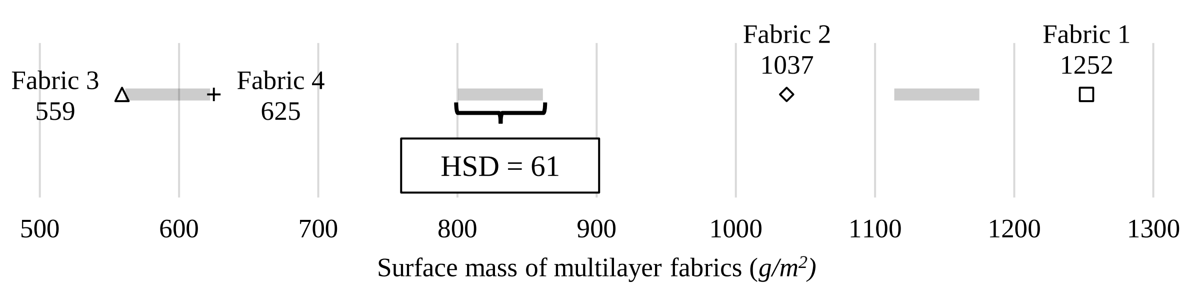

Figure 3.24 – Surface mass of multilayer fabrics

The third ANOVA compares the surface masses of single and multilayered versions of each fabric. The surface masses of every single and multilayer fabric are plotted in Figure 3.25, along with HSDs for each single/multilayer comparison.

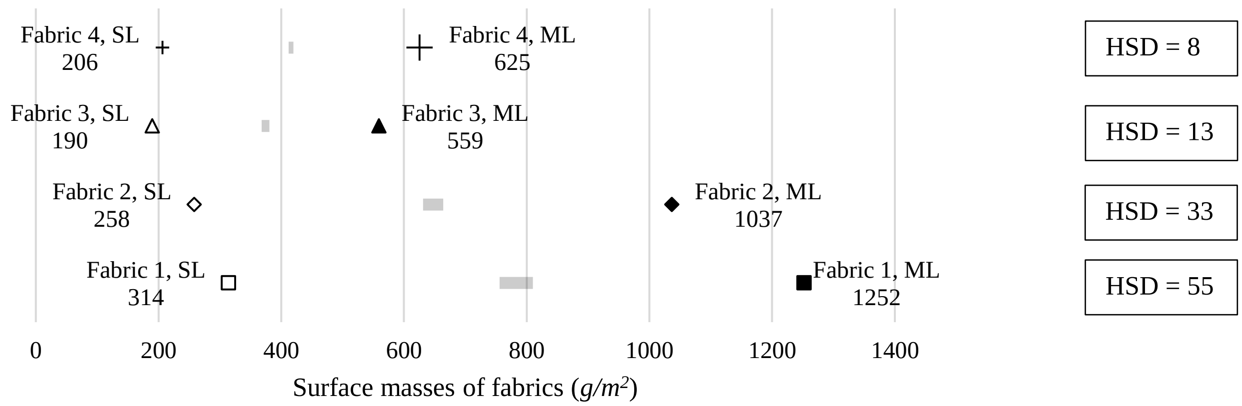

Figure 3.25 – Surface mass of fabrics

The surface masses of multilayer fabrics are detectably different from the surface masses of single layer fabrics. This result is expected, as multilayer versions of fabrics 1 to 4 are stacks of single layer fabrics. The ratios of multilayer to single layer fabrics are shown in Table 3.4.

Table 3.4 – Ratios of multilayer to single layer surface masses

Fabric	Single layer average surface mass (g/m^2)	Multilayer average surface mass (g/m^2)	Ratio of multilayer to single layer surface mass	Number of layers
Fabric 1	314	1252	3.99	4
Fabric 2	258	1037	4.02	4
Fabric 3	190	559	2.94	3
Fabric 4	206	625	3.03	3

DOEs were used for developing linear interpolation functions for the surface mass of fabrics. The surface mass of fabrics was measured on samples cut along three directions – the warp direction (0°), the bias direction (45°) and the weft direction (90°). Therefore, two piecewise linear functions are needed for interpolating the surface mass data. The first function is valid for yarn orientations between the warp (0°) and bias (45°) directions, and the second function is valid for yarn orientations between the bias (45°) and the weft (90°) directions. Every fabric has its own set of linear functions. The linear functions take the form

$$f(x) = C_0 + C_1 \cdot x_1 + C_2 \cdot x_2 + C_{12} \cdot x_1 x_2 \tag{3.4}$$

where C_0 is a constant, and C_1, C_2 and C_{12} are coefficients. Coefficient C_1 represents the effect of number of layers on surface mass, coefficient C_2 represents the effect of yarn orientation on surface mass, and C_{12} represents the interaction of number of layers and yarn orientation on surface mass. The constants and coefficients associated with each surface mass function are given in Table 3.5. Variables x_1 and x_2 are interpolation modalities that represent the number of layers and the yarn orientation. Interpolation modalities x_1 and x_2 are given in Table 3.6, where n is the number of layers used for creating the sample, and Φ is the yarn orientation of the fabric.

Table 3.5 – Interpolation function constants and coefficients

Fabric	**Range**	**C_0 (g/m^2)**	**C_1 (g/m^2)**	**C_2 (g/m^2)**	**C_{12} (g/m^2)**
Fabric 1	$0° < \phi \leq 45°$	758.75	454.75	32.25	20.25
	$45° < \phi \leq 90°$	815.00	489.50	24.00	14.50
Fabric 2	$0° < \phi \leq 45°$	671.00	404.00	50.00	32.00
	$45° < \phi \leq 90°$	697.25	421.25	-23.75	-14.75
Fabric 3	$0° < \phi \leq 45°$	388.25	193.75	3.25	0.75
	$45° < \phi \leq 90°$	377.50	185.50	-14.00	-9.00

Table 3.6 – Interpolation modalities

Fabric	Modality	Range	Interpolation
Fabric 1, Fabric 2	x_1	$1 < n \leq 4$	$\frac{1}{3}(2n-5)$
Fabric 3	x_1	$1 < n \leq 3$	$n-2$
All Fabrics	x_2	$0° < \phi \leq 45°$	$\frac{2}{45}\phi - 1$
All Fabrics	x_2	$45° < \phi \leq 90°$	$\frac{2}{45}\phi - 3$

The interpolation modalities are used for converting the yarn orientation and number of layers into a number between -1 and +1. This number is then multiplied by its estimated effect on the surface mass. During testing, the multilayer samples of Fabric 1 and Fabric 2 consisted of 4 layers, and the multilayer version of Fabric 3 consisted of 3 layers; therefore, the interpolation modality that represents the number of layers for Fabric 3 differs from the interpolation modalities of Fabric 1 and Fabric 2. The linear functions for Fabric 1, Fabric 2 and Fabric 3 are shown in Figure 3.26, Figure 3.27 and Figure 3.28 where the dashed lines represent the interpolation functions, and the data markers represent the data collected during experiments.

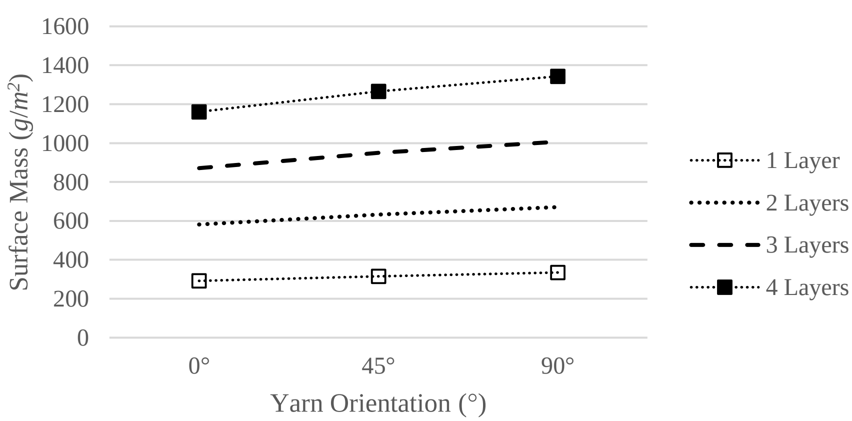

Figure 3.26 – Surface mass interpolation functions for Fabric 1

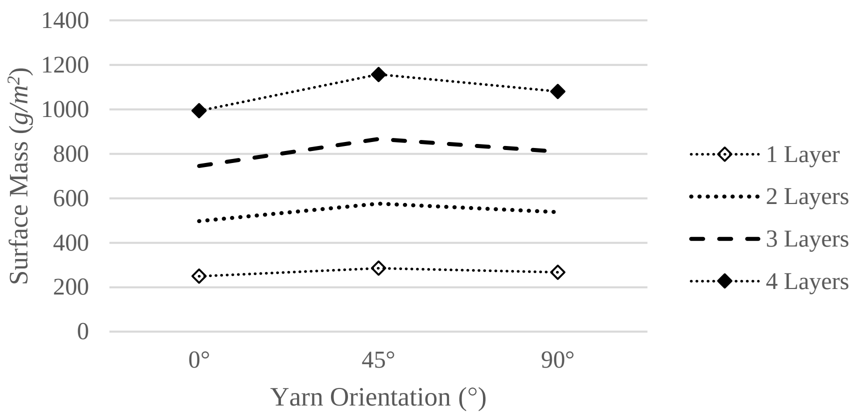

Figure 3.27 – Surface mass interpolation functions for Fabric 2

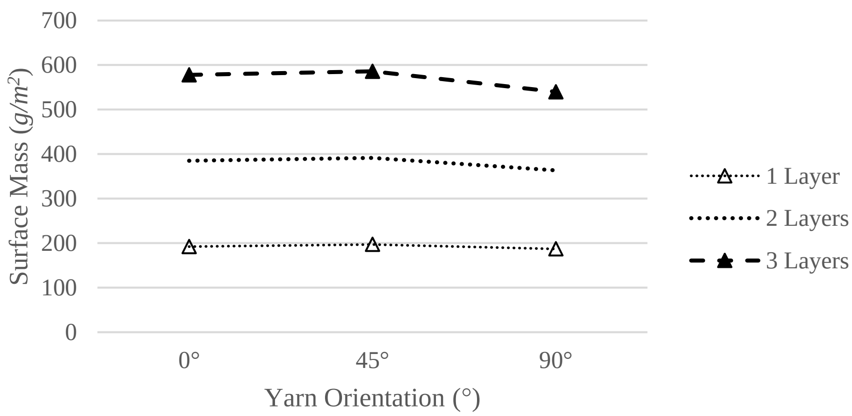

Figure 3.28 – Surface mass interpolation functions for Fabric 3

In all cases, the effect of yarn orientation is small in comparison to the effect of number of layers on the surface mass of fabrics.

Chapter 4. Results

This chapter presents data on bending stiffness, bending spring back, in-plane shear, in-plane shear spring back, inter layer friction, and pin stability for Fabrics 1, 2, 3 and 4, obtained using the characterization methods presented in Chapter 3. ANOVAs applied on results from each test enable objective comparisons of fabric characteristics, while DOEs enable the creation of linear functions interpolating the fabric characteristics. All analyses will be referred to by their respective heading numbers, shown Table 4.1. Complete statistical data for ANOVAs are available in Appendix A, while complete statistical data for DOEs are available in Appendix B.

Table 4.1 – Analysis terminology

Test	**Fabrics comparisons**	**Linear interpolation functions**
Bending stiffness	ANOVA 4.1.A	DOE 4.1.A
Overhang length	ANOVA 4.1.B	DOE 4.1.B
Convex bending spring back	ANOVA 4.2A	DOE 4.2.A
Concave bending spring back	ANOVA 4.2.B	DOE 4.2.B
In-plane shear load	ANOVA 4.3.A	DOE 4.3.A
In-plane shear spring back	ANOVA 4.3.B	N/A
Friction (Mean coefficient)	ANOVA 4.4.A	DOE 4.4.A
Friction (Mean deviation)	ANOVA 4.4.B	DOE 4.4.B
Pins (Load at failure)	ANOVA 4.5.A	DOE 4.5.A
Pins (Extension at failure)	ANOVA 4.5.B	DOE 4.5.B

4.1. Bending stiffness

The cantilever bending test was used for characterizing the bending stiffness of single and multilayered fabrics. Testing was conducted along the warp, along the weft, and at 45° bias from the warp for Fabrics 1, 2 and 3. Production imperatives at Hutchinson meant that data for Fabric 4 was only required along the warp and weft. Multilayered stacks of Fabrics 1 and 2 featured four layers, while those of Fabrics 3 and 4 featured three layers. Bending stiffness values for the tested fabrics are shown in Figure 4.1.

The average bending stiffness along the warp and weft directions are used for representing the bending stiffness of each fabric. Three ANOVAs are used for comparing bending stiffness of single layer fabrics (Figure 4.2), multilayer fabrics (Figure 4.3), and for comparing single and multilayer stacks of each fabric (Figure 4.4).

The bending stiffness of the single layers of Fabric 1 and Fabric 2 are not detectably different, while single layers of Fabric 2 and Fabric 3, Fabric 3 and Fabric 4, and Fabric 2 and Fabric 4 are detectably different. The bending stiffness of multilayer stacks of Fabric 1 and Fabric 2 are not detectably different, while multilayer stacks of Fabric 2 and Fabric 3, Fabric 3 and Fabric 4, and Fabric 2 and Fabric 4 are detectably different. The bending stiffness of single and multilayer stacks of each fabric are all detectably different.

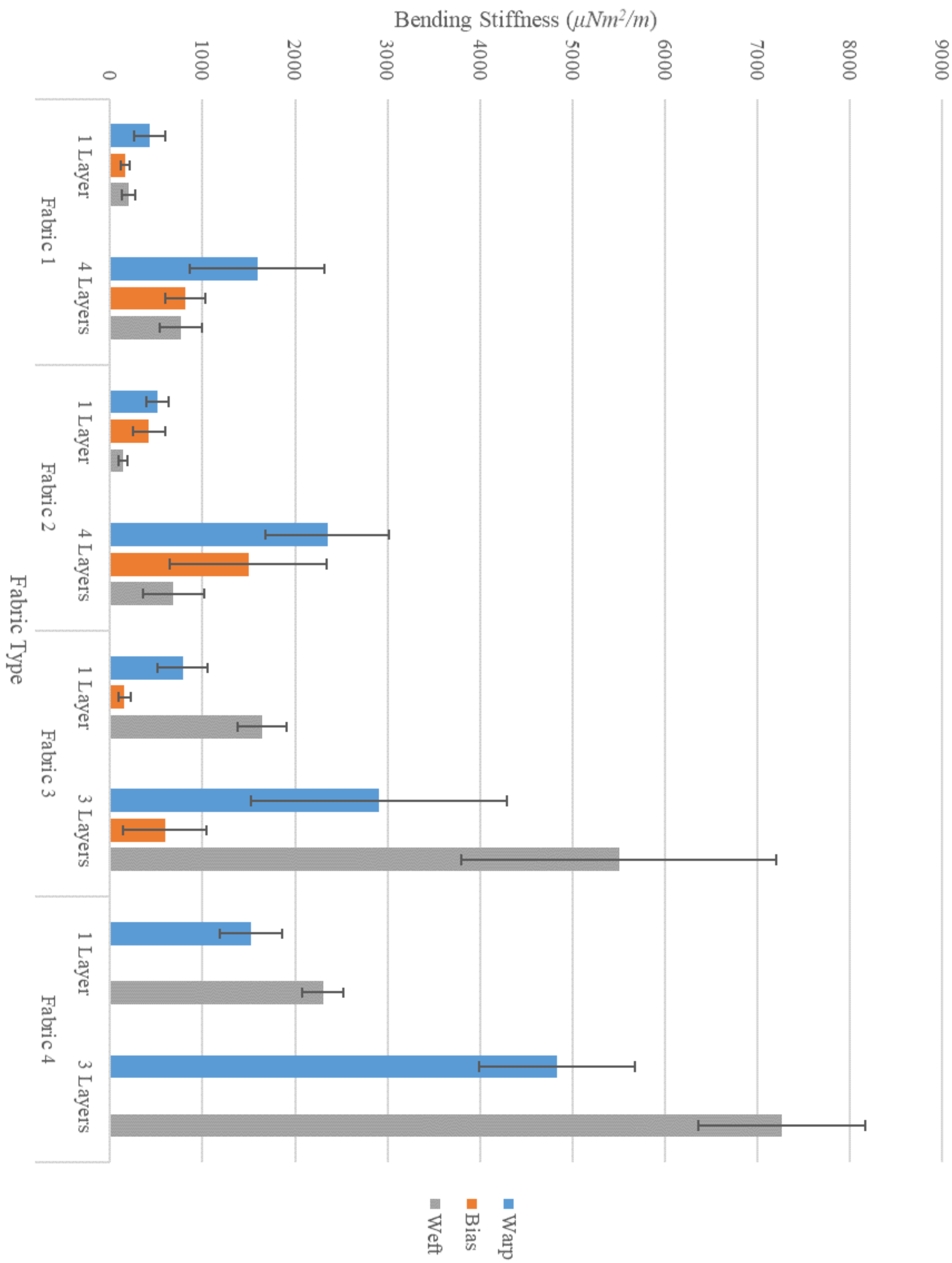

Figure 4.1 – Bending stiffness of tested fabrics

4.1.1. ANOVA 4.1.A – Bending stiffness

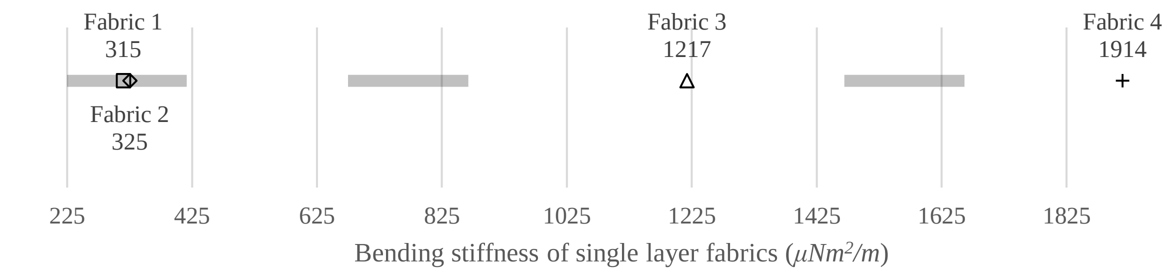

Figure 4.2 – Bending stiffness of single layer fabrics

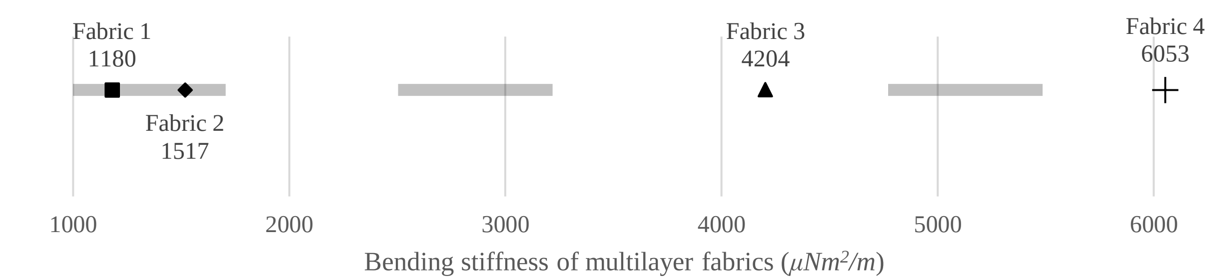

Figure 4.3 – Bending stiffness of multilayer fabrics

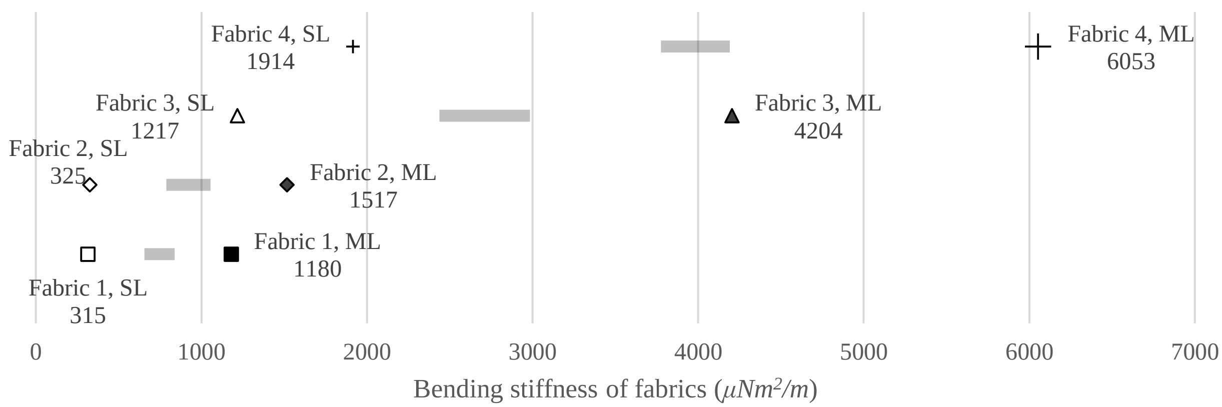

Figure 4.4 – Bending stiffness of fabrics

The ratio of multilayer to single layer bending stiffness of every fabric approaches the number of layers used in creating the sample (Table 4.2).

Table 4.2 – Ratio of multilayer to single layer bending stiffness

Fabric	Single layer average bending stiffness	Multilayer average bending stiffness	Ratio of multilayer to single layer bending stiffness	Number of layers
Fabric 1	315	1180	3.75	4
Fabric 2	325	1517	4.67	4
Fabric 3	1217	4204	3.45	3
Fabric 4	1914	6053	3.16	3

4.1.2. DOE 4.1.A – Bending stiffness

The linear functions used for interpolating the bending stiffness of fabrics take the form

$$f(x) = C_0 + C_1 \cdot x_1 + C_2 \cdot x_2 + C_{12} \cdot x_1 x_2 \tag{4.1}$$

where variables x_1 and x_2 are interpolation modalities listed in Table 4.3, where n is the number of layers and Φ is the yarn orientation. Constant C_0 is an average and C_1, C_2 and C_{12} are coefficients listed in Table 4.4. The linear functions for each fabric are shown in Figure 4.5, Figure 4.6 and Figure 4.7.

Table 4.3 – Interpolation modalities for bending stiffness

Fabric	Modality	Range	Interpolation
Fabric 1, Fabric 2	x_1	$1 < n \leq 4$	$\frac{1}{3}(2n-5)$
Fabric 3	x_1	$1 < n \leq 3$	$n-2$
All Fabrics	x_2	$0° < \phi \leq 45°$	$\frac{2}{45}\phi - 1$
All Fabrics	x_2	$45° < \phi \leq 90°$	$\frac{2}{45}\phi - 3$

Table 4.4 – Bending stiffness interpolation coefficients and constants

Fabric	**Range**	***C₀*** ***(μNm²/m)***	***C₁*** ***(μNm²/m)***	***C₂*** ***(μNm²/m)***	***C₁₂*** ***(μNm²/m)***
Fabric 1	$0° < \phi \leq 45°$	750.00	453.00	-259.50	-128.50
	$45° < \phi \leq 90°$	488.00	304.00	-2.50	-20.50
Fabric 2	$0° < \phi \leq 45°$	1,194.00	729.00	-237.50	-190.50
	$45° < \phi \leq 90°$	683.75	405.75	-272.75	-132.75
Fabric 3	$0° < \phi \leq 45°$	1,110.50	637.50	-736.00	-420.00
	$45° < \phi \leq 90°$	1,974.50	1,073.50	1,600.00	856.00

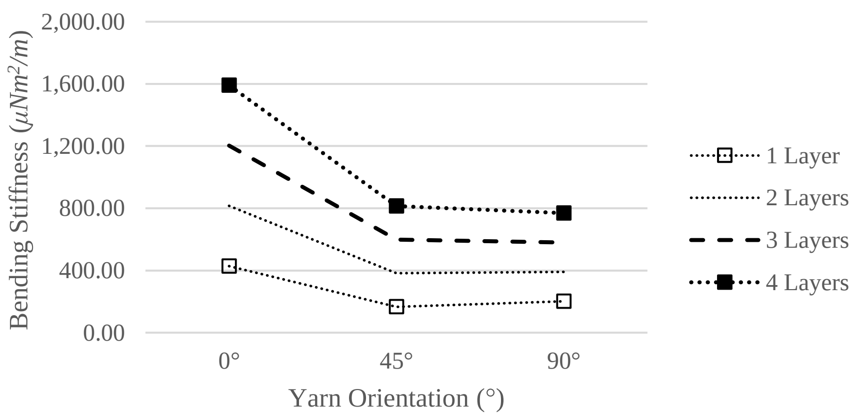

Figure 4.5 – Bending stiffness linear interpolation function for Fabric 1

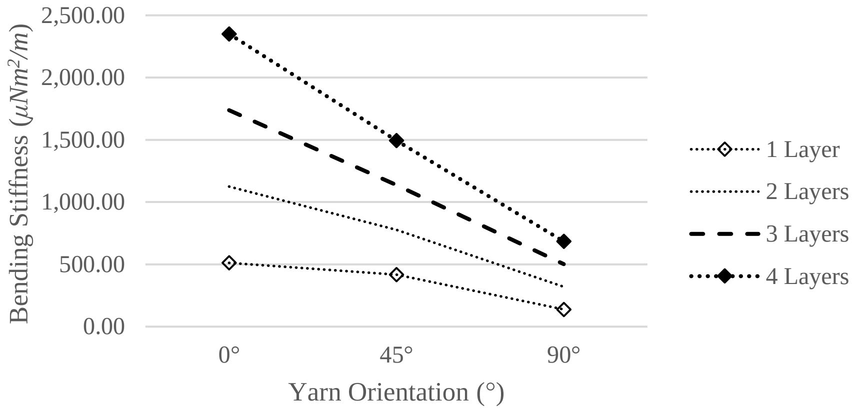

Figure 4.6 – Bending stiffness linear interpolation function for Fabric 2

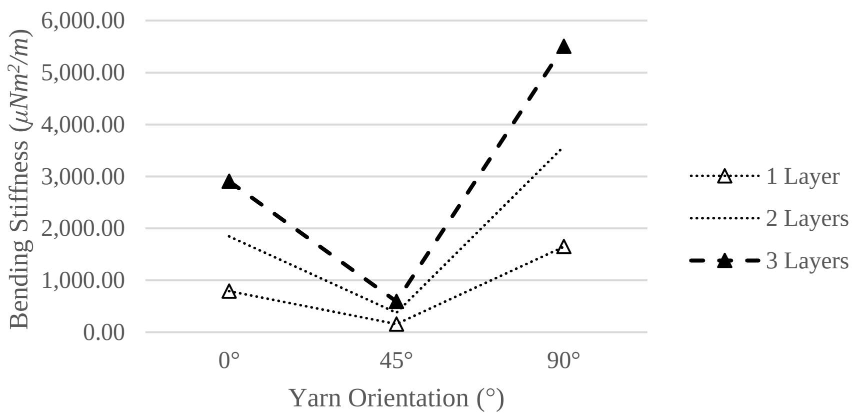

Figure 4.7 – Bending stiffness linear interpolation function for Fabric 3

The bending stiffness is a composite characteristic depending on the surface mass of the fabric and on the overhang length measured on the sample during the bending test. ANOVA and linear functions for the surface mass of fabrics were shown in Chapter Chapter 3. Raw measurements of overhang length are shown in Figure 4.8. ANOVA results are shown in Figure 4.9, Figure 4.10 and Figure 4.11.

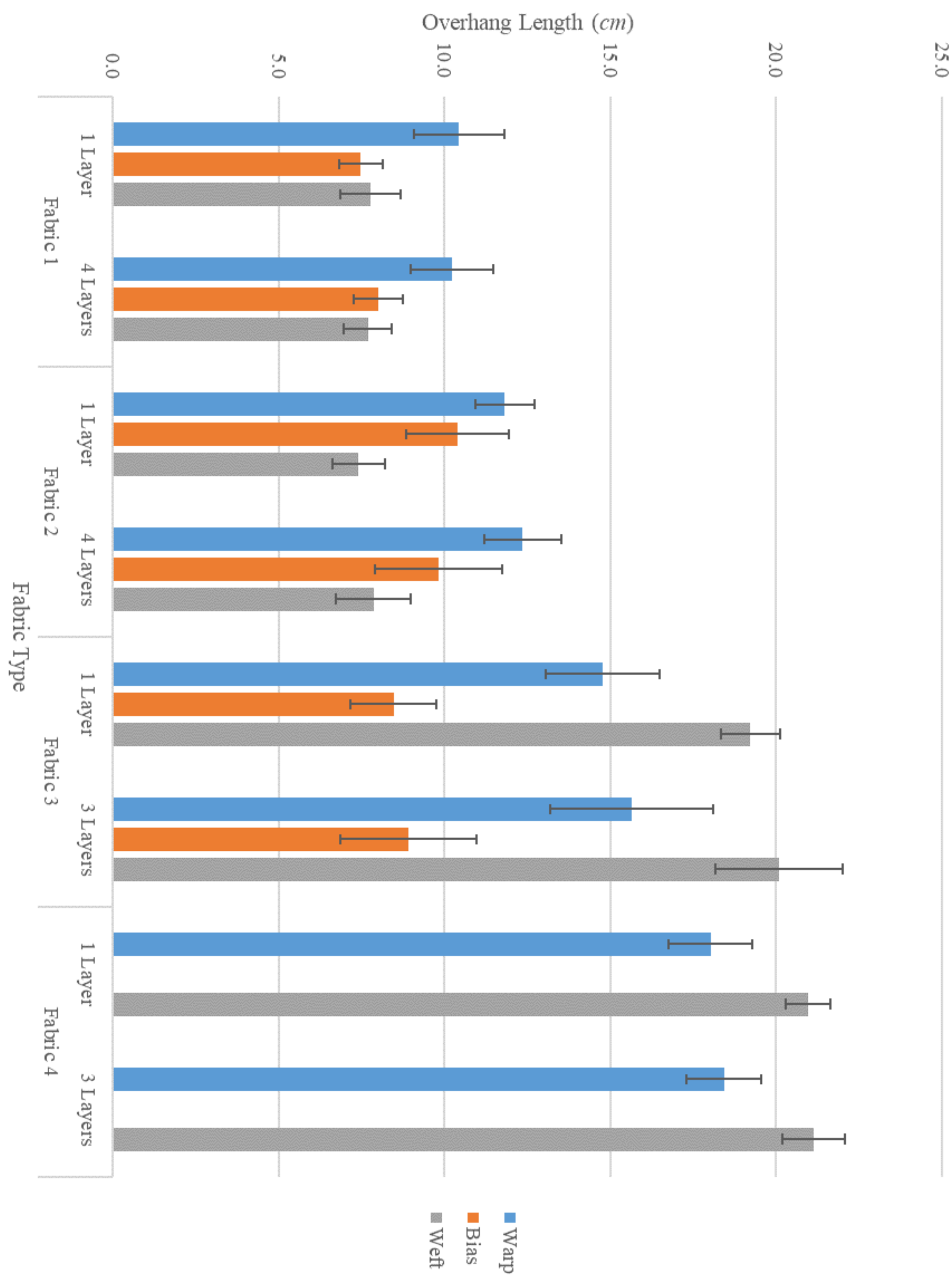

Figure 4.8 – Overhang lengths of tested fabrics

4.1.3. ANOVA 4.1.B – Overhang Length

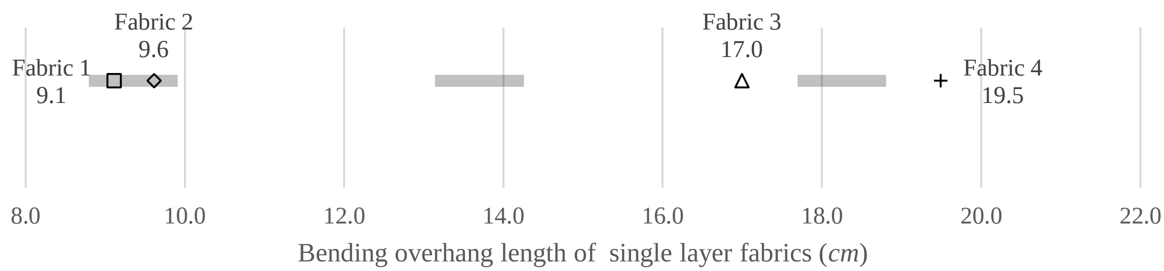

Figure 4.9 – Bending overhang length of single layer fabrics

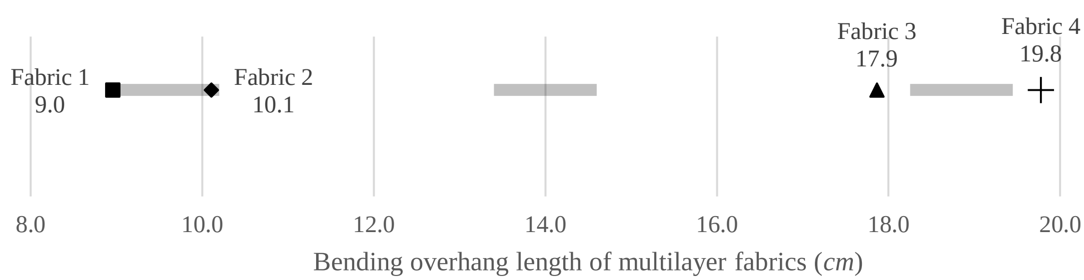

Figure 4.10 – Bending overhang length of multilayer fabrics

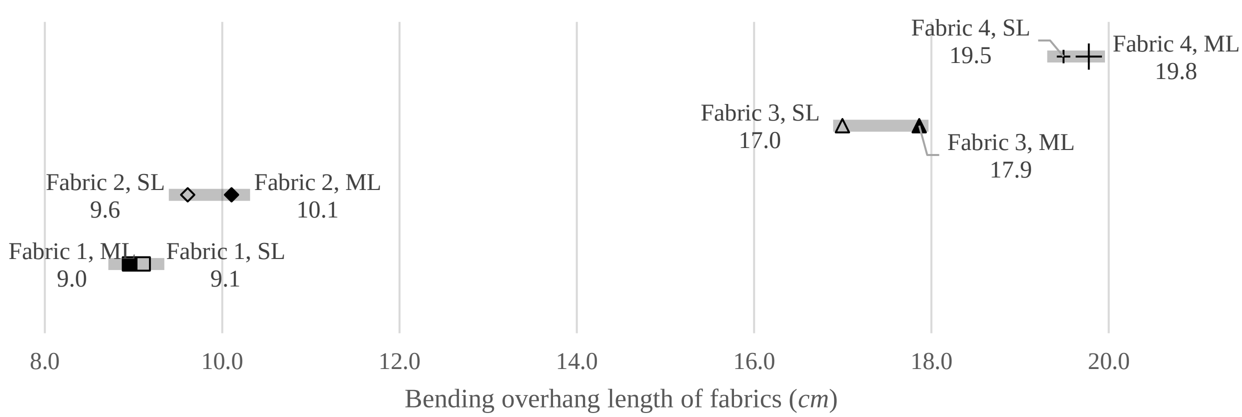

Figure 4.11 – Bending overhang length of fabrics

ANOVA results for overhang length are similar to ANOVA results for bending stiffness. The single layer and multilayer overhang lengths of Fabric 1 and Fabric 2 are not detectably different. The remaining single layer and multilayer overhang lengths are detectably different. Key differences between the overhang length and bending stiffness are shown in Figure 4.11, where there are no detectable differences between single and multilayer fabrics. Results of ANOVA for bending stiffness showed that there were detectable differences between single and multilayer bending stiffness values of each fabric.

4.1.4. DOE 4.1.B – Overhang Length

The linear functions used for interpolating the overhang length of fabrics take the same form as the bending stiffness linear functions. Interpolation modalities are also identical in their nature, although their values differ. Constants and coefficients for each linear function are shown in Table 4.5.

Table 4.5 – Linear function coefficients and constants for overhang length

Fabric	**Range**	***C_0* *(cm)***	***C_1* *(cm)***	***C_2* *(cm)***	***C_{12}* *(cm)***
Fabric 1	$0° < \theta \leq 45°$	9.03	0.07	-1.28	0.18
	$45° < \theta \leq 90°$	7.75	0.10	0.00	-0.15
Fabric 2	$0° < \theta \leq 45°$	11.10	0.00	-1.00	-0.30
	$45° < \theta \leq 90°$	8.88	-0.02	-1.23	0.28
Fabric 3	$0° < \theta \leq 45°$	11.95	0.30	-3.25	-0.10
	$45° < \theta \leq 90°$	14.18	0.33	5.48	0.13

The linear functions for each fabric appear in Figure 4.12 to Figure 4.14. The curves representing the overhang length of multilayer samples are virtually identical to those for the overhang length of single layer samples. Overhang length is most heavily affected by the yarn orientation of the fabric.

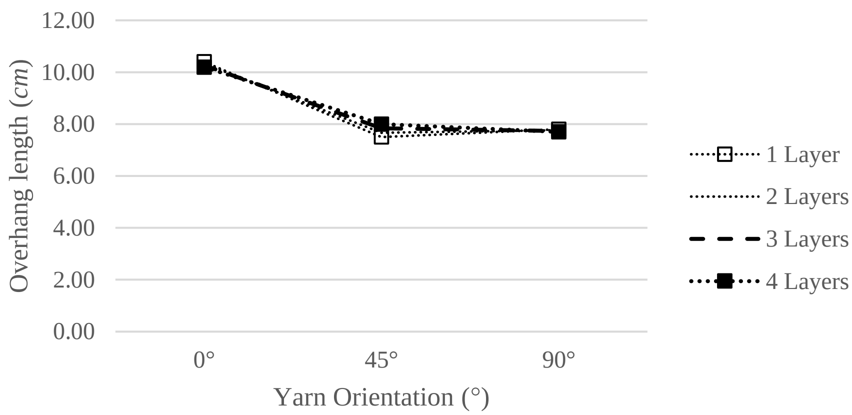

Figure 4.12 – Overhang length linear interpolation function for Fabric 1

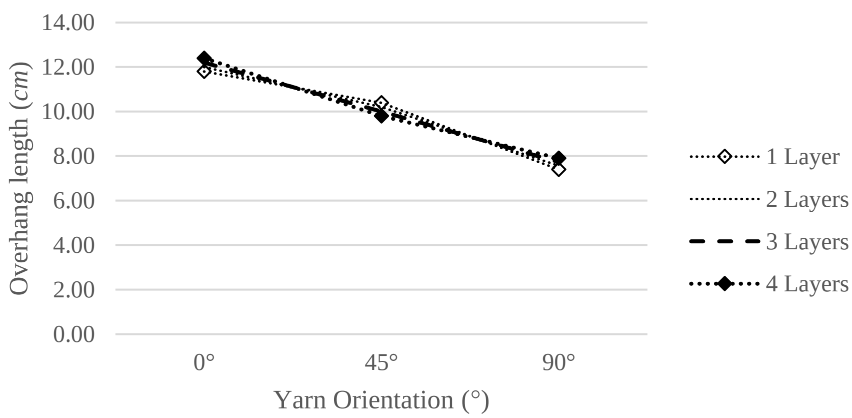

Figure 4.13 – Overhang length linear interpolation function for Fabric 2

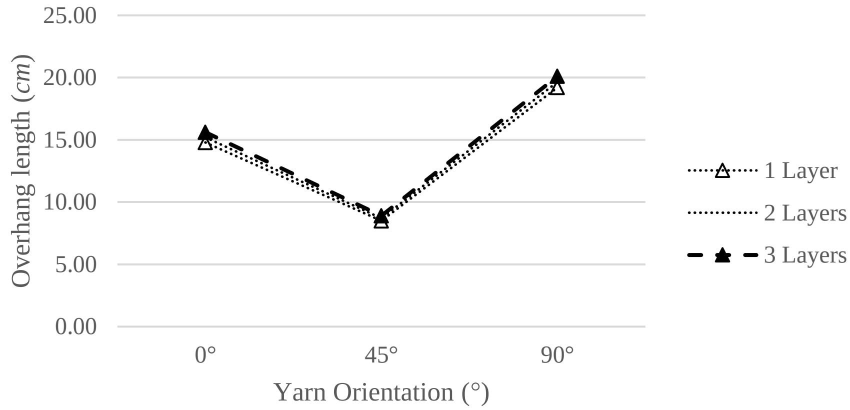

Figure 4.14 – Overhang length linear interpolation function for Fabric 3

These results suggest that each layer in multilayer fabrics bends individually, around their own neutral axis, because values of the bending stiffness of multilayer fabrics scale, approximately, to the number of layers in the multilayer fabric; the number of layers was not found to affect the overhang length of fabrics. The bending stiffness of multilayer fabrics along any orientation may be approximated by multiplying the single layer bending stiffness along said orientation by the number of layers used in the fabric.

4.2. Bending spring back

The measurement of bending spring back was introduced in this thesis as a novel method for quantifying behaviour observed in production. The procedure presented in Chapter 3 was used for characterizing the spring back behaviour of Fabrics 1, 2, 3 and 4, along the warp, bias and weft directions for Fabrics 1, 2 and 3 and along the warp and weft for Fabric 4. Multilayered stacks of Fabrics 1 and 2 featured four layers, and multilayered stacks of Fabrics 3 and 4 featured three layers. Tests were conducted over mould radii of 1.59 *mm* (1/16th *in*), 3.18 *mm* (1/8th *in*), 6.35 *mm* (1/4th *in*), 9.52 *mm* (3/8th *in*) and 12.70 *mm* (1/2 *in*) for both convex and concave corners.

4.2.1. Convex moulds

Results from convex spring back tests appear in Figure 4.15 and in Figure 4.16 for single layer and multilayer fabrics, respectively. The average SBR of the warp and weft directions are used for representing bending spring back of each fabric for a convex SMR of 1.59 *mm*. Three ANOVAs are used for comparing SBR of single layer fabrics in Figure 4.17, multilayer fabrics in Figure 4.18), and comparing the single layer and multilayer stacks of each fabric in Figure 4.19.

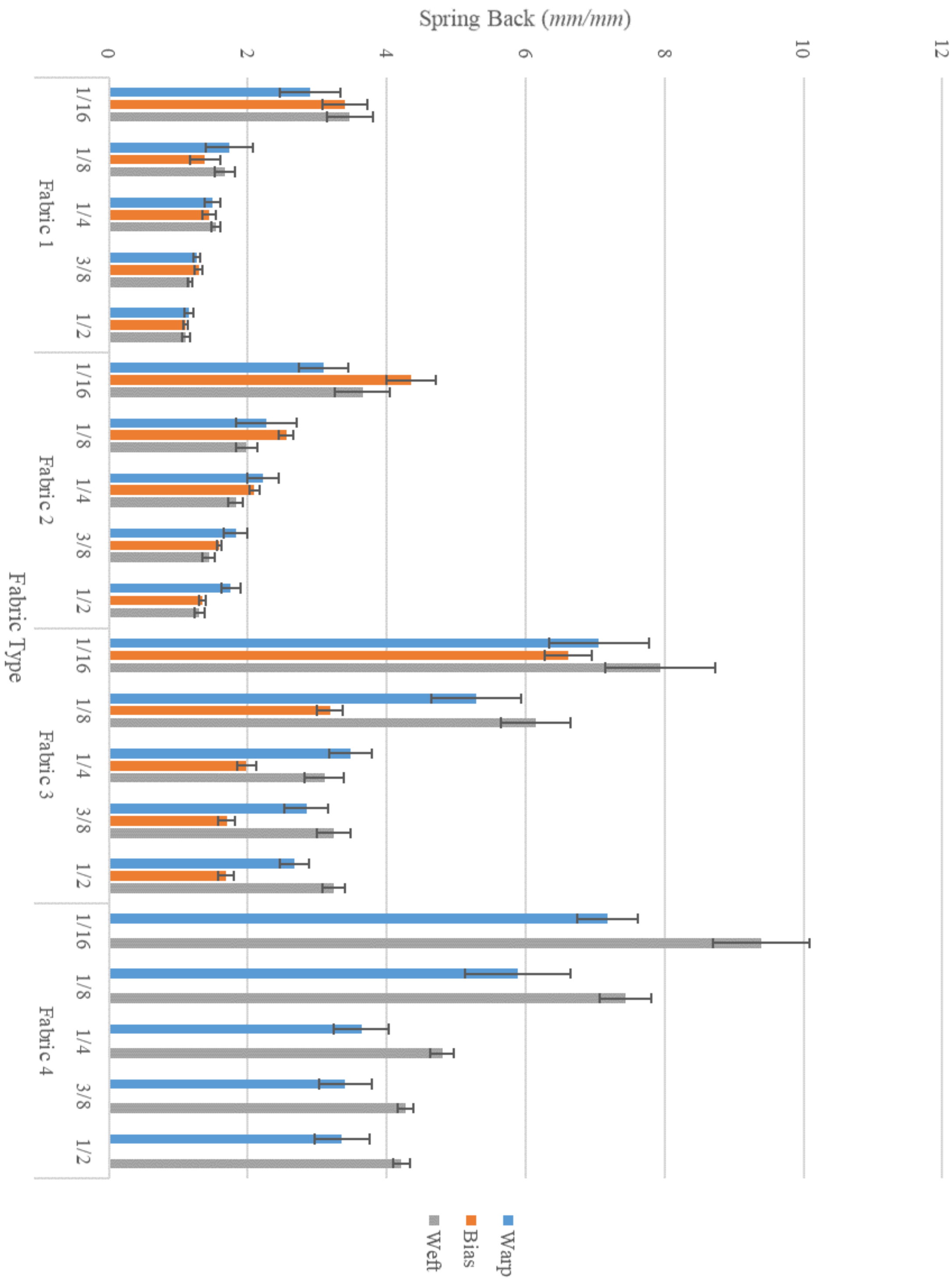

Figure 4.15 – Convex bending spring back of single layer fabrics

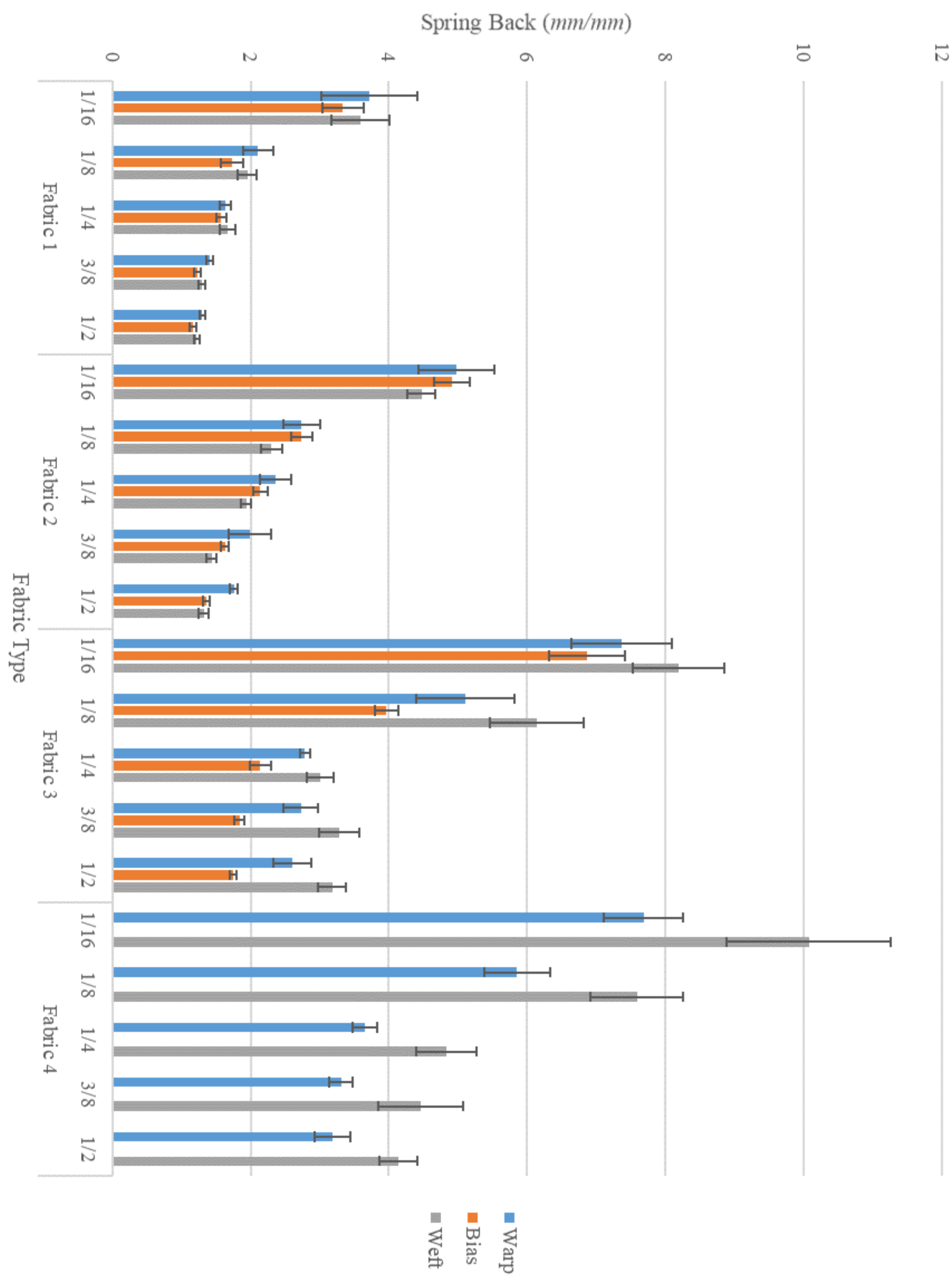

Figure 4.16 – Convex bending spring back of multilayer fabrics

4.2.1.1. ANOVA 4.2.A – Convex bending spring back

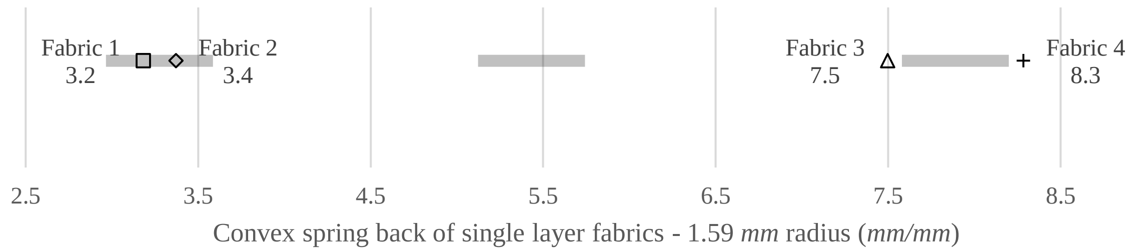

Figure 4.17 – Convex spring back of single layer fabrics – 1.59 *mm* (1/16th *in*) radius

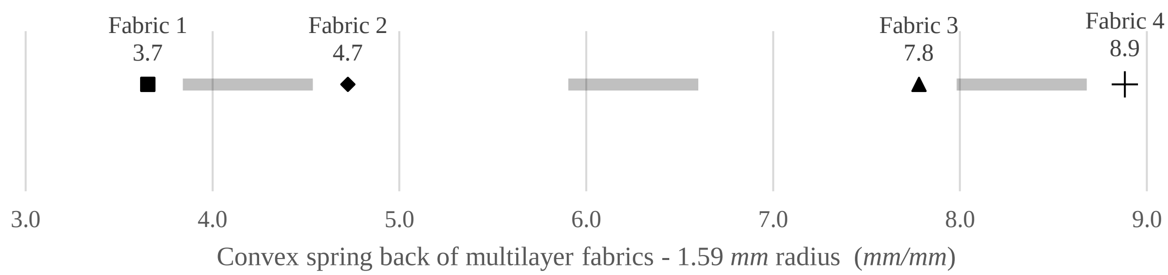

Figure 4.18 – Convex spring back of multilayer fabrics – 1.59 *mm* (1/16th *in*) radius

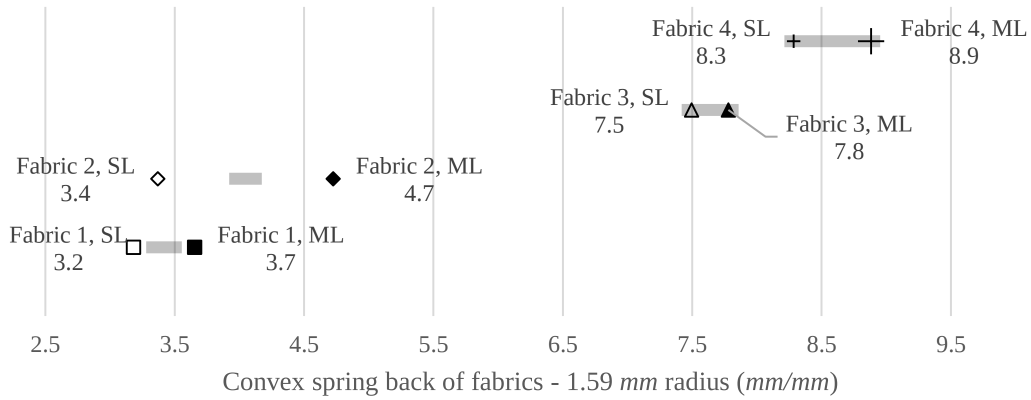

Figure 4.19 – Convex spring back of fabrics – 1.59 *mm* (1/16th *in*)

Convex spring back values of the single layer versions of Fabric 1 and Fabric 2 are not detectably different, while spring back values of single layer versions of Fabric 2, Fabric 3 and Fabric 4 are detectably different. All convex spring back values for multilayer fabrics are detectably different. The single layer and multilayer spring back values of Fabric 1 and Fabric 2 are detectably different, while the single layer and multilayer spring back values of Fabric 3 and Fabric 4 are not detectably different. The ratios of multilayer convex spring back values to single layer spring back of Fabric 1 and Fabric 2 are 1.16 and 1.38, respectively.

4.2.1.2. DOE 4.2.A – Convex bending spring back

Linear interpolation functions for the convex bending spring back take the form

$$f(x) = C_0 + C_1 \cdot x_1 + C_2 \cdot x_2 + C_{12} \cdot x_1 x_2 + C_3 x_3 + C_{13} x_1 x_3 + C_{23} x_2 x_3 + C_{123} x_1 x_2 x_3 \qquad (4.2)$$

where variables x_1 and x_2 are interpolation modalities for the number of layers in the fabric and for the yarn orientation – the same as the bending stiffness modalities, Table 4.3 – and variable x_3 is the interpolation modality for the mould radius, as listed in Table 4.6. Constant C_0 is an average and C_1, C_2, C_{12}, C_3, C_{13}, C_{23} and C_{123} are coefficients listed in Table 4.7. The convex spring back linear functions for each fabric are shown in Figure 4.20, Figure 4.21 and Figure 4.22.

Table 4.6 – Interpolation modalities for convex SBR

Fabric	Modality	Range	Interpolation
All Fabrics	x_3	$\frac{1}{16} < r \leq \frac{1}{8}$	$32\left(r - \frac{1}{16}\right) - 1$
All Fabrics	x_3	$\frac{1}{8} < r \leq \frac{1}{4}$	$16\left(r - \frac{1}{8}\right) - 1$
All Fabrics	x_3	$\frac{1}{4} < r \leq \frac{3}{8}$	$16\left(r - \frac{1}{4}\right) - 1$
All Fabrics	x_3	$\frac{3}{8} < r \leq \frac{1}{2}$	$16\left(r - \frac{3}{8}\right) - 1$

Table 4.7 – Linear function coefficients and constants for convex spring back interpolation functions

	Range		C_0	C_1	C_2	C_{12}	C_3	C_{13}	C_{23}	C_{123}
Fabric 1	$0° < \phi \leq 45°$	$\frac{1}{16} < r \leq \frac{1}{8}$	2.53	0.18	-0.08	-0.13	-0.80	0.00	-0.10	0.10
	$0° < \phi \leq 45°$	$\frac{1}{8} < r \leq \frac{1}{4}$	1.63	0.13	-0.10	0.00	-0.10	-0.05	0.08	0.03
	$0° < \phi \leq 45°$	$\frac{1}{4} < r \leq \frac{3}{8}$	1.41	0.04	-0.04	-0.01	-0.11	-0.04	-0.01	-0.04
	$0° < \phi \leq 45°$	$\frac{3}{8} < r \leq \frac{1}{2}$	1.25	0.03	-0.05	-0.03	-0.05	0.03	0.00	0.03
	$45° < \phi \leq 90°$	$\frac{1}{16} < r \leq \frac{1}{8}$	2.58	0.08	0.13	0.03	-0.88	0.08	0.02	-0.03
	$45° < \phi \leq 90°$	$\frac{1}{8} < r \leq \frac{1}{4}$	1.63	0.13	0.10	0.00	-0.08	-0.03	-0.05	0.00
	$45° < \phi \leq 90°$	$\frac{1}{4} < r \leq \frac{3}{8}$	1.40	0.05	0.03	0.03	-0.15	-0.05	-0.03	0.03
	$45° < \phi \leq 90°$	$\frac{3}{8} < r \leq \frac{1}{2}$	1.20	0.03	0.00	0.03	-0.05	0.03	0.00	-0.03
Fabric 2	$0° < \phi \leq 45°$	$\frac{1}{16} < r \leq \frac{1}{8}$	3.45	0.38	0.18	-0.20	-0.88	-0.25	-0.10	0.13
	$0° < \phi \leq 45°$	$\frac{1}{8} < r \leq \frac{1}{4}$	2.39	0.13	-0.10	0.00	-0.10	-0.05	0.08	0.03
	$0° < \phi \leq 45°$	$\frac{1}{4} < r \leq \frac{3}{8}$	1.98	0.04	-0.04	-0.01	-0.11	-0.04	-0.01	-0.04
	$0° < \phi \leq 45°$	$\frac{3}{8} < r \leq \frac{1}{2}$	1.66	0.03	-0.05	-0.03	-0.05	0.03	0.00	0.03
	$45° < \phi \leq 90°$	$\frac{1}{16} < r \leq \frac{1}{8}$	3.38	0.23	-0.25	0.05	-0.98	-0.13	0.00	0.00
	$45° < \phi \leq 90°$	$\frac{1}{8} < r \leq \frac{1}{4}$	2.19	0.13	0.10	0.00	-0.08	-0.03	-0.05	0.00
	$45° < \phi \leq 90°$	$\frac{1}{4} < r \leq \frac{3}{8}$	1.74	0.05	0.03	0.03	-0.15	-0.05	-0.03	0.03
	$45° < \phi \leq 90°$	$\frac{3}{8} < r \leq \frac{1}{2}$	1.41	0.03	0.00	0.03	-0.05	0.03	0.00	-0.03
Fabric 3	$0° < \phi \leq 45°$	$\frac{1}{16} < r \leq \frac{1}{8}$	5.70	0.15	-0.53	0.13	-1.30	0.00	-0.28	0.13
	$0° < \phi \leq 45°$	$\frac{1}{8} < r \leq \frac{1}{4}$	3.50	0.13	-0.10	0.00	-0.10	-0.05	0.08	0.03
	$0° < \phi \leq 45°$	$\frac{1}{4} < r \leq \frac{3}{8}$	2.43	0.04	-0.04	-0.01	-0.11	-0.04	-0.01	-0.04
	$0° < \phi \leq 45°$	$\frac{3}{8} < r \leq \frac{1}{2}$	2.21	0.03	-0.05	-0.03	-0.05	0.03	0.00	0.03
	$45° < \phi \leq 90°$	$\frac{1}{16} < r \leq \frac{1}{8}$	6.13	0.18	0.95	-0.10	-1.28	0.03	0.30	-0.10
	$45° < \phi \leq 90°$	$\frac{1}{8} < r \leq \frac{1}{4}$	3.70	0.13	0.10	0.00	-0.08	-0.03	-0.05	0.00
	$45° < \phi \leq 90°$	$\frac{1}{4} < r \leq \frac{3}{8}$	2.53	0.05	0.03	0.03	-0.15	-0.05	-0.03	0.03
	$45° < \phi \leq 90°$	$\frac{3}{8} < r \leq \frac{1}{2}$	2.48	0.03	0.00	0.03	-0.05	0.03	0.00	-0.03

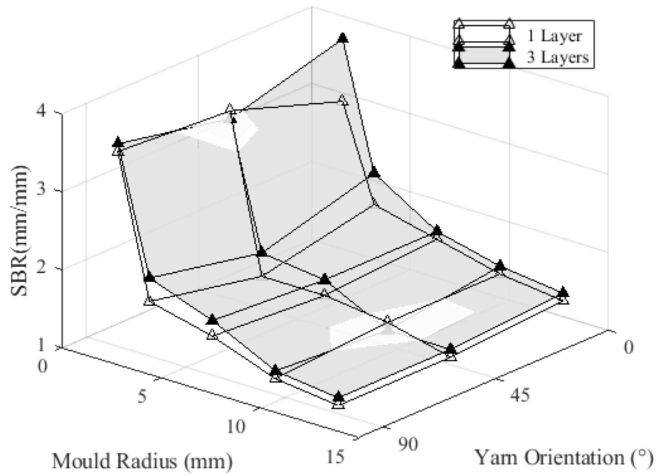

Figure 4.20 – Fabric 1 convex spring back interpolation function

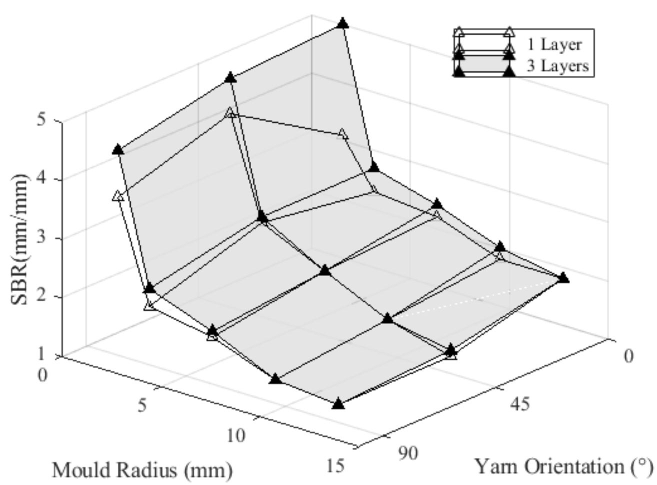

Figure 4.21 – Fabric 2 convex spring back interpolation function

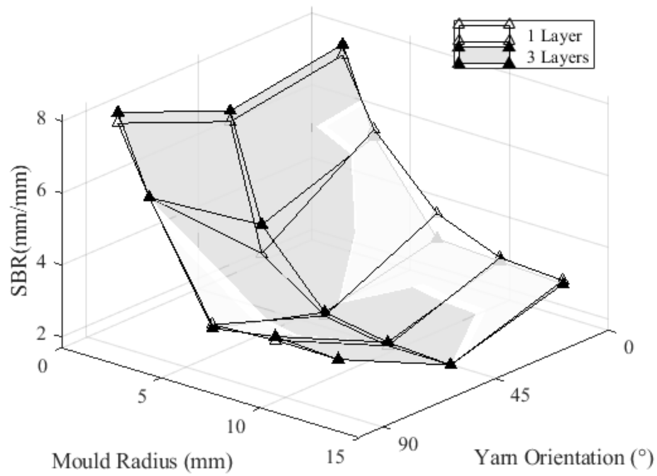

Figure 4.22 – Fabric 3 convex spring back interpolation function

Linear functions are shown for 1 layer of fabric and for 4 layers of fabric (Fabrics 1 and 2), or for 1 layer of fabric and for 3 layers of fabric (Fabric 3). The number of layers has a limited effect on the convex spring back of fabrics compared to the effect of the mould radius; however, the linear functions can still be used for interpolating spring back ratios for multilayer fabrics at any given number of layers.

4.2.2. Concave moulds

Results from concave spring back tests appear in Figure 4.23 and in Figure 4.24 for single layer and multilayer fabrics, respectively. The average SBR along the warp and weft directions are used for representing the bending spring back of each fabric for a concave SMR of 1.59 *mm*. Three ANOVAs are used for comparing concave SBR of single layer fabrics in Figure 4.25, multilayer fabrics in Figure 4.26, and for comparing the single and multilayer versions of each fabric, Figure 4.27.

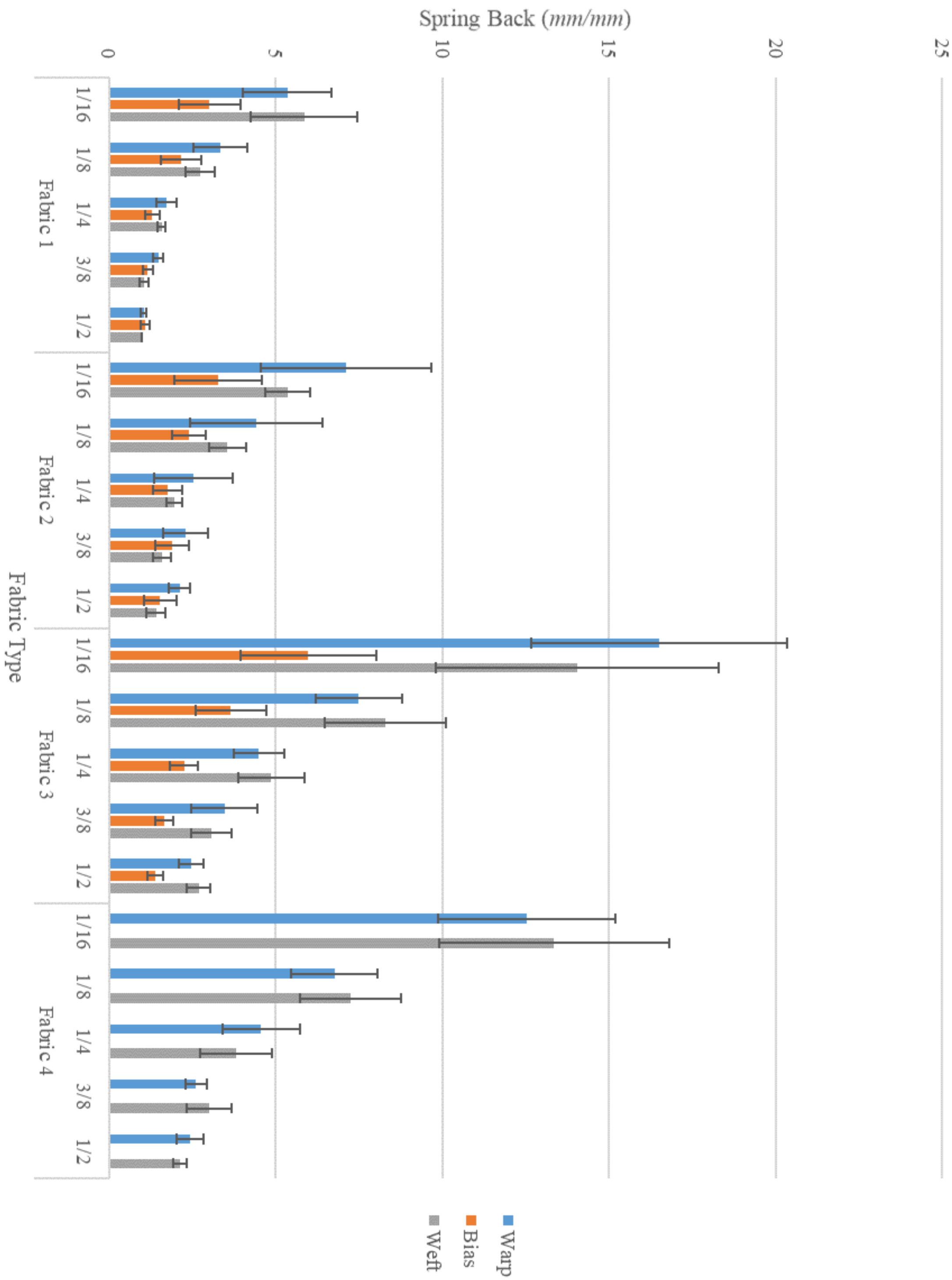

Figure 4.23 – Concave bending spring back of single layer fabrics

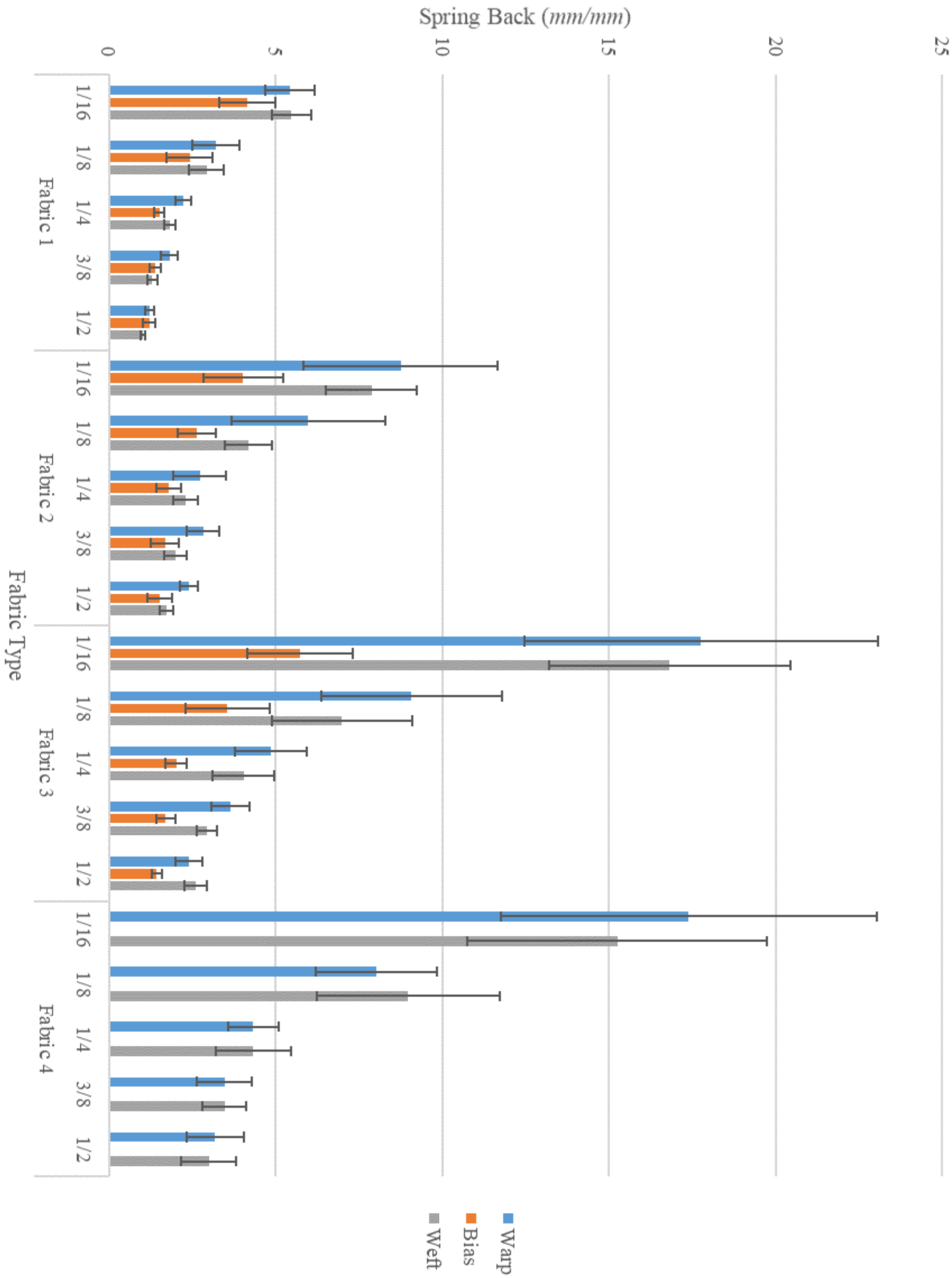

Figure 4.24 – Concave bending spring back of multilayer fabrics

4.2.2.1. ANOVA 4.2.B – Concave bending spring back

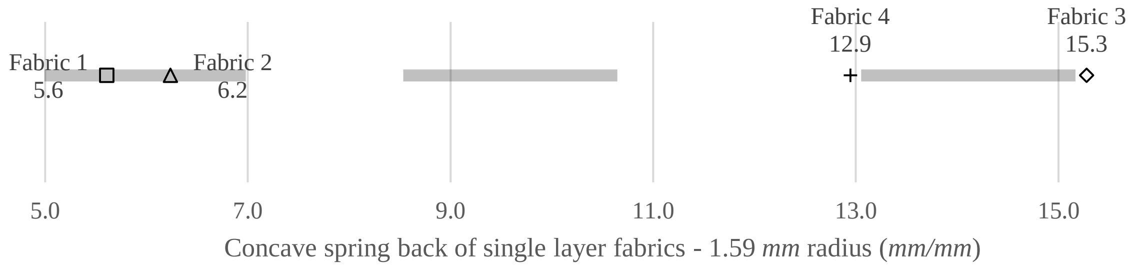

Figure 4.25 – Concave spring back of single layer fabrics – 1.59 *mm* radius

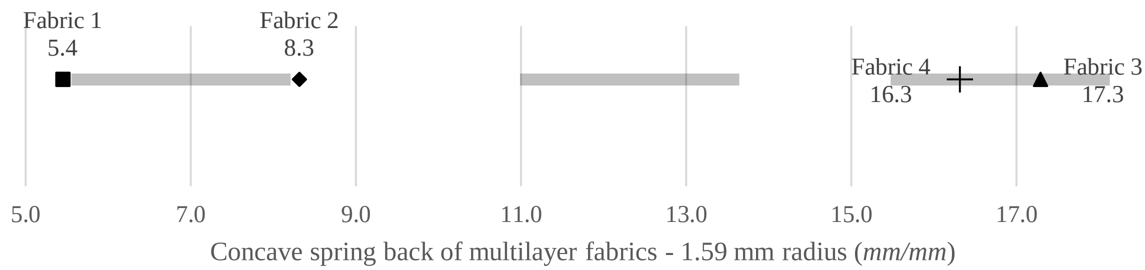

Figure 4.26 – Concave spring back of multilayer fabrics – 1.59 *mm* radius

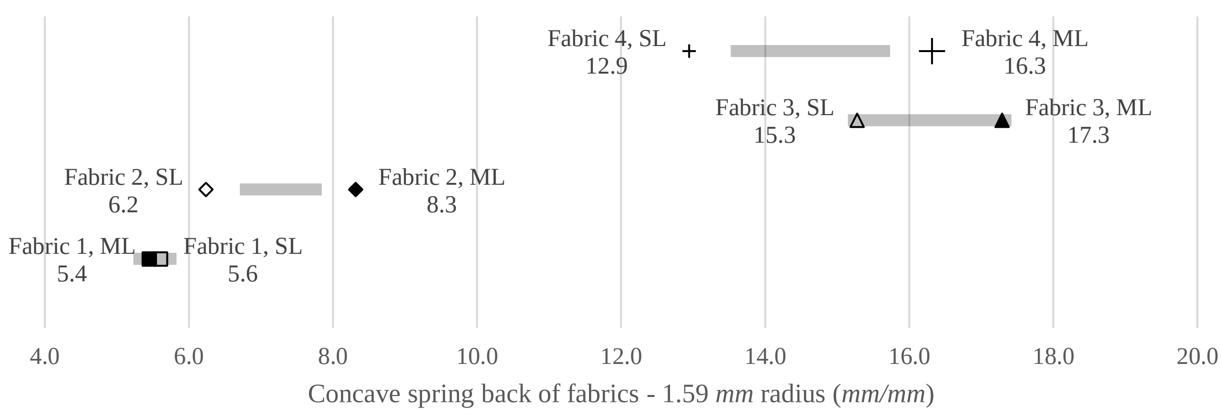

Figure 4.27 – Concave spring back of fabrics – 1.59 *mm* radius

Concave spring back values of single layer Fabric 1 and Fabric 2 are not detectably different, while the concave spring back values of single layer versions of Fabric 2, Fabric 3 and Fabric 4 are detectably different. The multilayer concave spring back values of Fabric 3 and Fabric 4 are not detectably different, while the spring back values of Fabric 1, Fabric 2 and Fabric 3 are detectably different. The spring back values of single and multilayer versions of Fabric 1 and Fabric 3 are not detectably different, while the spring back values of single and multilayer versions of Fabric 2 and Fabric 4 are detectably different. The ratios of multilayer to single layer spring back values of Fabric 2 and Fabric 4 are 1.34 and 1.26, respectively.

4.2.2.2. DOE 4.2.B – Concave bending spring back

The linear interpolation functions for the concave bending spring back take the form

$$f(x) = C_0 + C_1 \cdot x_1 + C_2 \cdot x_2 + C_{12} \cdot x_1 x_2 + C_3 x_3 + C_{13} x_1 x_3 + C_{23} x_2 x_3 + C_{123} x_1 x_2 x_3 \tag{4.3}$$

where C_0 is a constant average and C_1, C_2, C_{12}, C_3, C_{13}, C_{23} and C_{123} are coefficients listed in Table 4.8. All concave modalities are identical to convex modalities. The linear functions for each fabric are shown in Figure 4.28, Figure 4.29 and Figure 4.30.

Table 4.8 – Linear function coefficients and constants for concave spring back interpolation functions

	Range		C_0	C_1	C_2	C_{12}	C_3	C_{13}	C_{23}	C_{123}
Fabric 1	$0° < \phi \le 45°$	$\frac{1}{16} < r \le \frac{1}{8}$	3.64	0.16	-0.69	0.19	-0.86	-0.14	0.21	-0.11
	$0° < \phi \le 45°$	$\frac{1}{8} < r \le \frac{1}{4}$	2.23	0.10	-0.38	0.00	-0.55	0.08	0.10	-0.08
	$0° < \phi \le 45°$	$\frac{1}{4} < r \le \frac{3}{8}$	1.58	0.15	-0.23	-0.05	-0.10	-0.03	0.05	0.03
	$0° < \phi \le 45°$	$\frac{3}{8} < r \le \frac{1}{2}$	1.30	0.10	-0.07	-0.03	-0.18	-0.03	0.10	0.00
	$45° < \phi \le 90°$	$\frac{1}{16} < r \le \frac{1}{8}$	3.60	0.15	0.65	-0.20	-1.05	-0.05	-0.40	0.20
	$45° < \phi \le 90°$	$\frac{1}{8} < r \le \frac{1}{4}$	2.05	0.10	0.20	0.00	-0.50	0.00	-0.05	0.00
	$45° < \phi \le 90°$	$\frac{1}{4} < r \le \frac{3}{8}$	1.40	0.10	0.05	0.00	-0.15	0.00	-0.10	0.00
	$45° < \phi \le 90°$	$\frac{3}{8} < r \le \frac{1}{2}$	1.16	0.06	-0.06	-0.01	-0.09	-0.04	-0.01	-0.01
Fabric 2	$0° < \phi \le 45°$	$\frac{1}{16} < r \le \frac{1}{8}$	4.83	0.53	-1.75	-0.30	-0.98	-0.08	0.40	-0.05
	$0° < \phi \le 45°$	$\frac{1}{8} < r \le \frac{1}{4}$	3.03	0.10	-0.38	0.00	-0.55	0.08	0.10	-0.08
	$0° < \phi \le 45°$	$\frac{1}{4} < r \le \frac{3}{8}$	2.19	0.15	-0.23	-0.05	-0.10	-0.03	0.05	0.03
	$0° < \phi \le 45°$	$\frac{3}{8} < r \le \frac{1}{2}$	2.03	0.10	-0.07	-0.03	-0.18	-0.03	0.10	0.00
	$45° < \phi \le 90°$	$\frac{1}{16} < r \le \frac{1}{8}$	4.18	0.50	1.10	0.28	-0.98	-0.30	-0.40	-0.18
	$45° < \phi \le 90°$	$\frac{1}{8} < r \le \frac{1}{4}$	2.59	0.10	0.20	0.00	-0.50	0.00	-0.05	0.00
	$45° < \phi \le 90°$	$\frac{1}{4} < r \le \frac{3}{8}$	1.89	0.10	0.05	0.00	-0.15	0.00	-0.10	0.00
	$45° < \phi \le 90°$	$\frac{3}{8} < r \le \frac{1}{2}$	1.66	0.06	-0.06	-0.01	-0.09	-0.04	-0.01	-0.01
Fabric 3	$0° < \phi \le 45°$	$\frac{1}{16} < r \le \frac{1}{8}$	8.74	0.31	-3.99	-0.41	-2.76	0.06	1.66	-0.01
	$0° < \phi \le 45°$	$\frac{1}{8} < r \le \frac{1}{4}$	4.70	0.10	-0.38	0.00	-0.55	0.08	0.10	-0.08
	$0° < \phi \le 45°$	$\frac{1}{4} < r \le \frac{3}{8}$	3.03	0.15	-0.23	-0.05	-0.10	-0.03	0.05	0.03
	$0° < \phi \le 45°$	$\frac{3}{8} < r \le \frac{1}{2}$	2.28	0.10	-0.07	-0.03	-0.18	-0.03	0.10	0.00
	$45° < \phi \le 90°$	$\frac{1}{16} < r \le \frac{1}{8}$	8.18	0.18	3.43	0.28	-2.45	-0.45	-1.35	-0.50
	$45° < \phi \le 90°$	$\frac{1}{8} < r \le \frac{1}{4}$	4.51	0.10	0.20	0.00	-0.50	0.00	-0.05	0.00
	$45° < \phi \le 90°$	$\frac{1}{4} < r \le \frac{3}{8}$	2.81	0.10	0.05	0.00	-0.15	0.00	-0.10	0.00
	$45° < \phi \le 90°$	$\frac{3}{8} < r \le \frac{1}{2}$	2.18	0.06	-0.06	-0.01	-0.09	-0.04	-0.01	-0.01

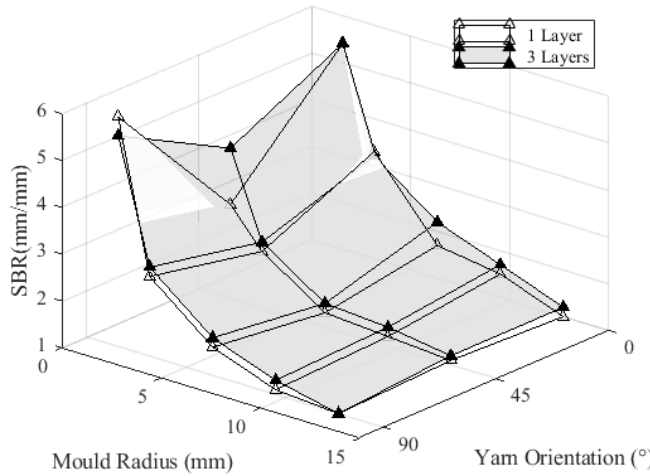

Figure 4.28 – Fabric 1 concave spring back linear function

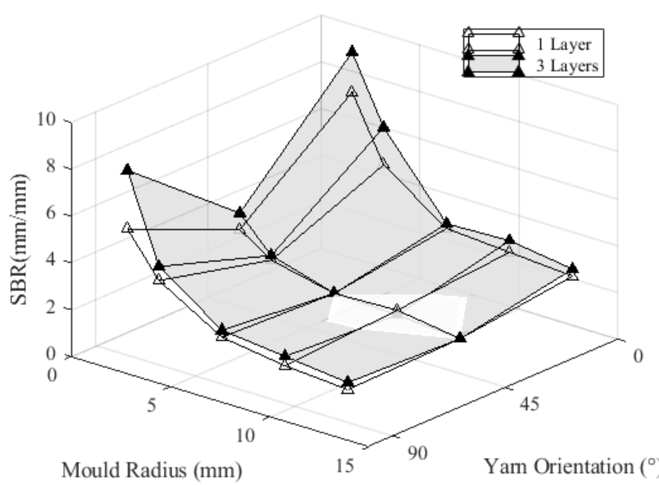

Figure 4.29 – Fabric 2 concave spring back linear function

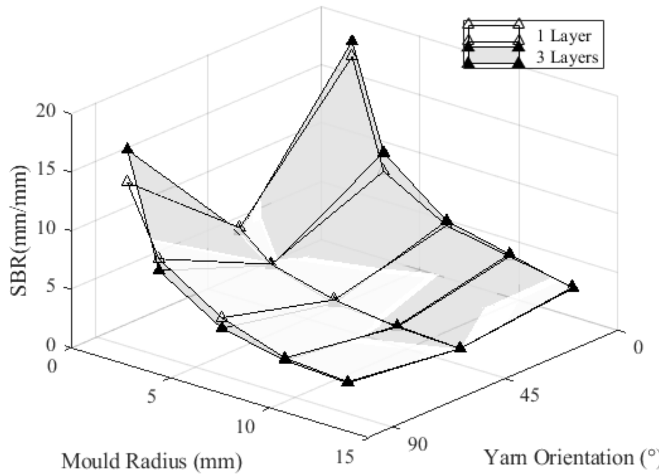

Figure 4.30 – Fabric 3 concave spring back linear function

Linear functions are shown for 1 layer of fabric and for 4 layers of fabric (Fabrics 1 and 2), or for 1 layer of fabric and for 3 layers of fabric (Fabric 3). The number of layers has a limited effect on the concave spring back of fabrics; however, the linear functions can still be used for interpolating spring back ratios for multilayer fabrics at any given number of layers.

4.3. In-plane shear

Fabrics undergo large in-plane shear deformations when draped onto moulds. The picture-frame shear test was used for characterizing the maximum in-plane shear load and the return angle of Fabrics 1, 2 and 3. Single and multilayer fabrics were tested. Multilayer samples of Fabrics 1 and 2 consisted of 4 layers of fabric; multilayer samples of Fabric 3 consisted of 3 layers of fabric. Five single layer and five multilayered samples were tested. Each sample was subjected to 5 cycles from 0° to 53° of shear. Extension rate of the universal testing frame was 60 *mm*/*min* for both loading and unloading portions of the cycles. Average normalized shear load plots from the 5th cycle testing are shown in Figure 4.31 for all tested fabrics. The ANOVA results appear in Figure 4.32 to Figure 4.34 for the maximum normalized shear load, and in Figure 4.35 to Figure 4.37 for the return angle.

The maximum normalized shear loads reached by single layer (Figure 4.32) and multilayer (Figure 4.33) fabrics are detectably different. The maximum normalized shear load of multilayer stacks of each fabric are detectably different from their single layer counterparts (Figure 4.34). The ratios of multilayer to single layer maximum normalized shear loads are 3.35, 2.67 and 2.72 for Fabric 1, Fabric 2 and Fabric 3 respectively.

The return angles of single layer fabrics are detectably different, Figure 4.35. The return angles of multilayer Fabric 1 and Fabric 2 are detectably different from Fabric 3. Multilayer return angles of Fabrics 1 and 2 are not detectably different, Figure 4.36. The return angles of multilayer fabrics are not detectably different from their single layer counterparts, Figure 4.37.

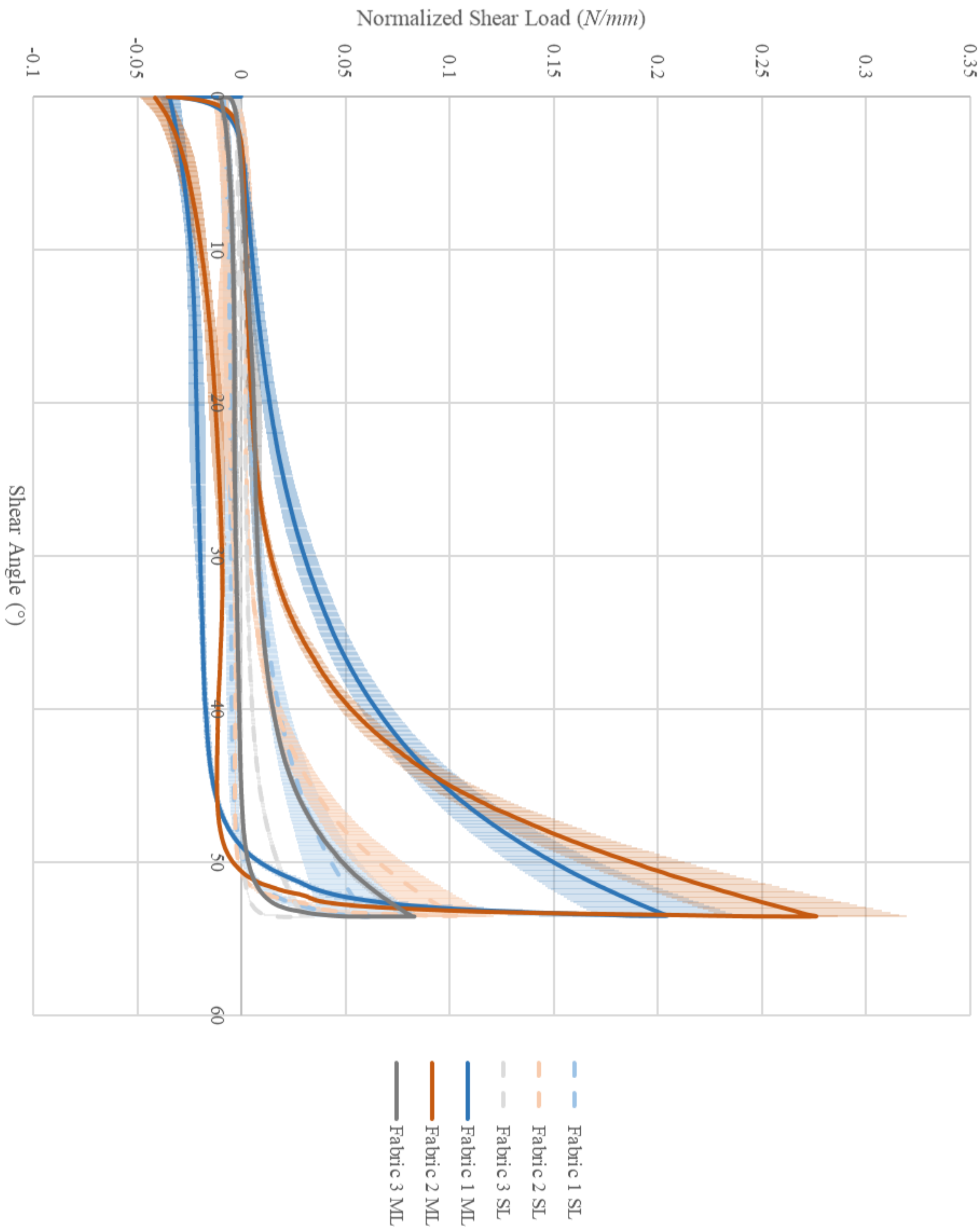

Figure 4.31 – Normalized shear load of tested fabrics

4.3.1. ANOVA 4.3.A – Normalized Shear Load

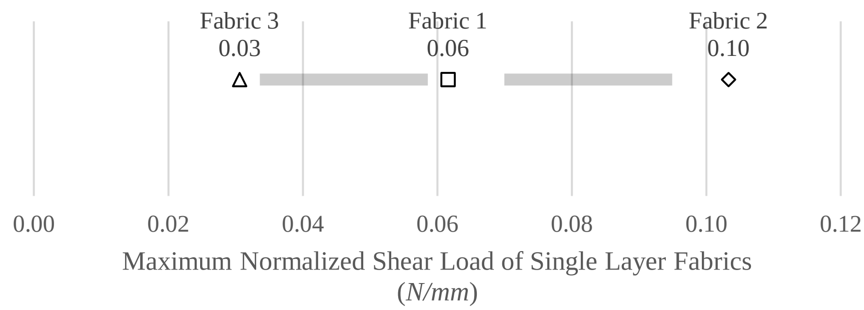

Figure 4.32 – Maximum normalized shear load of single layer fabrics

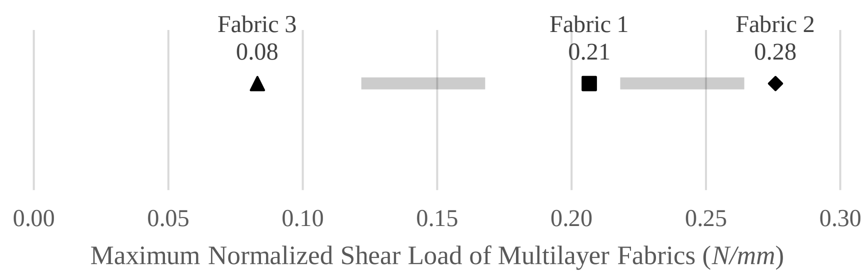

Figure 4.33 – Maximum normalized shear load of multilayer fabrics

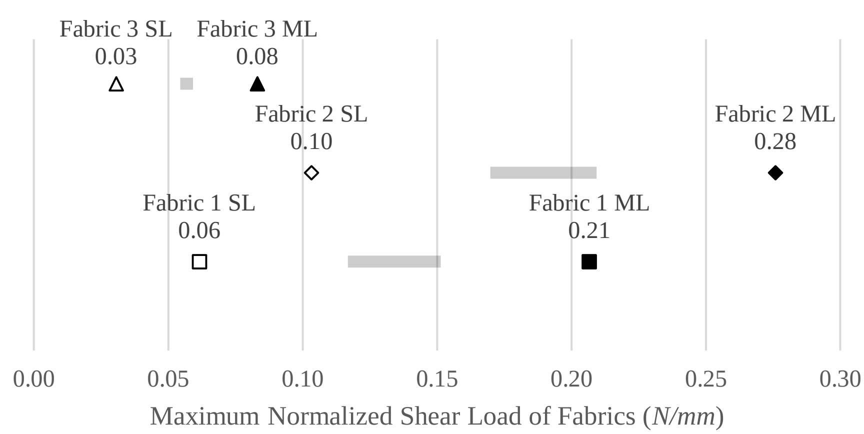

Figure 4.34 – Maximum normalized shear load of fabrics

4.3.2. ANOVA 4.3.B – Return Angle

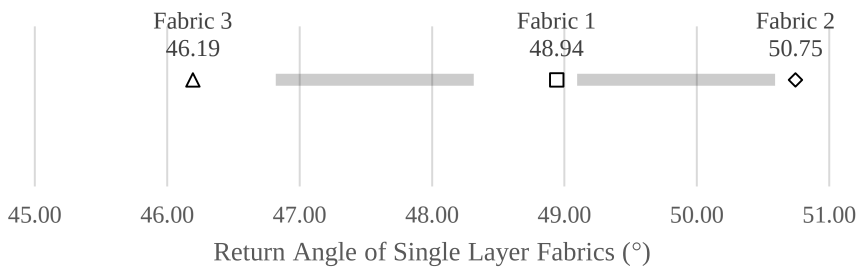

Figure 4.35 – Return angle of single layer fabrics

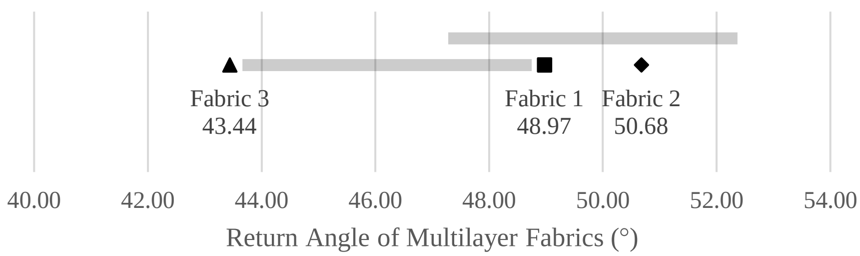

Figure 4.36 – Return angle of multilayer fabrics

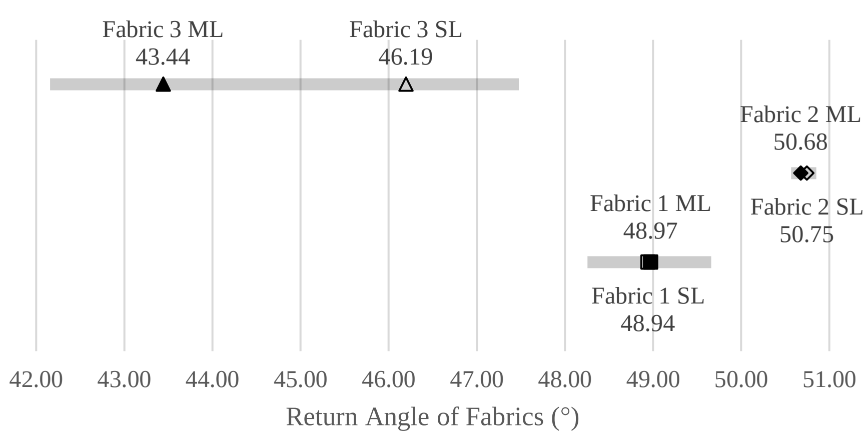

Figure 4.37 – Return angle of fabrics

4.3.3. DOE 4.3.A – Normalized Shear Load

While DOEs are extremely useful in creating linear interpolation functions for fabric characteristics when factors are set at two levels, the normalized shear load of fabrics is a function of the shear angle and number of layers in the fabric stack. This relation was shown in Figure 4.31 and it clearly is non-linear. Using multiple linear regression, polynomial regression equations can be used for estimating the normalized shear load of fabrics. In this work, fifth order polynomials are used for curve-fitting in-plane shear, Figure 4.38.

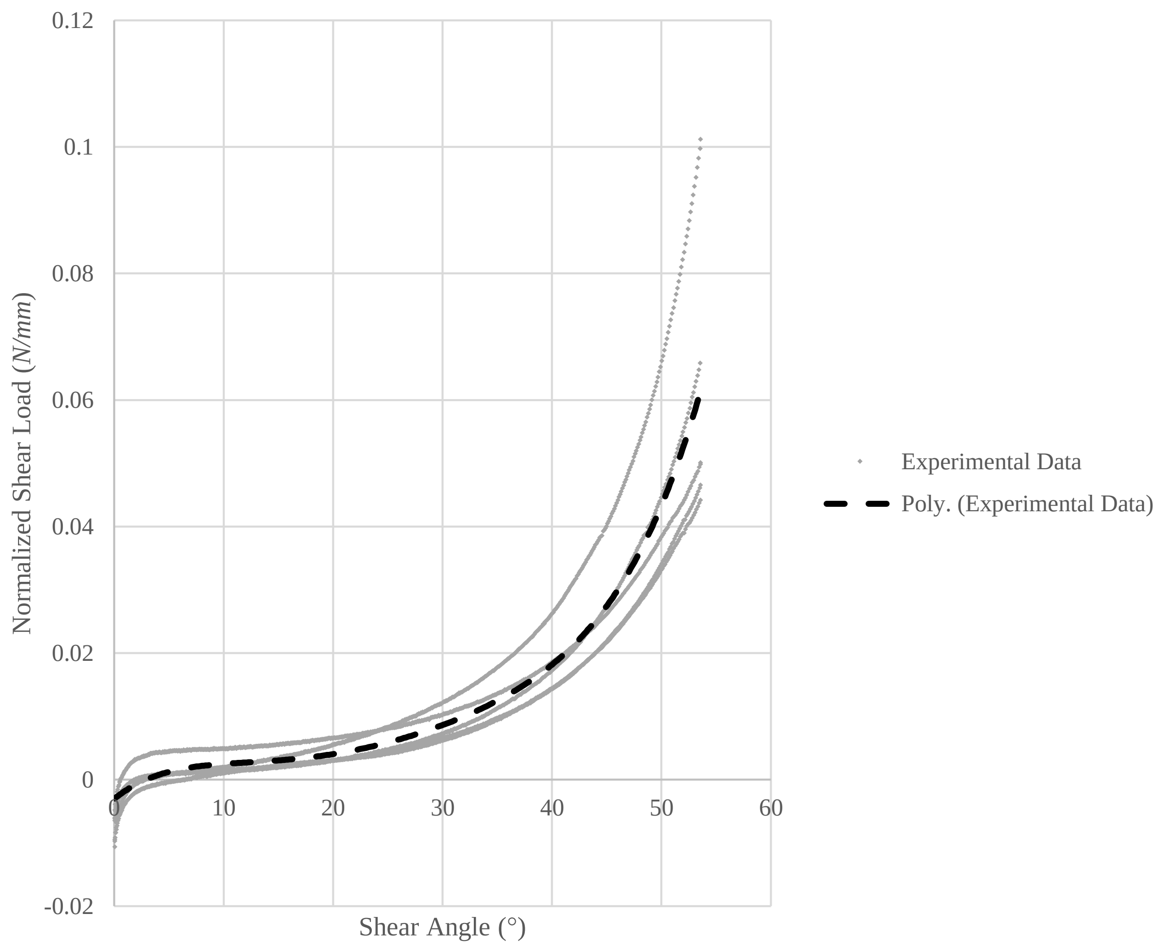

Figure 4.38 – Polynomial regressions for Fabric 1 single layer normalized shear load

The polynomial regression takes the form

$$f(x) = a_0 + a_1\gamma + a_2\gamma^2 + a_3\gamma^3 + a_4\gamma^4 + a_5\gamma^5 \quad (4.4)$$

where γ is the shear angle of the fabric (°). Coefficients a_0, a_1, a_2, a_3, a_4 and a_5, and the adjusted R^2 are listed in Table 4.9. Regressions are shown in Figure 4.39.

Table 4.9 – Polynomial regression coefficients for normalized shear load

	Number of layers	a_0	a_1	a_2	a_3	a_4	a_5	R^2
Fabric 1	1	-3.04E-03	1.39E-03	-1.35E-04	6.44E-06	-1.36E-07	1.15E-09	0.88
	4	-1.51E-02	5.16E-03	-4.84E-04	2.25E-05	-4.61E-07	3.79E-09	0.97
Fabric 2	1	-2.77E-03	1.85E-03	-2.00E-04	9.30E-06	-2.06E-07	1.92E-09	0.96
	4	-1.20E-02	4.13E-03	-4.09E-04	1.89E-05	-4.15E-07	3.99E-09	0.98
Fabric 3	1	-1.68E-03	7.34E-04	-7.90E-05	4.19E-06	-1.01E-07	9.22E-10	0.98
	3	-4.51E-03	1.44E-03	-1.28E-04	7.09E-06	-1.87E-07	1.87E-09	0.98

A comparison between average values of normalized shear load, Figure 4.31 and predicted values of normalized shear load using polynomial regressions, Figure 4.39 is shown in Table 4.10 and in Table 4.11. The polynomial regressions estimate the average normalized shear load accurately over the ranges of shear angles tested.

Table 4.10 – Average and regression normalized shear loads at smaller shear angles

	Number of layers	20°		30°	
		Average	Regression	Average	Regression
Fabric 1	1	4.24E-03	4.03E-03	8.46E-03	8.61E-03
	4	1.37E-02	1.29E-02	3.02E-02	3.04E-02
Fabric 2	1	2.07E-03	2.07E-03	4.14E-03	4.17E-03
	4	5.01E-03	4.37E-03	1.41E-02	1.44E-02
Fabric 3	1	1.75E-03	1.69E-03	2.80E-03	2.88E-03
	3	6.12E-03	5.68E-03	8.10E-0	8.61E-03

Table 4.11 – Average and regression normalized shear loads at larger shear angles

	Number of layers	45°		50°	
		Average	Regression	Average	Regression
Fabric 1	1	2.74E-02	2.74E-02	4.33E-02	4.33E-02
	4	9.70E-02	9.70E-02	1.49E-01	1.50E-01
Fabric 2	1	3.39E-02	3.36E-02	6.54E-02	6.61E-02
	4	1.00E-01	1.01E-01	1.87E-01	1.86E-01
Fabric 3	1	8.66E-03	8.83E-03	1.74E-02	1.77E-02
	3	2.51E-02	2.54E-02	4.84E-02	4.96E-02

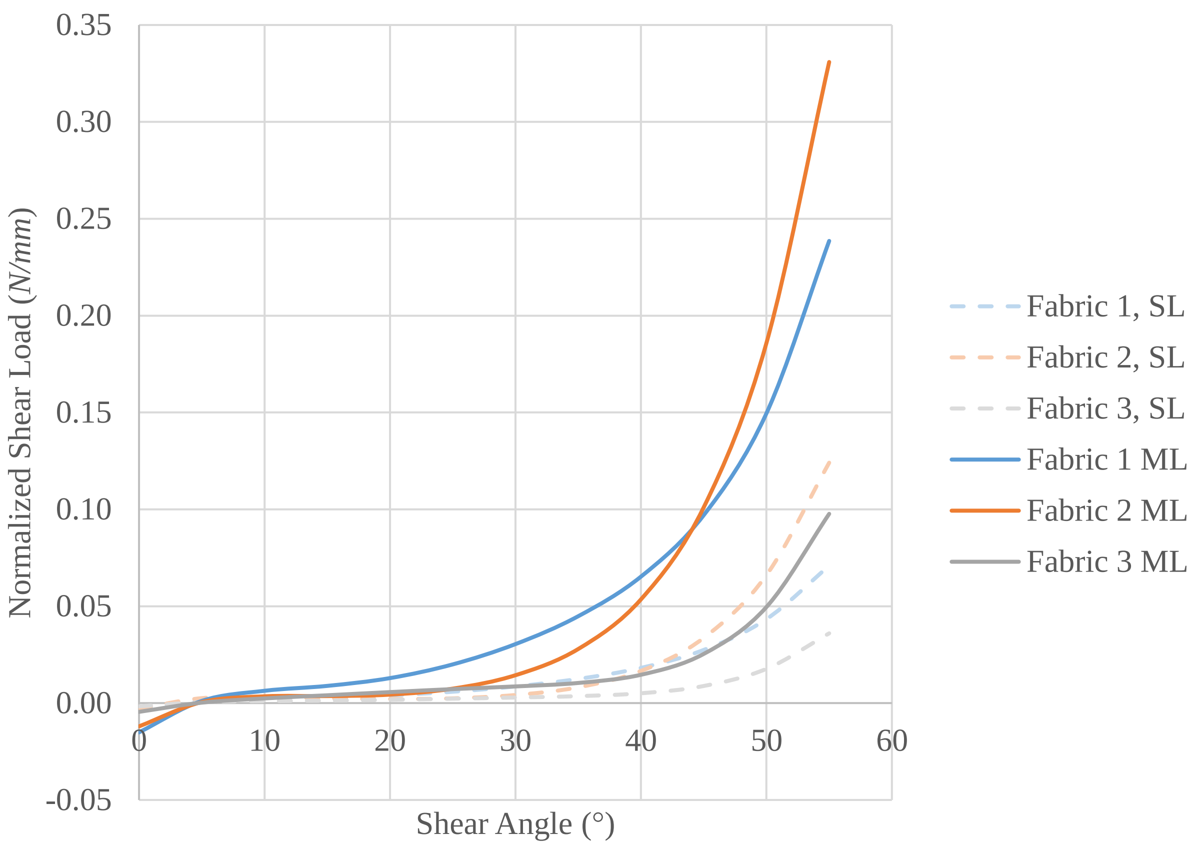

Figure 4.39 – Normalized shear regression of experimental data for tested fabrics

4.4. Friction

Individual layers of fabric within a multilayer stack may slide relative to each other while being draped onto moulds. This sliding causes significant difficulties to technicians manufacturing composite parts. The mean coefficient of friction and the mean deviation of the coefficient of friction were characterised for Fabric 1, Fabric 2 and Fabric 3 using the methodology presented in Chapter Chapter 3. Five tests per yarn orientation were conducted for every fabric. The frictional characteristics are defined over the first 5 *mm* of displacement, Section 3.2.4. The mean coefficient of friction for each fabric is shown in Figure 4.40, while the mean deviations of coefficient of friction are shown in Figure 4.41.

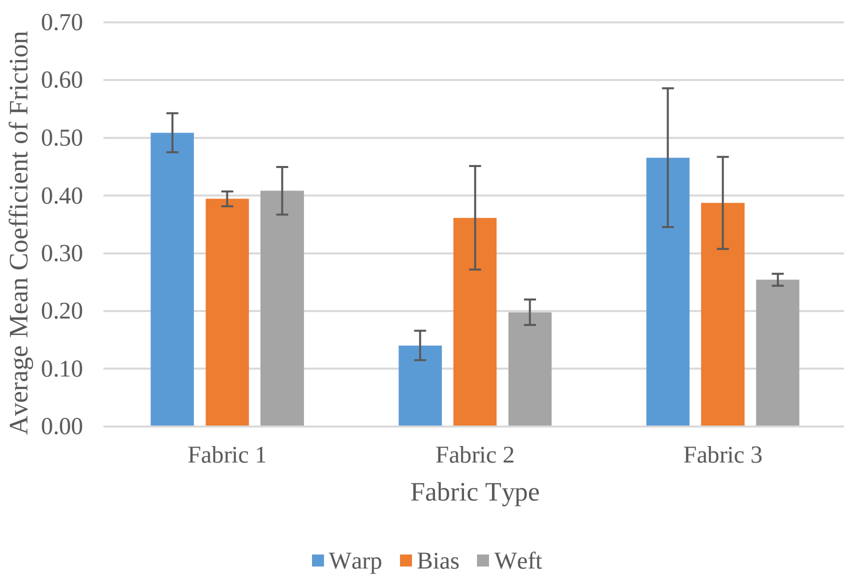

Figure 4.40 – Average mean coefficient of friction of Fabrics 1, 2 and 3

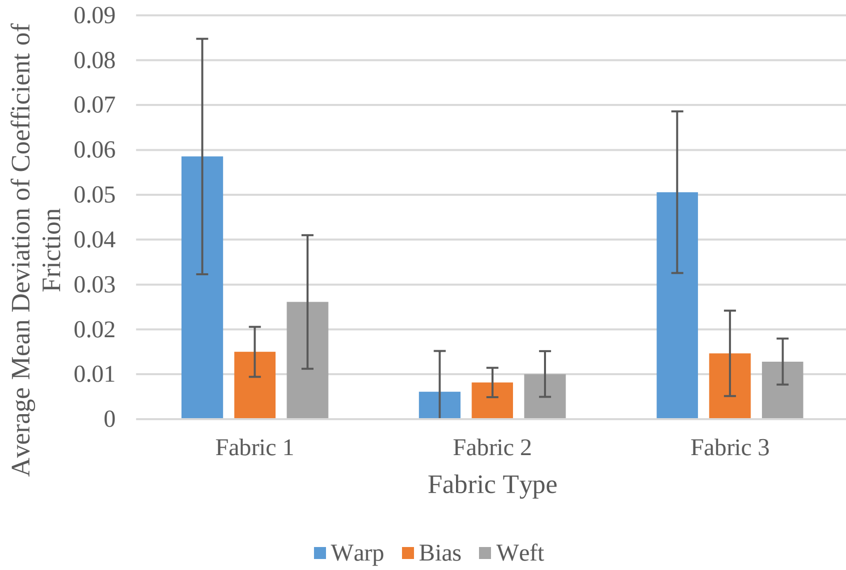

Figure 4.41 – Average mean deviation of the coefficient of friction of Fabrics 1, 2 and 3

4.4.1. ANOVA 4.4.A – Mean coefficient of friction

The average mean coefficients of friction along the warp and weft directions were used for comparing the performance of each fabric. The ANOVA for the mean coefficient of friction of each fabric is shown in Figure 4.42. The average mean coefficients of friction of every fabric were found to be detectably different.

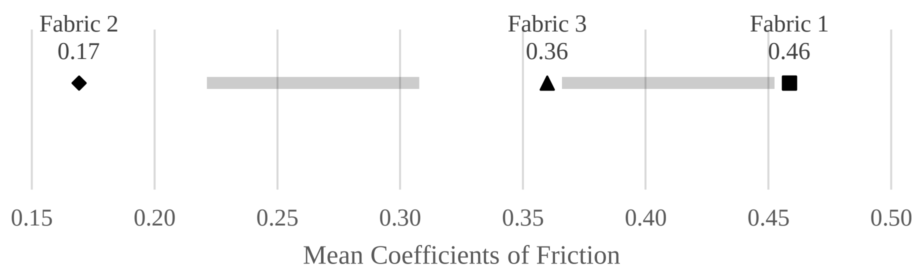

Figure 4.42 – Mean coefficient of friction of fabrics

4.4.2. DOE 4.4.A – Mean coefficient of friction

The linear functions used for interpolating the mean coefficient of friction of fabrics take the form

$$f(x) = C_0 + C_2 \cdot x_2 \tag{4.5}$$

where C_0 is a constant average and C_2 is a coefficient listed in Table 4.12. x_2 is an interpolation modality that represents the yarn orientation of the fabric, found in Table 4.3. The linear functions for all fabrics appear in Figure 4.43.

Table 4.12 – Linear function coefficients for mean coefficient of friction

Fabric	Range	C_0	C_2
Fabric 1	$0° < \phi \leq 45°$	4.52E-01	-2.86E-02
	$45° < \phi \leq 90°$	4.01E-01	3.49E-03
Fabric 2	$0° < \phi \leq 45°$	2.51E-01	5.53E-02
	$45° < \phi \leq 90°$	2.80E-01	-4.09E-02
Fabric 3	$0° < \phi \leq 45°$	4.26E-01	-1.96E-02
	$45° < \phi \leq 90°$	3.21E-01	-3.33E-02

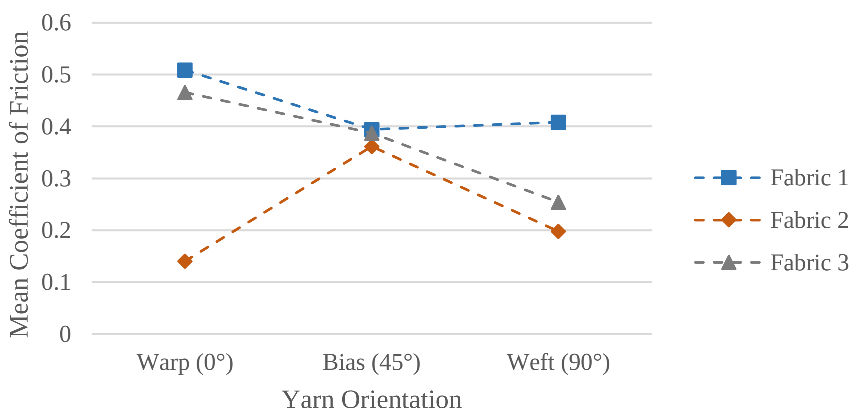

Figure 4.43 – Linear functions of mean coefficient of friction (all fabrics)

4.4.3. ANOVA 4.4.B – Mean deviation of coefficient of friction

The average mean deviations of coefficients of friction along the warp and weft directions were used for comparing the performance of each fabric. The ANOVA for the mean deviations of coefficient of friction is shown in Figure 4.44. The mean deviations of Fabric 1 and Fabric 3 are not detectably different, while the mean deviation of Fabric 2 is detectably smaller than that of both other fabrics.

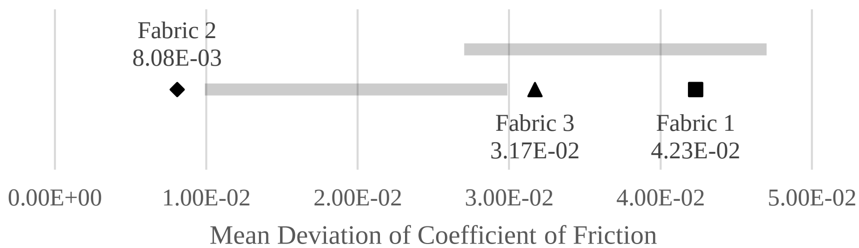

Figure 4.44 – Mean deviation of coefficient of friction of fabrics

4.4.4. DOE 4.4.B – Mean deviation of coefficient of friction

The linear functions used for interpolating the mean deviation of coefficient of friction take the same form as the linear functions for the mean coefficient of friction. The linear function coefficients are listed in Table 4.13. The linear functions for the mean deviation of coefficient of friction are shown in Figure 4.45.

Table 4.13 – Linear function coefficients and constants for mean deviation of coefficient of friction

Fabric	Range	C_0	C_2
Fabric 1	$0° < \phi \leq 45°$	3.68E-02	-1.09E-02
	$45° < \phi \leq 90°$	2.06E-02	2.78E-03
Fabric 2	$0° < \phi \leq 45°$	7.13E-03	5.19E-04
	$45° < \phi \leq 90°$	9.12E-03	4.74E-04
Fabric 3	$0° < \phi \leq 45°$	3.26E-02	-8.98E-03
	$45° < \phi \leq 90°$	1.38E-02	-4.57E-04

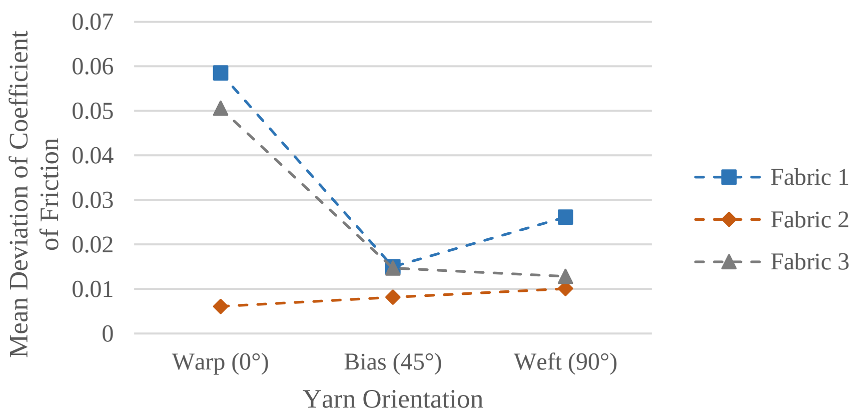

Figure 4.45 – Linear functions for mean deviation of coefficient of friction of fabrics

4.5. Pin stability

Hutchinson technicians make use of pins for securing textile preforms onto moulds as they are draped. A new test was developed in order to evaluate the stability of the fabrics while they are pinned to a mould. The procedure is detailed in Section 3.2.5. Load and extension were recorded throughout the entire tests. The recorded load increases as the fabric is being pulled through the pin and then drops to zero when the fabric fails. The point of failure of the samples was taken at the maximum load reached by the fabric during the test. Two metrics were used for comparing the performance of the fabrics: the load at failure, taken as the maximum load reached during the test; and the extension at failure, taken as the extension corresponding to the load at failure. The load at failure of the fabrics is shown in Figure 4.46.

ANOVA results for load at failure are shown in Figure 4.47, Figure 4.48 and Figure 4.49. The single layer loads at failure of Fabric 1 and Fabric 2 are not detectably different. The multilayer loads at failure of Fabric 1, Fabric 3 and Fabric 4 are not detectably different. The single and multilayer loads at failure of Fabric 4 are not detectably different.

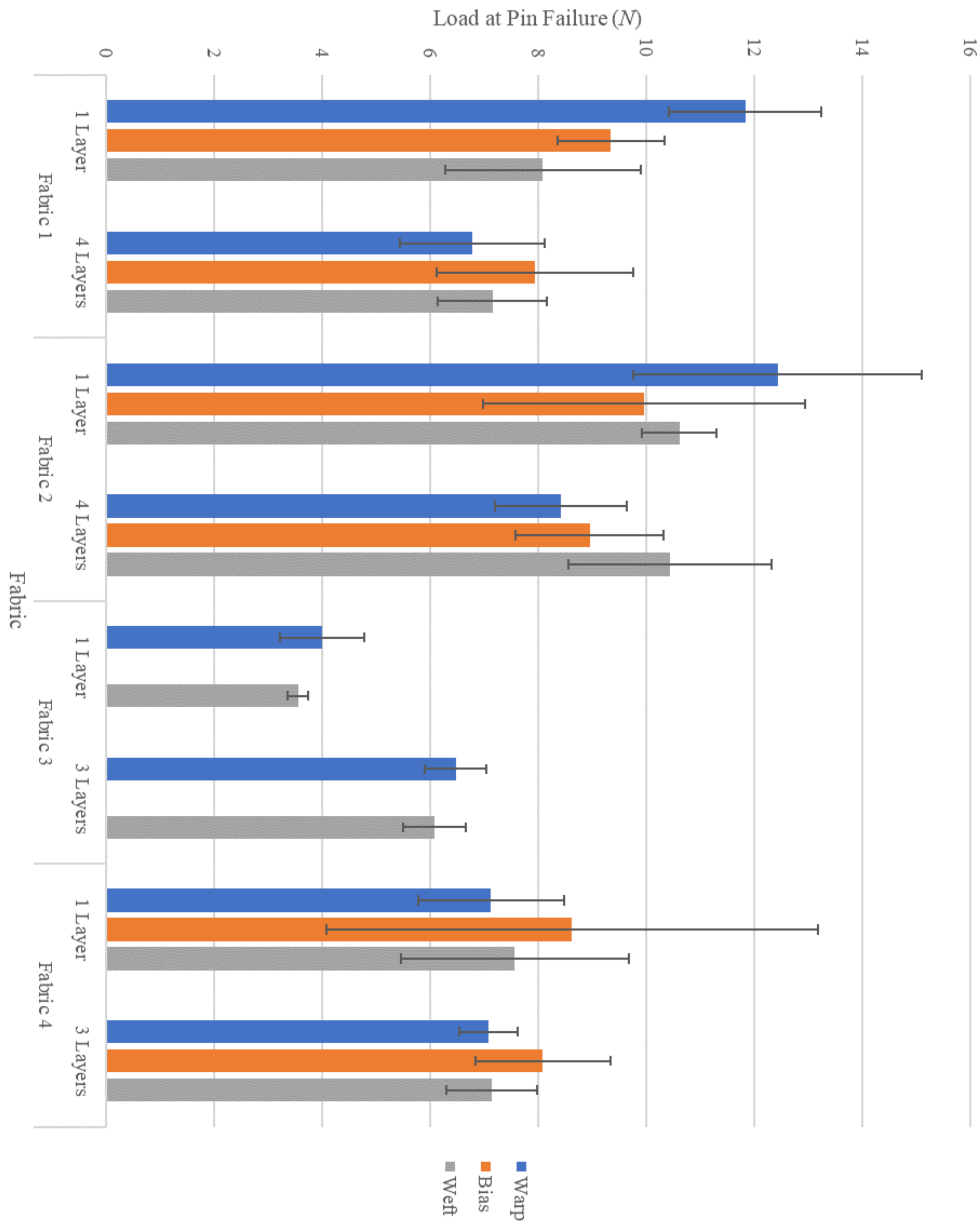

Figure 4.46 – Load at pin failure of fabrics

4.5.1. ANOVA 4.5.A – Load at pin failure

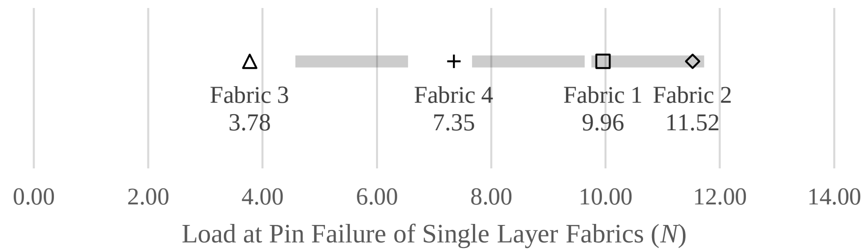

Figure 4.47 – Load at pin failure of single layer fabrics

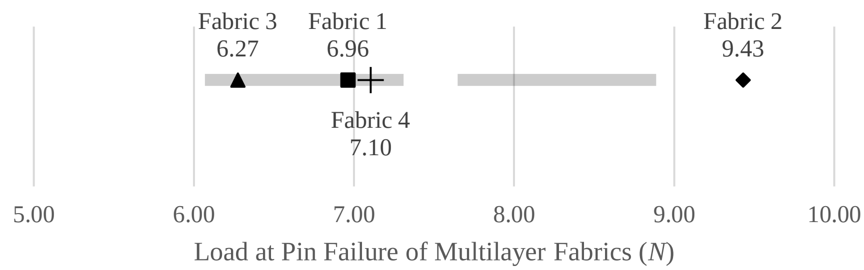

Figure 4.48 – Load at pin failure of multilayer fabrics

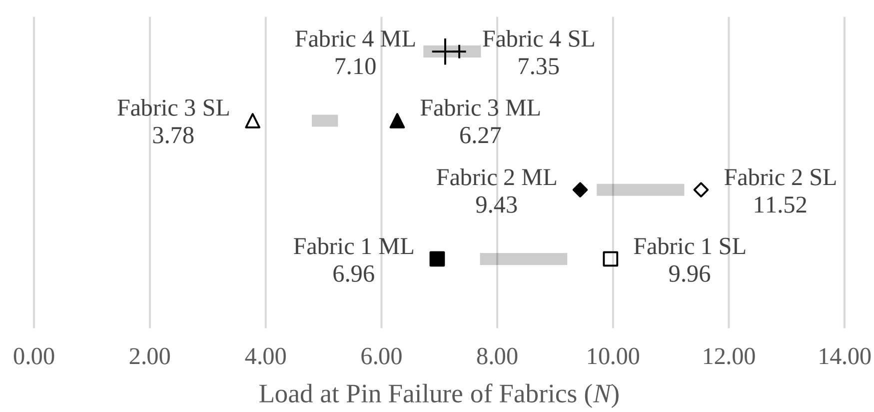

Figure 4.49 – Load pin at failure of fabrics

Load at failure of multilayer Fabric 1 and multilayer Fabric 2 were detectably lower than single layer versions, which suggests that some multilayer fabrics may be less stable than their single layer counterparts, as less force is required to make the pin fail.

4.5.2. DOE 4.5.A – Load at pin failure

The linear functions for interpolating the load at failure take the form

$$f(x) = C_0 + C_1 \cdot x_1 + C_2 \cdot x_2 + C_{12} \cdot x_1 x_2 \tag{4.6}$$

where C_0 is a constant average, and C_1, C_2 and C_{12} are coefficients, listed in Table 4.14. x_1 and x_2 are interpolation modalities, listed in Table 4.3. Linear functions for Fabric 1, Fabric 2 and Fabric 4 are shown in Figure 4.50, Figure 4.51 and Figure 4.52, respectively.

Table 4.14 – Linear function coefficients for load at failure of fabrics

Fabric	**Range**	C_0	C_1	C_2	C_{12}
Fabric 1	$0° < \phi \leq 45°$	8.97	-1.62	-0.33	0.91
	$45° < \phi \leq 90°$	8.13	-0.58	-0.51	0.12
Fabric 2	$0° < \phi \leq 45°$	9.94	-1.25	-0.49	0.75
	$45° < \phi \leq 90°$	9.99	-0.30	0.54	0.21
Fabric 4	$0° < \phi \leq 45°$	7.73	-0.15	0.63	-0.12
	$45° < \phi \leq 90°$	7.85	-0.24	-0.50	0.03

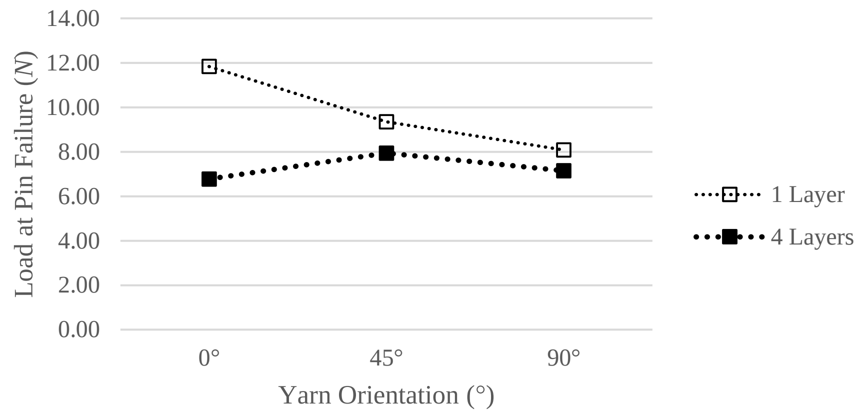

Figure 4.50 – Fabric 1 load at failure linear function

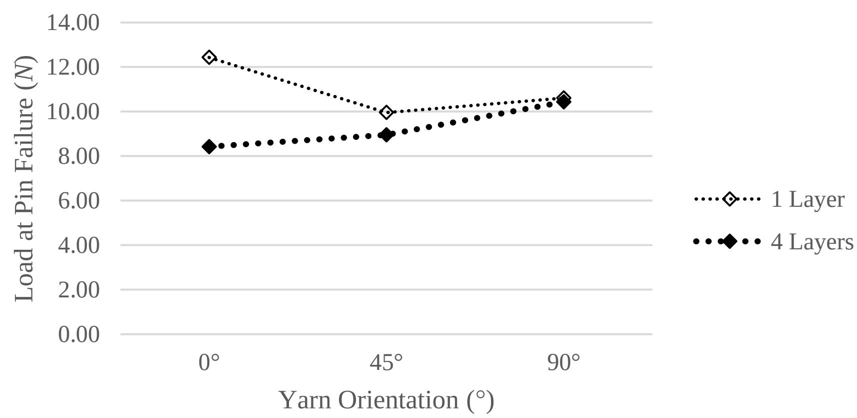

Figure 4.51 – Fabric 2 load at pin failure linear function

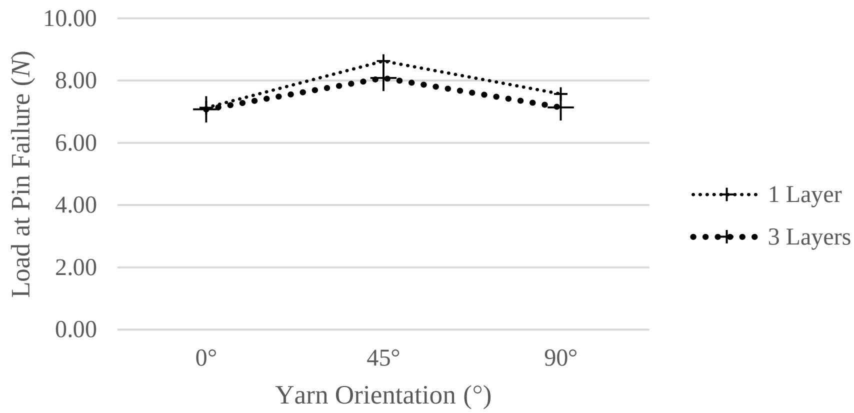

Figure 4.52 – Fabric 4 load at pin failure linear function

The extension at failure of the fabrics is shown in Figure 4.53. ANOVA results are shown in Figure 4.54, Figure 4.55 and Figure 4.56. Single layer fabric extensions at failure are not detectably different. The multilayer extensions at failure of Fabric 1 and 2, and of Fabric 2 and 3 are not detectably different, while the remaining pairwise comparisons reveal that the extensions at failure of multilayer fabrics are detectably different. Multilayer fabrics appear to show reduced stability for some fabrics, as some multilayer fabrics failed at smaller extensions, namely Fabric 1 and Fabric 4.

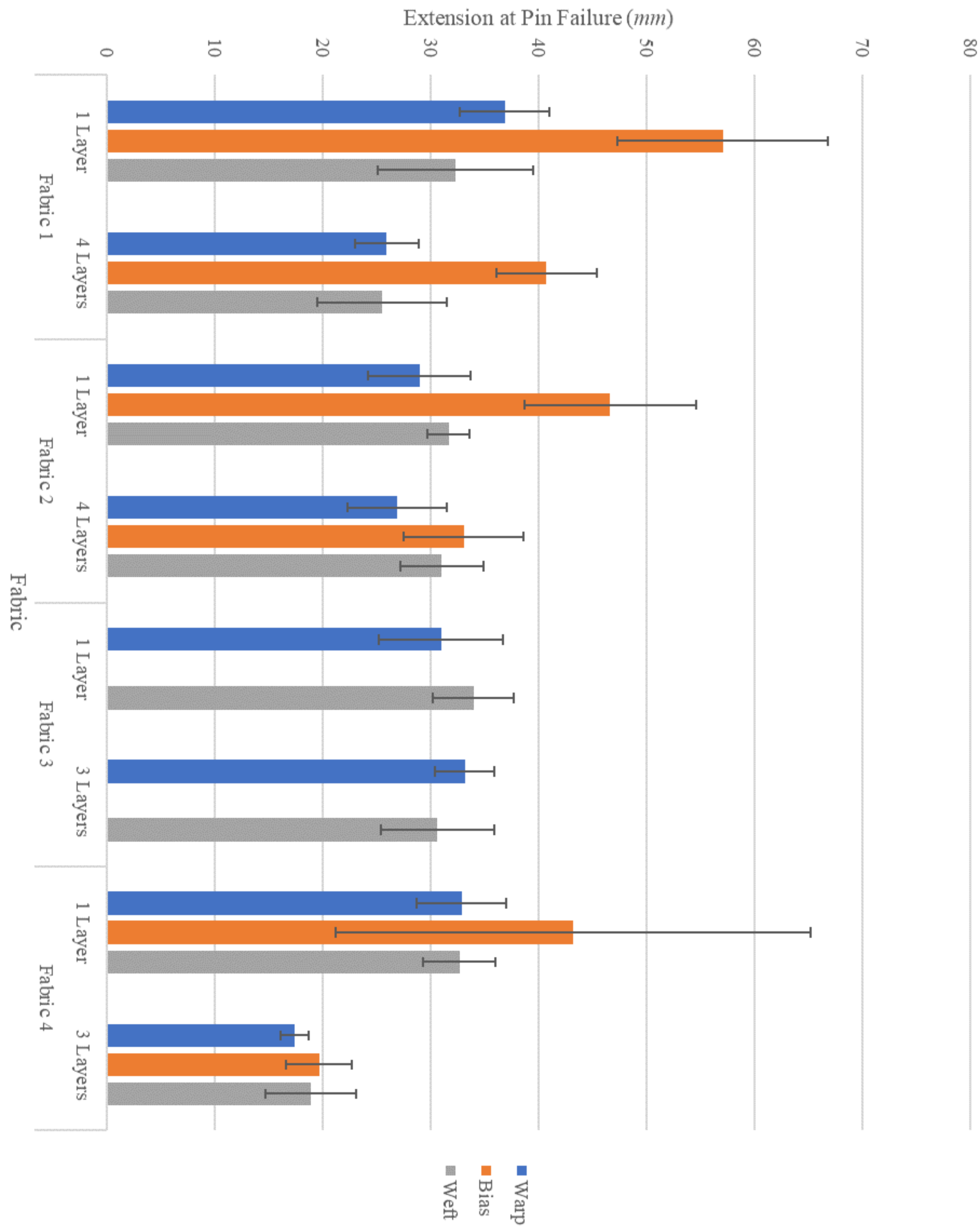

Figure 4.53 – Extension at pin failure of fabrics

4.5.3. ANOVA 4.5.B – Extension at pin failure under load

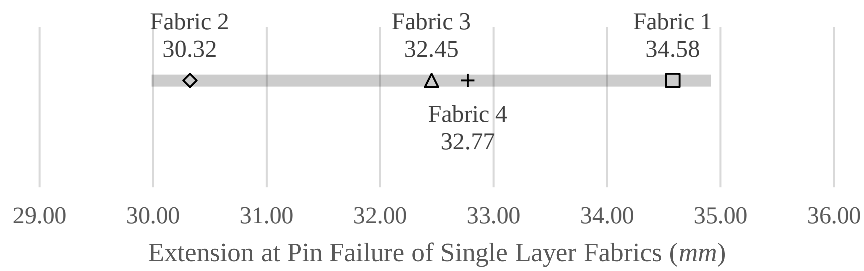

Figure 4.54 – Extension at pin failure of single layer fabrics

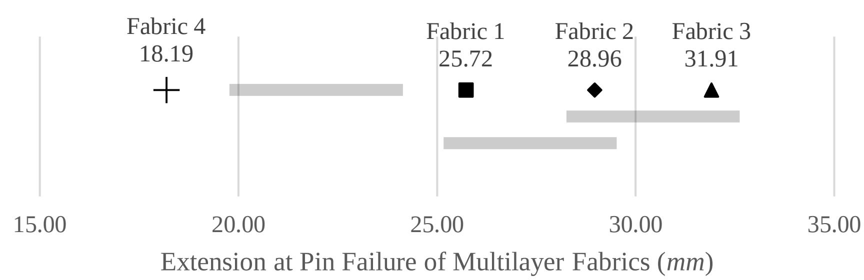

Figure 4.55 – Extension at pin failure of multilayer fabrics

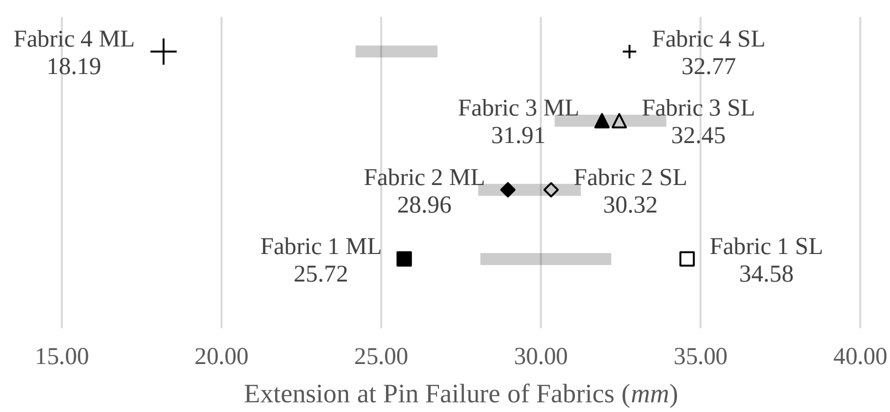

Figure 4.56 – Extension at pin failure of fabrics

4.5.4. DOE 4.5.B – Extension at pin failure under load

The linear functions for the extension at pin failure take the same form as the linear functions for the load at pin failure. The coefficients are listed in Table 4.15. The linear functions for Fabric 1, Fabric 2 and Fabric 4 are shown in Figure 4.57, Figure 4.58 and Figure 4.59.

Table 4.15 – Linear function coefficients for extension at failure of fabrics

Fabric	**Range**	***C_0***	***C_1***	***C_2***	***C_{12}***
Fabric 1	$0° < \phi \leq 45°$	40.15	-6.80	8.74	-1.35
	$45° < \phi \leq 90°$	38.90	-5.77	-9.99	2.37
Fabric 2	$0° < \phi \leq 45°$	33.89	-3.91	5.96	-2.88
	$45° < \phi \leq 90°$	35.60	-3.56	-4.24	3.23
Fabric 4	$0° < \phi \leq 45°$	28.30	-9.74	3.14	-2.02
	$45° < \phi \leq 90°$	28.62	-9.31	-2.82	2.45

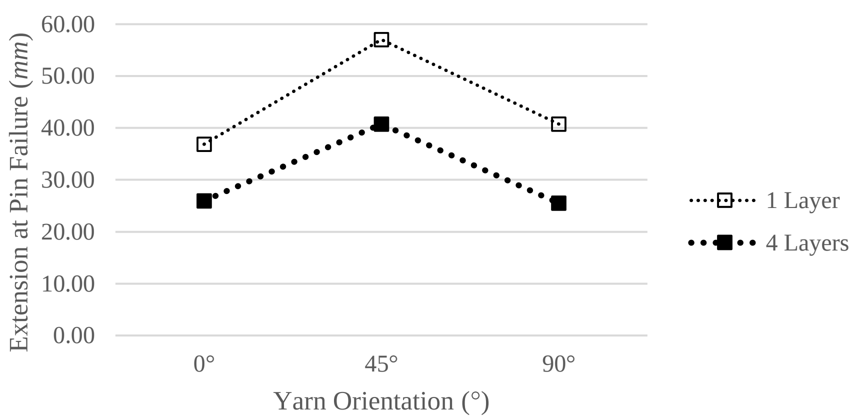

Figure 4.57 – Fabric 1 extension at pin failure linear function

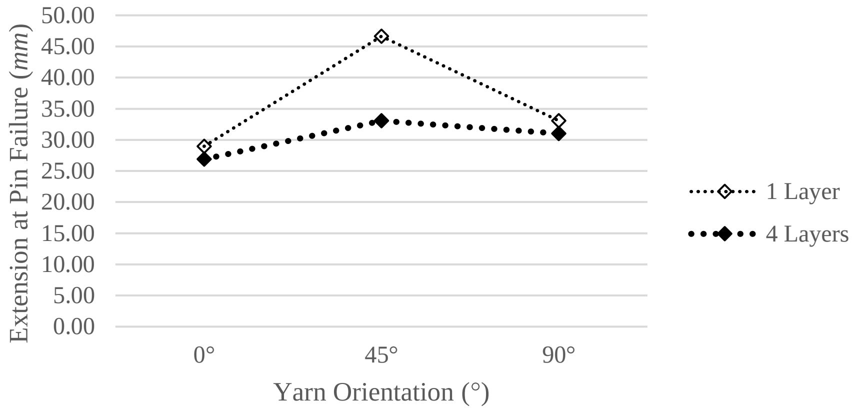

Figure 4.58 – Fabric 2 extension at failure linear function

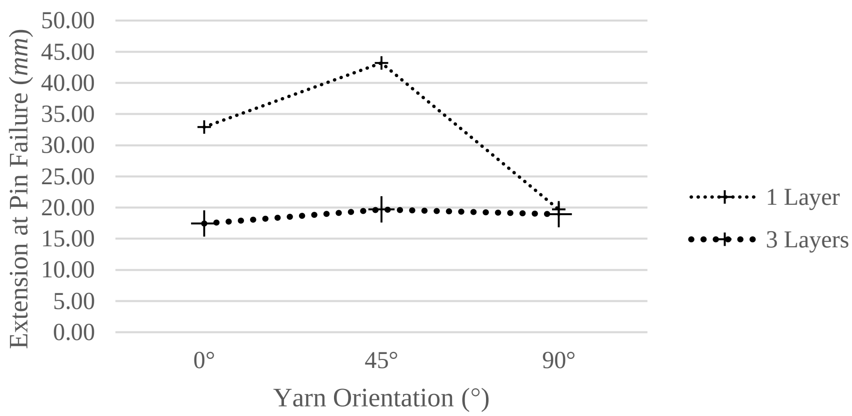

Figure 4.59 – Fabric 4 extension at failure linear function

Chapter 5. Drape energy

The focus of Chapter 4 was to present results that characterize the fabrics. ANOVAs were used for comparing results from each test, while DOE plans were used for creating linear interpolation functions. The goal of the present chapter is to introduce methods whereby further fabric characteristics are obtained towards selecting a fabric to be draped onto a mould. Results of characterisation tests are used for calculating values of energy associated with each test, fabric behaviour and deformation mode. In turn, energy values are used to inform the difficulty of draping a mould as well as the variability of the drape. The difficulty of draping a mould is associated with the average of new characteristics derived from bending stiffness, bending spring back, in-plane shear, in-plane shear spring back, friction and pin resistance, while the variability of the drape is associated with the standard deviations of these new characteristics.

This Chapter is separated in three parts. Firstly, Section 5.1 presents models that were developed for computing drape energies based on averages of fabric characteristics and mould geometry. These drape energies relate directly to the difficulty of draping a fabric. Secondly, Section 5.2 presents models that were developed for computing variability in drape energy, based on the spread of fabric characteristics and on mould geometry. Finally, Section 5.3 features a discussion on statistical considerations for estimating the variability of fabric behaviour.

5.1. Drape energy – difficulty

The difficulty of draping a fabric onto a mould, labeled drape difficulty henceforth, is strongly related to the strain energy required for draping the fabric onto the mould. A fabric that requires a larger quantity of strain energy towards being draped onto a mould is a fabric that is difficult to bend, difficult to shear in-plane, has high spring back in bending, and/or has high in-plane shear spring back. Higher strain energies also correspond to larger fabric samples, which are inherently more difficult to drape.

As a fabric is draped on a mould, it conforms to various single and double curvature surfaces that constitute the mould geometry. The method used for parameterizing these surfaces appears in [9]. Under normal circumstances, a fabric draped to a single curvature surface does not shear, while a fabric draped to a double curvature surface shears as it is draped. Different difficulties arise over single and double curvature base surfaces: bending stiffness and spring back impact draping onto single curvature base surfaces, whilst in-plane shear stiffness and spring back impact draping onto double curvature surfaces. Therefore, in this work bending and bending spring back energies are calculated only when fabrics are draped onto single curvature surfaces, while in-plane shear and in-plane spring back energies are calculated only when fabrics are draped onto double curvature surfaces.

The following subsections introduce methods for calculating the strain energies associated with bending, bending spring back, in-plane shear and in-plane shear spring back using the linear functions developed in Chapter 4.

5.1.1. Bending energy

The following assumptions are made towards calculating the bending energy of fabrics:

1. Bending behaviour is linear and elastic;
2. The single curvature surface has a circular shape with constant radius;
3. The bending moment along the length of the fabric is constant (pure bending);
4. Fabric thickness is negligible.

The bending strain energy of a linear elastic material is given by:

$$U_{bending} = \int_0^l \frac{M^2}{2B} dx \tag{5.1}$$

where *M* is the bending moment (*Nm*), *B* is the bending rigidity (*Nm*^{2}) and *l* is the length (*m*). The relation between bending moment and bending radius in pure bending is given by:

$$M = \frac{1}{R} B \tag{5.2}$$

where *R* is the radius of the fabric (*m*). Integrating Equation (5.1) and substituting Equation (5.2) gives:

$$U_{bending} = \frac{\left(\frac{1}{R} B\right)^2 l}{2B} \tag{5.3}$$

Simplifying Equation (5.3) results in

$$U_{bending} = \frac{\left(\frac{1}{R^2}\right) B^2 L}{2B} = \frac{BL}{2R^2} = \left(\frac{1}{2}\right)\left(\frac{B}{R}\right)\left(\frac{L}{R}\right) = \left(\frac{1}{2}\right) M\alpha_m \tag{5.4}$$

where α_m is the angle between both ends of the fabric (*rad*), referred to as the fabric opening angle. Once the fabric is draped onto the mould, angle α_m is the same for the fabric and the mould. The bending moment M can be calculated using the cantilever bending stiffness characterized in this work. Bending stiffness results presented in Chapter Chapter 4 are bending rigidity measurements normalized by unit width. Therefore, calculating the energy required for draping fabrics onto a single curvature surface can be done using:

$$U_{bending} = \left(\frac{1}{2}\right) B_{Peirce} b \frac{\alpha_m}{R_m} \tag{5.5}$$

where B_{Peirce} is the bending stiffness of the fabric ($\mu Nm^2/m$), b is the fabric width (mm) and R_m is the mould radius (mm). Examples of convex and concave corners are shown in Figure 5.1 and Figure 5.2. The units of bending energy are μNm.

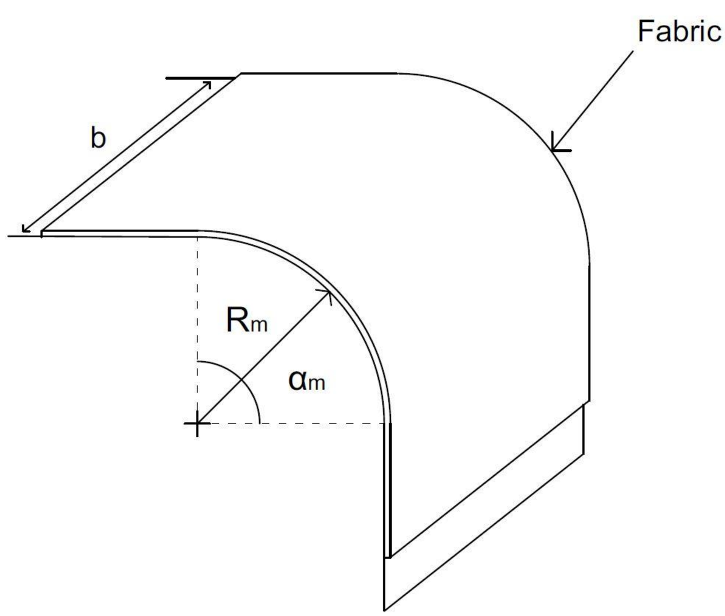

Figure 5.1 – Bending energy for a convex corner

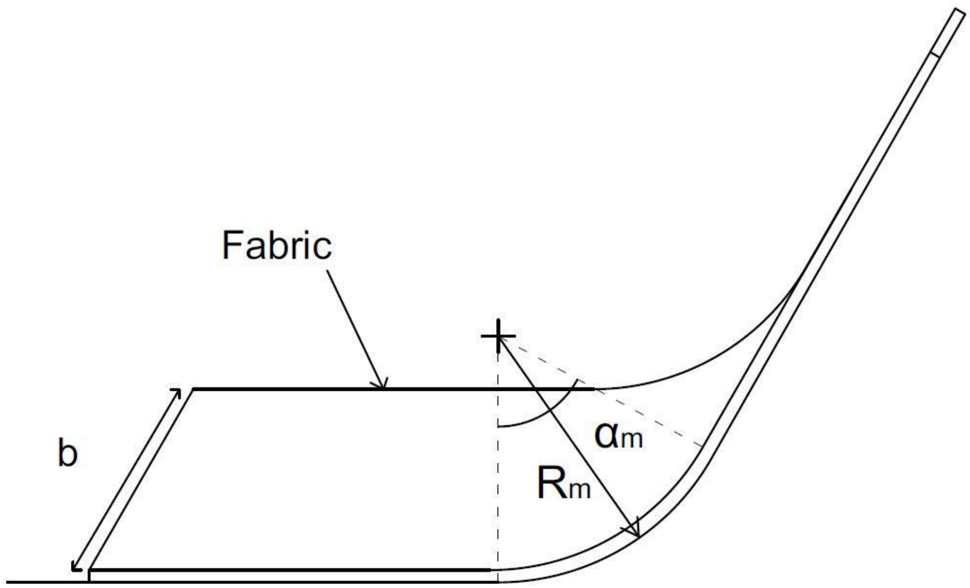

Figure 5.2 – Bending energy for a concave corner

5.1.2. Bending spring back energy

The bending spring back behaviour of fabrics is relatively complex, hence several simplifying assumptions were made in order to describe and quantify it. These assumptions are as follows:

1. The behaviour of a fabric upon initial bending is linear elastic; however, due to internal factors (frictional forces between yarns and frictional forces between fibres within the yarns), the fabric does not return to its initial shape;
2. Technicians need to provide more energy to ensure that a fabric that would spring back does stay draped onto the mould;
3. Fabric thickness is negligible;
4. The fabric is bent to a circular shape of constant radius.

In other words, a fabric showing limited spring back will require less additional energy to ensure that it stays draped on a mould, whilst a fabric showing important spring back will require more additional energy to ensure that it stays draped on the mould.

Recalling Equation (5.4), the bending moment-opening angle relation is linear. The bending energy corresponds to the area under the curve of the bending moment vs bending angle. The bending moment is a function of the fabric radius and fabric bending stiffness (Equation (5.2)); therefore, the slope of the bending moment vs bending angle plot changes depending on the fabric radius of curvature. A fabric that is bent to a larger radius of curvature requires less strain energy than the same fabric bent to a smaller radius of curvature, assuming the same fabric opening angle, as shown in Figure 5.3

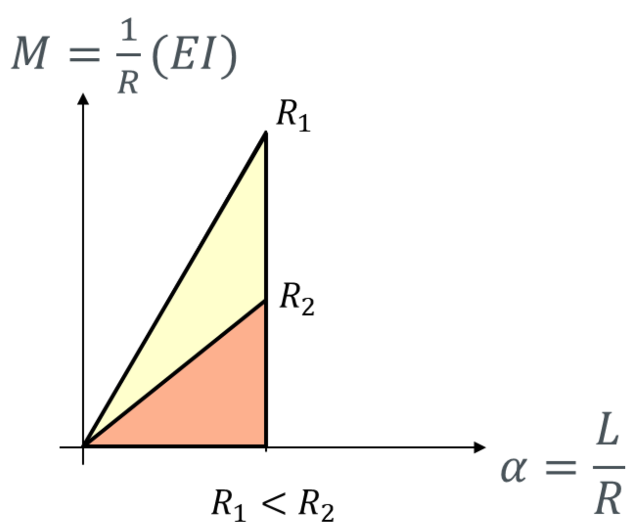

Figure 5.3 – Graphical representation of bending energy

When draping the fabric onto the mould, a specific amount of energy is needed for bending the fabric. As the fabric springs back, the opening angle of the fabric decreases and the fabric radius increases until the fabric reaches a new deformed state. Assumption 4 states that all bent shapes are circular, therefore a specific bending moment applied to the fabric corresponds to the shape of the fabric after spring back. The spring back energy represents the difference between the energy required initially for draping the fabric to the mould, minus the energy required for bending the fabric to its final shape after spring back. The spring back energy is shown in Figure 5.4 where the red area represents the energy required initially for bending the fabric to a deformed shape corresponding to the radius of the mould, and green area represents the energy required for bending the fabric to a deformed shape equivalent to its spring back state. The spring back energy, which is positive, is the difference between the former and the later terms.

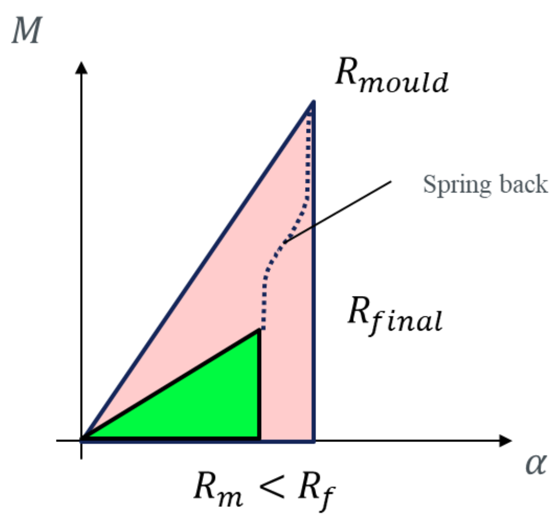

Figure 5.4 – Spring back energy

The bending spring back energy ($SBE_{Bending}$) can be calculated using:

$$SBE_{bending} = \left(\frac{1}{2}\right) B_{Peirce} b \left(\frac{\alpha_m}{R_m} - \frac{\alpha_f}{R_f}\right) \tag{5.6}$$

where α_f and R_f represent the final opening angle of the fabric and final radius after spring back. Equation (5.6) is an extension of the bending energy equation derived in Section 5.1.1, Equation (5.5). The units of the bending spring back energy are μNm.

Fabric spring back occurs over both convex and concave surfaces. Results of convex and concave bending spring back tests were presented in Chapter 4. Both cases of spring back require different methods for characterizing α_f and R_f.

5.1.2.1. Convex Bending Spring Back

Convex bending spring back of fabrics was characterized for a 90° bending angle for multiple SMRs. Throughout convex spring back testing, fabrics were held in place on the horizontal surface shown in Figure 5.5. Measurements of spring back β were taken horizontally with respect to the SMR origin. The circles representing the SMR (R_m) and the final fabric shape (R_f) are assumed tangent at the location where the fabric leaves the horizontal surface (point A). The centre of the fabric radius is therefore collinear with point A and the SMR origin.

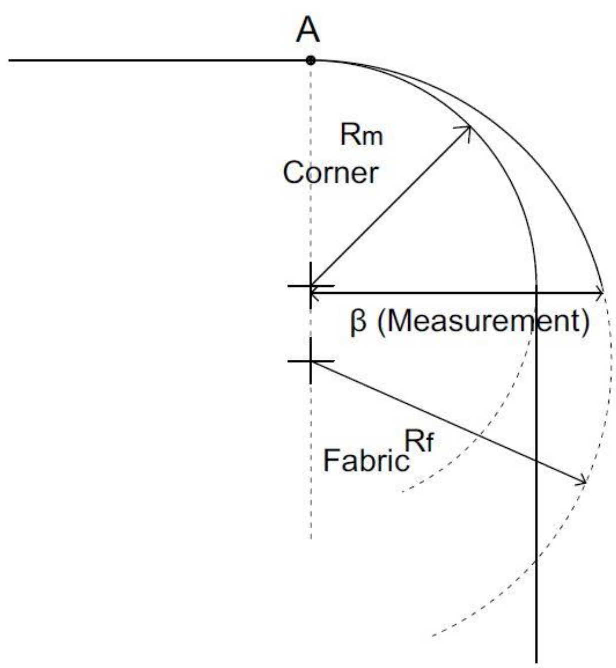

Figure 5.5 – Geometric assumptions, convex spring back

The final radius of the fabric can be calculated using:

$$R_f = \frac{R_m^2 + \beta^2}{2R_m} \tag{5.7}$$

The final opening angle of the fabric can be calculated using:

$$\alpha_f = \frac{\pi}{2} - \tan^{-1}\left(\frac{\beta}{2R_m} - \frac{R_m}{2\beta}\right) \tag{5.8}$$

5.1.2.2. Concave Bending Spring Back

Concave spring back was characterized for a 90° mould opening angle and multiple SMRs. Throughout testing, the fabrics were held in place at a distance of 4 *cm* from the vertical side-wall, Figure 5.6. Spring back measurements (β) were taken vertically with respect to the horizontal plane. The circles representing the SMR and the final fabric shape are assumed tangent to both the horizontal plane on which the fabric is resting, and the vertical side-wall (point B). Furthermore, the origins of both circles are assumed collinear with the intersection of the horizontal plane and the vertical side-wall.

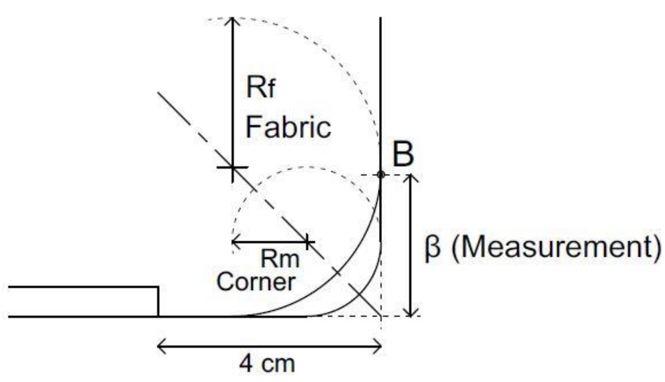

Figure 5.6 – Geometric assumptions, concave spring back

These assumptions result in the final fabric radius being equal to the measured value of spring back β, and the final opening angle of the fabric α_f being equal to the opening angle of the mould α_m.

The bending spring back energy of fabrics bent to concave moulds simplifies to:

$$SBE_{Bending} = \frac{1}{2} B_{Peirce} b \alpha_m \left(\frac{1}{R_m} - \frac{1}{R_f} \right) \tag{5.9}$$

5.1.3. In-plane shear energy

The elastic strain energy of a material subjected to in-plane shear is given by:

$$U_{shear} = \iiint \frac{\tau^2}{2G} dxdydz \tag{5.10}$$

where τ is the shear stress (*N/m*^{2}) and G is the shear stiffness (*N/m*^{2}). The in-plane shear behaviour of fabrics is non-linear and non-elastic as shown in Figure 4.31, Chapter 4. The return phase of the loading cycle shows that the in-plane behaviour is hysteretic. In Chapter 4, the in-plane shear behaviour of fabrics was modelled using a fifth order polynomial, where the shear angle is used for estimating the normalized shear load.

As units of energy are *Nm*, the energy required for shearing the fabric to a specified shear angle involves an integral. Two methods for calculating the shear energy were considered in this work. The first method involves integrating the normalized shear load (*N/mm*) with respect to the shear angle (*rad*). The resulting units of the integral are *N/mm*, because the shear load is normalized with respect to the sample and picture-frame dimensions. Taking the integral of the shear load without normalization (N) with respect to the shear angle (rad) results in units of N for the integrated quantity, which does not represent an energy.

The second approach involves integrating the raw picture-frame test data. The integration of the load applied on the picture frame (N) with respect to its extension results in integral units of Nm, which represents an energy. Therefore, numerical integration was performed on the raw data produced from the picture-frame tests. Results of numerical integrations appear in Figure 5.7 and Figure 5.8.

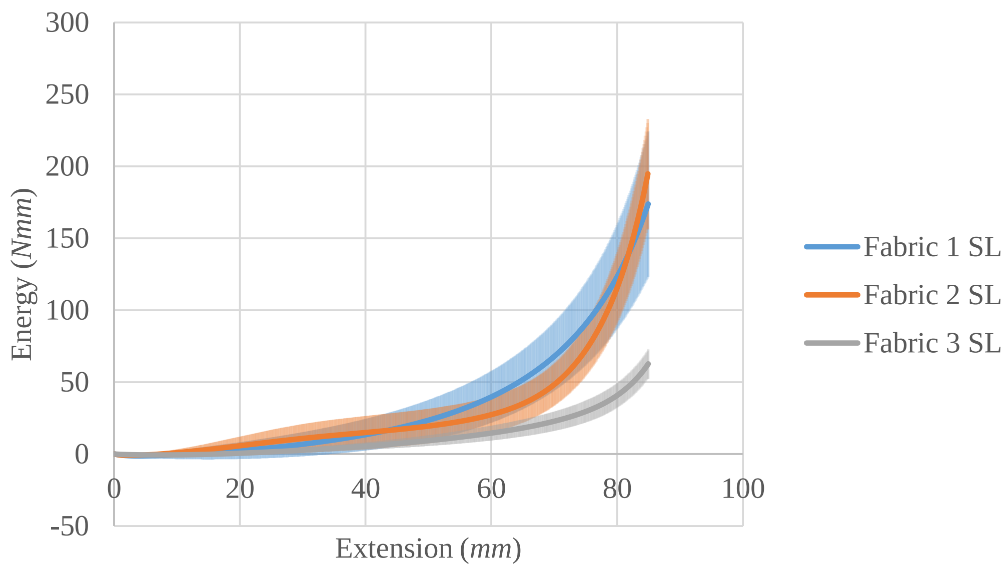

Figure 5.7 – Average and standard deviation of numerical integrations of raw picture-frame test results for single layer fabrics

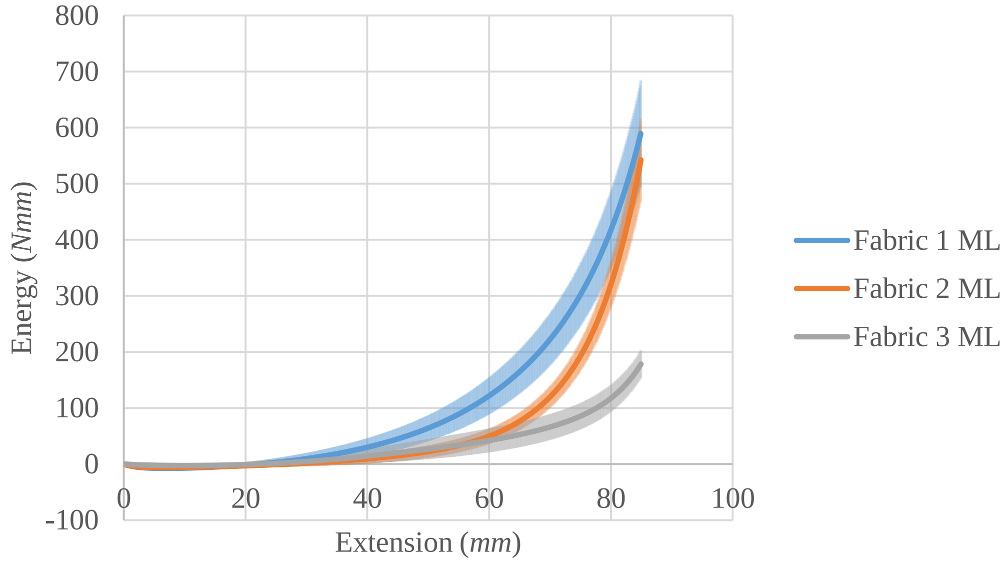

Figure 5.8 – Average and standard deviation of numerical integrations of raw picture frame test results for multilayer fabrics

In-plane shear was modelled using a fifth order polynomial, hence shear energy was modelled using a sixth order polynomial taking the form:

$$f(x) = C_0 + C_1x + C_2x^2 + C_3x^3 + C_4x^4 + C_5x^5 + C_6x^6 \tag{5.11}$$

where x is the extension of the picture-frame, and C_0, C_1, C_2, C_3, C_4, C_5 and C_6 are coefficients listed in Table 5.1. Regression curves are shown in Figure 5.9 and Figure 5.10.

Table 5.1 – Regression coefficients for shear energy

	Number of layers	C_0	C_1	C_2	C_3	C_4	C_5	C_6	R^2
Fabric 1	1	-6.465E-02	-5.778E-01	8.093E-02	-3.709E-03	9.111E-05	-1.071E-06	5.072E-09	0.87
	4	-5.496E-01	-2.533E+00	2.794E-01	-1.262E-02	3.093E-04	-3.611E-06	1.700E-08	0.96
Fabric 2	1	8.197E-01	-1.025E+00	1.637E-01	-8.009E-03	1.958E-04	-2.364E-06	1.137E-08	0.91
	4	6.970E-01	-2.993E+00	3.761E-01	-1.941E-02	4.987E-04	-6.172E-06	3.011E-08	0.96
Fabric 3	1	5.471E-01	-5.416E-01	6.586E-02	-3.117E-03	7.668E-05	-9.051E-07	4.133E-09	0.92
	3	7.589E-01	-1.139E+00	1.219E-01	-5.843E-03	1.575E-04	-2.007E-06	9.718E-09	0.89

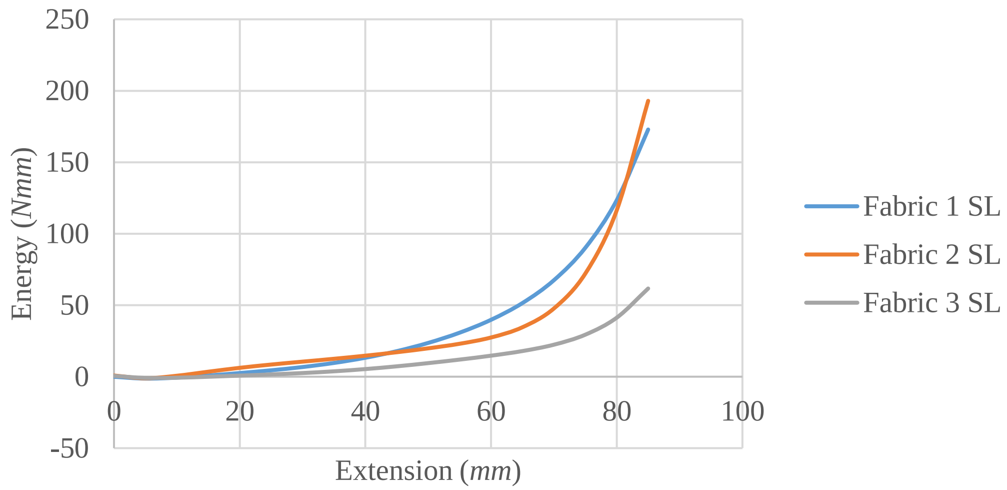

Figure 5.9 – Regression polynomials built on numerical integration of raw picture-frame test results for single layer fabrics

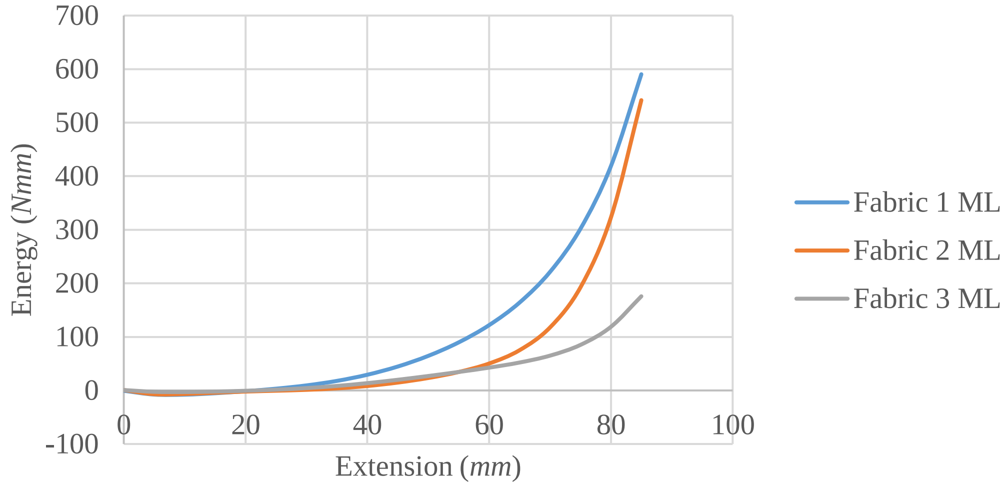

Figure 5.10 – Regression polynomials built on numerical integration of raw picture frame test results for multilayer fabrics

A comparison of average values of in-plane shear energy (Figure 5.7 and Figure 5.8) and predicted values of shear energy (Figure 5.9 and Figure 5.10) is shown in Table 4.10, Table 4.11, and Table 5.4. The polynomial regressions estimate the shear energy accurately over the range of shear angles tested.

Table 5.2 – Comparison of average and regression normalized shear energies at small shear angles

	Number of layers	20° (40 *mm*)			30° (55 *mm*)		
		Average	Regression	% Error	Average	Regression	% Error
Fabric 1	1	12.73 *Nmm*	12.61 *Nmm*	-0.01	31.45 *Nmm*	31.80 *Nmm*	0.01
	4	27.79 *Nmm*	27.30 *Nmm*	-0.02	92.33 *Nmm*	93.33 *Nmm*	0.01
Fabric 2	1	14.61 *Nmm*	14.33 *Nmm*	-0.02	23.08 *Nmm*	23.50 *Nmm*	0.02
	4	8.45 *Nmm*	7.52 *Nmm*	-0.11	34.50 *Nmm*	36.13 *Nmm*	0.05
Fabric 3	1	5.24 *Nmm*	5.06 *Nmm*	-0.03	12.01 *Nmm*	12.30 *Nmm*	0.02
	3	13.19 *Nmm*	12.76 *Nmm*	-0.03	34.73 *Nmm*	35.49 *Nmm*	0.02

Table 5.3 – Comparison of average and regression normalized shear energies at large shear angles

	Number of layers	45° (75 *mm*)			50° (80 *mm*)		
		Average	Regression	% Error	Average	Regression	% Error
Fabric 1	1	94.81 *Nmm*	95.07 *Nmm*	0.00	134.98 *Nmm*	135.41 *Nmm*	0.00
	4	317.73 *Nmm*	319.16 *Nmm*	0.00	455.42 *Nmm*	460.41 *Nmm*	0.01
Fabric 2	1	77.88 *Nmm*	78.13 *Nmm*	0.00	132.44 *Nmm*	134.00 *Nmm*	0.01
	4	209.04 *Nmm*	210.33 *Nmm*	0.01	370.00 *Nmm*	373.46 *Nmm*	0.01
Fabric 3	1	30.83 *Nmm*	31.03 *Nmm*	0.01	45.22 *Nmm*	45.97 *Nmm*	0.02
	3	89.39 *Nmm*	89.74 *Nmm*	0.00	130.11 *Nmm*	131.90 *Nmm*	0.01

Table 5.4 – In-plane shear energy of fabrics at 53°

	Number of layers	53° (85 *mm*)		
		Average	Regression	% Error
Fabric 1	1	173.75 *Nmm*	172.90 *Nmm*	0.00
	4	589.42 *Nmm*	590.39 *Nmm*	0.00
Fabric 2	1	194.76 *Nmm*	192.97 *Nmm*	-0.01
	4	542.60 *Nmm*	541.99 *Nmm*	0.00
Fabric 3	1	62.67 *Nmm*	61.69 *Nmm*	-0.02
	3	178.22 *Nmm*	175.81 *Nmm*	-0.01

In order to obtain the energy required for shearing a fabric to a specified shear angle, the effect of the mould geometry on the shear angle of the fabric must be known. Single curvature and flat mould features do not induce in-plane shear deformation on the fabric, while double curvature mould features can induce large in-plane shear deformations to the fabric.

Mould features were broken down into base surfaces in [9] using a five and a twelve parameter conical frustum models. Linear interpolation functions were created for estimating the shear angles at each base surface vertex and at the midpoints along each base surface edge. The five-parameter conical frustum model is shown in Figure 5.11. Linear function inputs are the frustum parameters, and three starting drape parameters.

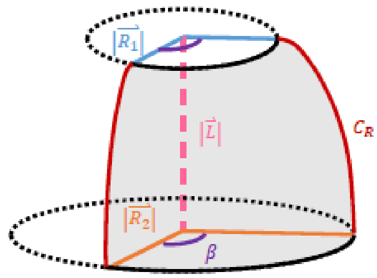

Figure 5.11 – Five-parameter conical frustum [9]

Sixteen models were used for capturing the effect of the mould geometry on the shear angle distribution, and 8 simulations per model were used for capturing the effect of drape starting parameters on the shear angle distribution [9]. The five-parameter frustum parameters of each model are listed in Table 5.5.

Table 5.5 – Frustum parameters for simulating shear angles [9]

	Frustum Parameters				
	R_1	R_2	C_R	$L_{5\text{-}para}$	$\beta_{5\text{-}para}$
Model 1	0 *cm*	1 *cm*	2 *cm*	0.5 *cm*	45°
Model 3	0 *cm*	1 *cm*	2 *cm*	0.5 *cm*	90°
Model 5	2 *cm*	1 *cm*	2 *cm*	0.5 *cm*	45°
Model 7	2 *cm*	1 *cm*	2 *cm*	0.5 *cm*	90°
Model 9	0 *cm*	1 *cm*	2 *cm*	2 *cm*	45°
Model 11	0 *cm*	1 *cm*	2 *cm*	2 *cm*	90°
Model 13	2 *cm*	1 *cm*	2 *cm*	2 *cm*	45°
Model 15	2 *cm*	1 *cm*	2 *cm*	2 *cm*	90°
Model 17	0 *cm*	2 *cm*	2 *cm*	0.5 *cm*	45°
Model 19	0 *cm*	2 *cm*	2 *cm*	0.5 *cm*	90°
Model 21	2 *cm*	2 *cm*	2 *cm*	0.5 *cm*	45°
Model 23	2 *cm*	2 *cm*	2 *cm*	0.5 *cm*	90°
Model 25	0 *cm*	2 *cm*	2 *cm*	2 *cm*	45°
Model 27	0 *cm*	2 *cm*	2 *cm*	2 *cm*	90°
Model 29	2 *cm*	2 *cm*	2 *cm*	2 *cm*	45°
Model 31	2 *cm*	2 *cm*	2 *cm*	2 *cm*	90°

The starting drape parameters of each simulation are listed in Table 5.6, where *Ps* is the starting drape position, *Os* is the starting yarn orientation, and *w* is the starting shear angle. The starting drape position was taken at the centre of the base surface, or at the centre of the longest edge of the base surface, labelled “C” and “MLE” respectively [9].

Table 5.6 – Starting drape parameters [9]

	Drape Parameters		
	Ps	*Os*	*w*
Simulation 1	MLE	0°	0°
Simulation 2	MLE	45°	0°
Simulation 3	MLE	0°	30°
Simulation 4	MLE	45°	30°
Simulation 5	C	0°	0°
Simulation 6	C	45°	0°
Simulation 7	C	0°	30°
Simulation 8	C	45°	30°

The linear functions built in [9] are used for obtaining shear angles at each base surface vertex and at the centre of each base surface edge, shown in Figure 5.12. Conical frustum parameters may be defined for base surfaces having three or four edges.

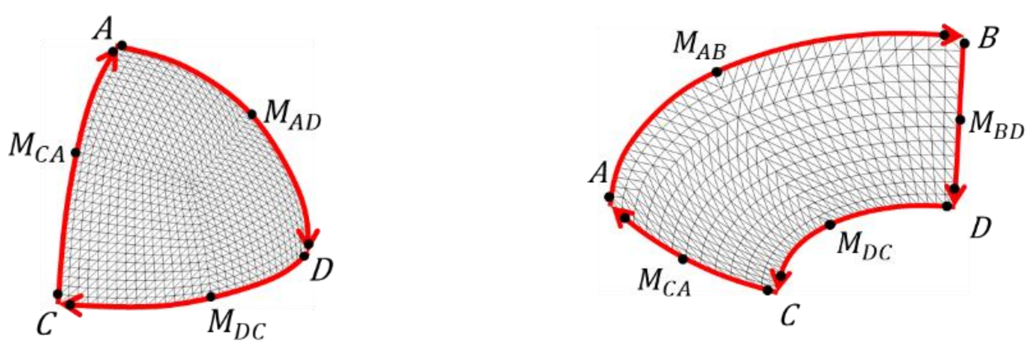

Figure 5.12 – Locations of shear angles for 3-edged (left) and 4-edged (right) base surfaces [9]

Once shear angles are estimated using the linear functions, in-plane shear energy can be estimated using the numerical integration of test results. The highest shear angle occurring along the base surface edges is taken to represent the shear angle over the entire base surface. While this decision is arbitrary, it should overestimate the actual drape energy required for draping the double curvature base surface, hence constitutes a prudent choice.

As discussed previously, the in-plane shear energy is calculated by numerical integration of raw test results as this result is expressed in appropriate units. Calculating the shear energy involves converting the shear angle (*rad*) to an extension (*mm*), which represents the extension of the picture frame during picture frame shear tests. Extension is calculated using:

$$x = 2l_{frame} \cos\left(\frac{90 - \gamma}{2}\right) - \sqrt{2}\, l_{frame} \tag{5.12}$$

where γ is the shear angle of the fabric and L_{frame} is the length of the picture-frame rig, Figure 5.13. Equation (5.12) was adapted from Equations (2.14) and (2.15), Chapter 2. The length of the frame used for characterizing the in-plane shear behaviour is 175 mm.

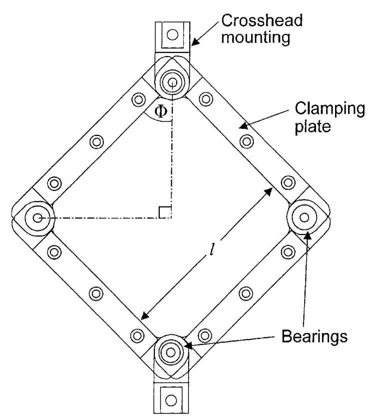

Figure 5.13 – Frame length L_{frame} [31]

Once the extension is known, the in-plane shear energy required for shearing the fabric to a specified shear angle can be obtained using the 6th order polynomial regression equation with coefficients listed in Table 5.1, or by using a table look-up function. The number of layers in the fabric and its surface area must also be considered when calculating the shear energy of fabrics.

Linear interpolation is used for estimating the shear energy of multilayer fabrics, and a scaling factor is used to adjust for the surface area of sheared fabric:

$$U_{shear}(n,\gamma) = \frac{S_{BS}}{S_{PF}}\left(\left(\frac{n-1}{3}\right)\cdot\left(U_{shear}(4,\gamma) - U_{shear}(1,\gamma)\right) + U_{shear}(1,\gamma)\right) \tag{5.13}$$

$$U_{shear}(n,\gamma) = \frac{S_{BS}}{S_{PF}}\left(\left(\frac{n-1}{2}\right)\cdot\left(U_{shear}(3,\gamma) - U_{shear}(1,\gamma)\right) + U_{shear}(1,\gamma)\right) \tag{5.14}$$

where $U_{shear}(n,\gamma)$ is the shear energy of fabrics, n is the number of layers in the fabric, S_{BS} is the surface area of the base surface, and S_{PF} is the surface area of the sheared fabric during the picture frame tests. The area of sheared fabric during the picture-frame tests is taken as 19 600 mm^2. Equation (5.13) is used for calculating the shear energies of Fabrics 1 and 2, as picture-frame shear tests were conducted for 1 layer and 4 layer samples of fabric. Equation (5.14) is used for interpolating the shear energy of Fabric 3, as picture-frame tests were conducted for 1 and 3 layers of fabric.

5.1.4. In–plane shear spring back energy

In-plane shear spring back was characterized by the return angle of fabrics. The return angle of fabrics was defined as the angle at which shear force vanished during the return phase of testing. In this work, shear energy calculations involve numerical integration of raw picture-frame test results. The in-plane shear spring back energy is represented by the area under the return phase of the cycle in Figure 4.31. The return phase of single layer fabrics is shown in Figure 5.14, and the return phase of multilayer fabrics is shown in Figure 5.15.

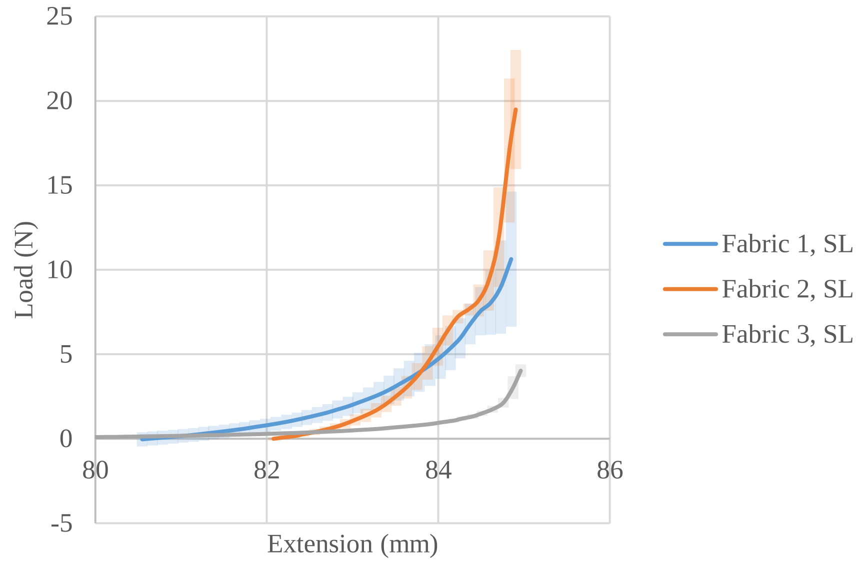

Figure 5.14 – Average and standard deviation of return phase of single layer fabrics

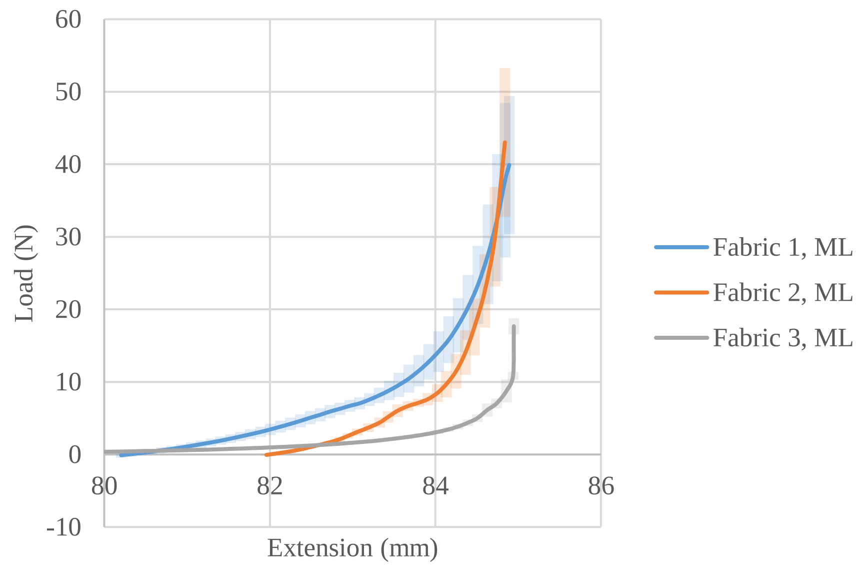

Figure 5.15 – Average and standard deviation of return phase of multilayer fabrics

In-plane shear spring back energies are known for a shear angle of 53°, corresponding to 85 mm extension on the picture-frame rig. The in-plane shear energies required for shearing every fabric to 53° are listed in Table 5.4.

Average values of shear spring back energies for the tested fabrics are listed in Table 5.7. Numerical integration of the return phase of fabrics was performed on average curves of test results; therefore, standard deviations of the spring back energies are not readily available. Regression polynomials were not created for the return phase of the tests, as the return phase depends on the maximum shear angle of the fabrics during the in-plane shear test due to the hysteretic nature of the shear behaviour of fabrics.

Table 5.7 – In-plane shear spring back energy of fabrics

	Single Layer (N mm)	Multilayer (N mm)
Fabric 1	11.08	38.09
Fabric 2	11.87	22.40
Fabric 3	3.20	10.55

The ratios of in-plane shear spring back energy to in-plane shear energy are listed in Table 5.8:

Table 5.8 – Average in-plane shear spring back ratio

	Single Layer	Multilayer
Fabric 1	6.38E-02	6.46E-02
Fabric 2	6.09E-02	4.13E-02
Fabric 3	5.11E-02	5.92E-02

The average ratio for all the fabrics is 5.68×10^{-2} and the ratios do display much variability. ANOVA statistical analysis can be performed on the ratios by using measurement uncertainty propagation to estimate the standard deviation of the spring back ratios. Equations of the propagation of dispersion are listed in Appendix C. For the spring back ratio of fabrics, the average and dispersion are calculated using:

$$\frac{U_{return} \pm \Delta U_{return}}{U_{53^\circ} \pm \Delta U_{53^\circ}} = \frac{U_{return}}{U_{53^\circ}} \pm \frac{U_{return}}{U_{53^\circ}}\left(\frac{\Delta U_{return}}{U_{return}} + \frac{\Delta U_{53^\circ}}{U_{53^\circ}}\right) \tag{5.15}$$

where U_{return} is the average return energy of the fabric, ΔU_{return} is the dispersion of the return energy, U_{53° is the average energy required for shearing the fabric to 53°, and ΔU_{53° is the dispersion of the energy required for shearing the fabric to 53°. The standard deviations shown in Figure 5.14 and Figure 5.15 appear small compared to the standard deviations shown in Figure 5.7 and Figure 5.8. Neglecting the dispersion of the return phase energy, $\Delta U_{return} \approx 0$, the standard deviation of the spring back ratios can be estimated using:

$$\Delta SBR_{shear} = \pm \frac{U_{return}}{U_{53^\circ}}\left(\frac{\Delta U_{53^\circ}}{U_{53^\circ}}\right) \tag{5.16}$$

Average spring back ratios and approximations of standard deviations using Equation (5.16) are listed in Table 5.9.

Table 5.9 – Average in-plane shear spring back ratio

	Single Layer		Multilayer	
	Average	Standard Deviation	Average	Standard Deviation
Fabric 1	6.38E-02	1.85E-02	6.46E-02	1.05E-02
Fabric 2	6.09E-02	1.19E-02	4.13E-02	5.64E-03
Fabric 3	5.11E-02	8.38E-03	5.92E-02	8.42E-03

The resulting ANOVA is shown in Figure 5.16 for $\alpha = 0.01$ confidence level.

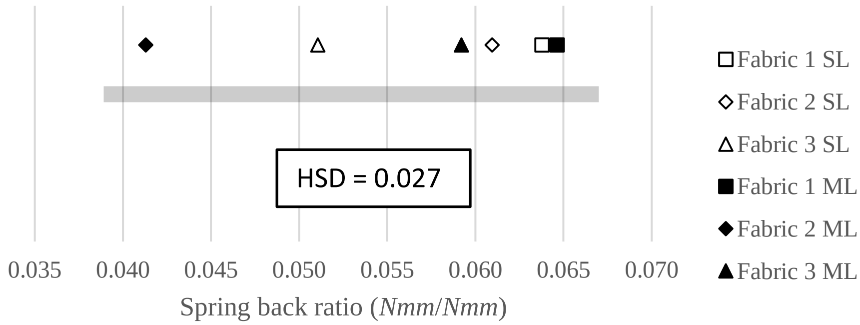

Figure 5.16 – Spring back ratio ANOVA

The ANOVA shows that there are no detectable differences between the spring back ratios of the fabrics. For simplicity, the in-plane shear spring back ratio is assumed constant for all tested fabrics and constant for all shear angles. The in-plane shear spring back energy SBE_{Shear} is obtained by multiplying the energy required for shearing the fabric to a given shear angle by the average in-plane shear spring back ratio for all fabrics, 5.68×10^{-2}:

$$SBE_{shear} = 5.68 \times 10^{-2} \cdot U_{shear}(n, \alpha) \tag{5.17}$$

5.2. Drape energy variability

Fabrics with more consistent draping behaviour are more predictable; therefore, it is easier for technicians to drape them. Fabric variability is therefore an important consideration for evaluating the difficulty of draping fabrics. In this work, draping difficulty is characterized through the drape energy as discussed in Section 5.1. On the other hand, the variability of fabric draping energy is used for characterizing the repeatability of the draping energy, and therefore the repeatability of the draping process. The variability of fabric draping energy is closely related to the variability of the fabric characteristics obtained via testing. The variability of fabric characteristics is difficult to predict, therefore two approaches that use the same data are presented in this work for characterizing the variability in drape energy.

In the first approach, linear functions are used for interpolating the standard deviations of fabric characteristics, in a process that is similar to the interpolating of averages of fabric characteristics as described in Chapter 4. The linear functions are developed in Section 5.2.1. The standard deviations of fabric characteristics represent the dispersion of each given characteristic used in calculating variations in energy for each fabric drape energy term.

In the second approach, the data used in building the linear functions for the fabric characteristics is used for calculating a confidence interval on the estimated value of the fabric characteristic. The prediction intervals represent the dispersion of the given characteristic in calculating the variation in energy for each fabric drape energy. This approach is detailed in section 5.2.2.

Mathematical proofs of all equations appearing in this Chapter are available in Appendix C.

5.2.1. Linear functions for standard deviation

In this approach, the standard deviations of fabric characteristics are correlated to the same independent variables as the linear functions for interpolating average fabric characteristics. Therefore, the DOE plans used for creating the linear functions for the standard deviation of fabric characteristics are the same as the DOE plans used for creating the linear functions for the average of fabric characteristics. Consequently, the linear functions take the form:

$$f(x) = C_0 + C_1x_1 + C_2x_2 + C_{12}\,x_1x_2 + C_3\,x_3 + C_{13}x_1x_3 + C_{23}x_2x_3 + C_{123}x_1x_2x_3 \qquad (5.18)$$

where x_1 and x_2 represent the number of layers in the fabric, and x_3 represents the mould radius. Interpolation modalities x_1 and x_2 are defined in Table 4.3, and interpolation modality x_3 is defined in Table 4.6. Constant C_0 is an average, and coefficients C_1, C_2, C_{12}, C_3, C_{13}, C_{23}, C_{123} are coefficients listed in Table 5.10, Table 5.11, and Table 5.12 for Fabrics 1, 2 and 3 respectively. It must be noted that linear functions for the standard deviations of bending stiffness characteristics (surface mass, overhang length, stiffness) and pin resistance characteristic (pin resistance, load and pin resistance, extension) only include entries for C_0, C_1, C_2 and C_{12} because their linear functions do not feature coefficient C_3, which represents the simulated mould radius during bending spring back tests. Furthermore, linear functions for the standard deviation of friction characteristics only feature C_0 and C_1; C_2 and C_3 are irrelevant as they are associated with the number of layers and the simulated mould radius in bending spring back tests. Furthermore, linear functions for the pin resistance of Fabric 3 are not defined due to difficulties in testing along the bias direction of the fabric.

Table 5.10 – Coefficients of linear functions for standard deviations, Fabric 1

	Range		C_0	C_1	C_2	C_{12}	C_3	C_{13}	C_{23}	C_{123}
Surface mass	$0° < \phi \leq 45°$	N/a	7.83	3.33	0.78	-2.23				
	$45° < \phi \leq 90°$	N/a	8.55	1.50	-0.05	0.40				
O. l.	$0° < \phi \leq 45°$	N/a	1.03	-0.03	-0.33	0.03				
	$45° < \phi \leq 90°$	N/a	0.75	-0.05	0.05	-0.05				
Stiffness	$0° < \phi \leq 45°$	N/a	289.50	180.50	-159.00	-96.00				
	$45° < \phi \leq 90°$	N/a	139.50	81.00	9.00	-3.50				
Convex spring back	$0° < \phi \leq 45°$	$\frac{1}{16} < r \leq \frac{1}{8}$	0.33	0.03	-0.08	-0.03	-0.10	-0.05	0.05	0.05
	$0° < \phi \leq 45°$	$\frac{1}{8} < r \leq \frac{1}{4}$	0.16	-0.01	-0.01	0.01	-0.06	0.01	0.01	-0.01
	$0° < \phi \leq 45°$	$\frac{1}{4} < r \leq \frac{3}{8}$	0.09	0.01	0.01	-0.01	-0.01	0.01	0.01	-0.01
	$0° < \phi \leq 45°$	$\frac{3}{8} < r \leq \frac{1}{2}$	0.05	0.00	0.00	0.00	-0.03	-0.03	-0.03	0.03
	$45° < \phi \leq 90°$	$\frac{1}{16} < r \leq \frac{1}{8}$	0.25	0.00	0.00	0.00	-0.08	-0.03	-0.03	-0.03
	$45° < \phi \leq 90°$	$\frac{1}{8} < r \leq \frac{1}{4}$	0.14	-0.01	-0.01	-0.01	-0.04	0.01	0.01	0.01
	$45° < \phi \leq 90°$	$\frac{1}{4} < r \leq \frac{3}{8}$	0.09	0.01	-0.01	0.01	-0.01	0.01	-0.01	0.01
	$45° < \phi \leq 90°$	$\frac{3}{8} < r \leq \frac{1}{2}$	0.05	0.00	0.00	0.00	-0.03	-0.03	0.03	-0.03
Concave spring back	$0° < \phi \leq 45°$	$\frac{1}{16} < r \leq \frac{1}{8}$	0.83	-0.08	-0.05	0.10	-0.13	0.08	0.00	-0.05
	$0° < \phi \leq 45°$	$\frac{1}{8} < r \leq \frac{1}{4}$	0.46	-0.01	-0.04	0.04	-0.24	-0.01	0.01	-0.01
	$0° < \phi \leq 45°$	$\frac{1}{4} < r \leq \frac{3}{8}$	0.20	0.00	-0.03	0.03	-0.03	0.03	0.00	0.00
	$0° < \phi \leq 45°$	$\frac{3}{8} < r \leq \frac{1}{2}$	0.15	0.03	0.00	0.03	-0.03	0.00	0.03	0.00
	$45° < \phi \leq 90°$	$\frac{1}{16} < r \leq \frac{1}{8}$	0.78	-0.10	0.00	-0.13	-0.23	0.15	-0.10	0.13
	$45° < \phi \leq 90°$	$\frac{1}{8} < r \leq \frac{1}{4}$	0.36	0.04	-0.06	0.01	-0.19	-0.01	0.04	0.01
	$45° < \phi \leq 90°$	$\frac{1}{4} < r \leq \frac{3}{8}$	0.16	0.04	-0.01	0.01	-0.01	0.01	0.01	-0.01
	$45° < \phi \leq 90°$	$\frac{3}{8} < r \leq \frac{1}{2}$	0.13	0.05	-0.03	0.00	-0.03	0.00	-0.03	0.00
Mean friction	$0° < \phi \leq 45°$	N/a	0.02		-0.01					
	$45° < \phi \leq 90°$	N/a	0.03		0.01					
Mean deviation	$0° < \phi \leq 45°$	N/a	0.02		-0.01					
	$45° < \phi \leq 90°$	N/a	0.01		0.00					
Pin resistance, load	$0° < \phi \leq 45°$	N/a	1.39	0.19	0.01	0.23				
	$45° < \phi \leq 90°$	N/a	1.41	0.01	0.00	-0.41				
Pin resistance, extension	$0° < \phi \leq 45°$	N/a	5.37	-1.58	1.83	-0.97				
	$45° < \phi \leq 90°$	N/a	6.89	-1.58	-0.32	0.98				

Table 5.11 – Coefficients for linear functions for standard deviations, Fabric 2

	Range		C_0	C_1	C_2	C_1C_2	C_3	C_1C_3	C_2C_3	$C_1C_2C_3$
Surface mass	$0° < \phi \leq 45°$	N/a	8.98	5.73	0.58	-1.08				
	$45° < \phi \leq 90°$	N/a	21.40	10.60	11.85	5.95				
O. l.	$0° < \phi \leq 45°$	N/a	1.38	0.18	0.33	0.03				
	$45° < \phi \leq 90°$	N/a	1.33	0.18	-0.38	-0.03				
Stiffness	$0° < \phi \leq 45°$	N/a	452.50	307.50	61.00	32.00				
	$45° < \phi \leq 90°$	N/a	351.75	240.25	-161.75	-99.25				
Convex spring back	$0° < \phi \leq 45°$	$\frac{1}{16} < r \leq \frac{1}{8}$	0.34	0.01	-0.09	-0.01	-0.09	-0.01	-0.01	0.06
	$0° < \phi \leq 45°$	$\frac{1}{8} < r \leq \frac{1}{4}$	0.20	-0.01	-0.01	0.01	-0.06	0.01	0.01	-0.01
	$0° < \phi \leq 45°$	$\frac{1}{4} < r \leq \frac{3}{8}$	0.15	0.01	0.01	-0.01	-0.01	0.01	0.01	-0.01
	$0° < \phi \leq 45°$	$\frac{3}{8} < r \leq \frac{1}{2}$	0.10	0.00	0.00	0.00	-0.03	-0.03	-0.03	0.03
	$45° < \phi \leq 90°$	$\frac{1}{16} < r \leq \frac{1}{8}$	0.25	-0.03	0.00	-0.03	-0.08	0.05	0.03	0.00
	$45° < \phi \leq 90°$	$\frac{1}{8} < r \leq \frac{1}{4}$	0.14	-0.01	-0.01	-0.01	-0.04	0.01	0.01	0.01
	$45° < \phi \leq 90°$	$\frac{1}{4} < r \leq \frac{3}{8}$	0.09	0.01	-0.01	0.01	-0.01	0.01	-0.01	0.01
	$45° < \phi \leq 90°$	$\frac{3}{8} < r \leq \frac{1}{2}$	0.06	0.00	0.00	0.00	-0.03	-0.03	0.03	-0.03
Concave spring back	$0° < \phi \leq 45°$	$\frac{1}{16} < r \leq \frac{1}{8}$	1.68	0.07	-0.78	-0.08	-0.33	0.03	-0.03	0.03
	$0° < \phi \leq 45°$	$\frac{1}{8} < r \leq \frac{1}{4}$	1.03	-0.01	-0.04	0.04	-0.24	-0.01	0.01	-0.01
	$0° < \phi \leq 45°$	$\frac{1}{4} < r \leq \frac{3}{8}$	0.61	0.00	-0.03	0.03	-0.03	0.03	0.00	0.00
	$0° < \phi \leq 45°$	$\frac{3}{8} < r \leq \frac{1}{2}$	0.45	0.03	0.00	0.03	-0.03	0.00	0.03	0.00
	$45° < \phi \leq 90°$	$\frac{1}{16} < r \leq \frac{1}{8}$	0.88	0.10	-0.03	0.10	-0.28	-0.05	0.08	-0.10
	$45° < \phi \leq 90°$	$\frac{1}{8} < r \leq \frac{1}{4}$	0.48	0.04	-0.06	0.01	-0.19	-0.01	0.04	0.01
	$45° < \phi \leq 90°$	$\frac{1}{4} < r \leq \frac{3}{8}$	0.36	0.04	-0.01	0.01	-0.01	0.01	0.01	-0.01
	$45° < \phi \leq 90°$	$\frac{3}{8} < r \leq \frac{1}{2}$	0.36	0.05	-0.03	0.00	-0.03	0.00	-0.03	0.00
Mean friction	$0° < \phi \leq 45°$	N/a	0.06		0.02					
	$45° < \phi \leq 90°$	N/a	0.06		-0.02					
Mean deviation	$0° < \phi \leq 45°$	N/a	0.01		0.00					
	$45° < \phi \leq 90°$	N/a	0.00		0.00					
Pin resistance, load	$0° < \phi \leq 45°$	N/a	2.06	0.19	0.01	0.23				
	$45° < \phi \leq 90°$	N/a	1.73	0.01	0.00	-0.41				
Pin resistance, extension	$0° < \phi \leq 45°$	N/a	5.68	-1.58	1.83	-0.97				
	$45° < \phi \leq 90°$	N/a	4.80	-1.58	-0.32	0.98				

Table 5.12 – Coefficients for linear functions for standard deviations, Fabric 3

	Range		C_0	C_1	C_2	C_1C_2	C_3	C_1C_3	C_2C_3	$C_1C_2C_3$
Surface mass	$0° < \phi \leq 45°$	N/a	4.90	-0.85	0.20	1.25				
	$45° < \phi \leq 90°$	N/a	8.38	1.48	3.28	1.08				
O. l.	$0° < \phi \leq 45°$	N/a	1.88	0.38	-0.23	-0.03				
	$45° < \phi \leq 90°$	N/a	1.53	0.43	-0.13	0.08				
Stiffness	$0° < \phi \leq 45°$	N/a	542.25	375.75	-284.75	-180.25				
	$45° < \phi \leq 90°$	N/a	620.00	459.50	362.50	264.00				
Convex spring back	$0° < \phi \leq 45°$	$\frac{1}{16} < r \leq \frac{1}{8}$	0.50	0.05	-0.18	0.03	-0.08	-0.03	-0.05	-0.05
	$0° < \phi \leq 45°$	$\frac{1}{8} < r \leq \frac{1}{4}$	0.30	-0.01	-0.01	0.01	-0.06	0.01	0.01	-0.01
	$0° < \phi \leq 45°$	$\frac{1}{4} < r \leq \frac{3}{8}$	0.18	0.01	0.01	-0.01	-0.01	0.01	0.01	-0.01
	$0° < \phi \leq 45°$	$\frac{3}{8} < r \leq \frac{1}{2}$	0.16	0.00	0.00	0.00	-0.03	-0.03	-0.03	0.03
	$45° < \phi \leq 90°$	$\frac{1}{16} < r \leq \frac{1}{8}$	0.50	0.05	0.18	-0.03	-0.10	0.00	0.03	0.08
	$45° < \phi \leq 90°$	$\frac{1}{8} < r \leq \frac{1}{4}$	0.30	-0.01	-0.01	-0.01	-0.04	0.01	0.01	0.01
	$45° < \phi \leq 90°$	$\frac{1}{4} < r \leq \frac{3}{8}$	0.19	0.01	-0.01	0.01	-0.01	0.01	-0.01	0.01
	$45° < \phi \leq 90°$	$\frac{3}{8} < r \leq \frac{1}{2}$	0.15	0.00	0.00	0.00	-0.03	-0.03	0.03	-0.03
Concave spring back	$0° < \phi \leq 45°$	$\frac{1}{16} < r \leq \frac{1}{8}$	2.39	0.34	-0.89	-0.39	-0.79	0.06	0.49	0.09
	$0° < \phi \leq 45°$	$\frac{1}{8} < r \leq \frac{1}{4}$	1.11	-0.01	-0.04	0.04	-0.24	-0.01	0.01	-0.01
	$0° < \phi \leq 45°$	$\frac{1}{4} < r \leq \frac{3}{8}$	0.59	0.00	-0.03	0.03	-0.03	0.03	0.00	0.00
	$0° < \phi \leq 45°$	$\frac{3}{8} < r \leq \frac{1}{2}$	0.41	0.03	0.00	0.03	-0.03	0.00	0.03	0.00
	$45° < \phi \leq 90°$	$\frac{1}{16} < r \leq \frac{1}{8}$	2.21	-0.06	0.71	-0.01	-0.64	0.19	-0.34	0.04
	$45° < \phi \leq 90°$	$\frac{1}{8} < r \leq \frac{1}{4}$	1.11	0.04	-0.06	0.01	-0.19	-0.01	0.04	0.01
	$45° < \phi \leq 90°$	$\frac{1}{4} < r \leq \frac{3}{8}$	0.51	0.04	-0.01	0.01	-0.01	0.01	0.01	-0.01
	$45° < \phi \leq 90°$	$\frac{3}{8} < r \leq \frac{1}{2}$	0.31	0.05	-0.03	0.00	-0.03	0.00	-0.03	0.00
Mean friction	$0° < \phi \leq 45°$	N/a	0.10		-0.01					
	$45° < \phi \leq 90°$	N/a	0.05		-0.02					
Mean deviation	$0° < \phi \leq 45°$	N/a	0.01		0.00					
	$45° < \phi \leq 90°$	N/a	0.01		0.00					
Pin resistance, load	$0° < \phi \leq 45°$	N/a								
	$45° < \phi \leq 90°$	N/a								
Pin resistance, extension	$0° < \phi \leq 45°$	N/a								
	$45° < \phi \leq 90°$	N/a								

5.2.2. Prediction intervals for regression functions

A prediction interval is the confidence interval on a predicted value in regression analysis. Linear functions built using DOE plans are a special case of multiple linear regression. The polynomial regression functions used for modelling the in-plane shear behaviour are also a special case of multiple linear regression. Prediction intervals for multiple linear regression models are generally calculated using:

$$\Delta y = \pm t_{\frac{\alpha}{2},df}\sqrt{\hat{\sigma}^2(1 + \boldsymbol{x_p^T}(\boldsymbol{X^T X})^{-1}\boldsymbol{x_p})} \tag{5.19}$$

where $t_{\frac{\alpha}{2},df}$ is a statistical parameter depending on the confidence level of the prediction interval α and the degrees of freedom of the mean square error df, $\hat{\sigma}^2$ is the mean square error of the regression, $\boldsymbol{x_p}$ is a vector representing the independent variables used for predicting the dependent variable, and $\boldsymbol{X}$ is the design matrix used in building the regression model [51].

A regression function built using dispersed data will create wider prediction intervals than a regression function built using less dispersed data, as the prediction interval depends on the mean square error of the regression, Equation (5.19). In this approach, the prediction interval represents the dispersion of the data interpolated using the linear functions developed in Chapter 4.

5.2.3. Bending energy variability

Dispersion of bending stiffness is used for characterizing the variability of bending energy. Recalling Section 5.1.1, the bending energy of a fabric is a function of the bending stiffness of that fabric B_{Peirce}, mould radius R_m, width b and opening angle α_m. Assuming that the mould radius, mould opening angle and curvature width are constant – each quantity does not have dispersion – the expression used for calculating the variability of the bending energy is:

$$\Delta U_{bending} = \left(\frac{1}{2}\right) b \frac{\alpha_m}{R_m} \Delta B_{Peirce} \tag{5.20}$$

where ΔB_{Peirce} is the dispersion of the bending stiffness.

5.2.4. Bending spring back energy variability

Geometric differences in convex and concave spring back tests resulted in two different expressions for characterizing the bending spring back energy of fabrics. This is also the case for the variability of bending spring back. In convex spring back cases, the final opening angle of the fabric is not identical to the opening angle of the mould; therefore, Equation (5.21) is used for calculating the variability of convex spring back energy:

$$\Delta SBE_{Bending} = \frac{1}{2} b \left(\Delta B_{Peirce} \cdot \frac{\alpha_m}{R_m} + \frac{B_{Peirce}\alpha_f}{R_f} \cdot \left(\frac{\Delta\alpha_f}{\alpha_f} + \frac{\Delta R_f}{R_f} + \frac{\Delta B_{Peirce}}{B_{Peirce}} \right) \right) \tag{5.21}$$

where ΔR_f is the final fabric radius and $\Delta\alpha_f$ is the final fabric opening angle. Equations used for obtaining ΔR_f and $\Delta\alpha_f$ are:

$$\Delta R_f = \frac{\beta}{R_m} \Delta\beta \tag{5.22}$$

$$\Delta\alpha_f = \frac{1}{R_f} \Delta\beta \tag{5.23}$$

where $\Delta\beta$ is the dispersion of this raw spring back data.

In the concave spring back case, the final opening angle of the fabric was assumed equal to the mould opening angle, and the final fabric radius was equal to the raw spring back measurement. Therefore, Equation (5.24) is used for calculating the variability of the concave spring back energy:

$$\Delta SBE_{Bending} = \frac{1}{2} \cdot \alpha_m \cdot b \left(\frac{\Delta B_{Peirce}}{R_m} + \frac{B_{Peirce}}{R_f} \left(\frac{\Delta B_{Peirce}}{B_{Peirce}} + \frac{\Delta R_f}{R_f} \right) \right) \tag{5.24}$$

In this case, raw spring back measurements were assumed equal to the final fabric radius. Therefore, dispersion of the final fabric radius is equal to the dispersion of spring back measurements.

5.2.5. In-plane shear energy variability

The strain energy required for shearing a fabric in-plane to a specified shear angle was previously defined as the integral of raw picture-frame test results. Two approaches were specified for obtaining the shear energy, both involving converting the shear angle to an extension, using Equation (5.12).

The first approach uses a table lookup function to find the standard deviation of the shear energy, and quantifies the variability of shear energy as the standard deviation of shear energy. Standard deviations of shear energy for different fabrics and numbers of layers are plotted as a function of picture-frame extension in Figure 5.17.

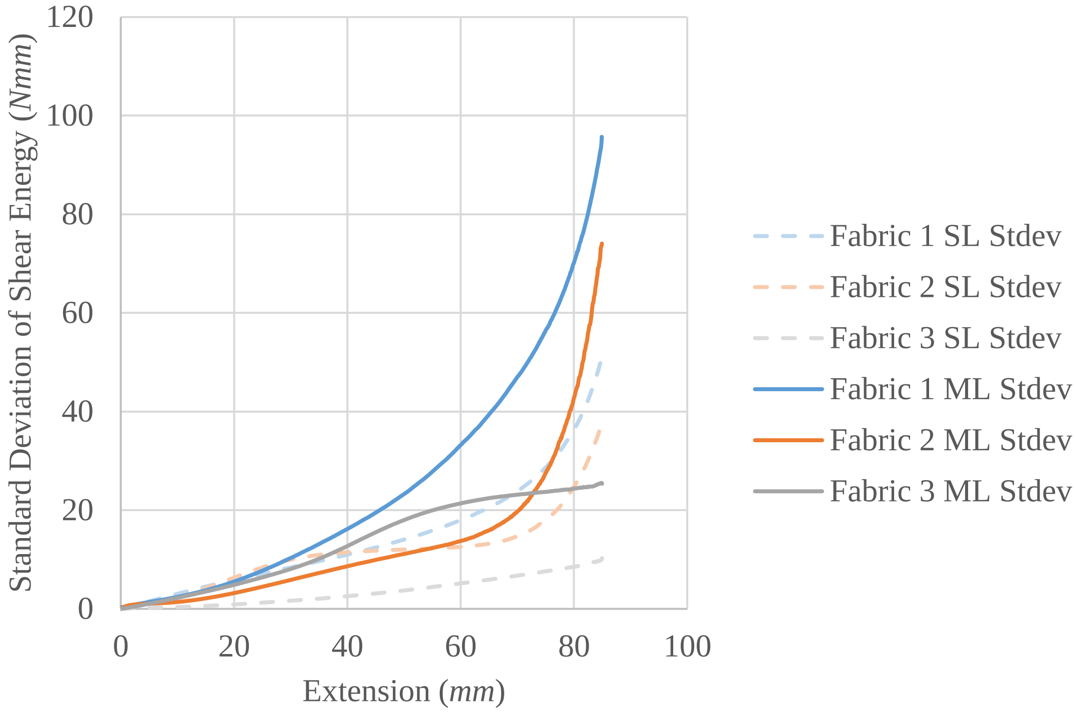

Figure 5.17 – Standard deviations of shear energy

The second approach uses the polynomial regression Equation (5.11) with the relevant regression coefficients listed in Table 5.1. The prediction interval is calculated using Equation (5.19) and is taken to represent the variability of shear energy. Polynomial regressions and prediction intervals for each fabric tested are shown in Figure 5.18 to Figure 5.23.

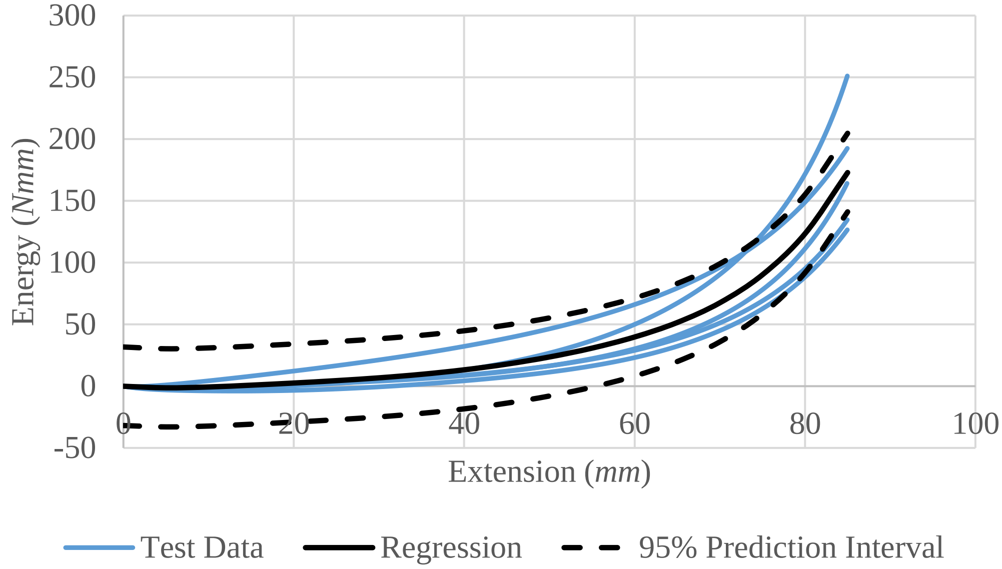

Figure 5.18 – Polynomial regression for Fabric 1, single layer

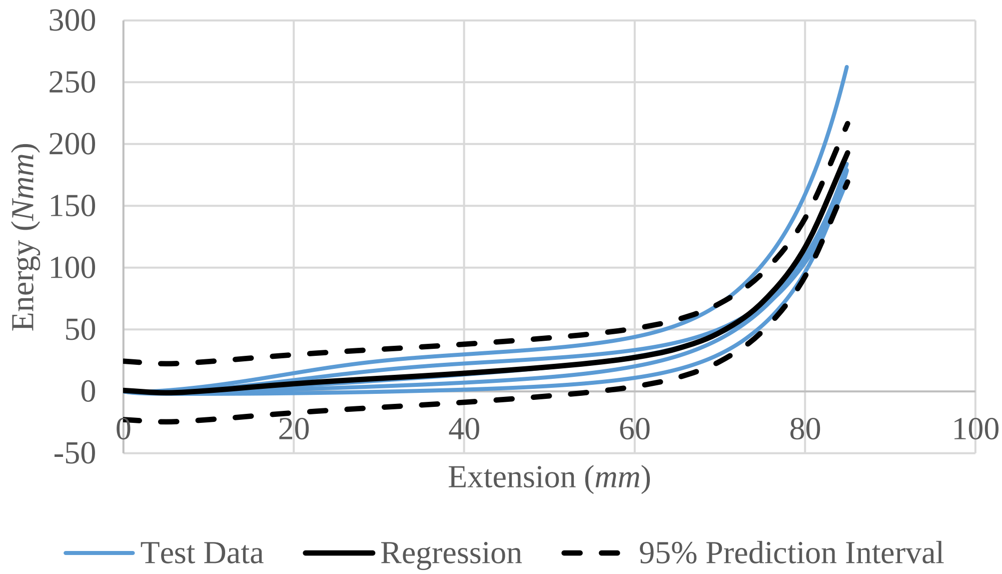

Figure 5.19 – Polynomial regression for Fabric 2, single layer

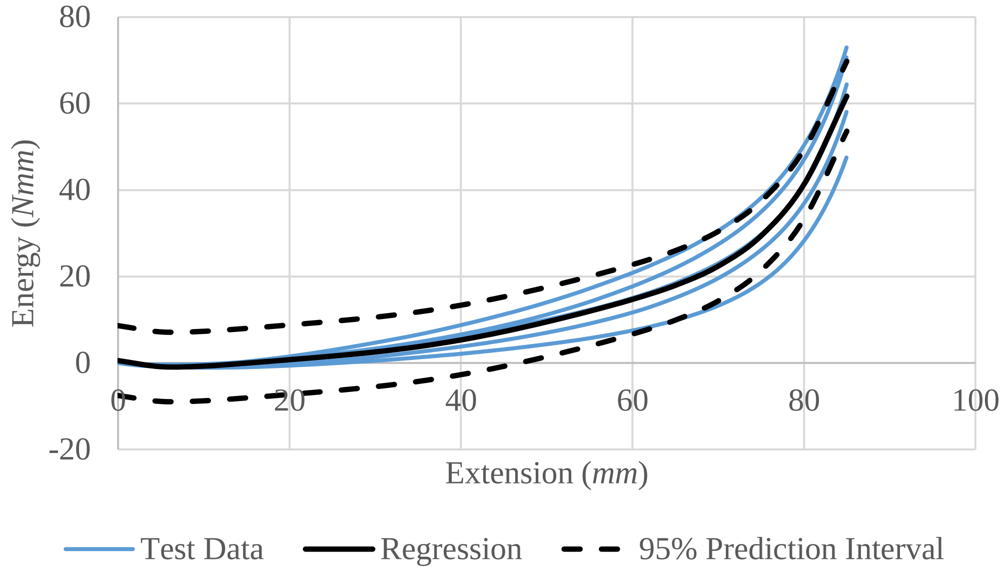

Figure 5.20 – Polynomial regression for Fabric 3, single layer

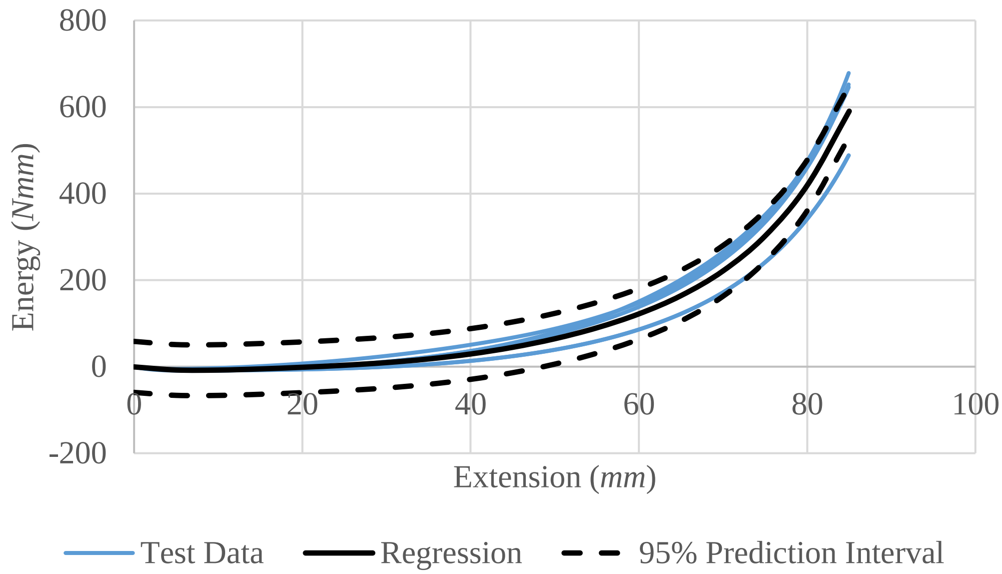

Figure 5.21 – Polynomial regression for Fabric 1, multilayer

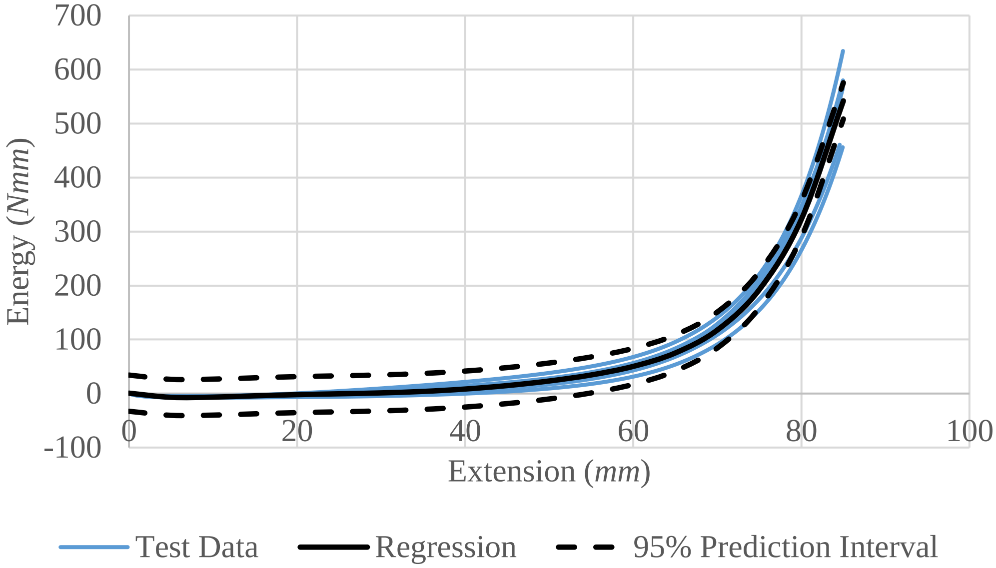

Figure 5.22 – Polynomial regression for Fabric 2, multilayer

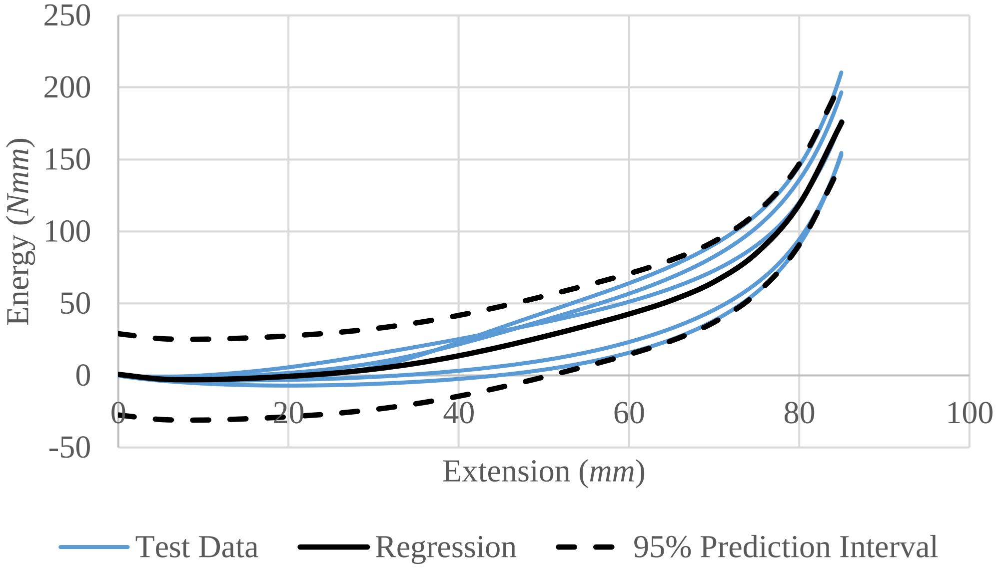

Figure 5.23 – Polynomial regression for Fabric 3, multilayer

Both approaches for quantifying the variability of the shear energy require linear interpolation for quantifying the variability of the shear energy of multilayer fabrics:

$$\Delta U_{shear}(n,\gamma) = \frac{S_{BS}}{S_{PF}}\left(\left(\frac{n-1}{3}\right)\cdot\left(\Delta U_{shear}(4,\gamma) - \Delta U_{shear}(1,\gamma)\right) + \Delta U_{shear}(1,\gamma)\right) \quad (5.25)$$

$$\Delta U_{shear}(n,\gamma) = \frac{S_{BS}}{S_{PF}}\left(\left(\frac{n-1}{2}\right)\cdot\left(\Delta U_{shear}(3,\gamma) - \Delta U_{shear}(1,\gamma)\right) + \Delta U_{shear}(1,\gamma)\right) \quad (5.26)$$

where $\Delta U_{shear}(n,\gamma)$ is the variability of the shear energy of fabrics, n is the number of layers in the fabric, S_{BS} is the surface area of the base surface, and S_{PF} is the surface area of the sheared fabric during the picture frame tests. The area of sheared fabric during the picture-frame tests is taken as 19 600 mm^2.

Equation (5.25) is used for interpolating the variability of the shear energy for Fabric 1 and Fabric 2, as picture-frame shear tests were conducted for 1 layer and for 4 layer samples of fabric. Equation (5.26) is used for interpolating the variability of the shear energy for Fabric 3, as tests were conducted for 1 layer and 3 layer samples.

5.2.6. In-plane shear spring back energy variability

The dispersion of in-plane shear energy is used for characterizing the variability of in-plane shear energy. Recalling Section 5.1.3, the shear energy of a fabric is a function of the shear angle and number of layers in the fabric stack. Recalling Section 5.1.4, the in-plane shear spring back ratio is assumed constant for all tested fabrics and for all shear angles, and is calculated using:

$$SBE_{shear} = 5.68 \times 10^{-2} \cdot U_{shear}(n,\gamma) \quad (5.27)$$

where SBR is the spring back ratio and $U_{shear}(n,\gamma)$ is the shear energy required for shearing a stack of n layers of fabric to γ degrees. The in-plane shear spring back energy variability is calculated using:

$$\Delta SBE_{shear} = 5.68 \times 10^{-2} \cdot \Delta U_{shear}(n, \gamma) \qquad (5.28)$$

where $\Delta U_{shear}(n,\gamma)$ is the variability of the shear energy required for shearing n layers of fabric to γ degrees.

5.3. Statistical considerations

This Section discusses statistical considerations related to quantifying fabric behaviour variability. Topics discussed include the use of prediction intervals versus interpolation of standard deviations, and the effect of the confidence level on the size of prediction intervals.

5.3.1. Prediction interval versus interpolation of standard deviation

As discussed in Section 5.2.2, a prediction interval represents a confidence interval for a predicted value in regression analysis. Calculations of prediction intervals for regression analysis are detailed in many textbooks, such as [51]. The linear functions that were developed in this thesis for interpolating the standard deviation of fabric characteristics are not a standard method for predicting the variability of fabric characteristics.

The linear functions developed in Chapter 4 are piecewise multiple linear regressions equations, defined for specified ranges of yarn orientations and/or simulated mould radii. It should be noted that the variability of fabric behaviour is only known at the lower and upper limits of each linear function. Furthermore, in cases where a parameter is probed at more than 2 modalities the prediction intervals are discontinuous at the upper and lower limits of the range of validity of the linear functions due to the piecewise nature of these linear functions. The 95% prediction interval for the overhang length of one layer of Fabric 1 is compared graphically to the standard deviation linear interpolation functions for the same characteristic in Figure 5.24. The discontinuity that is present at an orientation of 45° in the latter does not exist in the former.

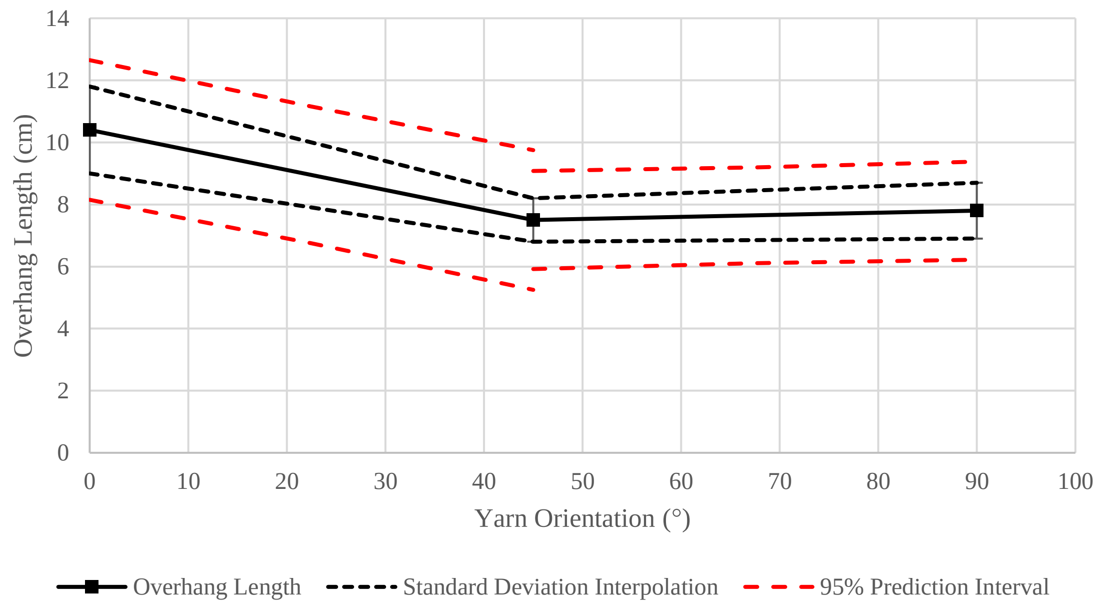

Figure 5.24 – Standard deviation interpolation vs. prediction interval, overhang length of one layer of Fabric 1

The prediction intervals provide a statistically sound estimate of the variability of fabric characteristics; however, the variability is discontinuous at the locations where the piecewise function is divided. The standard deviation interpolation functions provide continuous estimates of the variability of fabric characteristics from one section of piecewise function to the next; however, the statistical validity of this method is unclear.

In some cases, the prediction interval provided by the linear function is greater than the predicted value of the fabric characteristic. Such cases generally occur upon estimating the bending stiffness of fabrics. The bending stiffness linear function for one layer of Fabric 1 is shown in Figure 5.25.

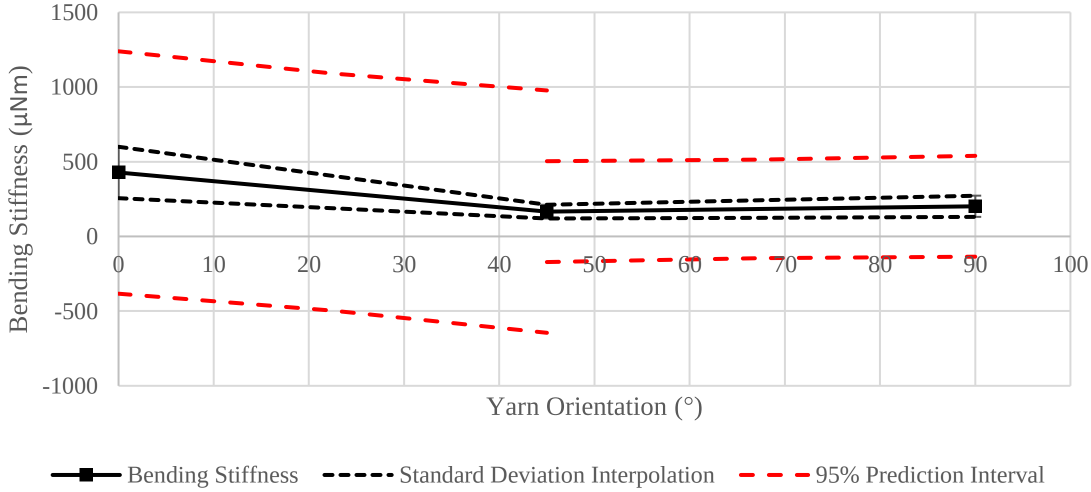

Figure 5.25 – Discontinuous prediction interval, bending stiffness of one layer of Fabric 1

The 95% prediction interval produces variability that is larger than the average value of the bending stiffness for the single layer of Fabric 1. Prediction intervals for four layers of Fabric 1 are shown in Figure 5.26, where the width of the interval approaches the standard deviation interpolation.

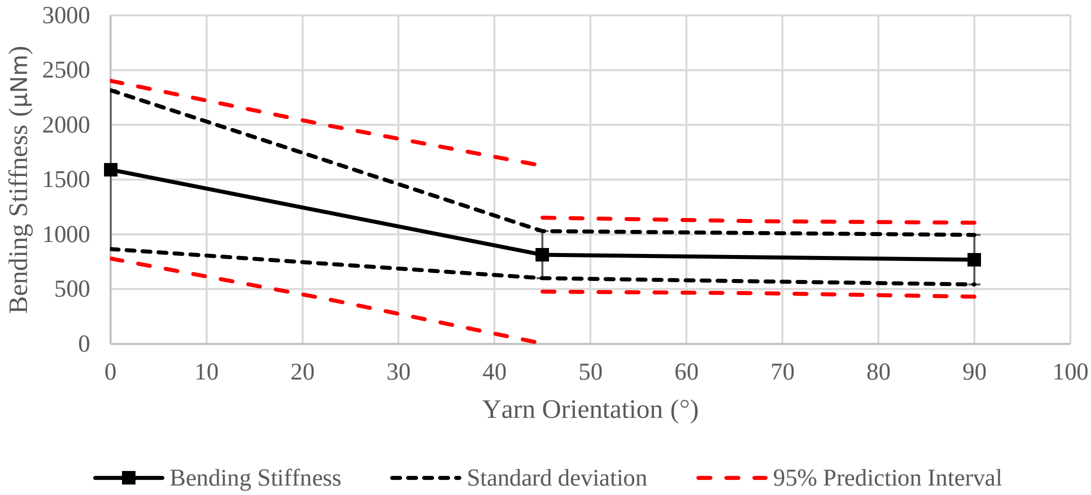

Figure 5.26 – Discontinuous prediction interval, bending stiffness of four layers of Fabric 1

The width of prediction intervals are nearly identical for single layer fabrics and for multilayer fabrics. Recalling Equation (5.19), the prediction interval is a function of the mean square error of the regression equation $\hat{\sigma}^2$, the independent variables used for predicting the bending stiffness $\boldsymbol{x_p}$, and the design matrix $\boldsymbol{X}$ used for building the regression equation. The design matrix $\boldsymbol{X}$ used for building bending stiffness linear functions and their prediction intervals is a 4x3 orthogonal matrix,

$$\boldsymbol{X} = \begin{bmatrix} -1 & -1 & 1 \\ 1 & -1 & -1 \\ -1 & 1 & -1 \\ 1 & 1 & 1 \end{bmatrix}$$

where each row represents one run of experiments. The first two columns represent the input variables used for building the linear functions; the first column represents the number of layers and the second column represents yarn orientation. The third column represents the interaction of both independent variables. Table 5.13 and Table 5.14 summarize the data used for building the piecewise linear functions.

Table 5.13 – Design matrix for bending stiffness linear functions, 0° to 45° yarn orientation

	Number of Layers	Yarn Orientation	Interaction	
Run 1	-1 = 1 Layer	-1 = 0° (Warp)	+1	5 Measurements
Run 2	+1 = 4 Layers	-1 = 0° (Warp)	-1	5 Measurements
Run 3	-1 = 1 Layer	+1 = 45° (Bias)	-1	5 Measurements
Run 4	+1 = 4 Layers	+1 = 45° (Bias)	+1	5 Measurements

Table 5.14 – Design matrix for bending stiffness linear functions, 45° to 90° yarn orientation

	Number of Layers	Yarn Orientation	Interaction	
Run 1	-1 = 1 Layer	-1 = 45° (Bias)	+1	5 Measurements
Run 2	+1 = 4 Layers	-1 = 45° (Bias)	-1	5 Measurements
Run 3	-1 = 1 Layer	+1 = 90° (Weft)	-1	5 Measurements
Run 4	+1 = 4 Layers	+1 = 90° (Weft)	+1	5 Measurements

The $(\boldsymbol{X^T X})^{-1}$ term in Equation (5.19) is the Moore-Penrose inverse of the design matrix used for building the linear functions. The same design matrix is used for both subdomains of the piecewise linear function. The Moore-Penrose inverse of the design matrix is given by:

$$(\boldsymbol{X^T X})^{-1} = \begin{bmatrix} \frac{1}{4} & 0 & 0 \\ 0 & \frac{1}{4} & 0 \\ 0 & 0 & \frac{1}{4} \end{bmatrix}$$

therefore, the calculation of the prediction interval can be simplified:

$$\Delta y = \pm t_{\frac{\alpha}{2},df} \sqrt{\hat{\sigma}^2 (1 + \frac{\mathbf{1}}{\mathbf{4}} \boldsymbol{x_p^T I_3 x_p})} \tag{5.29}$$

where $\boldsymbol{I_3}$ is the 3x3 identity matrix. The $\boldsymbol{x_p^T}$ term in Equation (5.29) is a row vector that represents the independent variables used for building the linear functions. The prediction interval calculation can then be further simplified to:

$$\Delta y = \pm t_{\frac{\alpha}{2},df}\sqrt{\hat{\sigma}^2(1+\frac{1}{4}\left(\boldsymbol{x_1^2}+\boldsymbol{x_2^2}+\boldsymbol{x_3^2}\right))} \tag{5.30}$$

where x_1, x_2 and x_3 are numbers between -1 and +1 that represent the number of layers, the yarn orientation, and the interaction of both variables on the bending stiffness of fabrics. The maximum value of the sum of the squared input variables x_1, x_2 and x_3 is 3, and the minimum value is 0, therefore the prediction intervals for the bending stiffness lie between $t_{\frac{\alpha}{2},df}\sqrt{\hat{\sigma}^2}$ and $1.32\ t_{\frac{\alpha}{2},df}\sqrt{\hat{\sigma}^2}$:

$$\Delta y = \pm\frac{\sqrt{7}}{2}t_{\frac{\alpha}{2},df}\hat{\sigma} \approx \pm 1.32\ t_{\frac{\alpha}{2},df}\sqrt{\hat{\sigma}^2} \tag{5.31}$$

$$\Delta y = \pm t_{\frac{\alpha}{2},df}\sqrt{\hat{\sigma}^2} \tag{5.32}$$

where $\hat{\sigma}^2$ is the mean square error of the regression. The number of layers does not dramatically affect the prediction interval given by the regression analysis; therefore the prediction intervals for single and multilayer fabrics are similar.

In the bending stiffness linear functions, the mean square error is estimated by averaging the statistical variances of each run used for building the linear function. The statistical variance is estimated by squaring the standard deviation of each run; therefore the prediction interval is closely related to the dispersion of the raw measurements of bending stiffness. The bending stiffness of fabrics is a function of the surface mass of fabrics and their overhang length, cubed.

In this thesis, every raw measurement of overhang length corresponded to one measurement of bending stiffness, meaning that small deviations of overhang length resulted in large deviations of bending stiffness. An alternate method for characterizing the variability of bending stiffness consists in using the linear function outputs for estimating the overhang length, a prediction interval for the overhang length, the surface mass of fabrics and a prediction interval for the surface mass of fabrics:

$$\Delta B_{Peirce} = \pm \frac{9.81 \times 10^{-6} \times M}{8} \times l^3 \left(\frac{\boldsymbol{\Delta M}}{M} + 3\frac{\boldsymbol{\Delta l}}{l}\right) \tag{5.33}$$

where ΔM is the prediction interval of the surface mass and Δl is the prediction interval of the overhang length of the fabric. The linear functions for the surface mass and overhang length make use of the same design matrix as for bending stiffness, therefore Equation (5.30) is valid for calculating their prediction intervals.

This method for calculating the variability of the bending stiffness appears to produce smaller estimates of that variability. The variability is proportional to the surface mass of the fabric, itself a function of the number of layers; therefore, the variability of the bending stiffness is a function of the number of layers in the stack of fabric. The variability of the bending stiffness defined in Equation (5.33) is henceforth used for characterizing the variability of the bending stiffness of fabrics.

5.3.2. Effect of confidence level on prediction intervals

A prediction interval is calculated using Equation (5.19), where $t_{\frac{\alpha}{2},df}$ is a statistical parameter that depends on the confidence level used for calculating that prediction interval. In the linear functions developed in this thesis, the prediction interval calculation is simplified due to the orthogonal design matrices used for creating the regression equations. Recalling Equations (5.31) and (5.32), the prediction intervals for bending stiffness linear functions were a function of $t_{\frac{\alpha}{2},df}$, a statistical parameter that depends on the confidence level used for calculating the prediction interval and the degrees of freedom of the mean square error. The mean square error of the bending stiffness linear functions have 76 degrees of freedom. *t*-statistic values for 76 degrees of freedom were generated using Excel and are listed in Table 5.15. Prediction intervals widen when the confidence level increases, because values of $t_{\frac{\alpha}{2},df}$ increase when the confidence level increases.

Table 5.15 – *t*-statistic values for given confidence level for 76 degrees of freedom

Confidence level	$t_{\frac{\alpha}{2},76}$
99.9%	3.42
99.0%	2.64
90.0%	1.67
67.98%	1.00

Higher confidence levels always result in wider prediction intervals, even when the prediction interval calculation is not simple, as was the case with the bending stiffness prediction interval. Shown in Figure 5.27, a higher confidence level results in a wider prediction interval for the shear energy of one layer of Fabric 1.

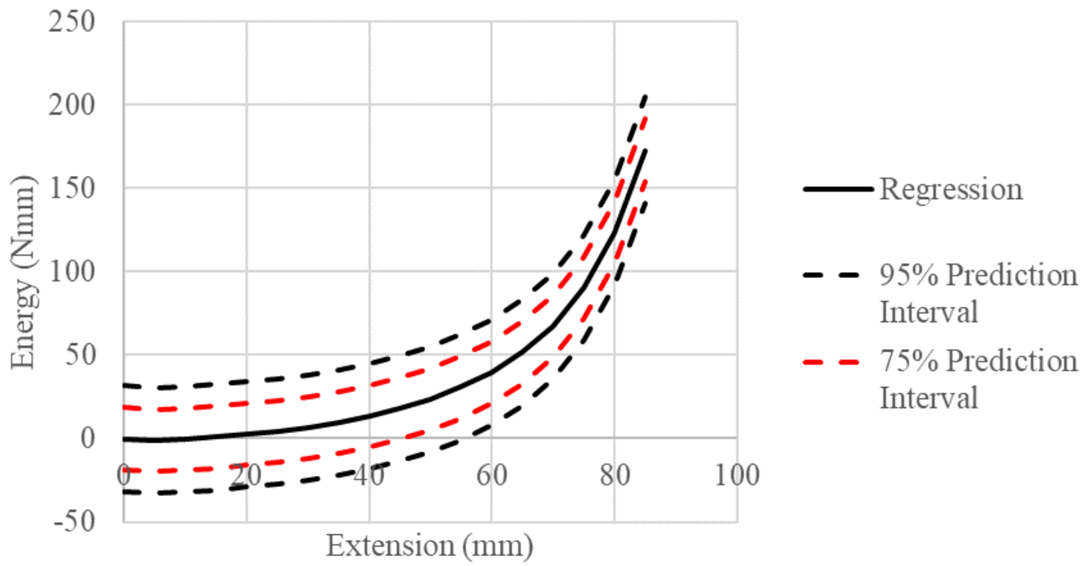

Figure 5.27 – 95% vs. 75% prediction intervals for one layer of Fabric 1

The confidence level used in demonstrating the drape energy and variability calculations in Chapter 6 is taken at 95%.

Chapter 6. Drape energy demonstration

Drape energy calculations were introduced in Chapter 5, making use of base surface parameters and mechanical fabric characteristics for calculating the drape energy and the variability of the drape energy required for draping one single base surface. The purpose of this chapter is to three draping strategies, defined as sequences of steps completed towards covering an entire mould with a single pattern [9]. Upon analyzing a given draping strategy, drape energy and variability calculations are made for each individual base surface, sequentially as they are covered. Fibre orientations, levels of shear, energy and variability on each base surface will vary from one strategy to another, enabling comparisons of the difficulty and variability of draping multiple fabrics using multiple draping strategies onto the entire mould.

This Chapter is divided into three Sections. Section 6.1 discusses a ruleset developed in [9] for creating a draping strategy.

Section 6.2 describes an industrial mould used for demonstrating the updated ruleset for creating a draping strategy. The industrial mould is broken down into multiple base surfaces modelled using a five parameter conical frustum. Three distinct draping strategies are introduced.

Section 6.3 demonstrates drape energy and variability calculations applied to the draping of the entire mould, using the three draping strategies introduced in Section 6.2. Energy and variability calculations are made using three fabrics. The resulting drape energy and variability of each fabric and each draping strategy are compared for informing fabric performance during the drape process.

6.1. Preliminary draping strategy

The draping strategy defined in [9] can be summarized into seven steps:

1. Break down the mould into multiple three and four edged base surfaces;
2. Model each base surface using the five parameter conical frustum;
3. Select a starting base surface;
4. Use linear functions for estimating the shear angles occurring along base surface edges;
5. Drape a base surface adjacent to the starting base surface;
6. Use linear functions for estimating the shear angles occurring along the base surface edges;
7. Repeat until all the base surfaces are covered.

This algorithm makes use of conical frustum base surface parameters and starting drape parameters for calculating the distribution of shear angles and yarn orientations along base surface edges using linear interpolation functions. The conical frustum parameters used for calculating shear angles and yarn orientations are shown in Figure 5.11. Definition of starting drape parameters is shown in Figure 6.2, Figure 6.3 and Figure 6.4.

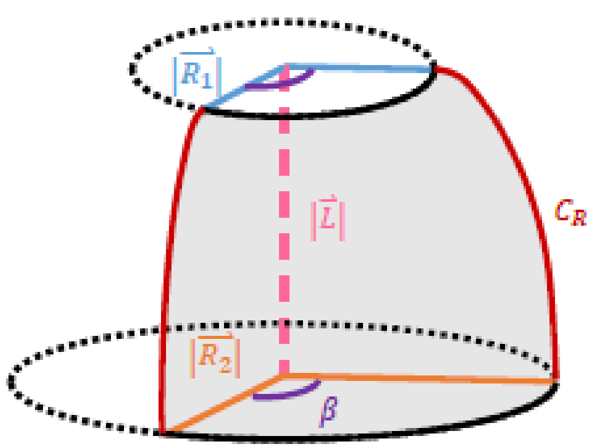

Figure 6.1 – Five-parameter conical frustum [9]

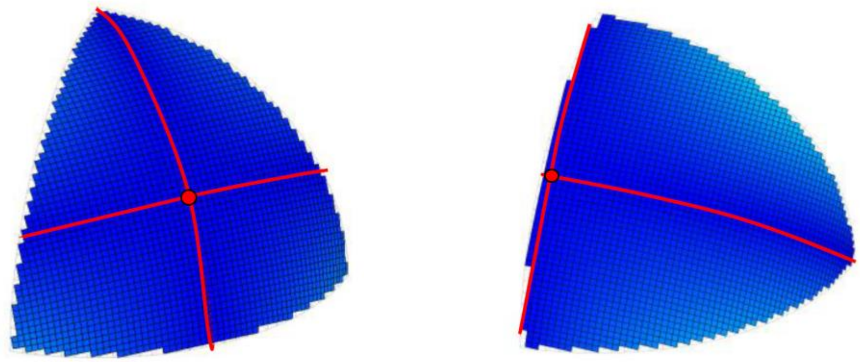

Figure 6.2 – Starting drape position (left: centre of base surface, right: middle of longest edge)

[9]

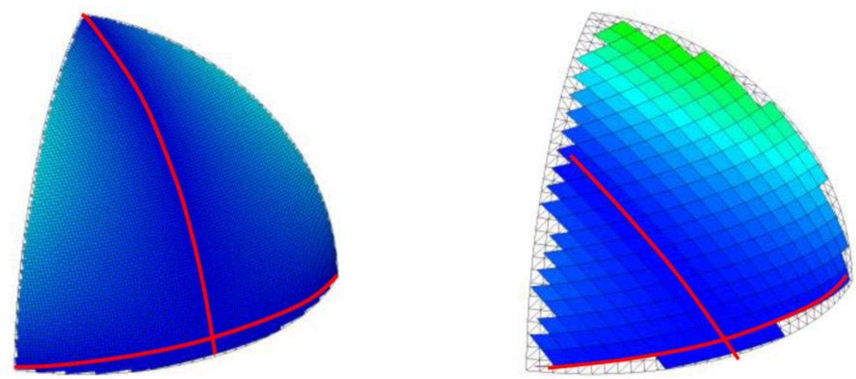

Figure 6.3 – Initial shear angle (left: 0° shear angle, right: 30° shear angle) [9]

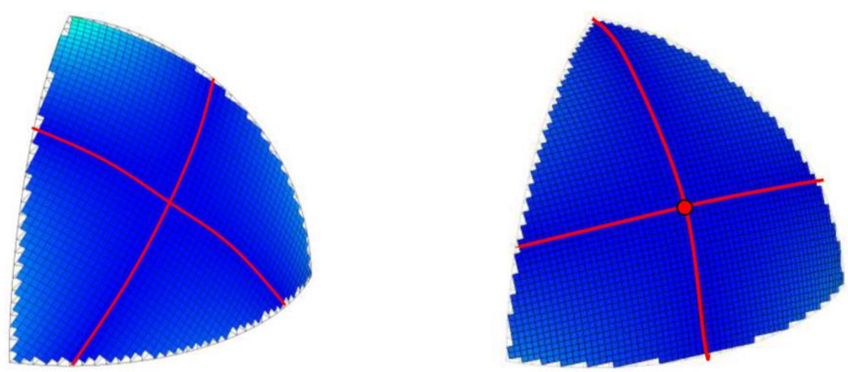

Figure 6.4 – Initial yarn orientation (left: 45°, right: 0°) [9]

Shear angles and yarn orientations on the base surfaces are calculated by selecting the starting drape position, and then by inputting the conical frustum parameters, starting yarn orientation and starting shear angle into the interpolation functions. The distribution of shear angles is given by providing estimates of the shear angles and yarn orientations at each base surface vertex and at the centre of each base surface edge, shown in Figure 6.7.

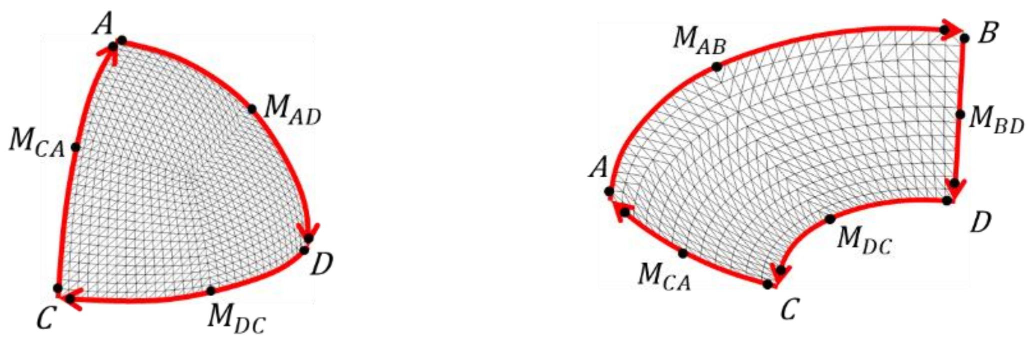

Figure 6.5 – Locations of shear angles for 3-edged (left) and 4-edged (right) base surfaces [9]

The preliminary drape algorithm defines a draping strategy as a sequence of steps for covering an entire mould with a single pattern [9]. The draping strategy contains two main components: connections between base surfaces, and the sequence along which the connections appear. Once any given mould is broken down into three and four edged base surfaces, a large number of possible draping strategies can be defined for a given mould. Consider an idealized mould with 8 base surfaces, shown in Figure 6.6. A draping strategy can be defined for this mould by starting the draping process on base surface 7, then covering base surfaces 8, 9, 6, 3, 2, 1, 4 and 5 sequentially.

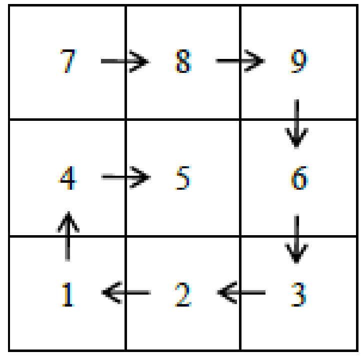

Figure 6.6 – Example of a draping strategy

In addition to the first iteration of the draping algorithm, several rules are listed in [9] for ensuring that all base surfaces are covered in a draping strategy, and for exploring multiple draping strategies:

1. There is only one starting surface;
2. The starting point is defined as the centre point on a single base surface, not as any other point on the base surface;
3. All surfaces are covered only once;
4. Surfaces are covered from an adjacent surface that is already covered, with both surfaces sharing at least one common edge. Surfaces are covered by draping through common edges only, not through vertices;
5. Once the first base surface in the draping strategy is covered, the drape starting position parameter for all subsequent base surfaces is at the middle of the edge that connects both base surfaces. This ensures that yarn orientations are continuous at the edges of base surfaces. Continuity of yarn orientations is shown in Figure 6.7;

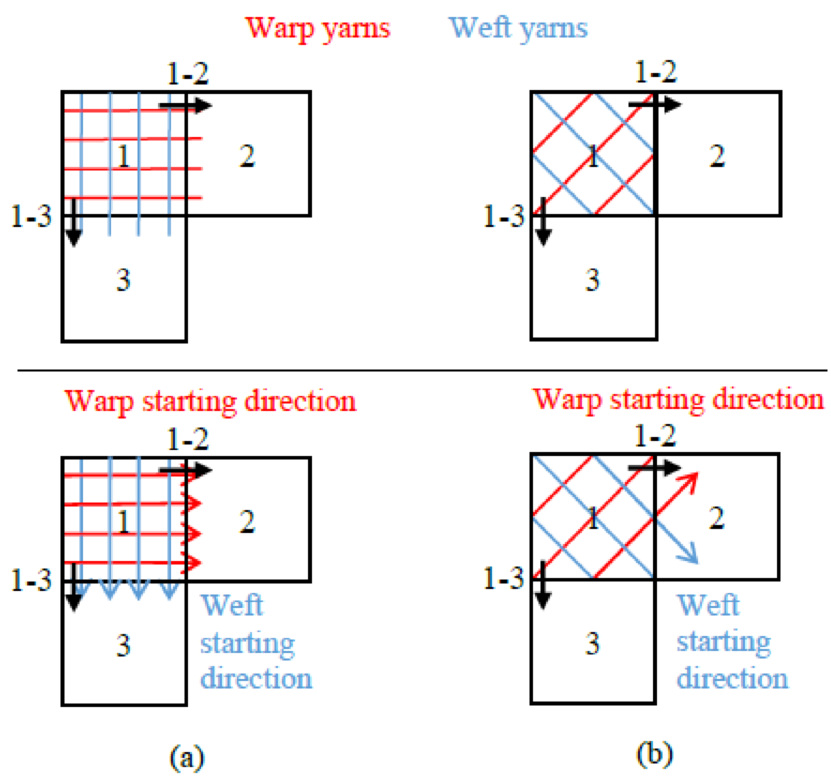

Figure 6.7 – Starting drape parameters for subsequent base surfaces [9]

6. When covering a given surface, some of the adjacent base surfaces may already be covered. An example of a strategy where an adjacent base surface is already covered is shown in Figure 6.8, where base surface 5 can be draped by entering from base surface 2 while base surface 4 is already covered. Base surface 5 can also be draped by entering from base surface 4 while base surface 2 is already covered;

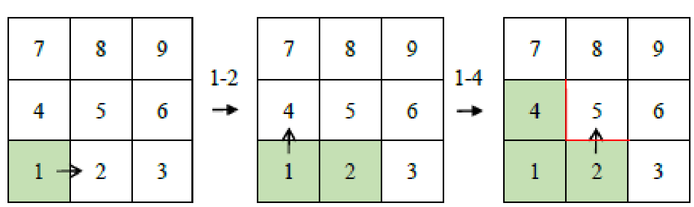

Figure 6.8 – Two starting positions

7. There is no method for distinguishing what would be regarded as theoretically possible but impractical strategies.

Rule 6 specifies that some of the adjacent base surfaces may already be covered while draping a base surface. The drape starting position parameter in the linear functions for calculating shear angles along base surface edges requires only one starting position; therefore, the rule appears problematic for calculating the shear angles and the yarn orientations along the base surface edges. In these cases, the average yarn orientation and shear angles are used for estimating the distribution of yarn orientations and shear angles across the base surfaces. Consider base surface 5 in Figure 6.9. Base surface 5 can be draped from base surface 2 or from base surface 4. One set of shear angles and yarn orientations results from draping the base surface from the middle of the edge connecting base surfaces 4 and 5. Another set of shear angles and yarn orientations results from draping the base surface from the middle of the edge connecting base surfaces 2 and 5. The averages of shear angles and yarn orientations calculated from both starting positions are used for estimating the shear angles and yarn orientations along the remaining two base surfaces.

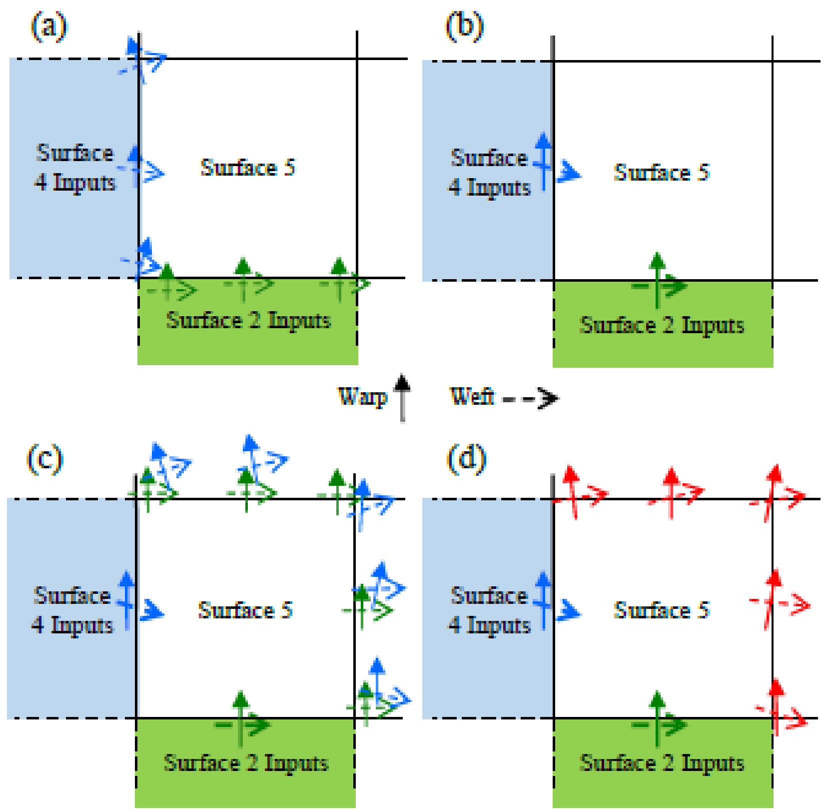

Figure 6.9 – Consolidation of boundary conditions: (a) boundary conditions; (b) chosen boundary condition input; (c) results from both boundary conditions; (d) average of results [9]

6.2. FR mould

The FR mould shown in Figure 6.10 was used for demonstrating drape energy and variability calculations over entire moulds. The FR mould was broken down into 22 base surfaces using the five-parameter frustum model [9], Figure 6.11. Base surface parameters for single and double curvature surfaces are listed in Table 6.1.

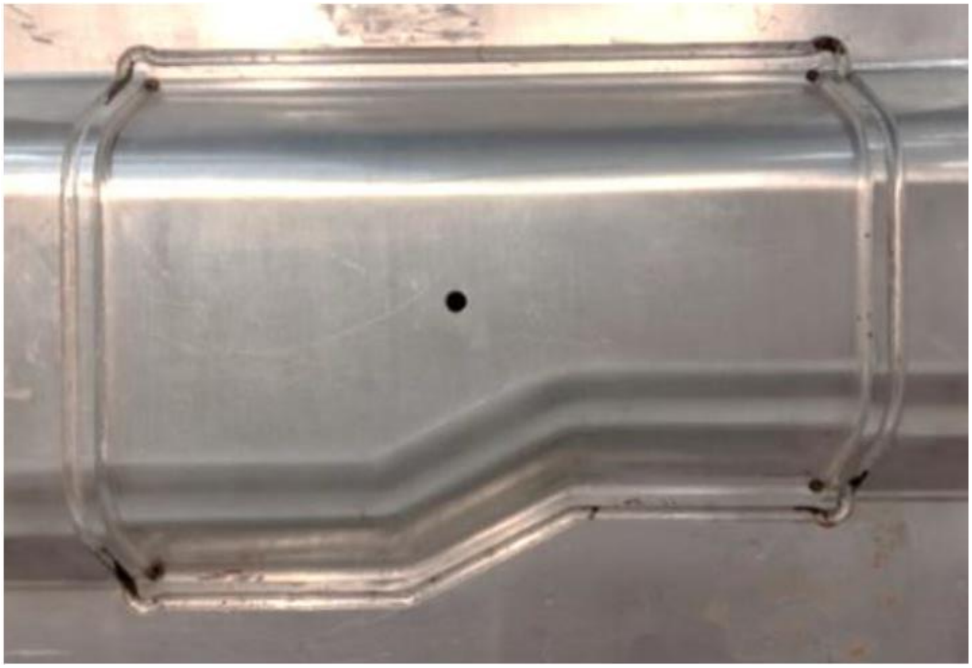

Figure 6.10 – FR demonstrator mould

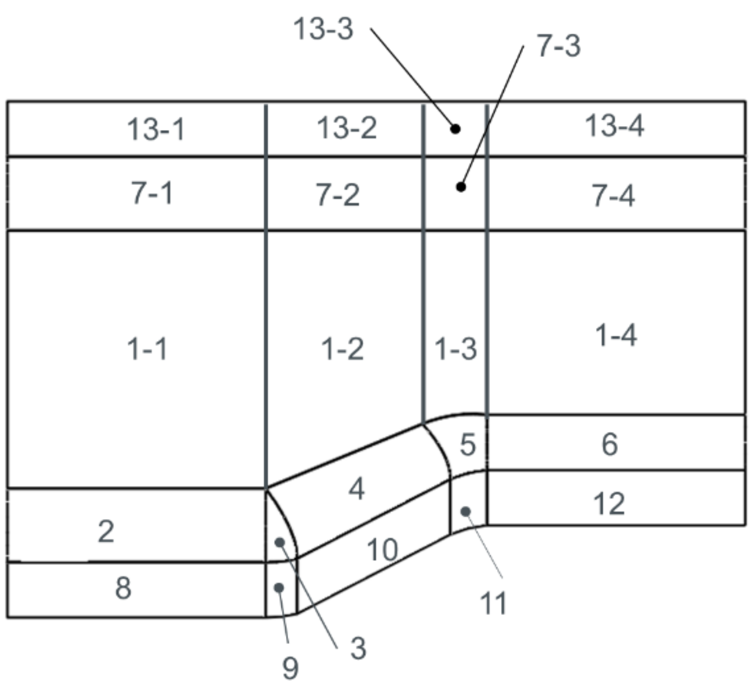

Figure 6.11 – Break down of base surfaces

Table 6.1 – FR mould five-parameter conical frustum parameters

Base surface	Five-parameter conical frustum parameters					Base Surface type
	R_1	R_2	C_R	$L_{5\text{-}para}$	$\beta_{5\text{-}para}$	
2	2.5 *cm*	2.5 *cm*	∞	7 *cm*	60°	Single curvature
3	0 *cm*	3 *cm*	2.5 *cm*	2.5 *cm*	18°	Double curvature
4	2.5 *cm*	2.5 *cm*	∞	4.75 *cm*	60°	Single curvature
5	3.5 *cm*	3 *cm*	2.5 *cm*	2.5 *cm*	23.5°	Double curvature
6	2.5 *cm*	2.5 *cm*	∞	7 *cm*	60°	Single curvature
7-1	2.5 *cm*	2.5 *cm*	∞	7 *cm*	60°	Single curvature
7-2	2.5 *cm*	2.5 *cm*	∞	3.8 *cm*	60°	Single curvature
7-3	2.5 *cm*	2.5 *cm*	∞	2.2 *cm*	60°	Single curvature
7-4	2.5 *cm*	2.5 *cm*	∞	7 *cm*	60°	Single curvature
9	2.75 *cm*	2.75 *cm*	∞	2.69 *cm*	18°	Single curvature
11	3 *cm*	3 *cm*	∞	3.2 *cm*	22°	Single curvature

Inputs used for calculating shear angles on double curvature surfaces and the resulting yarn orientations and shear angles are shown in Section 6.3.

6.2.1. FR mould, strategy 1

The first draping strategy initiates the draping process on base surface 10, with a 0°/90° yarn orientation. The warp yarns (blue arrows) are perpendicular to the edge connecting base surfaces 4 and 10, shown in Figure 6.12. Weft yarns (red arrows) are perpendicular to warp yarns. The first base surfaces covered in this strategy are base surfaces 4, 1-2, 7-2 and 13-2 (Figure 6.13). As these are single curvature or flat surfaces, the fabric is not sheared during this part of the draping sequence. Yarn orientations are known along all the base surface edges.

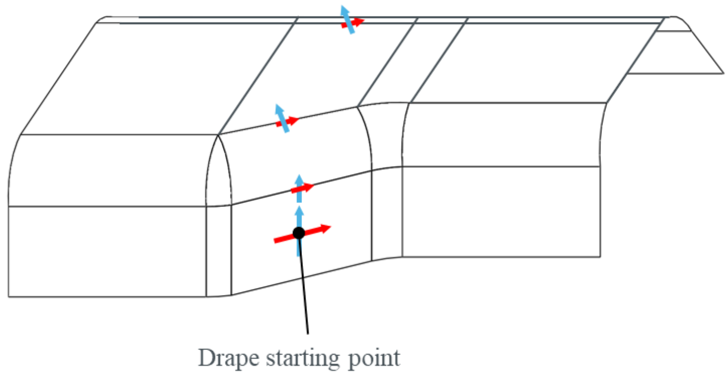

Figure 6.12 – Drape starting point

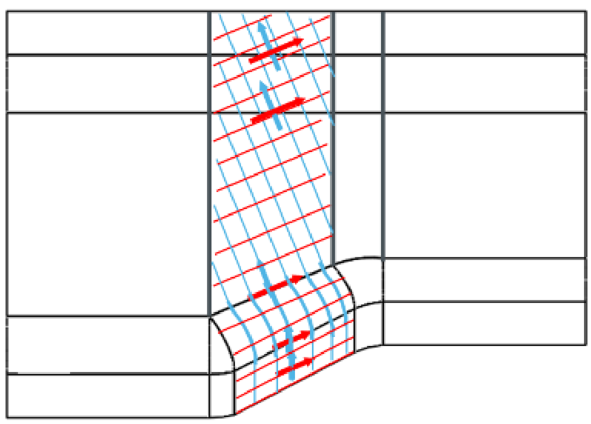

Figure 6.13 – Strategy 1, step 1

The second step of the drape strategy is to cover base surface 3 and from there, to cover base surfaces 2 and 9. Step 2 of the first strategy is shown in Figure 6.14.

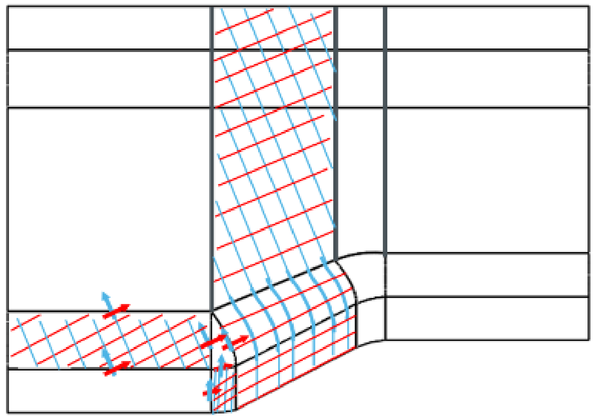

Figure 6.14 – Strategy 1, step 2

The third step of the drape strategy is to cover base 5, and single curvature or flat base surfaces that are connected to it, shown in Figure 6.15.

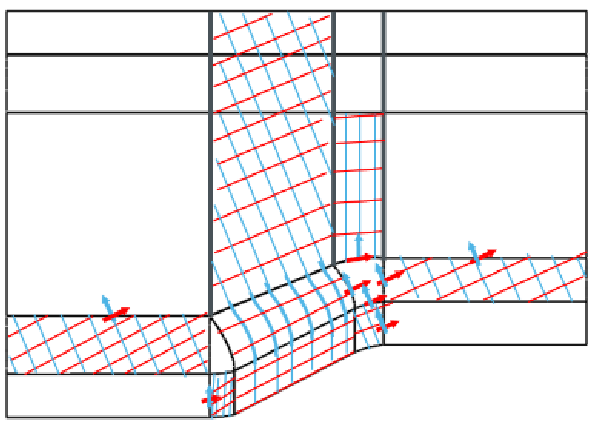

Figure 6.15 – Strategy 1, step 3

The last step of the draping strategy is to cover the remaining base surfaces on the mould, shown in Figure 6.16.

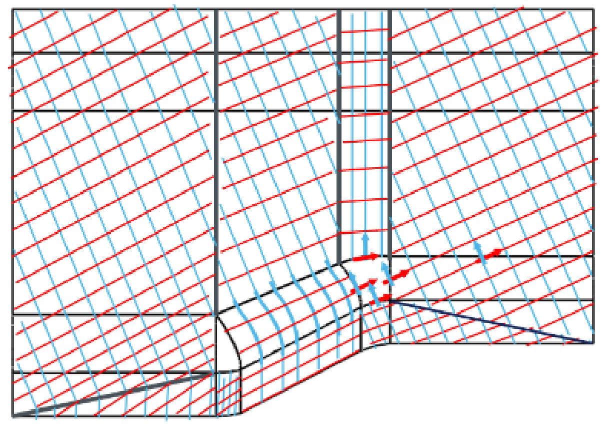

Figure 6.16 – Strategy 1, step 4

In this step of the strategy, base surfaces 1-1, 7-1 and 13-1 are covered using the yarn orientations from base surface 2, base surface 7-3 and 13-3 are covered using the yarn orientations from base surface 1-3, and base surfaces 1-4, 7-4 and 13-4 are covered using yarn orientations from base surface 6. Base surfaces 8 and 12 are arbitrarily split into two equally sized zones of fabric yarn orientations. Zones of continuous yarn orientations are shown in Figure 6.17. Yarn orientations over the mould are shown in Figure 6.18. Yarn orientations for a single curvature surface are defined by the angle between warp yarn and the line perpendicular to the connecting edge of the single curvature base surface.

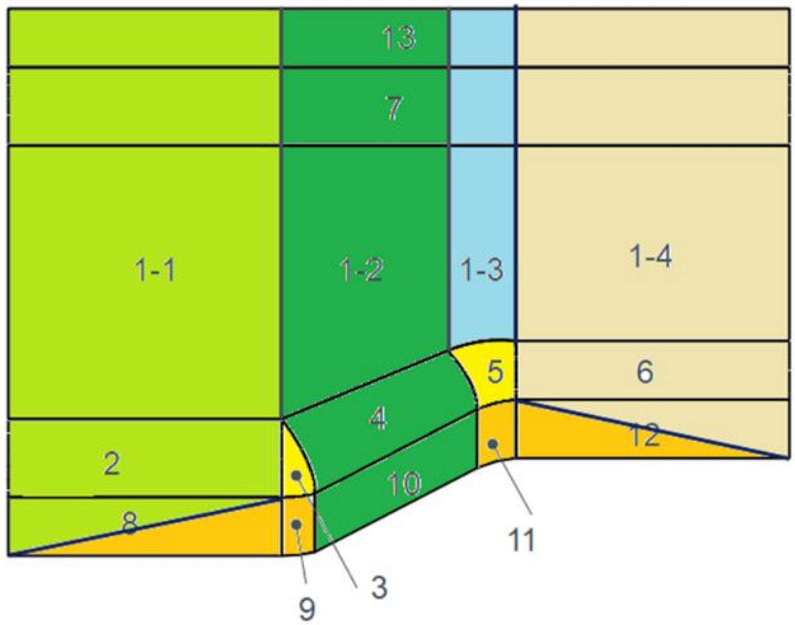

Figure 6.17 – Zones of continuous yarn orientations, strategy 1

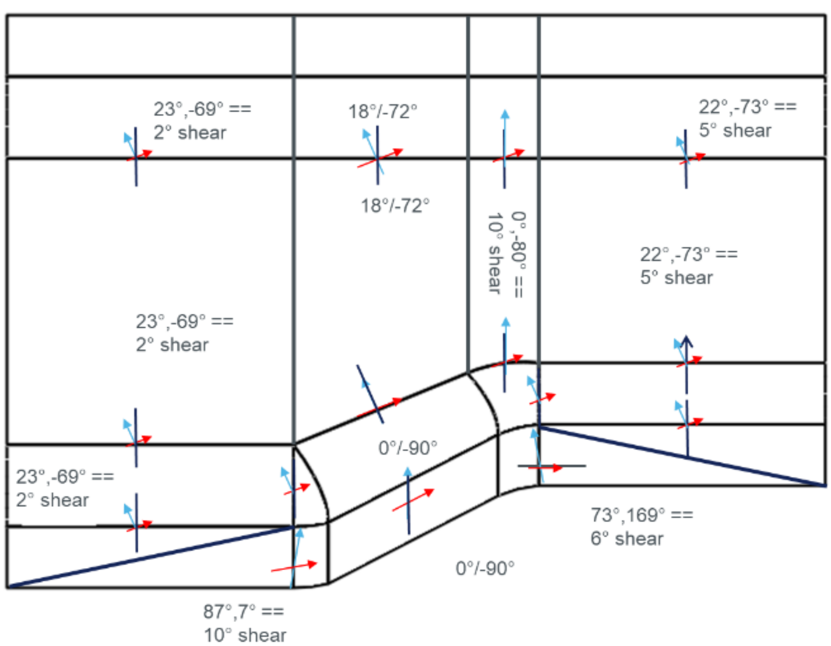

Figure 6.18 – Yarn orientations occurring on single curvature base surfaces, strategy 1

6.2.2. FR mould, strategy 2

The second draping strategy begins on base surface 13-1 with a 0°/90° yarn orientation. Warp yarns are perpendicular to the edge connecting base surfaces 13-1 and 7-1. The base surfaces covered in step 1 of this strategy are 7-1, 1-1, 2 and 8, shown in Figure 6.19.

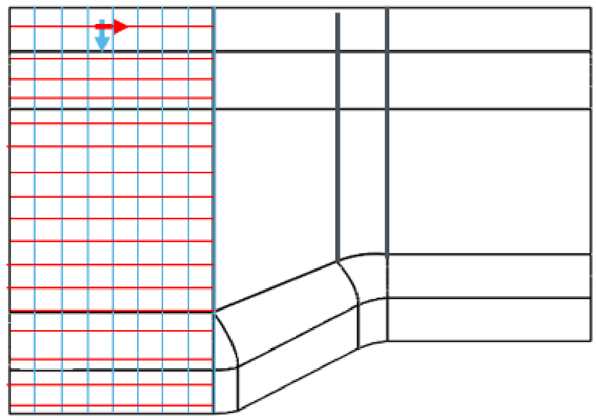

Figure 6.19 – Drape starting point and first step of strategy 2

The second step consists of draping base surfaces 3, 4 and 9. This step is shown in Figure 6.20.

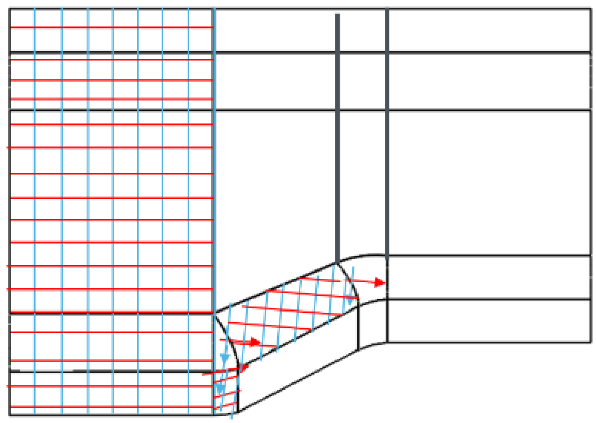

Figure 6.20 – Strategy 2, step 2

The third step consists of draping base surfaces 5, 1-3 and 6, as shown in Figure 6.21.

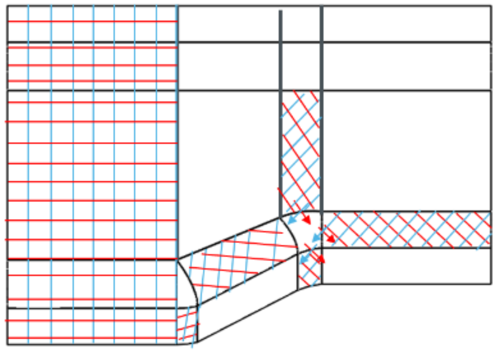

Figure 6.21 – Strategy 2, step 3

The last step in the strategy is shown in Figure 6.22, where base surfaces 1-2, 7-2 and 13-2 are covered using the yarn orientations on base surface 4. Base surfaces 7-3 and 13-3 are covered using the yarn orientations on base surface 1-3. Base surfaces 1-4, 7-4 and 13-4 are covered using the yarn orientations on base surface 6. Base surface 10 is arbitrarily split into three zones of fabric yarn orientations, while base surface 12 is split into two zones of fabric yarn orientations.

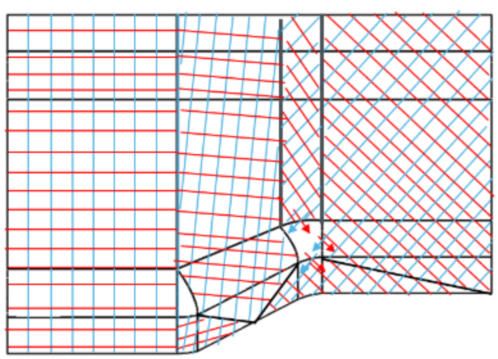

Figure 6.22 – Strategy 2, step 4

Zones of continuous yarn orientations are shown in Figure 6.23. Yarn orientations over the mould are shown in Figure 6.24. Yarn orientations for a single curvature surface are defined by the angle between the warp yarn and the direction of the single curvature base surface.

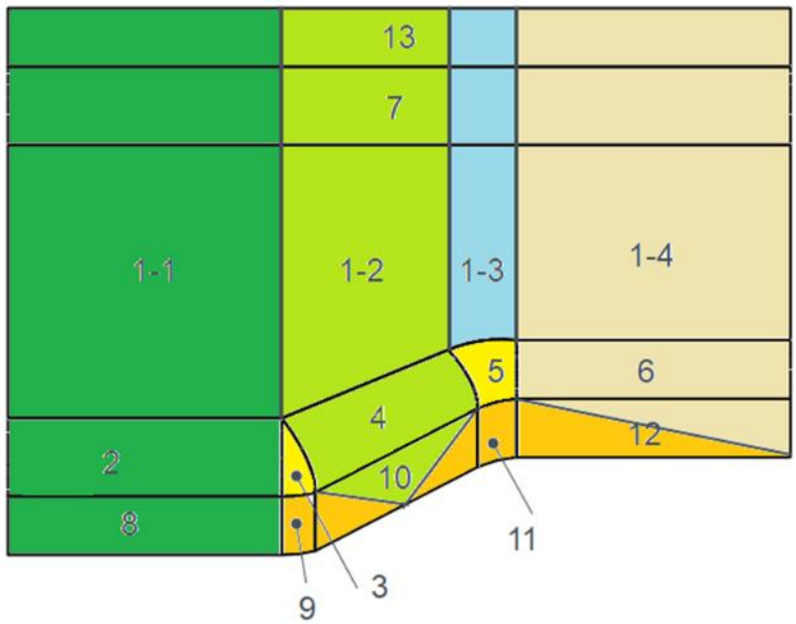

Figure 6.23 – Zones of continuous yarn orientations for strategy 2

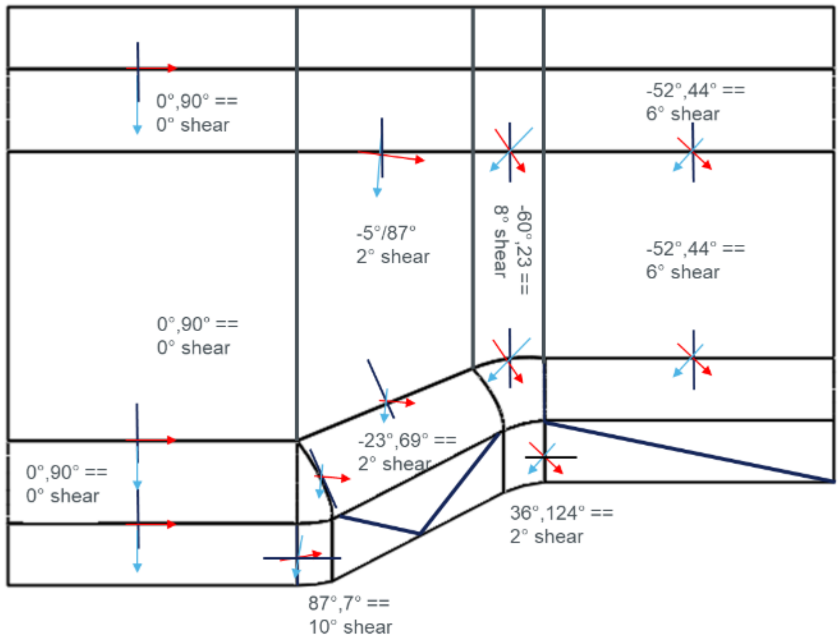

Figure 6.24 – Yarn orientations occurring on single curvature base surfaces, strategy 2

6.2.3. FR mould, strategy 3

The third strategy treats base surfaces 13-1, 13-2, 13-3 and 13-4 as one base surface, base surface 13. Base surfaces 7-1, 7-2, 7-3 and 7-4, and base surfaces 1-1, 1-2, 1-3 and 1-4 are also coalesced into two single base surfaces, base surface 7 and base surface 1 respectively. Base surfaces 13 and 1 are flat, and base surface 7 has a single curvature. In the third strategy, the starting base surface is base surface 13. Yarn orientation is 0°/90° and warp yarns are perpendicular to the edge connecting base surfaces 13 and 7. The first base surfaces covered in this strategy are base surface 7 and base surface 1. The first step of the draping strategy is shown in Figure 6.25.

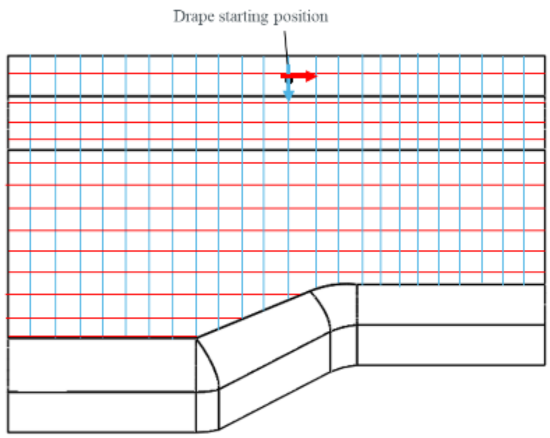

Figure 6.25 – Strategy 3, step 1

The second step is to cover base surface 5 and its adjacent base surfaces. This step is shown in Figure 6.26.

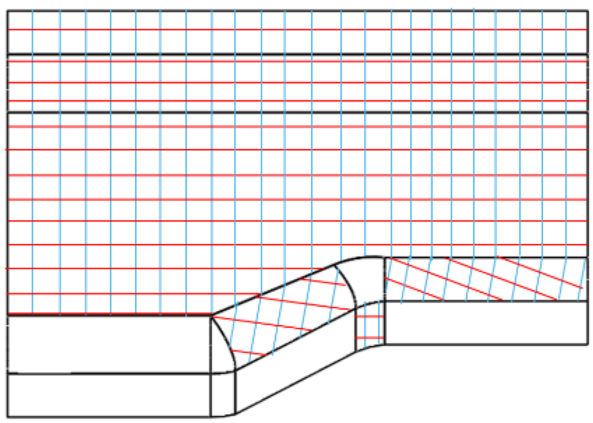

Figure 6.26 – Strategy 3, step 2

The third step is to cover base surface 3 and its adjacent base surfaces, shown in Figure 6.27.

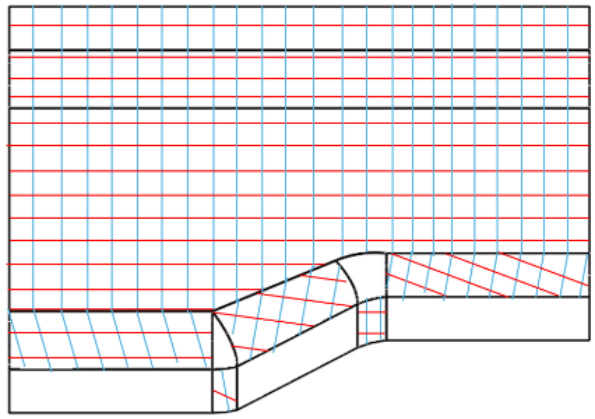

Figure 6.27 – Strategy 3, step 3

The last step is to drape the remaining base surfaces, which are all flat surfaces. Base surfaces 8 and 10 are split into two zones of yarn orientations, and base surface 10 is split into three zones of yarn orientations. The last step of the strategy is shown in Figure 6.28.

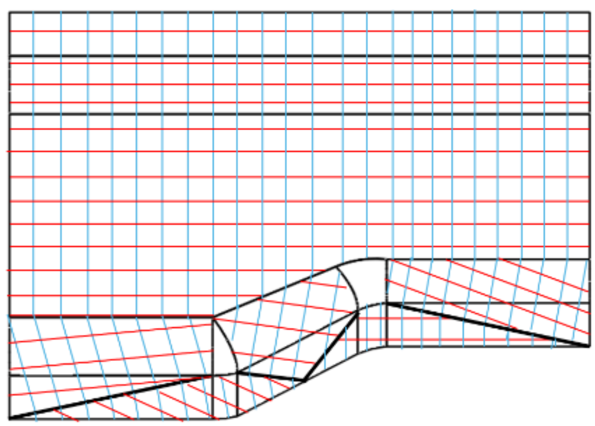

Figure 6.28 – Strategy 3, step 4

Zones of continuous yarn orientations are shown in Figure 6.29, and yarn orientations over the mould are shown in Figure 6.30.

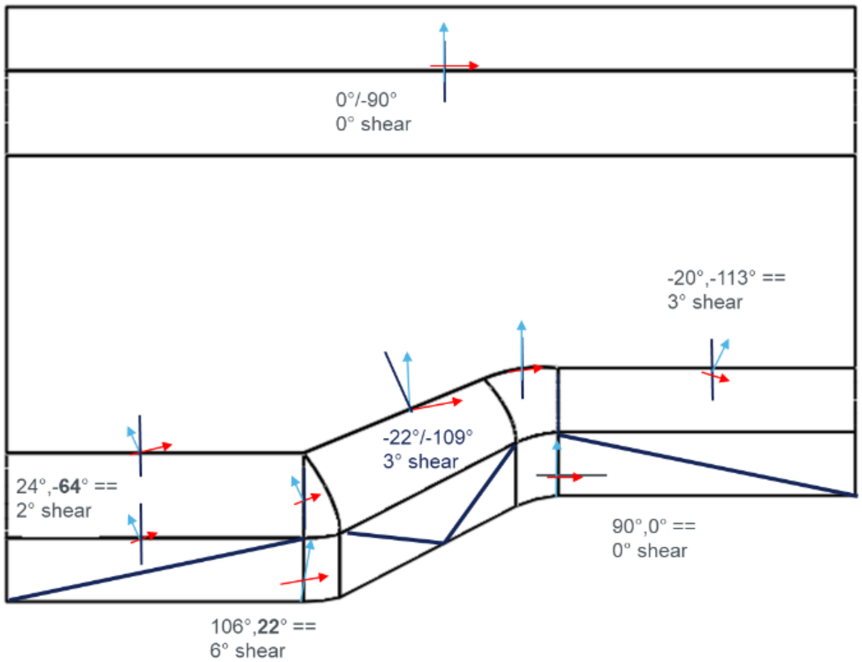

Figure 6.29 – Yarn orientations occurring on single curvature base surfaces, strategy 3

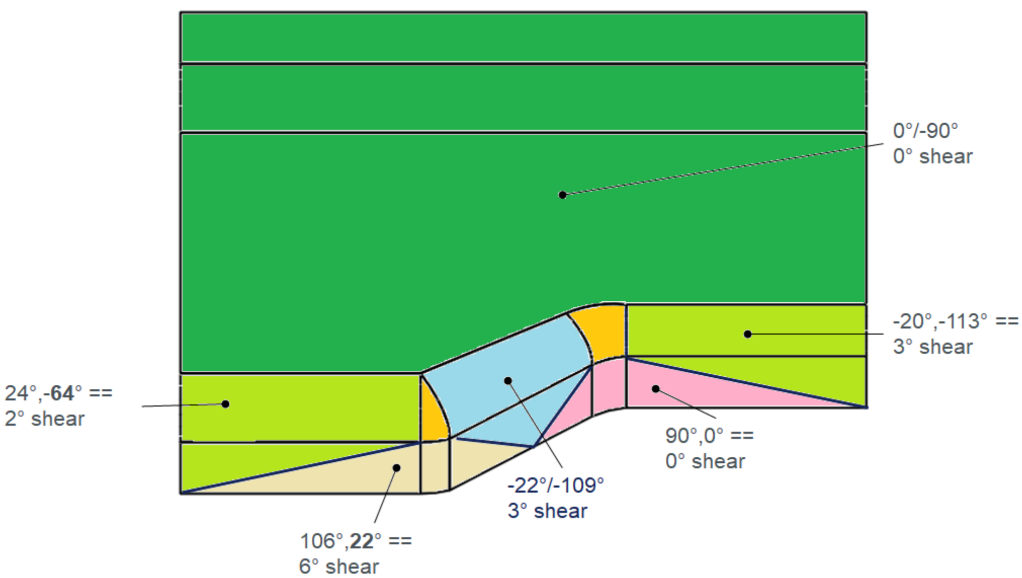

Figure 6.30 – Zones of continuous yarn orientations for strategy 3

6.3. Drape energy calculations

Drape energy and variability are calculated for all single curvature and double curvature base surfaces. The total drape energy is the sum of drape energies associated with each single and double curvature base surfaces. The total drape variability is the sum of drape variabilities associated with each single and double curvature base surfaces.

The drape energy and variability calculations depend on the mechanical characteristics of the fabric and on the mould geometry. Fabric characteristics are interpolated using linear functions introduced in Chapter 4. The mould geometry is broken down into multiple base surfaces, each parameterized using the five parameter conical frustum model. The frustum parameters are then used for estimating shear angles induced on the fabric by double curvature mould features. Limitations related to the usage of linear functions for estimating fabric mechanical characteristics and shear angles induced in the fabric are listed prior to introducing total drape energies and variabilities associated to each fabric and draping strategy.

6.3.1. Drape energy and variability limitations

6.3.1.1. Database B – Linear functions for fabric characteristics

Linear functions interpolating fabric spring back use spring back data for convex and concave corners of 1.59 *mm* to 12.70 *mm* in radius (1/16th *in*, 1/8th *in*, 1/4th *in*, 3/8th *in*, 1/2 *in*). Fabric spring back is known to vanish at larger mould radii, hence measured values of fabric radius are equivalent to the mould radius at large mould radii. In this thesis, spring back was characterized using the spring back ratio:

$$SBR = \frac{\beta}{SMR} \tag{6.1}$$

where β is the raw spring back measurement and SMR is the simulated mould radius. Raw measurements for convex and concave moulds are shown in Figure 6.31.

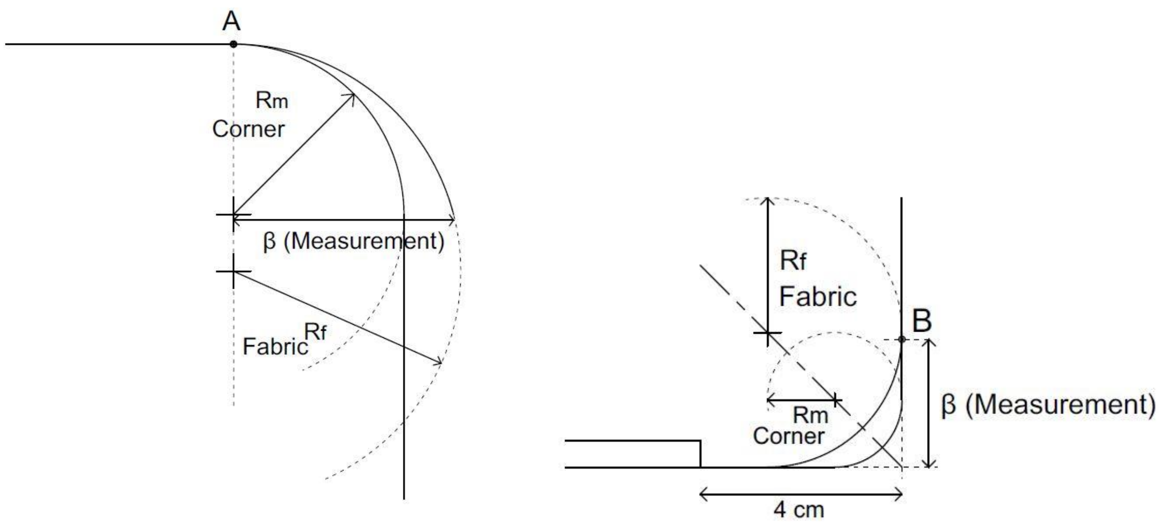

Figure 6.31 – Measurements of spring back (left: convex, right: concave)

The minimum value of the spring back ratio is exactly one, because the smallest possible measured spring back occurs when the fabric does not spring back. Extrapolation of spring back beyond 12.70 *mm* (1/2 *in*) may result in negative spring back ratios, because the slope of the interpolation of spring back between 9.52 *mm* ($3/8^{th}$ *in*) and 12.70 *mm* (1/2 *in*) is generally negative. Negative spring back ratios do not make physical sense. In order to avoid this problem, the largest mould radius used for calculating a bending spring back energy is 12.70 *mm* (1/2 *in*).

The bending spring back energy, Equation (5.6), is a function of the bending stiffness, mould radius and mould opening angle, Equation (5.7), and fabric opening angle, Equation (5.8). For concave spring back, the fabric opening angle is assumed equal to the mould opening angle, and the final radius of the fabric is equivalent to the measurement of spring back.

The effect of the mould opening and α_m on the spring back of fabrics is unknown, therefore mould opening angles of 90° should be used in all cases for calculating bending spring back energy, even when the mould opening angle is not 90°. A coefficient representing the effect of mould opening angle on the spring back should be determined experimentally by varying the mould opening angle during the spring back tests defined in Chapter 3.

In this work, the effect of mould opening angle on spring back is ignored; therefore it is impossible to determine the final fabric radius and final opening angle of the fabric when the mould radius is not 90°. Listed in Table 6.2, spring back energy calculations involving mould opening angles less than 90° appear to decrease the spring back energy for the same mould radius, while calculations involving opening angles greater than 90° appear to increase the spring back energy for the same mould radius. As the mould opening angle decreases (defined in Figure 5.1 for convex surfaces and Figure 5.2 for concave surfaces), the base surface becomes increasingly flat; therefore, the spring back energy should also decrease. It is noted that the spring back energy, Equation (5.6), represents additional energy required for ensuring that the fabric is draped on the mould once the fabric has sprung back from the mould; therefore, interpolated or extrapolated negative spring back values make no physical sense.

Table 6.2 – Spring back energy for one layer of Fabric 1 at 12.70 *mm* radius, 100 *mm* curvature width, 0° yarn orientation

Mould opening angle α_m (°)	Concave spring back energy (*Nmm*)	Convex spring back energy (*Nmm*)
30	0.00 $\pm$1.57	-1.04$\pm$2.47
90	0.00 $\pm$4.71	0.73 $\pm$3.75
150	0.00$\pm$ 7.85	2.49 $\pm$5.03

In-plane shear energy of fabrics is known over shear angles between 0° and 53°. The polynomial regressions can be used for predicting the shear energy beyond 53°; however, the actual shear behaviour beyond 53° is not known. Maximum values of in-plane shear energy should correspond to the shear energy at 53°.

In-plane shear spring back was characterized by shearing fabrics to 53°. Minimal differences between spring back ratios were reported for different fabrics in Chapter Chapter 5; therefore, the shear spring back energy was defined as 5.68% of the energy required for shearing a fabric to 53°. The spring back ratio may vary as the shear angle of a fabric is increased or decreased; the effect of shear angle on the shear spring back ratio is unknown.

6.3.1.2. Database A – Linear functions for estimating shear angles

Linear functions predicting the shear angles of fabrics are used for estimating yarn orientations and shear angles along the edges of a base surface. Base surface vertex labelling in database A is not always consistent while using the linear functions. The models used for simulating shear angles were listed in Table 5.5. Consider models 13 and 15 shown in Figure 6.32, with frustum parameters listed in Table 6.3.

Table 6.3 – Models 13 and 15 frustum parameters

	Frustum Parameters				
	R_1	R_2	C_R	L	β
Model 13	2 *cm*	1 *cm*	2 *cm*	2 *cm*	45°
Model 15	2 *cm*	1 *cm*	2 *cm*	2 *cm*	90°

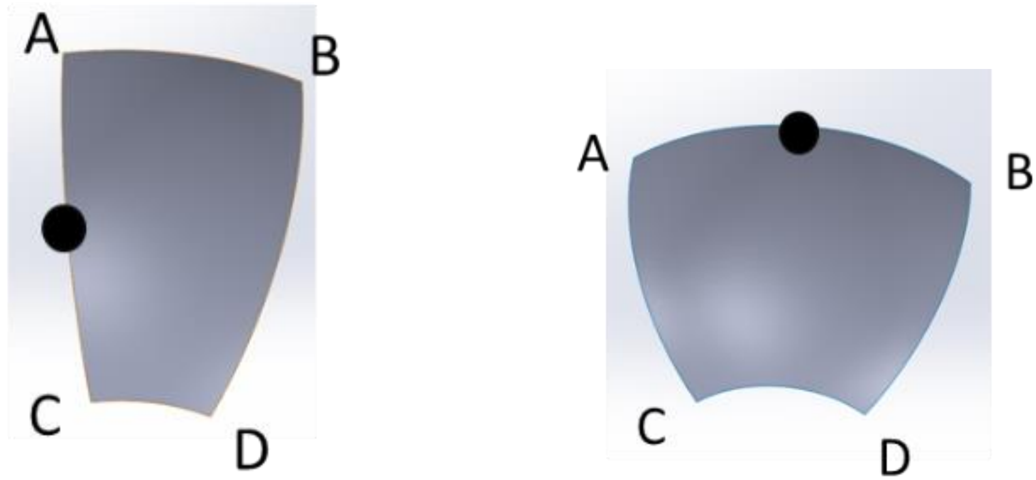

Figure 6.32 – Model 13 (right), model 15 (left)

The linear functions provide realistic shear angles along the base surface edges when the frustum parameters are identical to the frustum parameters of the models used for simulating fabric shear angles; however, nomenclature of vertex labelling is not fully consistent during database construction. For example, using Model 13 with starting drape parameters “MLE”, 0° shear angle and 0° yarn orientation results in shear angles and yarn orientations as listed in Table 6.4. The linear functions lead to a shear angle of 0° at the middle of edge BD, with weft yarns perpendicular to warp yarns. This result was expected, because the starting drape position was at the middle of the longest edge, and edges AC and BD are identical in length.

Table 6.4 – Shear angles and yarn orientations of model 13

Edge	Point	Shear Angle (°)	Warp Orientation (°)	Weft Orientation (°)
AB	A	15.0	164.5	89.6
	M_{AB}	9.5	170.6	90.1
	B	0.1	178.5	88.5
BD	B	-0.2	91.4	178.4
	M_{BD}	***0.0***	***89.8***	***179.7***
	D	0.6	88.3	177.7
DC	D	0.6	1.1	88.3
	M_{DC}	-5.9	11.1	106.9
	C	-11.2	24.4	125.6
CA	C	-11.2	65.0	36.2
	M_{CA}	-4.5	72.9	21.6
	A	14.5	74.5	1.0

Using Model 15 with starting drape parameters, the longest edge appears to be edge AB formed by parameter R_1 of the frustum model. Using "MLE", 0° shear angle and 0° yarn orientation starting parameters results in shear angles and yarn orientations as listed in Table 6.5.

Table 6.5 – Shear angles and yarn orientations of model 15

Edge	Point	Shear Angle (°)	Warp Orientation (°)	Weft Orientation (°)
AB	A	3.2	85.9	0.9
	M_{AB}	2.1	87.9	0.0
	B	1.0	89.9	0.9
BD	B	-0.8	0.3	90.5
	M_{BD}	15.8	19.6	93.9
	D	21.0	38.9	107.9
DC	D	20.9	127.7	163.3
	M_{DC}	***0.0***	***89.9***	***178.8***
	C	-21.1	52.2	163.3
CA	C	-21.1	141.0	107.9
	M_{CA}	-18.2	160.3	91.5
	A	3.2	175.7	88.9

The resulting shear angles are not consistent with expectations; the shear angle at point M_{AB} should be 0°, because the drape starting position was selected as the middle of the longest edge. Yarn orientations and shear angle at the middle of edge DC appears to best match the draping starting parameters. This seems to be a labelling problem; more consistent labelling in database A will be required for ensuring clear results that are easy to understand. In this thesis, it is assumed that edge AB corresponds to the circle formed by R_1, because setting $R_1 = 0$ results in three edged base surfaces that completely eliminate point B.

The definition of the drape starting position in [9] is also problematic, because the starting point is either at the centre of the base surface or at the middle of the longest edge. The database does not calculate the longest edge based on frustum parameters, and the longest edge often changed during database construction as shown in Figure 6.32. The longest edge of Model 13 is edge AC, while the longest edge of Model 15 is edge AB. The outputs of linear functions are listed in Table 6.6 for a model that interpolates between Models 13 and 15 – all parameters are identical except for $\beta_{5\text{-}para}$, which is set to 60°.

Table 6.6 – Shear angles and yarn orientations of interpolated model ($\beta_{5\text{-}para}$ = 60°)

Edge	Point	Shear Angle (°)	Warp Orientation (°)	Weft Orientation (°)
AB	A	11.1	138.3	60.0
	M_{AB}	***7.1***	***143.0***	***60.1***
	B	0.4	148.9	59.3
BD	B	-0.4	61.0	149.1
	M_{BD}	***5.3***	***66.4***	***151.1***
	D	7.4	71.8	154.5
DC	D	7.4	43.3	113.3
	M_{DC}	***-3.9***	***37.4***	***130.9***
	C	-14.5	33.7	138.1
CA	C	-14.5	90.3	60.1
	M_{CA}	***-9.0***	***102.0***	***44.9***
	A	10.7	108.3	30.3

The shear angle and yarn orientations at the middle of one of the base surface edges should correspond to the draping starting parameters: 0° shear angle and 0° yarn orientation. None of the shear angles on any of the edges corresponds to the expected shear angles and yarn orientations.

The shear angles and yarn orientations on the FR mould are calculated by approximating the base surfaces on the mould by one of the models used for creating Database A. These approximations will avoid the issues of confusing and at times illogical shear angle and yarn orientation output from the linear functions.

Shear angles along the edges of double curvature surfaces found on the FR mould were approximated by identifying a Model used for creating Database A that resembles each double curvature base surface on the mould. The base surface parameters and the models used for estimating the shear angles are listed in Table 6.7. Shear angles on base surface 3 were approximated using Model 9 parameters. Shear angles on base surface 5 were approximated using Model 13 parameters.

Table 6.7 – Models used for approximating the base surfaces

	Frustum Parameters				
	R_1	R_2	C_R	L	β
Base surface 3	0 *cm*	3 *cm*	2.5 *cm*	2.5 *cm*	18°
Model 9	**0 *cm***	**1 *cm***	**2 *cm***	**2 *cm***	**45°**
Base surface 5	3.5 *cm*	3 *cm*	2 *cm*	2.5 *cm*	23.5°
Model 13	**2 *cm***	**1 *cm***	**2 *cm***	**2 *cm***	**45°**

6.3.2. Strategy 1

The first draping strategy was detailed in Section 6.2.1. A summary of the result appears in Figure 6.33 . Drape energies required for covering all single curvature and double curvature surfaces are calculated for all single layer and multilayered fabrics tested. Fabric 1 drape energies for single curvature surfaces are listed in Table 6.8.

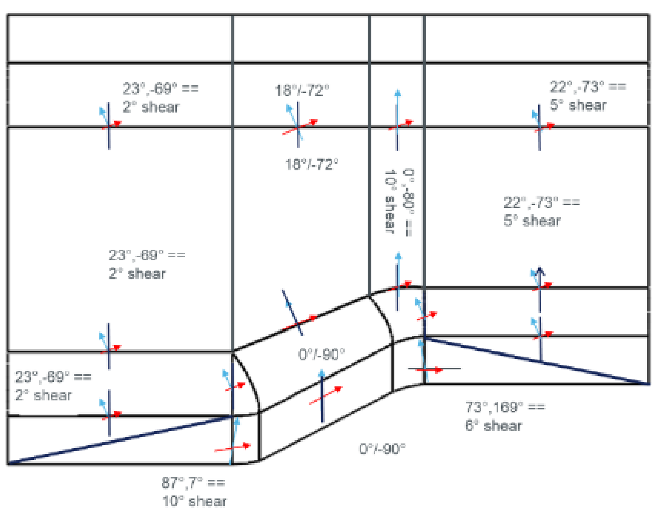

Figure 6.33 – Strategy 1 summary

Table 6.8 – Fabric 1 single layer drape energies, strategy one

BS #	Radius (*cm*)	Length (*cm*)	Theta (°)	Yarn orientation (°)	**Bending energy (*Nmm*)**	**Spring back energy (*Nmm*)**	**Bending variability (*Nmm*)**	**Spring back variability (*Nmm*)**
2	2.5 *cm*	7 *cm*	60°	23°	**0.43**	**0.27**	**0.61**	**2.06**
4	2.5 *cm*	4 *cm*	60°	0°	**0.36**	**0.29**	**0.58**	**1.50**
6	2.5 *cm*	7 *cm*	60°	22°	**0.44**	**0.28**	**0.62**	**2.09**
7-1	2.5 *cm*	7 *cm*	60°	23°	**0.43**	**0.27**	**0.61**	**2.06**
7-2	2.5 *cm*	3.8 *cm*	60°	18°	**0.26**	**0.17**	**0.36**	**1.19**
7-3	2.5 *cm*	2.2 *cm*	60°	0°	**0.20**	**0.16**	**0.32**	**0.83**
7-4	2.5 *cm*	7 *cm*	60°	22°	**0.44**	**0.28**	**0.62**	**2.09**
9	2.75 *cm*	2.69 *cm*	18°	87°	**0.03**	**0.05**	**0.05**	**0.48**
11	3.00 *cm*	3.2 *cm*	22°	73°	**0.04**	**0.06**	**0.06**	**0.53**

Shear angles that occur along the edges of double curvature base surfaces are shown in Figure 6.34 and Figure 6.35. The starting drape position is at the middle of the longest edge, the starting yarn orientation is 0°, and the starting shear angle is 0° for both base surfaces 3 and 5.

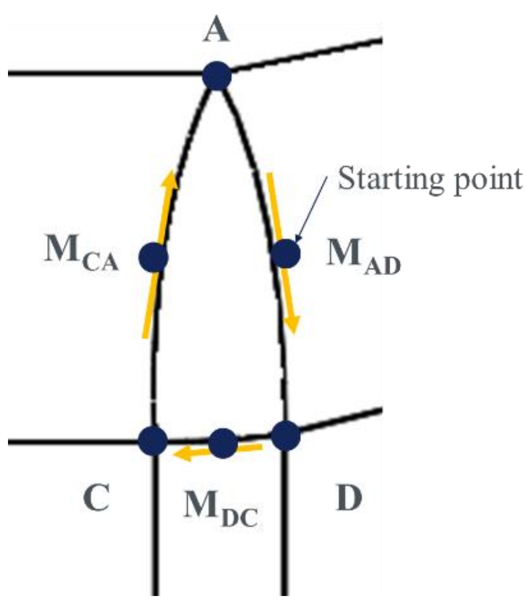

Points	**Shear Angles (°)**
A	0.7
M_{AD}	**0.0**
D	0.8
D	0.8
M_{DC}	-10.9
C	-34.4
C	-33.7
M_{CA}	1.6
A	0.7

Figure 6.34 – Shear angles on base surface 3, strategy 1

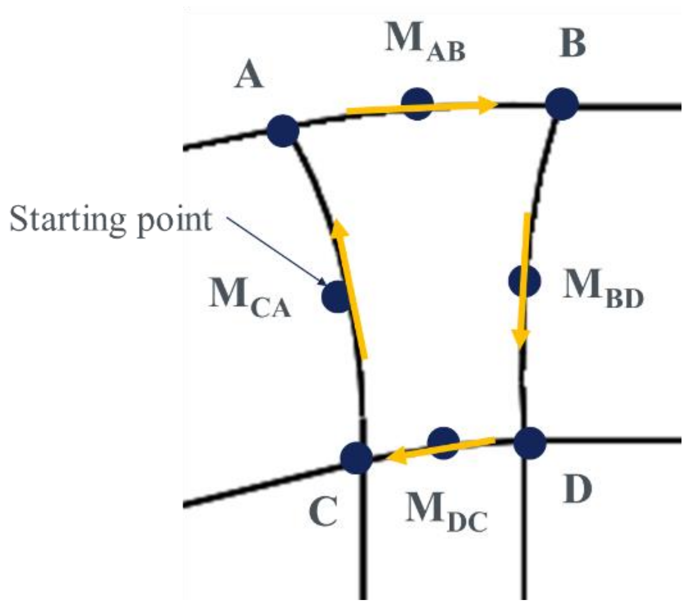

Points	**Shear Angles (°)**
A	0.1
M_{AB}	9.5
B	15.0
B	14.5
M_{BD}	-4.5
D	-11.2
D	-11.2
M_{DC}	-5.9
C	0.6
C	0.6
M_{CA}	**0.0**
A	-0.2

Figure 6.35 – Shear angles on base surface 5, strategy 1

The maximum shear angle that occurs on base surface 3 is 34.4°, and the maximum shear angle that occurs on base surface 5 is 15.0°. Drape energies for the double curvature surfaces are listed in Table 6.9.

Table 6.9 – Fabric 1 single layer drape energy, strategy one (double curvature)

BS #	Shear Angle (°)	Total Surface Area (*mm*^{2})	**Shear energy (*Nmm*)**	**Spring back energy (*Nmm*)**	**Shear energy variability (*Nmm*)**	**Spring back energy variability (*Nmm*)**
3	34.4	160 mm^2	**4.01**	**0.22**	**2.86**	**0.16**
5	15	284 mm^2	**0.82**	**0.05**	**3.8**	**0.21**

The total drape energies and variabilities for covering the entire mould with the tested fabrics are listed in Table 6.10. Tables containing the drape energies for individual base surfaces for Fabrics 2 and 3, single and multilayered, are listed in Appendix E.

Table 6.10 – Comparison of fabric drape energies, strategy one

	Totals	
	Energy (*Nmm*)	Energy variability (*Nmm*)
Fabric 1 SL	9.56	23.69
Fabric 2 SL	14.83	28.97
Fabric 3 SL	20.45	31.11
Fabric 1 ML	35.81	70.64
Fabric 2 ML	53.60	94.10
Fabric 3 ML	73.55	100.48

6.3.3. Strategy 2

The second draping strategy was detailed in Section 6.2.2. A summary of result is shown in Figure 6.36. Drape energies required for covering all single curvature and double curvature surfaces are calculated for all single layer and multilayered fabrics tested. Fabric 1 drape energies for single curvature surfaces are listed in Table 6.11.

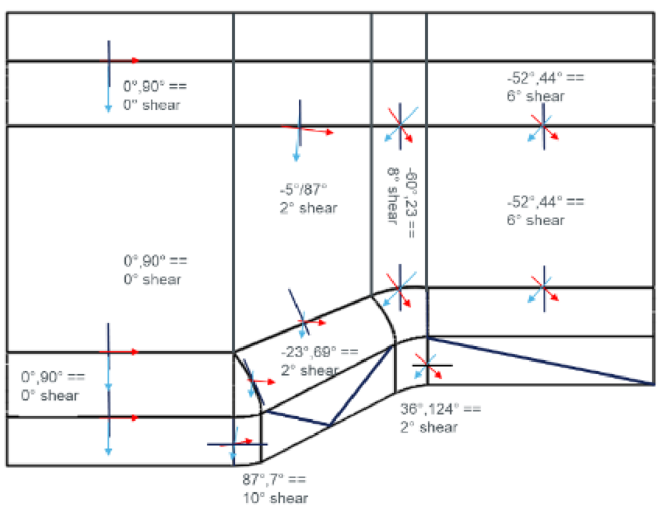

Figure 6.36 – Strategy 2 summary

Table 6.11 – Fabric 1 single layer drape energies, strategy two

BS #	Radius (*cm*)	Length (*cm*)	Theta (°)	Yarn orientation (°)	**Bending energy (*Nmm*)**	**Spring back energy (*Nmm*)**	**Bending variability (*Nmm*)**	**Spring back variability (*Nmm*)**
2	2.5 *cm*	7 *cm*	60°	0°	**0.63**	**0.51**	**1.02**	**2.63**
4	2.5 *cm*	4 *cm*	60°	23°	**0.25**	**0.16**	**0.35**	**1.18**
6	2.5 *cm*	7 *cm*	60°	52°	**0.25**	**0.11**	**0.35**	**1.09**
7-1	2.5 *cm*	7 *cm*	60°	0°	**0.63**	**0.51**	**1.02**	**2.63**
7-2	2.5 *cm*	3.8 *cm*	60°	5°	**0.32**	**0.25**	**0.48**	**1.36**
7-3	2.5 *cm*	2.2 *cm*	60°	60°	**0.08**	**0.04**	**0.10**	**0.35**
7-4	2.5 *cm*	7 *cm*	60°	52°	**0.25**	**0.11**	**0.35**	**1.09**
9	2.75 *cm*	2.69 *cm*	18°	87°	**0.03**	**0.05**	**0.05**	**0.48**
11	3.00 *cm*	3.2 *cm*	22°	36°	**0.04**	**0.08**	**0.10**	**0.78**

Shear angles along the edges of double curvature base surfaces are shown in Figure 6.37 and Figure 6.38. On base surface 3, Figure 6.37, the starting drape position is at the middle of the longest edge, with 0° starting yarn orientation and 0° starting shear angle. On base surface 5, Figure 6.38, the starting drape position is at the middle of the longest edge, with 23° starting yarn orientation and 1.6° starting shear angle.

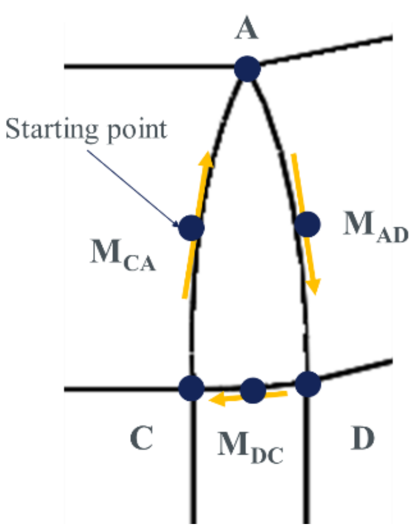

Points	**Shear Angles (°)**
A	0.7
M_{AD}	1.6
D	-33.7
D	-34.4
M_{DC}	-10.9
C	0.8
C	0.8
M_{CA}	**0.0**
A	0.7

Figure 6.37 – Shear angles on base surface 3, strategy 2

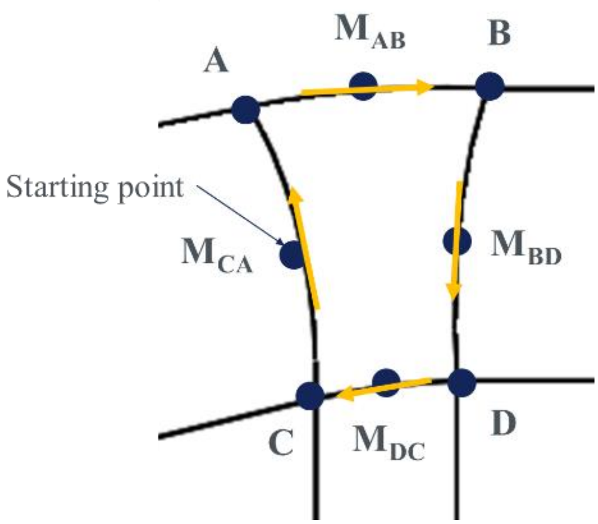

Points	Shear Angles (°)
A	3.6
M_{AB}	7.6
B	4.9
B	4.6
M_{BD}	-5.5
D	-0.8
D	-0.7
M_{DC}	2.1
C	4.4
C	4.4
M_{CA}	**1.7**
A	3.4

Figure 6.38 – Shear angles on base surface 5, strategy 2

The maximum shear angle that occurs on base surface 3 is 34.4°, and the maximum shear angle that occurs on base surface 5 is 7.6°. Drape energies for covering the double curvature surfaces are listed in Table 6.12.

Table 6.12 – Fabric 1 single layer drape energy, strategy two (double curvature)

BS #	Shear Angle (°)	Total Surface Area (mm^2)	**Shear energy (*Nmm*)**	**Spring back energy (*Nmm*)**	**Shear energy variability (*Nmm*)**	**Spring back energy variability (*Nmm*)**
3	34.4°	160 mm^2	**4.01**	**0.22**	**2.86**	**0.16**
5	7.6°	284 mm^2	**0.13**	**0.01**	**3.80**	**0.21**

The total drape energies and variabilities for covering the entire mould with the tested fabrics are listed in Table 6.13. Tables containing the drape energies for individual base surfaces for Fabrics 2 and 3, single and multilayered are listed in Appendix E.

Table 6.13 – Comparison of fabric drape energies, strategy two

	Totals	
	Energy (*Nmm*)	Energy Variability (*Nmm*)
Fabric 1 SL	8.67	22.44
Fabric 2 SL	13.1	32.09
Fabric 3 SL	20.53	31.52
Fabric 1 ML	34.31	66.46
Fabric 2 ML	50.34	94.29
Fabric 3 ML	74.00	99.95

6.3.4. Strategy 3

The third draping strategy was detailed in Section 6.2.3. A summary of the result appears in Figure 6.39. Drape energies required for covering all single curvature and double curvature surfaces are calculated for all single layer and multilayered fabrics tested. Fabric 1 drape energies for single curvature surfaces are listed in Table 6.14.

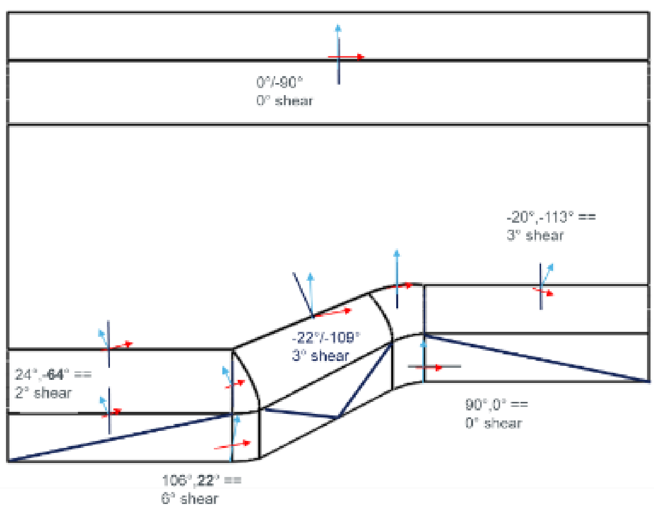

Figure 6.39 – Strategy 3 summary

Table 6.14 – Fabric 1 single layer drape energies, strategy three

BS #	Radius (*cm*)	Length (*cm*)	Theta (°)	Yarn orientation (°)	**Bending energy (*Nmm*)**	**Spring back energy (*Nmm*)**	**Bending variability (*Nmm*)**	**Spring back variability (*Nmm*)**
2	2.5 *cm*	7 *cm*	60°	24°	**0.42**	**0.26**	**0.60**	**2.04**
4	2.5 *cm*	4 *cm*	60°	22°	**0.25**	**0.16**	**0.35**	**1.19**
6	2.5 *cm*	7 *cm*	60°	20°	**0.46**	**0.30**	**0.64**	**2.14**
7	2.5 *cm*	20 *cm*	60°	0°	**1.79**	**1.46**	**2.91**	**7.51**
9	2.75 *cm*	2.69 *cm*	18°	16°	**0.05**	**0.13**	**0.08**	**0.86**
11	3.00 *cm*	3.2 *cm*	22°	90°	**0.04**	**0.13**	**0.08**	**0.95**

The shear angles along the edges of double curvature base surfaces are shown in Figure 6.40 and Figure 6.41. On base surface 3, the starting drape position is at the middle of the longest edge, with 22° yarn orientation and 3° shear angle. On base surface 5, the starting drape position is at the middle of the longest edge, with 0° starting yarn orientation and 0° starting shear angle.

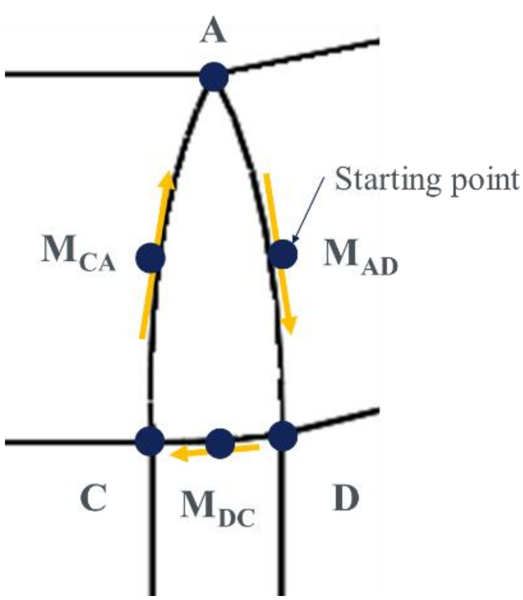

Points	**Shear Angles (°)**
A	6.8
M_{AD}	3.1
D	8.5
D	8.7
M_{DC}	6.3
C	-9.2
C	-9.0
M_{CA}	1.3
A	6.8

Figure 6.40 – Shear angles on base surface 3, strategy 3

In strategy three, Model 5 is used for calculating shear angles on base surface 5, because the starting drape position on the base surface is at the middle of edge AB. Model 5 frustum parameters are listed in Table 6.15.

Table 6.15 – Frustum parameters for estimating shear angles on base surface 5 (strategy 3)

	Frustum Parameters				
	R_1	R_2	C_R	L	β
Base surface 5	3.5 *cm*	3 *cm*	2 *cm*	2.5 *cm*	23.5°
Model 13	**2 *cm***	**1 *cm***	**2 *cm***	**0.5 *cm***	**45°**

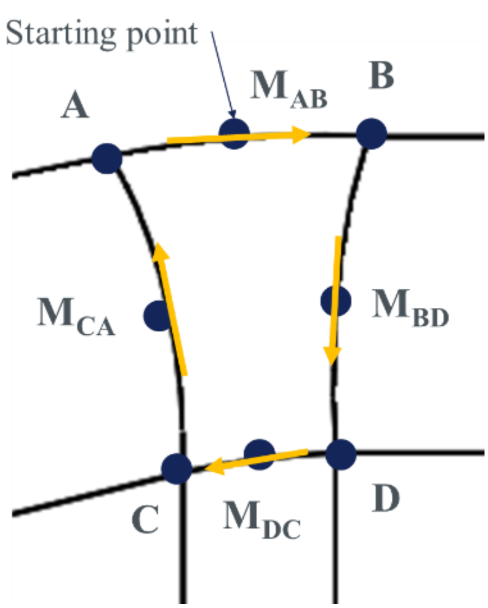

Points	**Shear Angles (°)**
A	1.2
M_{AB}	**0.0**
B	-0.7
B	-1.0
M_{BD}	-3.0
D	-2.8
D	-2.6
M_{DC}	-0.1
C	2.1
C	2.4
M_{CA}	3.1
A	1.6

Figure 6.41 – Shear angles on base surface 5, strategy 3

The maximum shear angle on base surface 3 is 9.2°, and the maximum shear angle on base surface 5 is 3.1°. Drape energies for covering the double curvature surfaces are listed in Table 6.16.

Table 6.16 – Fabric 1 single layer drape energy, strategy three (double curvature)

BS #	Shear Angle (°)	Total Surface Area (mm^2)	**Shear energy (*Nmm*)**	**Spring back energy (*Nmm*)**	**Shear energy variability (*Nmm*)**	**Spring back energy variability (*Nmm*)**
3	9.2°	160 mm^2	**0.19**	**0.01**	**2.86**	**0.16**
5	3.1°	284 mm^2	**-0.15**	**-0.01**	**3.81**	**0.21**

The total drape energies and variabilities for covering the entire mould with the tested fabrics are listed in Table 6.17. Tables containing the drape energies for individual base surfaces for Fabrics 2 and 3, single and multilayered, are listed in Appendix E.

Table 6.17 – Comparison of fabric drape energies, strategy three

	Totals	
	Energy (Nmm)	Energy Variability
Fabric 1 SL	5.81	26.39
Fabric 2 SL	12.49	30.88
Fabric 3 SL	19.30	33.48
Fabric 1 ML	26.32	78.4
Fabric 2 ML	56.15	103.47
Fabric 3 ML	72.57	109.52

6.3.5. Drape energy comparison

Total drape energies and total drape energy variabilities are listed in Table 6.18. Draping the FR mould using Fabric 1 results in the lowest drape energies for all draping strategies. Draping the mould using Fabric 3 results in the highest drape energies and variabilities for all draping strategies. Generally, Fabric 1 causes the least difficulties for technicians during the draping process, because it has a low bending stiffness and very limited bending spring back [10]. Generally, Fabric 3 causes the most difficulties during the draping process, due to large bending stiffness and bending spring back [10]. Drape energy totals are aligned with the difficulty of draping a fabric onto the mould.

Table 6.18 – Drape energy and variability comparison

		Fabrics	Totals: Energy (*Nmm*)	Totals: Energy Variability (*Nmm*)
Strategy 1	Single Layer	Fabric 1	9.56	23.69
		Fabric 2	14.83	28.97
		Fabric 3	20.45	31.11
	Multilayer	Fabric 1	35.81	70.64
		Fabric 2	53.60	94.10
		Fabric 3	73.55	100.48
Strategy 2	Single Layer	Fabric 1	8.67	22.44
		Fabric 2	13.10	32.09
		Fabric 3	20.53	31.52
	Multilayer	Fabric 1	34.31	66.46
		Fabric 2	50.34	94.29
		Fabric 3	74.00	99.95
Strategy 3	Single Layer	Fabric 1	5.81	26.39
		Fabric 2	12.49	30.88
		Fabric 3	19.30	33.48
	Multilayer	Fabric 1	26.32	78.4
		Fabric 2	56.15	103.47
		Fabric 3	72.57	109.52

Draping the mould using multilayer fabrics always results in higher drape energies and variabilities than for their single layer counterparts. Ratios of multilayer total drape energy to single layer total drape energy are listed in Table 6.19. The ratios are close to the number of layers in the fabric. Multilayer fabrics are generally more difficult to drape than single layer fabrics; however, the perceived difficulty is not deemed to correspond to the ratios listed in Table 6.19 for multilayer fabrics.

Table 6.19 – Comparison of single and multilayer drape energy

		Single layer	Multilayer	Ratio	Number of layers
Strategy 1	Fabric 1	9.56	35.81	3.74	4
	Fabric 2	14.83	53.60	3.61	4
	Fabric 3	20.45	73.55	3.60	3
Strategy 2	Fabric 1	8.67	34.31	3.96	4
	Fabric 2	13.10	50.34	3.84	4
	Fabric 3	20.53	74.00	3.60	3
Strategy 3	Fabric 1	5.81	26.32	4.53	4
	Fabric 2	12.49	56.15	4.50	4
	Fabric 3	19.30	72.57	3.76	3

Fabric 1 appears to produce draping strategies with smaller drape energy variability. Generally, Fabric 3 produces draping strategies that have higher drape energy variability, however, in draping strategy 2 the single layer version of Fabric 2 has a greater total drape energy variability than the single layer version Fabric 3. It is unclear if the totals of drape energy variability listed in Table 6.18 are realistic, as strong validating industrial data is not available.

Ratios of multilayer total drape energy variability to single layer total drape energy variability are listed in Table 6.20. The ratios are close to the number of layers in the fabrics. Fabric characterization tests showed that multilayer fabrics had greater dispersions, however it is unclear if the variability of total drape energy scales approximately to the number of layers in the fabric.

Table 6.20 – Comparison of single and multilayer drape energy variability

		Single layer	Multilayer	Ratio	Number of layers
Strategy 1	Fabric 1	23.69	70.64	2.98	4
	Fabric 2	28.97	94.10	3.25	4
	Fabric 3	31.11	100.48	3.23	3
Strategy 2	Fabric 1	22.44	66.46	2.96	4
	Fabric 2	32.09	94.29	2.94	4
	Fabric 3	31.52	99.95	3.17	3
Strategy 3	Fabric 1	26.39	78.40	2.97	4
	Fabric 2	30.88	103.47	3.35	4
	Fabric 3	33.48	109.52	3.27	3

Chapter 7. Conclusion

The draping performance, including draping difficulty and draping variability were characterized in this work, by using fabric mechanical parameters. Fabric mechanical parameters - bending stiffness, bending spring back, shearing behaviour, coefficient of friction and pin stability - were obtained via extensive testing.

The cantilever bending stiffness test is typically used for characterizing the bending stiffness of fabrics in the garment industry. In this thesis, the cantilever bending test was adapted for use on fabric reinforcements used in composite materials. Tests were conducted for single and multilayer versions of the tested fabrics, along multiple directions. Linear functions were created for interpolating the bending stiffness as a function of yarn orientation and number of layers in the fabric. The bending stiffness is used for calculating the bending energy of fabrics on single curvature surfaces on industrial moulds.

The bending spring back tests are a novel testing method developed in this work for characterizing the spring back behaviour of fabrics once draped on single curvature surfaces. The tests consisted of draping fabrics onto concave and convex curvature surfaces while varying the radius of curvature, and measuring their configuration after removal of the load. Interpolation functions similar to those developed for the bending stiffness were created for interpolating the spring back of fabrics as a function of yarn orientation, number of layers in the fabric, and radius of the single curvature feature on the mould. The bending spring back is used for calculating additional energy required for ensuring that the fabric stays on the mould after initial draping and spring back.

The picture-frame test is a well-established characterization method for testing in-plane shearing properties of fabric. Typically, the picture-frame test is used for identifying the locking angle of a fabric. In this thesis, the load was recording during loading and unloading cycles of the picture-frame test. The loading portion of the test was integrated for calculating the in-plane shear energy of fabrics. Fifth order polynomials were shown to have a strong interpolation ability of the shear load on the fabrics, while sixth order polynomials were shown to have a strong predictive ability of the shear energy of the fabrics. The shear spring back energy of fabrics was estimated by integrating the return portion of the test.

The drape energy considers bending and shearing deformation of fabrics as they are draped onto moulds. In order to calculate the drape energy, knowledge of the mould surfaces is required. In this work, the mould was broken down into multiple three and four edged base surfaces. Mould features are modelled using the five-parameter frustum developed in [9]. The five-parameter frustum allows for modelling single and double curvature base surfaces. Single curvature parameters are used in conjunction with the bending stiffness and spring back parameters for calculating drape energies associated to single curvature base surfaces.

A database of shear angles was created in [9] in the form of interpolation functions. The database allows for estimating the shear angles and yarn orientations of fabrics draped onto double curvature base surfaces. The results of the double-curvature base surface database are used in conjunction with the picture-frame test results for determining the drape energies associated to double curvature base surfaces.

The drape energy variability was used for estimating the repeatability of the draping process. The drape energy is calculated using the standard deviation of the testing results. Two methods were presented for estimating the dispersion of the fabric characteristics: interpolation functions for calculating the standard deviation of the fabric characteristics, and prediction interval calculations of the interpolated fabric characteristics. Both methods make use of the dispersion of the fabric characteristics.

The demonstrator mould showed that different drape energy and drape energy variability can result from draping the mould using different draping sequences. Fabric 1 was shown to be the fabric with the lowest drape energy and drape energy variability, while Fabric 3 was show to be the fabric with the highest drape energy and drape energy variability. This result aligns with technician experience: that Fabric 1 is an easy fabric to drape onto moulds, while Fabric 3 is a difficult fabric to drape onto moulds [10].

7.1. Future Work

There are several areas of interest that can be pursued in the context of the ongoing Hutchinson predictive draping project. The drape energy and energy variability calculations do not consider the pin stability of fabrics, and they do not consider the coefficient of friction of the fabrics. Both fabric characteristics affect the difficulty and quality of the drape [10]. In this work, these fabric characteristics were measured; however, they were not included in the drape energy and variability calculations. Integration of these parameters into the drape energy and drape energy variability calculations should be considered in future work for more realistic results of drape energy and drape energy variability.

Another area of interest is in creating rapid characterization methods for obtaining the fabric characteristics. In this work, bending spring back tests were conducted for convex and concave moulds of varying radii. The tests were time consuming; therefore expanding the database of fabric characteristics would require many resources. The rapid characterization of fabric bending spring back may involve developing more sophisticated models of the fabric bending behaviour. Rapid characterization methods would also allow for easily expanding the database of fabric mechanical parameters.

References

[1] "Alclad Aluminum 2024-T3." http://www.matweb.com/search/DataSheet.aspx?MatGUID=781ce4adb30c4d548320b0ab262a5d28 (accessed Oct. 07, 2020).

[2] W. Callister D., *Materials Science and Engineering*, 9th Edition. Wiley.

[3] "AISI 4340 Steel, annealed, 25 mm round." http://www.matweb.com/search/DataSheet.aspx?MatGUID=fd1b43a97a8a44129b32b9de0d7d6c1a (accessed Oct. 07, 2020).

[4] "Airbus technical magazine," Jun. 2013.

[5] J. Bachmann *et al.*, "Outlook on ecologically improved composites for aviation interior and secondary structures," *CEAS Aeronaut J*, vol. 9, no. 3, pp. 533–543, Sep. 2018, doi: 10.1007/s13272-018-0298-z.

[6] S. Prabhakaran, V. Krishnaraj, M. S. kumar, and R. Zitoune, "Sound and Vibration Damping Properties of Flax Fiber Reinforced Composites," *Procedia Engineering*, vol. 97, pp. 573–581, 2014, doi: 10.1016/j.proeng.2014.12.285.

[7] S. G. Hancock and K. D. Potter, "The use of kinematic drape modelling to inform the hand lay-up of complex composite components using woven reinforcements," *Composites Part A: Applied Science and Manufacturing*, vol. 37, no. 3, pp. 413–422, Mar. 2006, doi: 10.1016/j.compositesa.2005.05.044.

[8] S. Gagné, "Formage sous vide de renforts textiles de carbone et de verre pour fabrication de pièces composites pour l'aérospatiale," Thesis, Université d'Ottawa / University of Ottawa, 2017.

[9] J. Hoffer, “Development of a Draping Algorithm for Non-Structural Aerospace Composites,” Thesis, University of Ottawa, Ottawa, 2020.

[10] F. Guillemand, F. Salles, and C. Rannou, “Meeting with Shop Techinicians to Discuss Manufacturing Issues Related to Composites,” Mar. 2019.

[11] C. C. Chu, C. L. Cummings, and N. A. Teixeira, “Mechanics of Elastic Performance of Textile Materials: Part V: A Study of the Factors Affecting the Drape of Fabrics—The Development of a Drape Meter,” *Textile Research Journal*, vol. 20, no. 8, pp. 539–548, 1950, doi: 10.1177/004051755002000802.

[12] “Woven Textile Structure - an overview | ScienceDirect Topics.” https://www.sciencedirect.com/topics/engineering/woven-textile-structure (accessed Mar. 02, 2020).

[13] F. T. I. F. T. Peirce B.Sc. F. Inst. P., “26—the ‘Handle’ of Cloth as a Measurable Quantity,” *Journal of the Textile Institute Transactions*, vol. 21, no. 9, pp. T377–T416, Jan. 1930, doi: 10.1080/19447023008661529.

[14] R. G. Budynas, *Shigley’s mechanical engineering design*, 8th ed. Boston ; McGraw-Hill, 2008.

[15] P. Boisse, J. Colmars, N. Hamila, N. Naouar, and Q. Steer, “Bending and wrinkling of composite fiber preforms and prepregs. A review and new developments in the draping simulations,” *Composites Part B: Engineering*, vol. 141, pp. 234–249, May 2018, doi: 10.1016/j.compositesb.2017.12.061.

[16] M. Raheel, *Modern textile characterization methods*. 2017.

[17] S. Kawabata and M. Niwa, “Objective measurement of fabric mechanical property and quality: Its application to textile and clothing manufacturing,” *International Journal of Clothing Science and Technology*, vol. 3, no. 1, pp. 7–18, 1991, doi: 10.1108/eb002968.

[18] “KES-FB1-A/AW Tensile and Shear Tester | KATO TECH CO., LTD. | Pioneer of Texture Testers and Electronic Measuring Instruments.” https://english.keskato.co.jp/archives/products/kes-fb1-a (accessed Mar. 02, 2020).

[19] “KES-FB2-S Pure Bending Tester | KATO TECH CO., LTD. | Pioneer of Texture Testers and Electronic Measuring Instruments.” https://english.keskato.co.jp/archives/products/kes-fb2-s (accessed Mar. 02, 2020).

[20] “KES-FB3-A Compression Tester | KATO TECH CO., LTD. | Pioneer of Texture Testers and Electronic Measuring Instruments.” https://english.keskato.co.jp/archives/products/kes-fb3-a (accessed Mar. 02, 2020).

[21] “KES-FB4-A Surface Tester | KATO TECH CO., LTD. | Pioneer of Texture Testers and Electronic Measuring Instruments.” https://english.keskato.co.jp/archives/products/kes-fb4-a (accessed Mar. 02, 2020).

[22] J. Z. Yu, Z. Cai, and F. K. Ko, “Formability of textile preforms for composite applications. Part 1: Characterization experiments,” *Composites Manufacturing*, vol. 5, no. 2, pp. 113–122, 1994, doi: 10.1016/0956-7143(94)90062-0.

[23] S. V. Lomov, I. Verpoest, M. Barburski, and J. Laperre, “Carbon composites based on multiaxial multiply stitched preforms. Part 2. KES-F characterisation of the deformability of the preforms at low loads,” *Composites Part A: Applied Science and Manufacturing*, vol. 34, no. 4, pp. 359–370, Apr. 2003, doi: 10.1016/S1359-835X(03)00025-3.

[24] S. Kawabata and M. Niwa, “Fabric performance in clothing and clothing manufacture,” *Journal of the Textile Institute*, vol. 80, no. 1, pp. 19–50, 1989, doi: 10.1080/00405008908659184.

[25] A. S. Tam and T. G. Gutowski, “The kinematics for forming ideal aligned fibre composites into complex shapes,” *Composites Manufacturing*, vol. 1, no. 4, pp. 219–228, 1990, doi: 10.1016/0956-7143(90)90044-W.

[26] J. Cao *et al.*, “Characterization of mechanical behavior of woven fabrics: Experimental methods and benchmark results,” *Composites Part A: Applied Science and Manufacturing*, vol. 39, no. 6, pp. 1037–1053, Jun. 2008, doi: 10.1016/j.compositesa.2008.02.016.

[27] A. C. Long, B. J. Souter, F. Robitaille, and C. D. Rudd, “Effects of Fibre Architecture on Deformation during Preform Manufacture,” *Advanced Composites Letters*, vol. 8, no. 6, p. 096369359900800608, Nov. 1999, doi: 10.1177/096369359900800608.

[28] J. Launay, G. Hivet, A. V. Duong, and P. Boisse, “Experimental analysis of the influence of tensions on in plane shear behaviour of woven composite reinforcements,” *Composites Science and Technology*, vol. 68, no. 2, pp. 506–515, Feb. 2008, doi: 10.1016/j.compscitech.2007.06.021.

[29] F. Nosrat-Nezami, T. Gereke, C. Eberdt, and C. Cherif, “Characterisation of the shear–tension coupling of carbon-fibre fabric under controlled membrane tensions for precise simulative predictions of industrial preforming processes,” *Composites Part A: Applied Science and Manufacturing*, vol. 67, pp. 131–139, Dec. 2014, doi: 10.1016/j.compositesa.2014.08.030.

[30] A. G. Prodromou and J. Chen, "On the relationship between shear angle and wrinkling of textile composite preforms," *Composites Part A: Applied Science and Manufacturing*, vol. 28, no. 5, pp. 491–503, Jan. 1997, doi: 10.1016/S1359-835X(96)00150-9.

[31] A. C. Long, B. J. Souter, F. Robitaille, and C. D. Rudd, "Effects of fibre architecture on reinforcement fabric deformation," *Plastics, Rubber and Composites*, vol. 31, no. 2, pp. 87–97, Feb. 2002, doi: 10.1179/146580102225001391.

[32] X. Q. Peng, J. Cao, J. Chen, P. Xue, D. S. Lussier, and L. Liu, "Experimental and numerical analysis on normalization of picture frame tests for composite materials," *Composites Science and Technology*, vol. 64, no. 1, pp. 11–21, Jan. 2004, doi: 10.1016/S0266-3538(03)00202-1.

[33] I. Taha, Y. Abdin, and S. Ebeid, "Comparison of picture frame and Bias-Extension tests for the characterization of shear behaviour in natural fibre woven fabrics," *Fibers Polym*, vol. 14, no. 2, pp. 338–344, Feb. 2013, doi: 10.1007/s12221-013-0338-6.

[34] G. Lebrun, M. N. Bureau, and J. Denault, "Evaluation of bias-extension and picture-frame test methods for the measurement of intraply shear properties of PP/glass commingled fabrics," *Composite Structures*, vol. 61, no. 4, pp. 341–352, Sep. 2003, doi: 10.1016/S0263-8223(03)00057-6.

[35] P. Boisse, N. Hamila, E. Guzman-Maldonado, A. Madeo, G. Hivet, and F. dell'Isola, "The bias-extension test for the analysis of in-plane shear properties of textile composite reinforcements and prepregs: a review," *Int J Mater Form*, vol. 10, no. 4, pp. 473–492, Aug. 2017, doi: 10.1007/s12289-016-1294-7.

[36] L. Wang, J. Liu, R. Pan, and W. Gao, “Exploring the relationship between bending property and crease recovery of woven fabrics,” *Journal of the Textile Institute*, vol. 106, no. 11, pp. 1173–1179, 2015, doi: 10.1080/00405000.2014.977544.

[37] “Crease Recovery Tester | crease resistance tester,” *Testex*. https://www.testextextile.com/product/crease-recovery-tester-tf110a/ (accessed Mar. 02, 2020).

[38] F. Shi and Y. Wang, “Modelling crease recovery behaviour of woven fabrics,” *The Journal of The Textile Institute*, vol. 100, no. 3, pp. 218–222, Apr. 2009, doi: 10.1080/00405000701757560.

[39] L. Wang, J. Liu, R. Pan, and W. Gao, “Dynamic measurement of fabric wrinkle recovery angle by video sequence processing,” *Textile Research Journal*, vol. 84, no. 7, pp. 694–703, 2014, doi: 10.1177/0040517513507363.

[40] L. Fridrichova and K. Zelova, “Objective evaluation of multidirectional fabric creasing,” *Journal of the Textile Institute*, vol. 102, no. 8, pp. 719–725, 2011, doi: 10.1080/00405000.2010.515727.

[41] J. O. Ajayi, “Fabric Smoothness, Friction, and Handle,” *Textile Research Journal*, vol. 62, no. 1, pp. 52–59, Jan. 1992, doi: 10.1177/004051759206200108.

[42] B. S. Gupta and Textile Institute, Eds., *Friction in textile materials*. Boca Raton, Fla.: CRC Press [u.a.], 2008.

[43] “fabric friction tester | Science Museum Group Collection.” https://collection.sciencemuseumgroup.org.uk/objects/co8417503/fabric-friction-tester-fabric-friction-tester (accessed Feb. 27, 2020).

[44] “Renforts tissés | Hexcel.” https://www.hexcel.com/Resources/DataSheets/Reinforcements/Woven-Reinforcements?lS=HexForce+7500&lC=-1&lP=-1&fwl=&fwu=&ftl=&ftu=# (accessed Apr. 06, 2020).

[45] “Fabric Search | JPS Composite Materials.” https://jpscm.com/fabric-search/ (accessed Apr. 09, 2020).

[46] “1369,” *BGF Industries, Inc.* http://www.bgf.com/datasheet/1369/ (accessed Apr. 09, 2020).

[47] “PKHP-200 Powder,” *Gabriel*. https://www.gabrielchem.com/product/pkhp-200-powder/ (accessed Feb. 25, 2020).

[48] D13 Committee, “Test Method for Stiffness of Fabrics,” ASTM International. doi: 10.1520/D1388-18.

[49] F04 Committee, “Test Method for Determining the Flexural Stiffness of Medical Textiles,” ASTM International. doi: 10.1520/F3260-18.

[50] N. Lammens, M. Kersemans, G. Luyckx, W. Van Paepegem, and J. Degrieck, “Improved accuracy in the determination of flexural rigidity of textile fabrics by the Peirce cantilever test (ASTM D1388),” *Textile Research Journal*, vol. 84, no. 12, pp. 1307–1314, Jul. 2014, doi: 10.1177/0040517514523182.

[51] D. C. Montgomery, *Design and analysis of experiments*, Eighth edition. Hoboken, NJ: John Wiley & Sons, Inc, 2013.

Appendix

Appendix A. Analysis of variance results tables

A.1. Cantilever bending

A.1.1. Bending stiffness

Table A.1 – Bending stiffness ANOVA table – single layer fabrics

Source of Variance	Sum of Squares	Degrees of Freedom	Mean Squares	F-ratio	Critical F-ratio	Honestly Significant Difference
Between Groups	71,805,108.20	3	23,935,036.07	169.80	2.08	192.34
Within Groups	21,989,964.19	156	140,961.31			
Total	93,795,072.39	159				

Table A.2 – Bending stiffness ANOVA table – multilayer fabrics

Source of Variance	Sum of Squares	Degrees of Freedom	Mean Squares	F-ratio	Critical F-ratio	Honestly Significant Difference
Between Groups	642,188,710.85	3	214,062,903.62	110.10	2.08	714.33
Within Groups	303,314,533.49	156	1,944,323.93			
Total	945,503,244.34	159				

Table A.3 – Bending stiffness ANOVA table – Fabric 1 single layer vs multilayer

Source of Variance	Sum of Squares	Degrees of Freedom	Mean Squares	F-ratio	Critical F-ratio	Honestly Significant Difference
Between Groups	14,971,526.43	1	14,971,526.43	61.83	2.78	183.15
Within Groups	18,885,655.60	78	242,123.79			
Total	33,857,182.03	79				

Table A.4 – Bending stiffness ANOVA table – Fabric 2 single layer vs multilayer

Source of Variance	Sum of Squares	Degrees of Freedom	Mean Squares	F-ratio	Critical F-ratio	Honestly Significant Difference
Between Groups	28,417,683.58	1	28,417,683.58	55.41	2.78	266.56
Within Groups	40,006,321.30	78	512,901.56			
Total	68,424,004.87	79				

Table A.5 – Bending stiffness ANOVA table – Fabric 3 single layer vs multilayer

Source of Variance	Sum of Squares	Degrees of Freedom	Mean Squares	F-ratio	Critical F-ratio	Honestly Significant Difference
Between Groups	178,433,653.49	1	178,433,653.49	82.25	2.78	548.21
Within Groups	169,216,335.08	78	2,169,440.19			
Total	347,649,988.57	79				

Table A.6 – Bending stiffness ANOVA table – Fabric 4 single layer vs multilayer

Source of Variance	Sum of Squares	Degrees of Freedom	Mean Squares	F-ratio	Critical F-ratio	Honestly Significant Difference
Between Groups	342,576,886.19	1	342,576,886.19	274.92	2.78	415.48
Within Groups	97,196,185.70	78	1,246,104.94			
Total	439,773,071.89	79				

A.1.2. Overhang length

Table A.7 – Overhang length ANOVA table – single layer fabrics

Source of Variance	Sum of Squares	Degrees of Freedom	Mean Squares	F-ratio	Critical F-ratio	Honestly Significant Difference
Between Groups	3,285.45	3	1,095.15	231.27	2.08	1.11
Within Groups	738.71	156	4.74			
Total	4,024.16	159				

Table A.8 – Overhang length ANOVA table – multilayer fabrics

Source of Variance	Sum of Squares	Degrees of Freedom	Mean Squares	F-ratio	Critical F-ratio	Honestly Significant Difference
Between Groups	3,550.84	3	1,183.61	216.57	2.08	1.20
Within Groups	852.58	156	5.47			
Total	4,403.42	159				

Table A.9 – Overhang length ANOVA table – Fabric 1 single layer vs multilayer

Source of Variance	Sum of Squares	Degrees of Freedom	Mean Squares	F-ratio	Critical F-ratio	Honestly Significant Difference
Between Groups	0.48	1	0.48	0.17	2.78	0.63
Within Groups	225.01	78	2.88			
Total	225.49	79				

Table A.10 – Overhang length ANOVA table – Fabric 2 single layer vs multilayer

Source of Variance	Sum of Squares	Degrees of Freedom	Mean Squares	F-ratio	Critical F-ratio	Honestly Significant Difference
Between Groups	4.90	1	4.90	0.80	2.78	0.92
Within Groups	475.13	78	6.09			
Total	480.03	79				

Table A.11 – Overhang length ANOVA table – Fabric 3 single layer vs multilayer

Source of Variance	Sum of Squares	Degrees of Freedom	Mean Squares	F-ratio	Critical F-ratio	Honestly Significant Difference
Between Groups	15.05	1	15.05	1.80	2.78	1.08
Within Groups	652.67	78	8.37			
Total	667.72	79				

Table A.12 – Overhang length ANOVA table – Fabric 4 single layer vs multilayer

Source of Variance	Sum of Squares	Degrees of Freedom	Mean Squares	F-ratio	Critical F-ratio	Honestly Significant Difference
Between Groups	1.62	1	1.62	0.53	2.78	0.65
Within Groups	238.48	78	3.06			
Total	240.11	79				

A.2. Bending spring back

A.2.1. Convex spring back

Table A.13 – Convex bending spring back ANOVA table –single layer fabrics

Source of Variance	Sum of Squares	Degrees of Freedom	Mean Squares	F-ratio	Critical F-ratio	Honestly Significant Difference
Between Groups	432.37	3	144.12	206.23	2.17	0.62
Within Groups	53.11	76	0.70			
Total	485.48	79				

Table A.14 – Convex bending spring back ANOVA table – multilayer fabrics

Source of Variance	Sum of Squares	Degrees of Freedom	Mean Squares	F-ratio	Critical F-ratio	Honestly Significant Difference
Between Groups	366.70	3	122.23	138.90	2.17	0.70
Within Groups	66.88	76	0.88			
Total	433.58	79				

Table A.15 – Convex bending spring back ANOVA table – Fabric 1 single layer vs multilayer

Source of Variance	Sum of Squares	Degrees of Freedom	Mean Squares	F-ratio	Critical F-ratio	Honestly Significant Difference
Between Groups	2.23	1	2.23	8.17	2.85	0.28
Within Groups	10.38	38	0.27			
Total	12.61	39				

Table A.16 – Convex bending spring back ANOVA table – Fabric 2 single layer vs multilayer

Source of Variance	Sum of Squares	Degrees of Freedom	Mean Squares	F-ratio	Critical F-ratio	Honestly Significant Difference
Between Groups	18.34	1	18.34	81.51	2.85	0.25
Within Groups	8.55	38	0.23			
Total	26.89	39				

Table A.17 – Convex bending spring back ANOVA table – Fabric 3 single layer vs multilayer

Source of Variance	Sum of Squares	Degrees of Freedom	Mean Squares	F-ratio	Critical F-ratio	Honestly Significant Difference
Between Groups	0.80	1	0.80	1.16	2.85	0.44
Within Groups	26.33	38	0.69			
Total	27.13	39				

Table A.18 – Convex bending spring back ANOVA table – Fabric 4 single layer vs multilayer

Source of Variance	Sum of Squares	Degrees of Freedom	Mean Squares	F-ratio	Critical F-ratio	Honestly Significant Difference
Between Groups	3.58	1	3.58	1.82	2.85	0.74
Within Groups	74.74	38	1.97			
Total	78.32	39				

A.2.2. Concave spring back

Table A.19 – Concave bending spring back ANOVA table –single layer fabrics

Source of Variance	Sum of Squares	Degrees of Freedom	Mean Squares	F-ratio	Critical F-ratio	Honestly Significant Difference
Between Groups	1,399.48	3	466.49	57.41	2.17	2.11
Within Groups	617.54	76	8.13			
Total	2,017.02	79				

Table A.20 – Concave bending spring back ANOVA table –multilayer fabrics

Source of Variance	Sum of Squares	Degrees of Freedom	Mean Squares	F-ratio	Critical F-ratio	Honestly Significant Difference
Between Groups	2,060.31	3	686.77	53.63	2.17	2.65
Within Groups	973.15	76	12.80			
Total	3,033.46	79				

Table A.21 – Concave bending spring back ANOVA table –Fabric 1 single layer vs multilayer

Source of Variance	Sum of Squares	Degrees of Freedom	Mean Squares	F-ratio	Critical F-ratio	Honestly Significant Difference
Between Groups	0.25	1	0.25	0.19	2.85	0.60
Within Groups	48.55	38	1.28			
Total	48.80	39				

Table A.22 – Concave bending spring back ANOVA table –Fabric 2 single layer vs multilayer

Source of Variance	Sum of Squares	Degrees of Freedom	Mean Squares	F-ratio	Critical F-ratio	Honestly Significant Difference
Between Groups	43.21	1	43.21	9.34	2.85	1.14
Within Groups	175.78	38	4.63			
Total	218.99	39				

Table A.23 – Concave bending spring back ANOVA table – Fabric 3 single vs multilayer

Source of Variance	Sum of Squares	Degrees of Freedom	Mean Squares	F-ratio	Critical F-ratio	Honestly Significant Difference
Between Groups	40.63	1	40.63	2.20	2.85	2.27
Within Groups	701.03	38	18.45			
Total	741.66	39				

Table A.24 – Concave bending spring back ANOVA table –Fabric 4 single vs multilayer

Source of Variance	Sum of Squares	Degrees of Freedom	Mean Squares	F-ratio	Critical F-ratio	Honestly Significant Difference
Between Groups	113.57	1	113.57	6.49	2.85	2.21
Within Groups	665.34	38	17.51			
Total	778.91	39				

A.3. In-plane shear

A.3.1. Maximum normalized in-plane shear load

Table A.25 – Maximum normalized in-plane shear load ANOVA table –single layer fabrics

Source of Variance	Sum of Squares	Degrees of Freedom	Mean Squares	F-ratio	Critical F-ratio	Honestly Significant Difference
Between Groups	1.33E-02	2	6.65E-03	21.84	2.81	2.50E-02
Within Groups	3.66E-03	12	3.05E-04			
Total	1.70E-02	14				

Table A.26 – Maximum normalized in-plane shear load ANOVA table –multilayer fabrics

Source of Variance	Sum of Squares	Degrees of Freedom	Mean Squares	F-ratio	Critical F-ratio	Honestly Significant Difference
Between Groups	9.53E-02	2	4.77E-02	45.89	2.81	4.61E-02
Within Groups	1.25E-02	12	1.04E-03			
Total	1.08E-01	14				

Table A.27 – Maximum normalized in-plane shear load ANOVA table –Fabric 1 single vs multilayer

Source of Variance	Sum of Squares	Degrees of Freedom	Mean Squares	F-ratio	Critical F-ratio	Honestly Significant Difference
Between Groups	5.26E-02	1	5.26E-02	60.75	3.46	3.46E-02
Within Groups	6.93E-03	8	8.66E-04			
Total	5.95E-02	9				

Table A.28 – Maximum normalized in-plane shear load ANOVA table –Fabric 2 single vs multilayer

Source of Variance	Sum of Squares	Degrees of Freedom	Mean Squares	F-ratio	Critical F-ratio	Honestly Significant Difference
Between Groups	7.44E-02	1	7.44E-02	65.73	3.46	3.96E-02
Within Groups	9.06E-03	8	1.13E-03			
Total	8.35E-02	9				

Table A.29 – Maximum normalized in-plane shear load ANOVA table –Fabric 3 single vs multilayer

Source of Variance	Sum of Squares	Degrees of Freedom	Mean Squares	F-ratio	Critical F-ratio	Honestly Significant Difference
Between Groups	6.89E-03	1	6.89E-03	414.31	3.46	4.80E-03
Within Groups	1.33E-04	8	1.66E-05			
Total	7.03E-03	9				

A.3.2. Return angle

Table A.30 – Return angle ANOVA table –single layer fabrics

Source of Variance	Sum of Squares	Degrees of Freedom	Mean Squares	F-ratio	Critical F-ratio	Honestly Significant Difference
Between Groups	52.52	2	26.26	24.02	2.81	1.50
Within Groups	13.12	12	1.09			
Total	65.63	14				

Table A.31 – Return angle ANOVA table –multilayer fabrics

Source of Variance	Sum of Squares	Degrees of Freedom	Mean Squares	F-ratio	Critical F-ratio	Honestly Significant Difference
Between Groups	143.08	2	71.54	5.66	2.81	5.09
Within Groups	151.65	12	12.64			
Total	294.74	14				

Table A.32 – Return angle ANOVA table –Fabric 1 single vs multilayer

Source of Variance	Sum of Squares	Degrees of Freedom	Mean Squares	F-ratio	Critical F-ratio	Honestly Significant Difference
Between Groups	0.00	1	0.00	0.00	3.46	1.27
Within Groups	9.30	8	1.16			
Total	9.30405	9				

Table A.33 – Return angle ANOVA table –Fabric 2 single vs multilayer

Source of Variance	Sum of Squares	Degrees of Freedom	Mean Squares	F-ratio	Critical F-ratio	Honestly Significant Difference
Between Groups	0.01	1	0.01	0.77	3.46	0.15
Within Groups	0.13	8	0.02			
Total	0.14	9				

Table A.34 – Return angle ANOVA table –Fabric 3 single vs multilayer

Source of Variance	Sum of Squares	Degrees of Freedom	Mean Squares	F-ratio	Critical F-ratio	Honestly Significant Difference
Between Groups	18.97	1	18.97	0.98	3.46	5.18
Within Groups	155.34	8	19.42			
Total	174.31	9				

A.4. Friction

A.4.1. Mean coefficient of friction

Table A.35 – Mean coefficient of friction ANOVA table

Source of Variance	Sum of Squares	Degrees of Freedom	Mean Squares	F-ratio	Critical F-ratio	Honestly Significant Difference
Between Groups	4.33E-01	2	2.16E-01	26.62	2.51	8.65E-02
Within Groups	2.19E-01	27	8.13E-03			
Total	6.52E-01	29				

A.4.2. Mean deviation of coefficient of friction

Table A.36 – Mean deviation of coefficient of friction ANOVA table

Source of Variance	Sum of Squares	Degrees of Freedom	Mean Squares	F-ratio	Critical F-ratio	Honestly Significant Difference
Between Groups	6.15E-03	2	3.07E-03	7.09	2.51	2.00E-02
Within Groups	1.17E-02	27	4.34E-04			
Total	1.79E-02	29				

A.5. Pin stability

A.5.1. Load at pin failure

Table A.37 – Load at pin failure ANOVA table –single layer fabrics

Source of Variance	Sum of Squares	Degrees of Freedom	Mean Squares	F-ratio	Critical F-ratio	Honestly Significant Difference
Between Groups	344.02	3	114.67	33.37	2.24	1.97
Within Groups	123.72	36	3.44			
Total	467.74	39				

Table A.38 – Load at pin failure ANOVA table –multilayer fabrics

Source of Variance	Sum of Squares	Degrees of Freedom	Mean Squares	F-ratio	Critical F-ratio	Honestly Significant Difference
Between Groups	56.63	3	18.88	13.89	2.24	1.24
Within Groups	48.92	36	1.36			
Total	105.55	39				

Table A.39 – Load at pin failure ANOVA table –Fabric 1 single vs multilayer

Source of Variance	Sum of Squares	Degrees of Freedom	Mean Squares	F-ratio	Critical F-ratio	Honestly Significant Difference
Between Groups	44.81	1	44.81	11.86	3.01	1.51
Within Groups	67.99	18	3.78			
Total	112.80	19				

Table A.40 – Load at pin failure ANOVA table –Fabric 2 single vs multilayer

Source of Variance	Sum of Squares	Degrees of Freedom	Mean Squares	F-ratio	Critical F-ratio	Honestly Significant Difference
Between Groups	21.85	1	21.85	5.71	3.01	1.52
Within Groups	68.85	18	3.82			
Total	90.70	19				

Table A.41 – Load at pin failure ANOVA table –Fabric 3 single vs multilayer

Source of Variance	Sum of Squares	Degrees of Freedom	Mean Squares	F-ratio	Critical F-ratio	Honestly Significant Difference
Between Groups	31.20	1	31.20	91.51	3.01	0.45
Within Groups	6.14	18	0.34			
Total	37.34	19				

Table A.42 – Load at pin failure ANOVA table –Fabric 4 single vs multilayer

Source of Variance	Sum of Squares	Degrees of Freedom	Mean Squares	F-ratio	Critical F-ratio	Honestly Significant Difference
Between Groups	0.29	1	0.29	0.18	3.01	0.99
Within Groups	29.67	18	1.65			
Total	29.96	19				

A.5.2. Extension at pin failure

Table A.43 – Extension at pin failure ANOVA table –single layer fabrics

Source of Variance	Sum of Squares	Degrees of Freedom	Mean Squares	F-ratio	Critical F-ratio	Honestly Significant Difference
Between Groups	91.31	3	30.44	1.42	2.24	4.93
Within Groups	772.19	36	21.45			
Total	863.50	39				

Table A.44 – Extension at pin failure ANOVA table –multilayer fabrics

Source of Variance	Sum of Squares	Degrees of Freedom	Mean Squares	F-ratio	Critical F-ratio	Honestly Significant Difference
Between Groups	1047.10	3	349.03	20.75	2.24	4.37
Within Groups	605.45	36	16.82			
Total	1652.55	39				

Table A.45 – Extension at pin failure ANOVA table –Fabric 1 single vs multilayer

Source of Variance	Sum of Squares	Degrees of Freedom	Mean Squares	F-ratio	Critical F-ratio	Honestly Significant Difference
Between Groups	391.97	1	391.97	14.00	3.01	4.10
Within Groups	504.11	18	28.01			
Total	896.08	19				

Table A.46 – Extension at pin failure ANOVA table –Fabric 2 single vs multilayer

Source of Variance	Sum of Squares	Degrees of Freedom	Mean Squares	F-ratio	Critical F-ratio	Honestly Significant Difference
Between Groups	9.24	1	9.24	0.54	3.01	3.21
Within Groups	309.40	18	17.19			
Total	318.63	19				

Table A.47 – Extension at pin failure ANOVA table –Fabric 3 single vs multilayer

Source of Variance	Sum of Squares	Degrees of Freedom	Mean Squares	F-ratio	Critical F-ratio	Honestly Significant Difference
Between Groups	1.46	1	1.46	0.07	3.01	3.50
Within Groups	366.69	18	20.37			
Total	368.15	19				

Table A.48 – Extension at pin failure ANOVA table –Fabric 4 single vs multilayer

Source of Variance	Sum of Squares	Degrees of Freedom	Mean Squares	F-ratio	Critical F-ratio	Honestly Significant Difference
Between Groups	1063.92	1	1063.92	96.99	3.01	2.57
Within Groups	197.44	18	10.97			
Total	1261.36	19				

Appendix B. Design of experiments result tables (linear functions)

B.1. Cantilever bending

B.1.1. Bending stiffness

Table B.1 – Bending stiffness of Fabric 1

		C_1	C_2	C_{12}		
Fabric 1 $0° < \phi \le 45°$	Contrasts	1,812.00	-1,038.00	-514.00	Grand Average	Mean Squares Within
	Adjustment Term	0.20	0.20	0.20		
	Sum of Squares	16,416,720.00	5,387,220.00	1,320,980.00	**750.00**	150,887.50
	F-ratio	108.80	35.70	8.75		
	Coefficient	**453.00**	**-259.50**	**-128.50**		
Fabric 1 $45° < \phi \le 90°$	Contrasts	1,216.00	-10.00	-82.00	Grand Average	Mean Squares Within
	Adjustment Term	0.20	0.20	0.20		
	Sum of Squares	7,393,280.00	500.00	33,620.00	**488.00**	26,114.50
	F-ratio	283.11	0.02	1.29		
	Coefficient	**304.00**	**-2.50**	**-20.50**		

Table B.2 – Bending stiffness of Fabric 2

		C_1	C_2	C_{12}	Grand Average	Mean Squares Within
Fabric 2 $0° < \phi \leq 45°$	Contrasts	2,916.00	-950.00	-762.00		
	Adjustment Term	0.20	0.20	0.20		
	Sum of Squares	42,515,280.00	4,512,500.00	2,903,220.00	**1,194.00**	304,057.50
	F-ratio	139.83	14.84	9.55		
	Coefficient	**729.00**	**-237.50**	**-190.50**		
Fabric 2 $45° < \phi \leq 90°$	Contrasts	1,623.00	-1,091.00	-531.00		
	Adjustment Term	0.20	0.20	0.20		
	Sum of Squares	13,170,645.00	5,951,405.00	1,409,805.00	**683.75**	217,461.75
	F-ratio	60.57	27.37	6.48		
	Coefficient	**405.75**	**-272.75**	**-132.75**		

Table B.3 – Bending stiffness of Fabric 3

		C_1	C_2	C_{12}	Grand Average	Mean Squares Within
Fabric 3 $0° < \phi \leq 45°$	Contrasts	2,550.00	-2,944.00	-1,680.00		
	Adjustment Term	0.20	0.20	0.20		
	Sum of Squares	32,512,500.00	43,335,680.00	14,112,000.00	**1,110.50**	548,795.75
	F-ratio	59.24	78.97	25.71		
	Coefficient	**637.50**	**-736.00**	**-420.00**		
Fabric 3 $45° < \phi \leq 90°$	Contrasts	4,294.00	6,400.00	3,424.00		
	Adjustment Term	0.20	0.20	0.20		
	Sum of Squares	92,192,180.00	204,800,000.00	58,618,880.00	**1,974.50**	796,642.50
	F-ratio	115.73	257.08	73.58		
	Coefficient	**1,073.50**	**1,600.00**	**856.00**		

B.1.2. Overhang length

Table B.4 – Overhang length of Fabric 1

		C_1	C_2	C_{12}		
Fabric 1 $0° < \phi \leq 45°$	Contrasts	0.30	-5.10	0.70	Grand Average	Mean Squares Within
	Adjustment Term	0.20	0.20	0.20		
	Sum of Squares	0.45	130.05	2.45	**9.03**	1.16
	F-ratio	0.39	112.35	2.12		
	Coefficient	**0.07**	**-1.28**	**0.18**		
Fabric 1 $45° < \phi \leq 90°$	Contrasts	0.40	0.00	-0.60	Grand Average	Mean Squares Within
	Adjustment Term	0.20	0.20	0.20		
	Sum of Squares	0.80	0.00	1.80	**7.75**	0.57
	F-ratio	1.40	0.00	3.16		
	Coefficient	**0.10**	**0.00**	**-0.15**		

Table B.5 – Overhang length of Fabric 2

		C_1	C_2	C_{12}		
Fabric 2 $0° < \phi \leq 45°$	Contrasts	0.00	-4.00	-1.20	Grand Average	Mean Squares Within
	Adjustment Term	0.20	0.20	0.20		
	Sum of Squares	0.00	80.00	7.20	**11.10**	2.03
	F-ratio	0.00	39.46	3.55		
	Coefficient	**0.00**	**-1.00**	**-0.30**		
Fabric 2 $45° < \phi \leq 90°$	Contrasts	-0.10	-4.90	1.10	Grand Average	Mean Squares Within
	Adjustment Term	0.20	0.20	0.20		
	Sum of Squares	0.05	120.05	6.05	**8.88**	1.93
	F-ratio	0.03	62.28	3.14		
	Coefficient	**-0.02**	**-1.23**	**0.28**		

Table B.6 – Overhang length of Fabric 1

		C_1	C_2	C_{12}		
Fabric 3 $0° < \phi \leq 45°$	Contrasts	1.20	-13.00	-0.40	Grand Average	Mean Squares Within
	Adjustment Term	0.20	0.20	0.20		
	Sum of Squares	7.20	845.00	0.80	**11.95**	3.71
	F-ratio	1.94	227.92	0.22		
	Coefficient	**0.30**	**-3.25**	**-0.10**		
Fabric 3 $45° < \phi \leq 90°$	Contrasts	1.30	21.90	0.50	Grand Average	Mean Squares Within
	Adjustment Term	0.20	0.20	0.20		
	Sum of Squares	8.45	2,398.05	1.25	**14.18**	2.53
	F-ratio	3.34	948.78	0.49		
	Coefficient	**0.33**	**5.48**	**0.13**		

B.2. Bending spring back

B.2.1. Convex spring back

Table B.7 – Convex spring back of Fabric 1, 0° < Φ ≤45° yarn orientation

		C_1	C_2	C_{12}	C_3	C_{13}	C_{23}	C_{123}		
$0 < \phi \leq 45$ $\frac{1}{16} < r \leq \frac{1}{8}$	Contrasts	1.40	-0.60	-1.00	-6.40	0.00	-0.80	0.80	Grand Average	Mean Squares Within
	Adjustment Term	0.80	0.80	0.80	0.80	0.80	0.80	0.80		
	Sum of Squares	2.45	0.45	1.25	51.20	0.00	0.80	0.80	**2.53**	0.13
	F-ratio	18.85	3.46	9.62	393.85	0.00	6.15	6.15		
	Coefficient	**0.18**	**-0.08**	**-0.13**	**-0.80**	**0.00**	**-0.10**	**0.10**		
$0 < \phi \leq 45$ $\frac{1}{8} < r \leq \frac{1}{4}$	Contrasts	1.00	-0.80	0.00	-0.80	-0.40	0.60	0.20	Grand Average	Mean Squares Within
	Adjustment Term	0.80	0.80	0.80	0.80	0.80	0.80	0.80		
	Sum of Squares	1.25	0.80	0.00	0.80	0.20	0.45	0.05	**1.63**	0.03
	F-ratio	40.00	25.60	0.00	25.60	6.40	14.40	1.60		
	Coefficient	**0.13**	**-0.10**	**0.00**	**-0.10**	**-0.05**	**0.08**	**0.03**		
$0 < \phi \leq 45$ $\frac{1}{4} < r \leq \frac{3}{8}$	Contrasts	0.30	-0.30	-0.10	-0.90	-0.30	-0.10	-0.30	Grand Average	Mean Squares Within
	Adjustment Term	0.80	0.80	0.80	0.80	0.80	0.80	0.80		
	Sum of Squares	0.11	0.11	0.01	1.01	0.11	0.01	0.11	**1.41**	0.01
	F-ratio	12.86	12.86	1.43	115.71	12.86	1.43	12.86		
	Coefficient	**0.04**	**-0.04**	**-0.01**	**-0.11**	**-0.04**	**-0.01**	**-0.04**		
$0 < \phi \leq 45$ $\frac{3}{8} < r \leq \frac{1}{2}$	Contrasts	0.20	-0.40	-0.20	-0.40	0.20	0.00	0.20	Grand Average	Mean Squares Within
	Adjustment Term	0.80	0.80	0.80	0.80	0.80	0.80	0.80		
	Sum of Squares	0.05	0.20	0.05	0.20	0.05	0.00	0.05	**1.25**	0.01
	F-ratio	10.00	40.00	10.00	40.00	10.00	0.00	10.00		
	Coefficient	**0.03**	**-0.05**	**-0.03**	**-0.05**	**0.03**	**0.00**	**0.03**		

Table B.8 – Convex spring back of Fabric 1, 45° < $\Phi \leq$ 90°

		C_1	C_2	C_{12}	C_3	C_{13}	C_{23}	C_{123}		
$45 < \phi \leq 90$ $\frac{1}{16} < r \leq \frac{1}{8}$	Contrasts	0.60	1.00	0.20	-7.00	0.60	0.20	-0.20	Grand Average	Mean Squares Within
	Adjustment Term	0.80	0.80	0.80	0.80	0.80	0.80	0.80	**2.58**	0.07
	Sum of Squares	0.45	1.25	0.05	61.25	0.45	0.05	0.05		
	F-ratio	6.43	17.86	0.71	875.00	6.43	0.71	0.71		
	Coefficient	**0.08**	**0.13**	**0.03**	**-0.88**	**0.08**	**0.02**	**-0.03**		
$45 < \phi \leq 90$ $\frac{1}{8} < r \leq \frac{1}{4}$	Contrasts	1.00	0.80	0.00	-0.60	-0.20	-0.40	0.00	Grand Average	Mean Squares Within
	Adjustment Term	0.80	0.80	0.80	0.80	0.80	0.80	0.80	**1.63**	0.02
	Sum of Squares	1.25	0.80	0.00	0.45	0.05	0.20	0.00		
	F-ratio	58.82	37.65	0.00	21.18	2.35	9.41	0.00		
	Coefficient	**0.13**	**0.10**	**0.00**	**-0.08**	**-0.03**	**-0.05**	**0.00**		
$45 < \phi \leq 90$ $\frac{1}{4} < r \leq \frac{3}{8}$	Contrasts	0.40	0.20	0.20	-1.20	-0.40	-0.20	0.20	Grand Average	Mean Squares Within
	Adjustment Term	0.80	0.80	0.80	0.80	0.80	0.80	0.80	**1.40**	0.01
	Sum of Squares	0.20	0.05	0.05	1.80	0.20	0.05	0.05		
	F-ratio	22.86	5.71	5.71	205.71	22.86	5.71	5.71		
	Coefficient	**0.05**	**0.03**	**0.03**	**-0.15**	**-0.05**	**-0.03**	**0.03**		
$45 < \phi \leq 90$ $\frac{3}{8} < r \leq \frac{1}{2}$	Contrasts	0.20	0.00	0.20	-0.40	0.20	0.00	-0.20	Grand Average	Mean Squares Within
	Adjustment Term	0.80	0.80	0.80	0.80	0.80	0.80	0.80	**1.20**	0.01
	Sum of Squares	0.05	0.00	0.05	0.20	0.05	0.00	0.05		
	F-ratio	10.00	0.00	10.00	40.00	10.00	0.00	10.00		
	Coefficient	**0.03**	**0.00**	**0.03**	**-0.05**	**0.03**	**0.00**	**-0.03**		

Table B.9 – Convex spring back of Fabric 2, 0° < $\Phi \leq$45° yarn orientation

		C_1	C_2	C_{12}	C_3	C_{13}	C_{23}	C_{123}		
$0 < \phi \leq 45$ $\frac{1}{16} < r \leq \frac{1}{8}$	Contrasts	3.00	1.40	-1.60	-7.00	-2.00	-0.80	1.00	Grand Average	Mean Squares Within
	Adjustment Term	0.80	0.80	0.80	0.80	0.80	0.80	0.80	**3.45**	0.13
	Sum of Squares	11.25	2.45	3.20	61.25	5.00	0.80	1.25		
	F-ratio	84.11	18.32	23.93	457.94	37.38	5.98	9.35		
	Coefficient	**0.38**	**0.18**	**-0.20**	**-0.88**	**-0.25**	**-0.10**	**0.13**		
$0 < \phi \leq 45$ $\frac{1}{8} < r \leq \frac{1}{4}$	Contrasts	1.00	-0.80	0.00	-0.80	-0.40	0.60	0.20	Grand Average	Mean Squares Within
	Adjustment Term	0.80	0.80	0.80	0.80	0.80	0.80	0.80	**2.39**	0.05
	Sum of Squares	1.25	0.80	0.00	0.80	0.20	0.45	0.05		
	F-ratio	25.00	16.00	0.00	16.00	4.00	9.00	1.00		
	Coefficient	**0.13**	**-0.10**	**0.00**	**-0.10**	**-0.05**	**0.08**	**0.03**		
$0 < \phi \leq 45$ $\frac{1}{4} < r \leq \frac{3}{8}$	Contrasts	0.30	-0.30	-0.10	-0.90	-0.30	-0.10	-0.30	Grand Average	Mean Squares Within
	Adjustment Term	0.80	0.80	0.80	0.80	0.80	0.80	0.80	**1.98**	0.03
	Sum of Squares	0.11	0.11	0.01	1.01	0.11	0.01	0.11		
	F-ratio	3.75	3.75	0.42	33.75	3.75	0.42	3.75		
	Coefficient	**0.04**	**-0.04**	**-0.01**	**-0.11**	**-0.04**	**-0.01**	**-0.04**		
$0 < \phi \leq 45$ $\frac{3}{8} < r \leq \frac{1}{2}$	Contrasts	0.20	-0.40	-0.20	-0.40	0.20	0.00	0.20	Grand Average	Mean Squares Within
	Adjustment Term	0.80	0.80	0.80	0.80	0.80	0.80	0.80	**1.66**	0.02
	Sum of Squares	0.05	0.20	0.05	0.20	0.05	0.00	0.05		
	F-ratio	2.50	10.00	2.50	10.00	2.50	0.00	2.50		
	Coefficient	**0.03**	**-0.05**	**-0.03**	**-0.05**	**0.03**	**0.00**	**0.03**		

Table B.10 – Convex spring back of Fabric 2, 45° < $\Phi \le$ 90°

		C_1	C_2	C_{12}	C_3	C_{13}	C_{23}	C_{123}		
$45 < \phi \le 90$ $\frac{1}{16} < r \le \frac{1}{8}$	Contrasts	1.80	-2.00	0.40	-7.80	-1.00	0.00	0.00	Grand Average	Mean Squares Within
	Adjustment Term	0.80	0.80	0.80	0.80	0.80	0.80	0.80		
	Sum of Squares	4.05	5.00	0.20	76.05	1.25	0.00	0.00	**3.38**	0.07
	F-ratio	55.86	68.97	2.76	1048.97	17.24	0.00	0.00		
	Coefficient	**0.23**	**-0.25**	**0.05**	**-0.98**	**-0.13**	**0.00**	**0.00**		
$45 < \phi \le 90$ $\frac{1}{8} < r \le \frac{1}{4}$	Contrasts	1.00	0.80	0.00	-0.60	-0.20	-0.40	0.00	Grand Average	Mean Squares Within
	Adjustment Term	0.80	0.80	0.80	0.80	0.80	0.80	0.80		
	Sum of Squares	1.25	0.80	0.00	0.45	0.05	0.20	0.00	**2.19**	0.02
	F-ratio	58.82	37.65	0.00	21.18	2.35	9.41	0.00		
	Coefficient	**0.13**	**0.10**	**0.00**	**-0.08**	**-0.03**	**-0.05**	**0.00**		
$45 < \phi \le 90$ $\frac{1}{4} < r \le \frac{3}{8}$	Contrasts	0.40	0.20	0.20	-1.20	-0.40	-0.20	0.20	Grand Average	Mean Squares Within
	Adjustment Term	0.80	0.80	0.80	0.80	0.80	0.80	0.80		
	Sum of Squares	0.20	0.05	0.05	1.80	0.20	0.05	0.05	**1.74**	0.01
	F-ratio	22.86	5.71	5.71	205.71	22.86	5.71	5.71		
	Coefficient	**0.05**	**0.03**	**0.03**	**-0.15**	**-0.05**	**-0.03**	**0.03**		
$45 < \phi \le 90$ $\frac{3}{8} < r \le \frac{1}{2}$	Contrasts	0.20	0.00	0.20	-0.40	0.20	0.00	-0.20	Grand Average	Mean Squares Within
	Adjustment Term	0.80	0.80	0.80	0.80	0.80	0.80	0.80		
	Sum of Squares	0.05	0.00	0.05	0.20	0.05	0.00	0.05	**1.41**	0.01
	F-ratio	8.00	0.00	8.00	32.00	8.00	0.00	8.00		
	Coefficient	**0.03**	**0.00**	**0.03**	**-0.05**	**0.03**	**0.00**	**-0.03**		

Table B.11 – Convex spring back of Fabric 3, 0° < $\Phi \le$45° yarn orientation

		C_1	C_2	C_{12}	C_3	C_{13}	C_{23}	C_{123}		
$0 < \phi \le 45$ $\frac{1}{16} < r \le \frac{1}{8}$	Contrasts	1.20	-4.20	1.00	-10.40	0.00	-2.20	1.00	Grand Average	Mean Squares Within
	Adjustment Term	0.80	0.80	0.80	0.80	0.80	0.80	0.80		
	Sum of Squares	1.80	22.05	1.25	135.20	0.00	6.05	1.25	**5.70**	0.30
	F-ratio	6.10	74.75	4.24	458.31	0.00	20.51	4.24		
	Coefficient	**0.15**	**-0.53**	**0.13**	**-1.30**	**0.00**	**-0.28**	**0.13**		
$0 < \phi \le 45$ $\frac{1}{8} < r \le \frac{1}{4}$	Contrasts	1.00	-0.80	0.00	-0.80	-0.40	0.60	0.20	Grand Average	Mean Squares Within
	Adjustment Term	0.80	0.80	0.80	0.80	0.80	0.80	0.80		
	Sum of Squares	1.25	0.80	0.00	0.80	0.20	0.45	0.05	**3.50**	0.14
	F-ratio	9.26	5.93	0.00	5.93	1.48	3.33	0.37		
	Coefficient	**0.13**	**-0.10**	**0.00**	**-0.10**	**-0.05**	**0.08**	**0.03**		
$0 < \phi \le 45$ $\frac{1}{4} < r \le \frac{3}{8}$	Contrasts	0.30	-0.30	-0.10	-0.90	-0.30	-0.10	-0.30	Grand Average	Mean Squares Within
	Adjustment Term	0.80	0.80	0.80	0.80	0.80	0.80	0.80		
	Sum of Squares	0.11	0.11	0.01	1.01	0.11	0.01	0.11	**2.43**	0.04
	F-ratio	3.00	3.00	0.33	27.00	3.00	0.33	3.00		
	Coefficient	**0.04**	**-0.04**	**-0.01**	**-0.11**	**-0.04**	**-0.01**	**-0.04**		
$0 < \phi \le 45$ $\frac{3}{8} < r \le \frac{1}{2}$	Contrasts	0.20	-0.40	-0.20	-0.40	0.20	0.00	0.20	Grand Average	Mean Squares Within
	Adjustment Term	0.80	0.80	0.80	0.80	0.80	0.80	0.80		
	Sum of Squares	0.05	0.20	0.05	0.20	0.05	0.00	0.05	**2.21**	0.04
	F-ratio	1.38	5.52	1.38	5.52	1.38	0.00	1.38		
	Coefficient	**0.03**	**-0.05**	**-0.03**	**-0.05**	**0.03**	**0.00**	**0.03**		

Table B.12 – Convex spring back of Fabric 3, 45° < $\Phi \leq 90°$

		C_1	C_2	C_{12}	C_3	C_{13}	C_{23}	C_{123}		
$45 < \phi \leq 90$ $\frac{1}{16} < r \leq \frac{1}{8}$	Contrasts	1.40	7.60	-0.80	-10.20	0.20	2.40	-0.80	Grand Average	Mean Squares Within
	Adjustment Term	0.80	0.80	0.80	0.80	0.80	0.80	0.80	**6.13**	0.30
	Sum of Squares	2.45	72.20	0.80	130.05	0.05	7.20	0.80		
	F-ratio	8.17	240.67	2.67	433.50	0.17	24.00	2.67		
	Coefficient	**0.18**	**0.95**	**-0.10**	**-1.28**	**0.03**	**0.30**	**-0.10**		
$45 < \phi \leq 90$ $\frac{1}{8} < r \leq \frac{1}{4}$	Contrasts	1.00	0.80	0.00	-0.60	-0.20	-0.40	0.00	Grand Average	Mean Squares Within
	Adjustment Term	0.80	0.80	0.80	0.80	0.80	0.80	0.80	**3.70**	0.13
	Sum of Squares	1.25	0.80	0.00	0.45	0.05	0.20	0.00		
	F-ratio	10.00	6.40	0.00	3.60	0.40	1.60	0.00		
	Coefficient	**0.13**	**0.10**	**0.00**	**-0.08**	**-0.03**	**-0.05**	**0.00**		
$45 < \phi \leq 90$ $\frac{1}{4} < r \leq \frac{3}{8}$	Contrasts	0.40	0.20	0.20	-1.20	-0.40	-0.20	0.20	Grand Average	Mean Squares Within
	Adjustment Term	0.80	0.80	0.80	0.80	0.80	0.80	0.80	**2.53**	0.04
	Sum of Squares	0.20	0.05	0.05	1.80	0.20	0.05	0.05		
	F-ratio	4.85	1.21	1.21	43.64	4.85	1.21	1.21		
	Coefficient	**0.05**	**0.03**	**0.03**	**-0.15**	**-0.05**	**-0.03**	**0.03**		
$45 < \phi \leq 90$ $\frac{3}{8} < r \leq \frac{1}{2}$	Contrasts	0.20	0.00	0.20	-0.40	0.20	0.00	-0.20	Grand Average	Mean Squares Within
	Adjustment Term	0.80	0.80	0.80	0.80	0.80	0.80	0.80	**2.48**	0.03
	Sum of Squares	0.05	0.00	0.05	0.20	0.05	0.00	0.05		
	F-ratio	1.67	0.00	1.67	6.67	1.67	0.00	1.67		
	Coefficient	**0.03**	**0.00**	**0.03**	**-0.05**	**0.03**	**0.00**	**-0.03**		

B.2.2. Concave spring back

Table B.13 – Concave spring back of Fabric 1, 0° < $\Phi \leq 45°$ yarn orientation

		C_1	C_2	C_{12}	C_3	C_{13}	C_{23}	C_{123}		
$0 < \phi \leq 45$ $\frac{1}{16} < r \leq \frac{1}{8}$	Contrasts	1.30	-5.50	1.50	-6.90	-1.10	1.70	-0.90	Grand Average	Mean Squares Within
	Adjustment Term	0.80	0.80	0.80	0.80	0.80	0.80	0.80	**3.64**	0.72
	Sum of Squares	2.11	37.81	2.81	59.51	1.51	3.61	1.01		
	F-ratio	2.92	52.34	3.89	82.37	2.09	5.00	1.40		
	Coefficient	**0.16**	**-0.69**	**0.19**	**-0.86**	**-0.14**	**0.21**	**-0.11**		
$0 < \phi \leq 45$ $\frac{1}{8} < r \leq \frac{1}{4}$	Contrasts	0.80	-3.00	0.00	-4.40	0.60	0.80	-0.60	Grand Average	Mean Squares Within
	Adjustment Term	0.80	0.80	0.80	0.80	0.80	0.80	0.80	**2.23**	0.27
	Sum of Squares	0.80	11.25	0.00	24.20	0.45	0.80	0.45		
	F-ratio	2.92	41.10	0.00	88.40	1.64	2.92	1.64		
	Coefficient	**0.10**	**-0.38**	**0.00**	**-0.55**	**0.08**	**0.10**	**-0.08**		
$0 < \phi \leq 45$ $\frac{1}{4} < r \leq \frac{3}{8}$	Contrasts	1.20	-1.80	-0.40	-0.80	-0.20	0.40	0.20	Grand Average	Mean Squares Within
	Adjustment Term	0.80	0.80	0.80	0.80	0.80	0.80	0.80	**1.58**	0.04
	Sum of Squares	1.80	4.05	0.20	0.80	0.05	0.20	0.05		
	F-ratio	42.35	95.29	4.71	18.82	1.18	4.71	1.18		
	Coefficient	**0.15**	**-0.23**	**-0.05**	**-0.10**	**-0.03**	**0.05**	**0.03**		
$0 < \phi \leq 45$ $\frac{3}{8} < r \leq \frac{1}{2}$	Contrasts	0.80	-0.60	-0.20	-1.40	-0.20	0.80	0.00	Grand Average	Mean Squares Within
	Adjustment Term	0.80	0.80	0.80	0.80	0.80	0.80	0.80	**1.30**	0.03
	Sum of Squares	0.80	0.45	0.05	2.45	0.05	0.80	0.00		
	F-ratio	32.00	18.00	2.00	98.00	2.00	32.00	0.00		
	Coefficient	**0.10**	**-0.07**	**-0.03**	**-0.18**	**-0.03**	**0.10**	**0.00**		

Table B.14 – Concave spring back of Fabric 1, 45° < $\Phi \leq$ 90°

		C_1	C_2	C_{12}	C_3	C_{13}	C_{23}	C_{123}		
$45 < \phi \leq 90$ $\frac{1}{16} < r \leq \frac{1}{8}$	Contrasts	1.20	5.20	-1.60	-8.40	-0.40	-3.20	1.60	Grand Average **3.60**	Mean Squares Within 0.73
	Adjustment Term	0.80	0.80	0.80	0.80	0.80	0.80	0.80		
	Sum of Squares	1.80	33.80	3.20	88.20	0.20	12.80	3.20		
	F-ratio	2.48	46.62	4.41	121.66	0.28	17.66	4.41		
	Coefficient	**0.15**	**0.65**	**-0.20**	**-1.05**	**-0.05**	**-0.40**	**0.20**		
$45 < \phi \leq 90$ $\frac{1}{8} < r \leq \frac{1}{4}$	Contrasts	0.80	1.60	0.00	-4.00	0.00	-0.40	0.00	Grand Average **2.05**	Mean Squares Within 0.17
	Adjustment Term	0.80	0.80	0.80	0.80	0.80	0.80	0.80		
	Sum of Squares	0.80	3.20	0.00	20.00	0.00	0.20	0.00		
	F-ratio	4.60	18.42	0.00	115.11	0.00	1.15	0.00		
	Coefficient	**0.10**	**0.20**	**0.00**	**-0.50**	**0.00**	**-0.05**	**0.00**		
$45 < \phi \leq 90$ $\frac{1}{4} < r \leq \frac{3}{8}$	Contrasts	0.80	0.40	0.00	-1.20	0.00	-0.80	0.00	Grand Average **1.40**	Mean Squares Within 0.03
	Adjustment Term	0.80	0.80	0.80	0.80	0.80	0.80	0.80		
	Sum of Squares	0.80	0.20	0.00	1.80	0.00	0.80	0.00		
	F-ratio	27.83	6.96	0.00	62.61	0.00	27.83	0.00		
	Coefficient	**0.10**	**0.05**	**0.00**	**-0.15**	**0.00**	**-0.10**	**0.00**		
$45 < \phi \leq 90$ $\frac{3}{8} < r \leq \frac{1}{2}$	Contrasts	0.50	-0.50	-0.10	-0.70	-0.30	-0.10	-0.10	Grand Average **1.16**	Mean Squares Within 0.02
	Adjustment Term	0.80	0.80	0.80	0.80	0.80	0.80	0.80		
	Sum of Squares	0.31	0.31	0.01	0.61	0.11	0.01	0.01		
	F-ratio	15.63	15.63	0.62	30.63	5.63	0.63	0.62		
	Coefficient	**0.06**	**-0.06**	**-0.01**	**-0.09**	**-0.04**	**-0.01**	**-0.01**		

Table B.15 – Concave spring back of Fabric 2, 0° < $\Phi \leq$45° yarn orientation

		C_1	C_2	C_{12}	C_3	C_{13}	C_{23}	C_{123}		
$0 < \phi \leq 45$ $\frac{1}{16} < r \leq \frac{1}{8}$	Contrasts	4.20	-14.00	-2.40	-7.80	-0.60	3.20	-0.40	Grand Average **4.83**	Mean Squares Within 3.53
	Adjustment Term	0.80	0.80	0.80	0.80	0.80	0.80	0.80		
	Sum of Squares	22.05	245.00	7.20	76.05	0.45	12.80	0.20		
	F-ratio	6.26	69.50	2.04	21.57	0.13	3.63	0.06		
	Coefficient	**0.53**	**-1.75**	**-0.30**	**-0.98**	**-0.08**	**0.40**	**-0.05**		
$0 < \phi \leq 45$ $\frac{1}{8} < r \leq \frac{1}{4}$	Contrasts	0.80	-3.00	0.00	-4.40	0.60	0.80	-0.60	Grand Average **3.03**	Mean Squares Within 1.54
	Adjustment Term	0.80	0.80	0.80	0.80	0.80	0.80	0.80		
	Sum of Squares	0.80	11.25	0.00	24.20	0.45	0.80	0.45		
	F-ratio	0.52	7.32	0.00	15.74	0.29	0.52	0.29		
	Coefficient	**0.10**	**-0.38**	**0.00**	**-0.55**	**0.08**	**0.10**	**-0.08**		
$0 < \phi \leq 45$ $\frac{1}{4} < r \leq \frac{3}{8}$	Contrasts	1.20	-1.80	-0.40	-0.80	-0.20	0.40	0.20	Grand Average **2.19**	Mean Squares Within 0.44
	Adjustment Term	0.80	0.80	0.80	0.80	0.80	0.80	0.80		
	Sum of Squares	1.80	4.05	0.20	0.80	0.05	0.20	0.05		
	F-ratio	4.06	9.13	0.45	1.80	0.11	0.45	0.11		
	Coefficient	**0.15**	**-0.23**	**-0.05**	**-0.10**	**-0.03**	**0.05**	**0.03**		
$0 < \phi \leq 45$ $\frac{3}{8} < r \leq \frac{1}{2}$	Contrasts	0.80	-0.60	-0.20	-1.40	-0.20	0.80	0.00	Grand Average **2.03**	Mean Squares Within 0.22
	Adjustment Term	0.80	0.80	0.80	0.80	0.80	0.80	0.80		
	Sum of Squares	0.80	0.45	0.05	2.45	0.05	0.80	0.00		
	F-ratio	3.68	2.07	0.23	11.26	0.23	3.68	0.00		
	Coefficient	**0.10**	**-0.07**	**-0.03**	**-0.18**	**-0.03**	**0.10**	**0.00**		

Table B.16 – Concave spring back of Fabric 2, 45° < $\Phi \leq$ 90°

		C_1	C_2	C_{12}	C_3	C_{13}	C_{23}	C_{123}		
$45 < \phi \leq 90$ $\frac{1}{16} < r \leq \frac{1}{8}$	Contrasts	4.00	8.80	2.20	-7.80	-2.40	-3.20	-1.40	Grand Average	Mean Squares Within
	Adjustment Term	0.80	0.80	0.80	0.80	0.80	0.80	0.80		
	Sum of Squares	20.00	96.80	6.05	76.05	7.20	12.80	2.45	**4.18**	0.88
	F-ratio	22.73	110.00	6.88	86.42	8.18	14.55	2.78		
	Coefficient	**0.50**	**1.10**	**0.28**	**-0.98**	**-0.30**	**-0.40**	**-0.18**		
$45 < \phi \leq 90$ $\frac{1}{8} < r \leq \frac{1}{4}$	Contrasts	0.80	1.60	0.00	-4.00	0.00	-0.40	0.00	Grand Average	Mean Squares Within
	Adjustment Term	0.80	0.80	0.80	0.80	0.80	0.80	0.80		
	Sum of Squares	0.80	3.20	0.00	20.00	0.00	0.20	0.00	**2.59**	0.25
	F-ratio	3.23	12.93	0.00	80.81	0.00	0.81	0.00		
	Coefficient	**0.10**	**0.20**	**0.00**	**-0.50**	**0.00**	**-0.05**	**0.00**		
$45 < \phi \leq 90$ $\frac{1}{4} < r \leq \frac{3}{8}$	Contrasts	0.80	0.40	0.00	-1.20	0.00	-0.80	0.00	Grand Average	Mean Squares Within
	Adjustment Term	0.80	0.80	0.80	0.80	0.80	0.80	0.80		
	Sum of Squares	0.80	0.20	0.00	1.80	0.00	0.80	0.00	**1.89**	0.14
	F-ratio	5.77	1.44	0.00	12.97	0.00	5.77	0.00		
	Coefficient	**0.10**	**0.05**	**0.00**	**-0.15**	**0.00**	**-0.10**	**0.00**		
$45 < \phi \leq 90$ $\frac{3}{8} < r \leq \frac{1}{2}$	Contrasts	0.50	-0.50	-0.10	-0.70	-0.30	-0.10	-0.10	Grand Average	Mean Squares Within
	Adjustment Term	0.80	0.80	0.80	0.80	0.80	0.80	0.80		
	Sum of Squares	0.31	0.31	0.01	0.61	0.11	0.01	0.01	**1.66**	0.14
	F-ratio	2.21	2.21	0.09	4.34	0.80	0.09	0.09		
	Coefficient	**0.06**	**-0.06**	**-0.01**	**-0.09**	**-0.04**	**-0.01**	**-0.01**		

Table B.17 – Concave spring back of Fabric 3, 0° < $\Phi \leq$45° yarn orientation

		C_1	C_2	C_{12}	C_3	C_{13}	C_{23}	C_{123}		
$0 < \phi \leq 45$ $\frac{1}{16} < r \leq \frac{1}{8}$	Contrasts	2.50	-31.90	-3.30	-22.10	0.50	13.30	-0.10	Grand Average	Mean Squares Within
	Adjustment Term	0.80	0.80	0.80	0.80	0.80	0.80	0.80		
	Sum of Squares	7.81	1272.01	13.61	610.51	0.31	221.11	0.01	**8.74**	7.62
	F-ratio	1.03	166.90	1.79	80.11	0.04	29.01	0.00		
	Coefficient	**0.31**	**-3.99**	**-0.41**	**-2.76**	**0.06**	**1.66**	**-0.01**		
$0 < \phi \leq 45$ $\frac{1}{8} < r \leq \frac{1}{4}$	Contrasts	0.80	-3.00	0.00	-4.40	0.60	0.80	-0.60	Grand Average	Mean Squares Within
	Adjustment Term	0.80	0.80	0.80	0.80	0.80	0.80	0.80		
	Sum of Squares	0.80	11.25	0.00	24.20	0.45	0.80	0.45	**4.70**	1.73
	F-ratio	0.46	6.51	0.00	14.00	0.26	0.46	0.26		
	Coefficient	**0.10**	**-0.38**	**0.00**	**-0.55**	**0.08**	**0.10**	**-0.08**		
$0 < \phi \leq 45$ $\frac{1}{4} < r \leq \frac{3}{8}$	Contrasts	1.20	-1.80	-0.40	-0.80	-0.20	0.40	0.20	Grand Average	Mean Squares Within
	Adjustment Term	0.80	0.80	0.80	0.80	0.80	0.80	0.80		
	Sum of Squares	1.80	4.05	0.20	0.80	0.05	0.20	0.05	**3.03**	0.44
	F-ratio	4.13	9.28	0.46	1.83	0.11	0.46	0.11		
	Coefficient	**0.15**	**-0.23**	**-0.05**	**-0.10**	**-0.03**	**0.05**	**0.03**		
$0 < \phi \leq 45$ $\frac{3}{8} < r \leq \frac{1}{2}$	Contrasts	0.80	-0.60	-0.20	-1.40	-0.20	0.80	0.00	Grand Average	Mean Squares Within
	Adjustment Term	0.80	0.80	0.80	0.80	0.80	0.80	0.80		
	Sum of Squares	0.80	0.45	0.05	2.45	0.05	0.80	0.00	**2.28**	0.24
	F-ratio	3.35	1.88	0.21	10.26	0.21	3.35	0.00		
	Coefficient	**0.10**	**-0.07**	**-0.03**	**-0.18**	**-0.03**	**0.10**	**0.00**		

Table B.18 – Concave spring back of Fabric 3, 45° < $\Phi \leq$ 90°

		C_1	C_2	C_{12}	C_3	C_{13}	C_{23}	C_{123}		
$45 < \phi \leq 90$ $\frac{1}{16} < r \leq \frac{1}{8}$	Contrasts	1.40	27.40	2.20	-19.60	-3.60	-10.80	-4.00	Grand Average	Mean Squares Within
	Adjustment Term	0.80	0.80	0.80	0.80	0.80	0.80	0.80		
	Sum of Squares	2.45	938.45	6.05	480.20	16.20	145.80	20.00	**8.18**	5.96
	F-ratio	0.41	157.36	1.01	80.52	2.72	24.45	3.35		
	Coefficient	**0.18**	**3.43**	**0.28**	**-2.45**	**-0.45**	**-1.35**	**-0.50**		
$45 < \phi \leq 90$ $\frac{1}{8} < r \leq \frac{1}{4}$	Contrasts	0.80	1.60	0.00	-4.00	0.00	-0.40	0.00	Grand Average	Mean Squares Within
	Adjustment Term	0.80	0.80	0.80	0.80	0.80	0.80	0.80		
	Sum of Squares	0.80	3.20	0.00	20.00	0.00	0.20	0.00	**4.51**	1.58
	F-ratio	0.51	2.03	0.00	12.69	0.00	0.13	0.00		
	Coefficient	**0.10**	**0.20**	**0.00**	**-0.50**	**0.00**	**-0.05**	**0.00**		
$45 < \phi \leq 90$ $\frac{1}{4} < r \leq \frac{3}{8}$	Contrasts	0.80	0.40	0.00	-1.20	0.00	-0.80	0.00	Grand Average	Mean Squares Within
	Adjustment Term	0.80	0.80	0.80	0.80	0.80	0.80	0.80		
	Sum of Squares	0.80	0.20	0.00	1.80	0.00	0.80	0.00	**2.81**	0.34
	F-ratio	2.38	0.59	0.00	5.35	0.00	2.38	0.00		
	Coefficient	**0.10**	**0.05**	**0.00**	**-0.15**	**0.00**	**-0.10**	**0.00**		
$45 < \phi \leq 90$ $\frac{3}{8} < r \leq \frac{1}{2}$	Contrasts	0.50	-0.50	-0.10	-0.70	-0.30	-0.10	-0.10	Grand Average	Mean Squares Within
	Adjustment Term	0.80	0.80	0.80	0.80	0.80	0.80	0.80		
	Sum of Squares	0.31	0.31	0.01	0.61	0.11	0.01	0.01	**2.18**	0.12
	F-ratio	2.69	2.69	0.11	5.27	0.97	0.11	0.11		
	Coefficient	**0.06**	**-0.06**	**-0.01**	**-0.09**	**-0.04**	**-0.01**	**-0.01**		

B.3. Friction

B.3.1. Mean coefficient of friction

Table B.19 – Fabric 1 mean coefficient of friction

		C_2		
Fabric 1 $0° < \phi \leq 45°$	Contrasts	-1.15E-01	Grand Average	Mean Squares Within
	Adjustment Term	4.00E-01		
	Sum of Squares	3.28E-02	**0.45**	6.53E-04
	F-ratio	50.26		
	Coefficient	**-2.86E-02**		
Fabric 1 $45° < \phi \leq 90°$	Contrasts	1.40E-02	Grand Average	Mean Squares Within
	Adjustment Term	4.00E-01		
	Sum of Squares	4.88E-04	**0.40**	9.32E-04
	F-ratio	0.52		
	Coefficient	**3.49E-03**		

Table B.20 – Fabric 2 mean coefficient of friction

		C_2		
Fabric 2 $0° < \phi \leq 45°$	Contrasts	2.21E-01	Grand Average	Mean Squares Within
	Adjustment Term	4.00E-01		
	Sum of Squares	1.22E-01	**0.25**	4.34E-03
	F-ratio	28.15		
	Coefficient	**5.53E-02**		
Fabric 2 $45° < \phi \leq 90°$	Contrasts	-1.64E-01	Grand Average	Mean Squares Within
	Adjustment Term	4.00E-01		
	Sum of Squares	6.69E-02	**0.28**	4.26E-03
	F-ratio	15.70		
	Coefficient	**-4.09E-02**		

Table B.21 – Fabric 3 mean coefficient of friction

		C_2		
Fabric 3 $0° < \phi \leq 45°$	Contrasts	-7.83E-02	Grand Average	Mean Squares Within
	Adjustment Term	4.00E-01		
	Sum of Squares	1.53E-02	**0.43**	1.04E-02
	F-ratio	1.48		
	Coefficient	**-1.96E-02**		
Fabric 3 $45° < \phi \leq 90°$	Contrasts	-1.33E-01	Grand Average	Mean Squares Within
	Adjustment Term	4.00E-01		
	Sum of Squares	4.43E-02	**0.32**	3.23E-03
	F-ratio	13.71		
	Coefficient	**-3.33E-02**		

B.3.2. Mean deviation of coefficient of friction

Table B.22 – Fabric 1 mean deviation of coefficient of friction

		C_2		
Fabric 1 $0° < \phi \leq 45°$	Contrasts	-4.35E-02	Grand Average	Mean Squares Within
	Adjustment Term	4.00E-01		
	Sum of Squares	4.74E-03	**3.68E-02**	3.60E-04
	F-ratio	13.17		
	Coefficient	**-1.09E-02**		
Fabric 1 $45° < \phi \leq 90°$	Contrasts	1.11E-02	Grand Average	Mean Squares Within
	Adjustment Term	4.00E-01		
	Sum of Squares	3.09E-04	**2.06E-02**	1.26E-04
	F-ratio	2.45		
	Coefficient	**2.78E-03**		

Table B.23 – Fabric 2 mean deviation of coefficient of friction

		C_2		
Fabric 2 $0° < \phi \leq 45°$	Contrasts	2.08E-03	Grand Average	Mean Squares Within
	Adjustment Term	4.00E-01		
	Sum of Squares	1.08E-05	**7.13E-03**	4.68E-05
	F-ratio	0.23		
	Coefficient	**5.19E-04**		
Fabric 2 $45° < \phi \leq 90°$	Contrasts	1.89E-03	Grand Average	Mean Squares Within
	Adjustment Term	4.00E-01		
	Sum of Squares	8.97E-06	**9.12E-03**	1.83E-05
	F-ratio	0.49		
	Coefficient	**4.74E-04**		

Table B.24 – Fabric 3 mean deviation of coefficient of friction

		C_2		
Fabric 3 $0° < \phi \leq 45°$	Contrasts	-3.59E-02	Grand Average	Mean Squares Within
	Adjustment Term	4.00E-01		
	Sum of Squares	3.22E-03	**3.26E-02**	2.08E-04
	F-ratio	15.54		
	Coefficient	**-8.98E-03**		
Fabric 3 $45° < \phi \leq 90°$	Contrasts	-1.83E-03	Grand Average	Mean Squares Within
	Adjustment Term	4.00E-01		
	Sum of Squares	8.37E-06	**1.38E-02**	5.84E-05
	F-ratio	0.14		
	Coefficient	**-4.57E-04**		

B.4. Pin stability

B.4.1. Load at pin failure

Table B.25 – Load at pin failure

		C_1	C_2	C_{12}		
Fabric 1 $0° < \phi \leq 45°$	Contrasts	-6.46	-1.32	3.65	Grand Average	Mean Squares Within
	Adjustment Term	0.80	0.80	0.80		
	Sum of Squares	52.22	2.18	16.67	**8.97**	2.03
	F-ratio	25.78	1.08	8.23		
	Coefficient	**-1.62**	**-0.33**	**0.91**		
Fabric 1 $45° < \phi \leq 90°$	Contrasts	-2.34	-2.06	0.48	Grand Average	Mean Squares Within
	Adjustment Term	0.80	0.80	0.80		
	Sum of Squares	6.82	5.30	0.28	**8.13**	2.15
	F-ratio	3.16	2.46	0.13		
	Coefficient	**-0.58**	**-0.51**	**0.12**		
Fabric 2 $0° < \phi \leq 45°$	Contrasts	-5.01	-1.95	3.00	Grand Average	Mean Squares Within
	Adjustment Term	0.80	0.80	0.80		
	Sum of Squares	31.38	4.76	11.24	**9.94**	4.85
	F-ratio	6.47	0.98	2.32		
	Coefficient	**-1.25**	**-0.49**	**0.75**		
Fabric 2 $45° < \phi \leq 90°$	Contrasts	-1.18	2.14	0.83	Grand Average	Mean Squares Within
	Adjustment Term	0.80	0.80	0.80		
	Sum of Squares	1.75	5.73	0.86	**9.99**	3.70
	F-ratio	0.47	1.55	0.23		
	Coefficient	**-0.30**	**0.54**	**0.21**		
Fabric 4 $0° < \phi \leq 45°$	Contrasts	-0.60	2.51	-0.49	Grand Average	Mean Squares Within
	Adjustment Term	0.80	0.80	0.80		
	Sum of Squares	0.45	7.89	0.30	**7.73**	6.11
	F-ratio	0.07	1.29	0.05		
	Coefficient	**-0.15**	**0.63**	**-0.12**		
Fabric 4 $45° < \phi \leq 90°$	Contrasts	-0.98	-2.01	0.11	Grand Average	Mean Squares Within
	Adjustment Term	0.80	0.80	0.80		
	Sum of Squares	1.19	5.05	0.02	**7.85**	6.88
	F-ratio	0.17	0.73	0.00		
	Coefficient	**-0.24**	**-0.50**	**0.03**		

B.4.2. Extension at pin failure

Table B.26 – Extension at failure

		C_1	C_2	C_{12}		
Fabric 1 $0° < \phi \leq 45°$	Contrasts	-27.20	34.97	-5.38	Grand Average	Mean Squares Within
	Adjustment Term	0.80	0.80	0.80		
	Sum of Squares	925.00	1,528.96	36.21	**40.15**	35.67
	F-ratio	25.93	42.86	1.01		
	Coefficient	**-6.80**	**8.74**	**-1.35**		
Fabric 1 $45° < \phi \leq 90°$	Contrasts	-23.09	-39.97	9.49	Grand Average	Mean Squares Within
	Adjustment Term	0.80	0.80	0.80		
	Sum of Squares	666.44	1,997.46	112.69	**38.90**	50.99
	F-ratio	13.07	39.18	2.21		
	Coefficient	**-5.77**	**-9.99**	**2.37**		
Fabric 2 $0° < \phi \leq 45°$	Contrasts	-15.65	23.84	-11.51	Grand Average	Mean Squares Within
	Adjustment Term	0.80	0.80	0.80		
	Sum of Squares	306.02	710.54	165.48	**33.89**	34.09
	F-ratio	8.98	20.84	4.85		
	Coefficient	**-3.91**	**5.96**	**-2.88**		
Fabric 2 $45° < \phi \leq 90°$	Contrasts	-14.22	-16.97	12.93	Grand Average	Mean Squares Within
	Adjustment Term	0.80	0.80	0.80		
	Sum of Squares	252.91	359.83	208.93	**35.60**	27.86
	F-ratio	9.08	12.91	7.50		
	Coefficient	**-3.56**	**-4.24**	**3.23**		
Fabric 4 $0° < \phi \leq 45°$	Contrasts	-38.98	12.56	-8.07	Grand Average	Mean Squares Within
	Adjustment Term	0.80	0.80	0.80		
	Sum of Squares	1,898.93	197.32	81.50	**28.30**	127.77
	F-ratio	14.86	1.54	0.64		
	Coefficient	**-9.74**	**3.14**	**-2.02**		
Fabric 4 $45° < \phi \leq 90°$	Contrasts	-37.25	-11.28	9.80	Grand Average	Mean Squares Within
	Adjustment Term	0.80	0.80	0.80		
	Sum of Squares	1,734.34	158.93	120.10	**28.62**	130.24
	F-ratio	13.32	1.22	0.92		
	Coefficient	**-9.31**	**-2.82**	**2.45**		

Appendix C. Mathematical proofs

This appendix is for showing proofs that were omitted from the main body of the thesis. Proofs for Equations (5.7) and (5.8) are based on the geometry of the problem, and proofs for Equations (5.20), (5.21), (5.22), and (5.23) are based on manipulation of measurement uncertainties. The mathematical manipulation of the measurement uncertainties is presented first, followed by the proofs for Equations (5.7), (5.8), (5.21), (5.22), and (5.23).

C.1. Measurement uncertainties

In the body of the thesis, two methods are suggested for predicting the variability of the fabric characteristics. The first method consisted of creating linear functions for interpolating the standard deviation of the fabric characteristics. The independent variables in this method are identical to the independent variables used for creating the linear functions for interpolating the fabric characteristics. The second method consisted of calculating a confidence interval for the predicted value of the fabric characteristics.

In both cases, the methods for calculating the variability of the fabric characteristics are taken to represent the measurement uncertainty of the fabric characteristic. The measurement uncertainty of the fabric characteristics are then used for calculating the variability of the drape energy. Useful identities are presented below, and are then used for deriving expressions for the variability of drape energy.

C.1.1. Addition and subtraction

In this thesis, addition and subtraction of measurement error is conducted in the following manner:

$$(a \pm \Delta a) + (b \pm \Delta b) = (a + b) \ \pm (\Delta a + \Delta b)$$
$$(a \pm \Delta a) - (b \pm \Delta b) = (a - b) \ \pm (\Delta a + \Delta b) \tag{C.1}$$

These equations are obtained by summing or taking the difference of the maximum and minimum possible values of a and b. The proof given here is for the sum of two measurements; however it is also valid for the difference of two measurements. The maximum and minimum of the sum are:

$$S_{max} = (a + \Delta a) + (b + \Delta b) = (a + b) + (\Delta a + \Delta b)$$

$$S_{min} = (a - \Delta a) + (b - \Delta b) = (a + b) - (\Delta a + \Delta b)$$

The S_{max} and S_{min} values represent the range of possible values for the sum of the two measurements. The measurement uncertainty is therefore half the difference of S_{max} and S_{min}.

$$\Delta S = \frac{S_{max} - S_{min}}{2} = \frac{\big((a + b) + (\Delta a + \Delta b)\big) - ((a + b) - (\Delta a + \Delta b))}{2}$$

$$\boldsymbol{\Delta S = \Delta a + \Delta b}$$

C.1.2. Multiplication and division

Multiplication of measurement error is obtained by adding the proportions of measurement error for each variable, and multiplying the sum by the multiplication of the two measurements.

$$(a \pm \Delta a) \times (b \pm \Delta b) = ab \ \pm ab(\frac{\Delta a}{a} + \frac{\Delta b}{b}) \tag{C.2}$$

The maximum result of the multiplication is obtained by multiplying the maximum values of *a* and *b*, and the minimum result of the multiplication is obtained by multiplying the minimum values of *a* and *b*.

$$M_{max} = (a + \Delta a) \times (b + \Delta b) = ab + a\Delta b + b\Delta a + \Delta a\Delta b$$

$$M_{min} = (a - \Delta a) \times (b - \Delta b) = ab - a\Delta b - b\Delta a + \Delta a\Delta b$$

The difference of the maximum and minimum values of the multiplication are then halved for calculating the measurement uncertainty:

$$\Delta M = \frac{M_{max} - M_{min}}{2} = \frac{(ab + a\Delta b + b\Delta a + \Delta a\Delta b) - (ab - a\Delta b - b\Delta a + \Delta a\Delta b)}{2}$$

$$\Delta M = \frac{2a\Delta b + 2b\Delta a}{2} = a\Delta b + b\Delta a$$

$$\boldsymbol{\Delta M = ab(\frac{\Delta a}{a} + \frac{\Delta b}{b})}$$

Division of measurement error is obtained by adding the proportions of measurement error for each variable, and multiplying the sum by the quotient of the two measurements

$$\frac{(a \pm \Delta a)}{(b \pm \Delta b)} = \frac{a}{b} \pm \frac{a}{b}(\frac{\Delta a}{a} + \frac{\Delta b}{b}) \qquad \text{(C.3)}$$

This maximum value of the division is obtained by dividing the maximum value of *a* by the minimum value of *b*, and the minimum value of the division is obtained by dividing the minimum value of *a* by the maximum value of *b*.

$$D_{max} = \frac{(a + \Delta a)}{(b - \Delta b)}$$

$$D_{min} = \frac{(a - \Delta a)}{(b + \Delta b)}$$

The difference of the maximum and minimum values of the division are then halved for calculating the measurement uncertainty

$$\Delta D = \frac{D_{max} - D_{min}}{2} = \frac{\left(\frac{(a + \Delta a)}{(b - \Delta b)}\right) - \left(\frac{(a - \Delta a)}{(b + \Delta b)}\right)}{2}$$

$$\Delta D = \frac{(a + \Delta a)(b + \Delta b) - \ (a - \Delta a)(b - \Delta b)}{2(b - \Delta b)(b + \Delta b)}$$

$$\Delta D = \frac{ab + a\Delta b + b\Delta a + \Delta a\Delta b - ab + a\Delta b + b\Delta a - \Delta a\Delta b)}{2(b^2 + b\Delta b - b\Delta b - \Delta b^2)}$$

$$\Delta D = \frac{2a\Delta b + 2b\Delta a}{2(b^2 - \Delta b^2)}$$

$$\Delta D = \frac{ab\left(\frac{\Delta a}{a} + \frac{\Delta b}{b}\right)}{b^2 - \Delta b^2}$$

Term Δb^2 is assumed small compared to term b^2, therefore the expression is approximated by:

$$\Delta D = \ \frac{ab\left(\frac{\Delta a}{a} + \frac{\Delta b}{b}\right)}{b^2}$$

$$\boldsymbol{\Delta D} = \ \frac{\boldsymbol{a}}{\boldsymbol{b}}\left(\frac{\boldsymbol{\Delta a}}{\boldsymbol{a}} + \frac{\boldsymbol{\Delta b}}{\boldsymbol{b}}\right)$$

C.1.3. Uncertainty of a transformation of a variable

When a measurement is transformed by a function, the uncertainty of the output result is given by

$$f(a \pm \Delta a) = f(a) \pm \ f'(a)\Delta a \qquad \text{(C.4)}$$

This result is obtained by Taylor series expansion of the function around *x* = *a*.

$$f(x) = f(a) \pm\ f'(a) + \frac{f''(x-a)^2}{2!} + \frac{f'''(x-a)^3}{3!} + \cdots$$

Omitting higher order terms, the Taylor series expansion at $x = a$ is given by

$$f(x) \approx f(a) +\ f'(a)(x-a)$$

The uncertainty is obtained by calculating the Taylor series expansion at $x = a + \Delta a$ and at point $x = a - \Delta a$. The expansion at $x = a + \Delta a$ is given by

$$f(a + \Delta a) = f(a) +\ f'(a)(a + \Delta \mathrm{a} - a)$$

$$f(a + \Delta a) = f(a) +\ f'(a)\mathit{\Delta} a$$

and the expansion at $x = a - \Delta a$ is given by

$$f(a - \Delta a) = f(a) +\ f'(a)(a - \Delta \mathrm{a} - a)$$

$$f(a - \Delta a) = f(a) -\ f'(a)\mathit{\Delta} a$$

Therefore,

$$f(a \pm \Delta a) = f(a) \pm\ f'(a)\Delta a$$

C.2. Equation 5.7

Equation (5.7) is required for calculating the radius of the final shape of the fabric in convex bending cases. It is then used for calculating the spring back energy of fabrics when draped to convex corners, assuming the spring back shape of the fabric is circular. The fabric is assumed tangent to the SMR at point A, shown in Figure C.1. This point is assumed vertical to the SMR origin. The measurements of spring back are taken horizontally from the SMR origin.

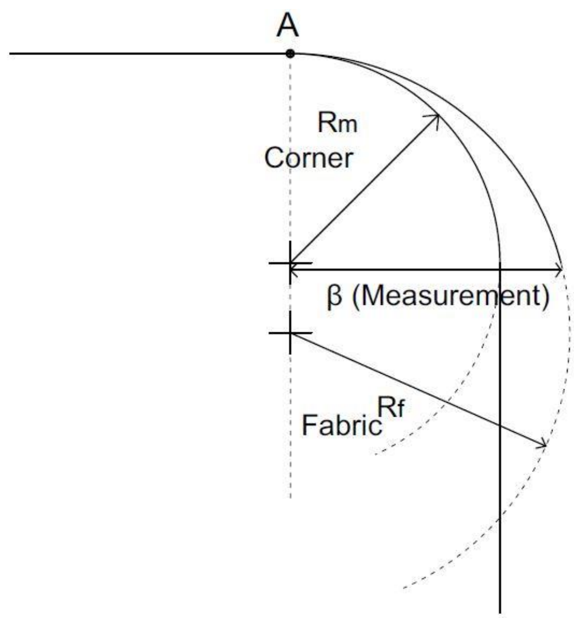

Figure C.1 – Geometric assumptions, convex spring back radius

The circle formed by the fabric is given by

$$x^2 + y^2 = R_f^2 \tag{C.5}$$

where R_f is the radius of the fabric. This is re-expressed as

$$y = \sqrt{R_f^2 - x^2} \tag{C.6}$$

Assuming point B on the circle formed by the fabric, its horizontal coordinate is the measurement of spring back β (2) and its vertical coordinate at point B is obtained by replacing *x* by β in Equation (C.6).

$$y = \sqrt{R_f^2 - \beta^2} \tag{C.7}$$

The vertical coordinate represents the same quantity as the difference between the SMR and fabric radii, shown in Figure C.2, therefore the following simplifications are made.

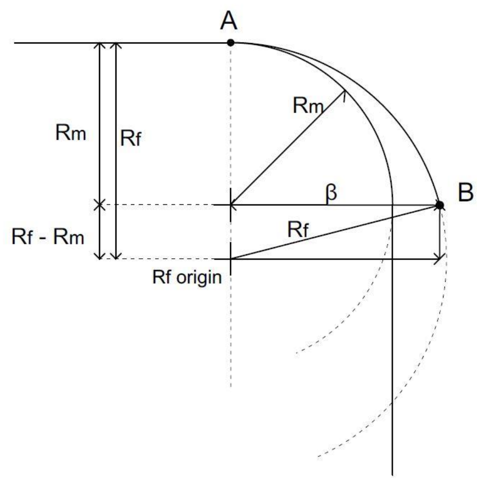

Figure C.2 – Vertical coordinate of point B

$$\sqrt{R_f^2 - \beta^2} = R_f - R_m$$

$$R_f^2 - \beta^2 = \left(R_f - R_m\right)^2$$

$$\left(R_f - R_m\right)^2 = R_f^2 - 2R_fR_m + R_m^2$$

$$R_f^2 - \beta^2 = R_f^2 - 2R_fR_m + R_m^2$$

$$\cancel{R_f^2 - R_f^2} = -2R_fR_m + R_m^2 + \beta^2$$

$$2R_f R_m = R_m^2 + \beta^2$$

And finally,

$$R_f = \frac{R_m^2 + \beta^2}{2R_m}$$

C.3. Equation 5.8

Equation (5.8) is also required for calculating the final opening angle of the fabric in calculating the convex spring back energy of fabrics. The opening angle is shown in Figure C.3.

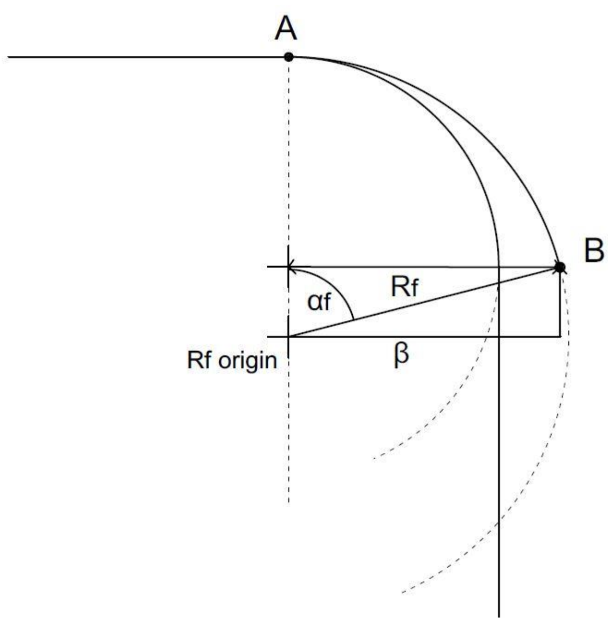

Figure C.3 – Geometric assumptions, convex spring back opening angle

The opening angle is obtained by taking the arctangent of the spring back measurement and vertical distance between the origins of the SMR and fabric radii. It should be noted that many expressions can be derived for calculating this angle. The result presented below is selected for simplifying calculations of final opening angle of fabrics.

$$\theta_f = \frac{\pi}{2} - \tan^{-1}\frac{R_f - R_m}{\beta} \tag{C.8}$$

The final radius of the fabric (Equation (5.7)) is substituted into Equation (C.8). The following simplifications are made for calculating the final opening angle of fabrics, based only on the measurement of spring back β and the mould radius, R_m.

$$\theta_f = \frac{\pi}{2} - \tan^{-1}\left(\frac{\frac{R_m^2 + \beta^2}{2R_m} - R_m}{\beta}\right)$$

$$\theta_f = \frac{\pi}{2} - \tan^{-1}\left(\frac{\frac{R_m^2 + \beta^2 - 2R_m^2}{2R_m}}{\beta}\right)$$

$$\theta_f = \frac{\pi}{2} - \tan^{-1}\left(\frac{\beta^2 - R_m^2}{2R_m\beta}\right)$$

$$\theta_f = \frac{\pi}{2} - \tan^{-1}\left(\frac{\beta^2}{2R_m\beta} - \frac{R_m^2}{2R_m\beta}\right)$$

$$\theta_f = \frac{\pi}{2} - \tan^{-1}\left(\frac{\beta}{2R_m} - \frac{R_m}{2\beta}\right)$$

The result is an expression for calculating the final opening angle of fabrics, Equation (5.8)

$$\theta_f = \frac{\pi}{2} - \tan^{-1}\left(\frac{\beta}{2R_m} - \frac{R_m}{2\beta}\right)$$

C.4. Equation 5.20

The variability of the bending energy is calculated by applying the measurement uncertainty formulas derived in this appendix to the calculation of the drape energies. The bending energy of fabrics was shown in Chapter 5 to be given by

$$U_{bending} = \left(\frac{1}{2}\right) B_{Peirce} b \frac{\alpha_m}{R_m}$$

The curvature width b, mould radius R_m and the mould opening angle α_m are all constants (i.e. no dispersion). The fabric has an average bending stiffness B_{Peirce} and a dispersion of bending stiffness ΔB_{Peirce}. The expression for bending energy is re-written as

$$U_{bending} = \frac{1}{2} b \frac{\alpha_m}{R_m} \times (B_{Peirce} \pm \Delta B_{Peirce})$$

therefore, the bending energy and its uncertainty are calculated using:

$$U_{bending} \pm \Delta U_{bending} = \frac{1}{2}\ G_{Peirce} w \frac{\theta_m}{R_m} \pm \frac{1}{2}\ \Delta G_{Peirce} w \frac{\theta_m}{R_m}$$

$$U_{bending} = \left(\frac{1}{2}\right) G_{Peirce} w \frac{\theta_m}{R_m}$$

$$\Delta U_{bending} = \pm \frac{1}{2}\ \Delta G_{Peirce} w \frac{\theta_m}{R_m}$$

C.5. Equation 5.21

The convex bending spring back of fabrics was shown to be calculated using

$$SBE_{convex} = \left(\frac{1}{2}\right) B_{Peirce} b \left(\frac{\alpha_m}{R_m} - \frac{\alpha_f}{R_f}\right)$$

where B_{Peirce} is the bending stiffness, b is the curvature width, α_m is the mould opening angle, R_m is the mould radius, α_f is the final opening angle of the fabric and R_f is the final radius of the fabric. The equation for spring back energy is re-written to include the uncertainties of each measured quantity

$$SBE_{convex} = \left(\frac{1}{2}\right) (B_{Peirce} \pm \Delta B_{Peirce}) b \left(\frac{\alpha_m}{R_m} - \frac{(\alpha_f \pm \Delta\alpha_f)}{(R_f \pm \Delta R_f)}\right)$$

and expanded to

$$\begin{aligned} SBE_{convex} = &\left(\frac{1}{2}\right) (B_{Peirce} \pm \Delta B_{Peirce}) b \frac{\alpha_m}{R_m} \\ &- \left(\frac{1}{2}\right) (B_{Peirce} \pm \Delta B_{Peirce}) b \frac{(\alpha_f \pm \Delta\alpha_f)}{(R_f \pm \Delta R_f)} \end{aligned} \tag{C.9}$$

The first term of this expression is

$$\left(\frac{1}{2}\right) (B_{Peirce} \pm \Delta B_{Peirce}) b \frac{\alpha_m}{R_m} = \left(\frac{1}{2}\right) B_{Peirce} b \frac{\alpha_m}{R_m} \pm \left(\frac{1}{2}\right) \Delta B_{Peirce} b \frac{\alpha_m}{R_m} \tag{C.10}$$

The second term of this expression requires a bit more development, because it includes a multiplication of uncertainties and a division of uncertainties. Using Equation (C.2) for multiplying the bending stiffness by the final opening angle of the fabric , the second part of the expression is re-written as

$$\left(\frac{1}{2}\right) b\left(B_{Peirce} \pm \Delta B_{Peirce}\right) \frac{\left(\alpha_f \pm \Delta\alpha_f\right)}{\left(R_f \pm \Delta R_f\right)} = \frac{\left(\frac{1}{2}\right) bB_{Peirce}\alpha_f \pm \left(\frac{1}{2}\right) bB_{Peirce}\alpha_f \left(\frac{\Delta B_{Peirce}}{B_{Peirce}} + \frac{\Delta\alpha_f}{\alpha_f}\right)}{\left(R_f \pm \Delta R_f\right)} \tag{C.11}$$

The final step is to use using Equation (C.3) to divide the numerator by the denominator in Equation (C.11). The division can be re-written as

$$\left(\frac{1}{2}\right) bB_{Peirce}\frac{\alpha_f}{R_f} \pm \left(\frac{1}{2}\right) bB_{Peirce}\frac{\alpha_f}{R_f}\left(\frac{\left(\frac{1}{2}\right) bB_{Peirce}\alpha_f \left(\frac{\Delta B_{Peirce}}{B_{Peirce}} + \frac{\Delta\alpha_f}{\alpha_f}\right)}{\left(\frac{1}{2}\right) bB_{Peirce}\alpha_f} + \frac{\Delta R_f}{R_f}\right)$$

And then simplified to

$$\left(\frac{1}{2}\right) bB_{Peirce}\frac{\alpha_f}{R_f} \pm \left(\frac{1}{2}\right) bB_{Peirce}\frac{\alpha_f}{R_f}\left(\frac{\Delta B_{Peirce}}{B_{Peirce}} + \frac{\Delta\alpha_f}{\alpha_f} + \frac{\Delta R_f}{R_f}\right) \tag{C.12}$$

Combining Equations (C.10) and (C.12) of the SBE results in

$$\left(\frac{1}{2}\right) B_{Peirce} b\frac{\alpha_m}{R_m} \pm \left(\frac{1}{2}\right) \Delta B_{Peirce} b\frac{\alpha_m}{R_m} - \left(\frac{1}{2}\right) bB_{Peirce}\frac{\alpha_f}{R_f} \pm \left(\frac{1}{2}\right) bB_{Peirce}\frac{\alpha_f}{R_f}\left(\frac{\Delta B_{Peirce}}{B_{Peirce}} + \frac{\Delta\alpha_f}{\alpha_f} + \frac{\Delta R_f}{R_f}\right)$$

The expression is re-organized to show the variability of the drape energy:

$$\left(\frac{1}{2}\right) B_{Peirce} b\left(\frac{\alpha_m}{R_m} - \frac{\alpha_f}{R_f}\right) \pm \left(\frac{1}{2}\right) b\left(\mathit{\Delta} B_{Peirce}\cdot\frac{\alpha_m}{R_m} + \frac{B\alpha_f}{R_f}\cdot\left(\frac{\mathit{\Delta}\alpha_f}{\alpha_f} + \frac{\Delta R_f}{R_f} + \frac{\mathit{\Delta} B_{Peirce}}{B_{Peirce}}\right)\right)$$

The calculations of the uncertainty of convex spring back energy requires calculations for the final fabric radius and the final fabric opening angle. Recalling Equation (5.7), the final radius of the fabric is given by

$$R_f = \frac{R_m^2 + \beta^2}{2R_m}$$

where R_m is the mould radius and β is the measurement of spring back obtained via spring back tests. The mould radius is assumed to have no dispersion; therefore, the uncertainty of the final fabric radius is calculated by replacing β by $\beta + \Delta\, \beta$:

$$R_f \pm \Delta R_f = \frac{R_m^2 + (\beta \pm \Delta\beta)^2}{2R_m} = \frac{1}{2}R_m + \frac{1}{2R_m}(\beta \pm \Delta\beta)^2$$

$$R_f \pm \Delta R_f = \frac{1}{2}R_m + \frac{1}{2R_m}(\beta \pm \Delta\beta)(\beta \pm \Delta\beta)$$

In this case, Equation (C.2) is used for multiplying uncertainties is used for developing the equation:

$$R_f \pm \Delta R_f = \frac{1}{2}R_m + \frac{1}{2R_m}\left\{\beta^2 \pm \beta\beta\left(\frac{\Delta\beta}{\beta} + \frac{\Delta\beta}{\beta}\right)\right\}$$

$$R_f \pm \Delta R_f = \frac{1}{2}R_m + \frac{\beta^2}{2R_m} \pm \frac{\beta\beta\left(\frac{\Delta\beta}{\beta} + \frac{\Delta\beta}{\beta}\right)}{2R_m}$$

$$R_f \pm \Delta R_f = \frac{1}{2}R_m + \frac{\beta^2}{2R_m} \pm \frac{\beta(\Delta\beta)}{R_m}$$

$$R_f \pm \Delta R_f = \frac{R_m^2 + \beta^2}{2R_m} \pm \frac{\beta(\Delta\beta)}{R_m}$$

Finally, the uncertainty of the radius of the fabric is given by

$$\Delta R_f = \pm \frac{\beta(\Delta\beta)}{R_m}$$

Recalling Equation (5.8), the final fabric opening angle is given by

$$\theta_f = \frac{\pi}{2} - \tan^{-1}\left(\frac{\beta}{2R_m} - \frac{R_m}{2\beta}\right)$$

Clearly stated, the fabric opening angle is a function of the mould radius and the spring back measurement. The mould radius here is known and is assumed to have no dispersion, therefore it is treated as a constant without dispersion. Written as a function of the spring back measurements β, the fabric opening angle is given by

$$\alpha_f = f(\beta) = \frac{\pi}{2} - \tan^{-1}\left(\frac{\beta}{2R_m} - \frac{R_m}{2\beta}\right)$$

The calculation of α_f involves the arctangent function, therefore the calculation of $\Delta\alpha_f$ involves Equation (C.4):

$$f(a \pm \Delta a) = f(a) \pm f'(a)\Delta a$$

The derivative of the arctangent function is given by:

$$\frac{d}{d\beta}(\tan^{-1} u) = \frac{1}{1+u^2}\frac{du}{d\beta}$$

where

$$u = \frac{\beta}{2R_m} - \frac{R_m}{2\beta}$$

Therefore, the fabric opening angle is calculated:

$$\alpha_f \pm \Delta\alpha_f = f(\beta) \pm f'(\beta)\Delta\beta = \left\{\frac{\pi}{2} - \tan^{-1}\left(\frac{\beta}{2R_m} - \frac{R_m}{2\beta}\right)\right\} \pm \frac{1}{1+u^2}\frac{du}{d\beta}\Delta\beta$$

The uncertainty of the fabric opening angle is given by:

$$\Delta\alpha_f = \pm\frac{1}{1+u^2}\frac{du}{d\beta}\Delta\beta$$

$$\Delta\alpha_f = \pm\frac{1}{1+\left(\frac{\beta}{2R_m} - \frac{R_m}{2\beta}\right)^2}\frac{d}{d\beta}\left(\frac{\beta}{2R_m} - \frac{R_m}{2\beta}\right)\Delta\beta$$

The above expression is then developed and simplified for calculating the dispersion of the fabric opening angle:

$$\Delta\alpha_f = \pm\frac{1}{1+\left(\frac{\beta}{2R_m} - \frac{R_m}{2\beta}\right)^2}\boldsymbol{\frac{d}{d\beta}\left(\frac{\beta}{2R_m} - \frac{R_m}{2\beta}\right)}\Delta\beta$$

$$\Delta\alpha_f = \pm\frac{1}{1+\boldsymbol{\left(\frac{\beta}{2R_m} - \frac{R_m}{2\beta}\right)^2}}\boldsymbol{\left(\frac{1}{2R_m} + \frac{R_m}{2\beta^2}\right)}\Delta\beta$$

$$\Delta\alpha_f = \pm\frac{1}{1+\boldsymbol{\left(\frac{\beta^2}{4R_m^2} - 2\frac{R_m}{2\beta}\frac{\beta}{2R_m} + \frac{R_m^2}{4\beta^2}\right)}}\boldsymbol{\left(\frac{1}{2R_m} + \frac{R_m}{2\beta^2}\right)}\Delta\beta$$

$$\Delta\alpha_f = \pm\frac{1}{1+\boldsymbol{\left(\frac{\beta^2}{4R_m^2} - \frac{1}{2} + \frac{R_m^2}{4\beta^2}\right)}}\boldsymbol{\left(\frac{1}{2R_m} + \frac{R_m}{2\beta^2}\right)}\Delta\beta$$

$$\Delta\alpha_f = \pm\frac{1}{\frac{1}{2}+\left(\frac{\beta^2}{4R_m^2} + \frac{R_m^2}{4\beta^2}\right)}\left(\frac{1}{2R_m} + \frac{R_m}{2\beta^2}\right)\Delta\beta$$

$$\Delta\alpha_f = \pm \frac{1}{\frac{8R_m^2\beta^2}{16R_m^2\beta^2} + \left(\frac{4\beta^4 + 4R_m^4}{16R_m^2\beta^2}\right)} \left(\frac{1}{2R_m} + \frac{R_m}{2\beta^2}\right) \Delta\beta$$

$$\Delta\alpha_f = \pm \frac{16R_m^2\beta^2}{4\beta^4 + 8R_m^2\beta^2 + 4R_m^4} \left(\frac{1}{2R_m} + \frac{R_m}{2\beta^2}\right) \Delta\beta$$

$$\Delta\alpha_f = \pm \frac{4(4R_m^2\beta^2)}{4(\beta^4 + 2R_m^2\beta^2 + R_m^4)} \left(\frac{1}{2}\right) \left(\frac{1}{R_m} + \frac{R_m}{\beta^2}\right) \Delta\beta$$

$$\Delta\alpha_f = \pm \frac{(4R_m^2\beta^2)}{(\beta^4 + 2R_m^2\beta^2 + R_m^4)} \left(\frac{1}{2}\right) \left(\frac{\beta^2 + R_m^2}{R_m\beta^2}\right) \Delta\beta$$

$$\Delta\alpha_f = \pm \frac{(4R_m^2\beta^2)}{(\beta^2 + R_m^2)^2} \left(\frac{1}{\beta^2}\right) \left(\boldsymbol{\frac{\beta^2 + R_m^2}{2R_m}}\right) \Delta\beta$$

$$\Delta\alpha_f = \pm \frac{(4R_m^2)}{(\beta^2 + R_m^2)^2} \boldsymbol{R_f} \, \Delta\beta$$

$$\Delta\alpha_f = \pm \frac{(2R_m)^2}{(\beta^2 + R_m^2)^2} R_f \, \Delta\beta$$

$$\Delta\alpha_f = \pm \left(\frac{1}{R_f}\right)^2 R_f \, \Delta\beta$$

And finally,

$$\Delta\alpha_f = \pm \frac{1}{R_f} \, \Delta\beta$$

C.6. Equation 5.23

The calculation of the concave bending spring back energy is more simple to derive, because the fabric opening angle is assumed to be identical to the mould opening angle. The concave spring back energy equation (Equation (5.6)) is simplified to

$$SBE_{Bending} = \left(\frac{1}{2}\right) B_{Peirce} b\alpha_m \left(\frac{1}{R_m} - \frac{1}{R_f}\right)$$

The concave bending spring back energy variability is obtained by writing the equation to include the uncertainty of each variable characterized via testing:

$$SBE_{Bending} = \left(\frac{1}{2}\right) (B_{Peirce} \pm \Delta B_{Peirce}) b\alpha_m \left(\frac{1}{R_m} - \frac{1}{(R_f \pm \Delta R_f)}\right)$$

The expression is then expanded and developed as follows as follows:

$$SBE = \left(\frac{1}{2}\right) b\alpha_m \left(\frac{(B_{Peirce} \pm \Delta B_{Peirce})}{R_m} - \frac{(B_{Peirce} \pm \Delta B_{Peirce})}{(R_f \pm \Delta R_f)}\right)$$

$$SBE = \left(\frac{1}{2}\right) b\alpha_m \left(\frac{B_{Peirce}}{R_m} \pm \frac{\Delta B_{Peirce}}{R_m} - \frac{(B_{Peirce} \pm \Delta B_{Peirce})}{(R_f \pm \Delta R_f)}\right)$$

$$SBE = \left(\frac{1}{2}\right) b\alpha_m \left(\frac{B_{Peirce}}{R_m} \pm \frac{\Delta B_{Peirce}}{R_m} - \left(\frac{B_{Peirce}}{R_m} \pm \frac{B_{Peirce}}{R_m}\left(\frac{\Delta B_{Peirce}}{B_{Peirce}} + \frac{\Delta R_f}{R_f}\right)\right)\right)$$

$$SBE = \left(\frac{1}{2}\right) b\alpha_m \left(\frac{B_{Peirce}}{R_m} \pm \frac{\Delta B_{Peirce}}{R_m} - \frac{B_{Peirce}}{R_m} \pm \frac{B_{Peirce}}{R_m}\left(\frac{\Delta B_{Peirce}}{B_{Peirce}} + \frac{\Delta R_f}{R_f}\right)\right)$$

$$SBE = \left(\frac{1}{2}\right) b\alpha_m \left(\frac{B_{Peirce}}{R_m} - \frac{B_{Peirce}}{R_m} \pm \frac{\Delta B_{Peirce}}{R_m} \pm \frac{B_{Peirce}}{R_m}\left(\frac{\Delta B_{Peirce}}{B_{Peirce}} + \frac{\Delta R_f}{R_f}\right)\right)$$

$$SBE = \left(\frac{1}{2}\right) b\alpha_m B_{Peirce}\left(\frac{1}{R_m} - \frac{1}{R_m}\right)$$

$$\pm\left(\frac{1}{2}\right) b\alpha_m\left(\frac{\Delta B_{Peirce}}{R_m} + \frac{B_{Peirce}}{R_m}\left(\frac{\Delta B_{Peirce}}{B_{Peirce}} + \frac{\Delta R_f}{R_f}\right)\right)$$

Therefore, the variability of the spring back energy is given by:

$$\Delta SBE_{concave} = \frac{1}{2}\cdot b\alpha_m\left(\frac{\Delta B_{Peirce}}{R_m} + \frac{B_{Peirce}}{R_f}\left(\frac{\Delta B_{Peirce}}{B_{Peirce}} + \frac{\Delta R_f}{R_f}\right)\right)$$

Appendix D. Draping ruleset

D.1. Additional drape algorithm hypotheses

The draping algorithm developed in [1] was limited to theoretical 2 dimensional moulds that do not consider mould features such as flat surfaces, single curvature surfaces, and double curvature surfaces. There is also no method for distinguishing completely impractical strategies. This Section lists additional draping hypotheses for ensuring realistic draping strategies while estimating the distribution of shear angles and yarn orientations that occur on the mould.

The draping algorithm used in this thesis makes use of existing knowledge related to the effect of mould features on the shear angles and yarn orientations of fabrics:

- Flat surfaces have no effect on yarn orientations or shear angles of fabrics;
- Single curvature surfaces have no effect on yarn orientations or shear angles of fabrics;
- Fabrics draped onto double curvature surfaces are sheared as they are draped onto the mould.

In addition to the previous iteration of the draping algorithm, new rules are introduced for obtaining draping strategies:

i. The draping sequence begins on a flat surface, because the shear angles and yarn orientations are known along the base surface edges;

ii. The first steps in the draping strategy cover as many flat and/or single curvature base surfaces, while moving in one direction across the mould. All single curvature or flat surfaces are to be covered until the mould boundary or a double curvature surface is encountered. Shear is not induced in fabrics draped on flat or single curvature surfaces;

therefore, yarn orientations and shear angles are known along all covered base surface edges;

iii. If a double curvature surface is connected to any of the covered base surfaces, use yarn orientation and shear angle linear functions for estimating the yarn orientations and shear angles along the base surface edges. If there are no double curvature base surfaces connected to any of the covered base surfaces, repeat previous step;

iv. Drape all single curvature or flat surfaces connected to the edges of the double curvature surface until mould boundary is reached;

v. Repeat steps iii and iv until all double curvature surfaces on the mould are covered.

vi. Once all double curvature base surfaces are covered, most of the base surfaces should be covered by the draping strategy. Cover all remaining base surfaces, respecting rule ii. Discontinuous yarn orientations can occur along boundaries of flat or single curvature base surfaces. Some of the remaining base surfaces can be draped from multiple starting positions. Flat base surfaces are split if they are draped from two or more single curvature surfaces.

The new set of rules partially eliminates rule 5 because double curvature surfaces are only draped from one base surface. All other adjacent base surfaces connected to a double curvature surface are not yet covered by the draping strategy. As listed in rule vi, the last base surfaces that are covered in this strategy are usually flat base surfaces that are in the vicinity of double curvature surfaces.

D.2. Draping ruleset limitations

The draping ruleset defined in this thesis was based on producing draping strategies for the FR mould introduced in Section 6.2. The ruleset appears to produce realistic draping strategies for the FR mould. However, it was not tested extensively on moulds with more base surfaces or on moulds with more complex geometries. The ruleset was developed primarily for the context and purpose of this thesis.

A first limitation is associated with the occurrence of shear progression. Certain sequences for the draping of base surfaces can result in changes in yarn orientations and shear angles occurring over single curvature or flat base surfaces, as illustrated in Figure D.1. The draping ruleset does not consider such changes in shear angles on single curvature and flat base surfaces, which are labelled as shear progression.

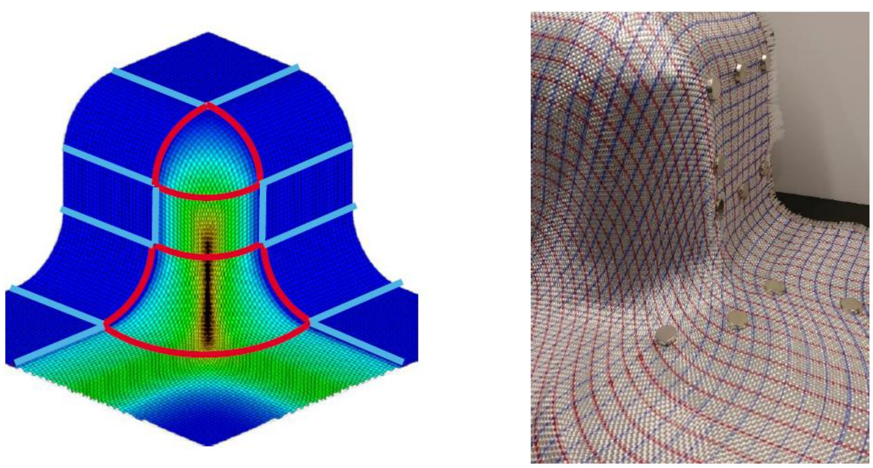

Figure D.1 – Shear progression example

In most cases, flat and single curvature base surfaces do not change yarn orientations, hence fabrics are not sheared as they are draped onto such f base surfaces. Cases where shear progression occurs are not clearly identified; however, several combinations of base surfaces leading to shear progression on flat and single curvature base surfaces were discovered in [1]. Such cases occur when a flat or a single curvature base surface is draped from a double curvature base surface. Again, the above drape strategy ruleset does not consider such occurrences.

The second limitation to the ruleset is associated with the draping of a base surface from more than one neighbouring base surfaces. In many cases, the draping strategy ruleset results in flat base surfaces draped from multiple neighbouring base surfaces. Figure D.2 shows a case where the flat base surface on the bottom left of the FR mould can be draped from the base surface above it, or from the base surface to its right.

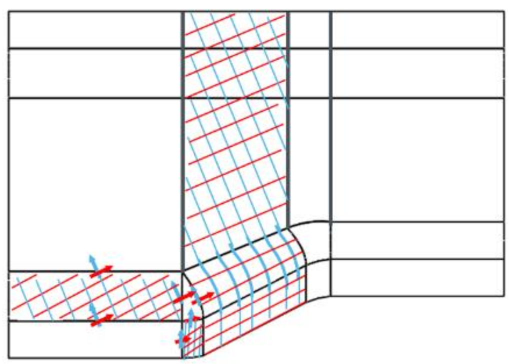

Figure D.2 – Step 5, Sequence 1

In these cases, the ruleset specifies to drape part of the flat base surface using yarn orientations from one of the base surface connected to it, and to drape the other part of the base surface using yarn orientations from the other base surface connected to it, shown in Figure D.3.

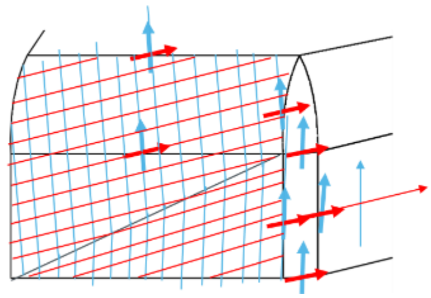

Figure D.3 – Flat base surface split into two parts

The line that splits the zones of differing yarn orientations on flat base surfaces is henceforth labelled a discontinuity line. Discontinuity lines are not an actual phenomenon that occurs while draping a fabric onto a mould, they are only the conceptual result of the rulesets that define the draping strategy, which is used for estimating the drape energy required for draping a fabric onto a mould.

Yarn orientations and shear angles may also appear discontinuous along an edge connecting two flat base surfaces, along an edge connecting a flat base surface and a single curvature surface, or along an edge connecting two single curvature base surfaces. The drape energy and variability calculations do not account for any discontinuities on the base surfaces.

The draping rulesets allows for multiple draping strategies to be generated. The draping strategies used in this thesis were defined manually and for comparison purposes only. The identification of an optimal draping strategy is not the scope of this work. The draping strategies were introduced in this work for demonstrating the calculation of drape energy and variability.

Appendix E. Drape energies

This section contains the drape energies and variabilities for the three draping strategies defined in Chapter 6.

E.1. Strategy 1 drape energy and variability

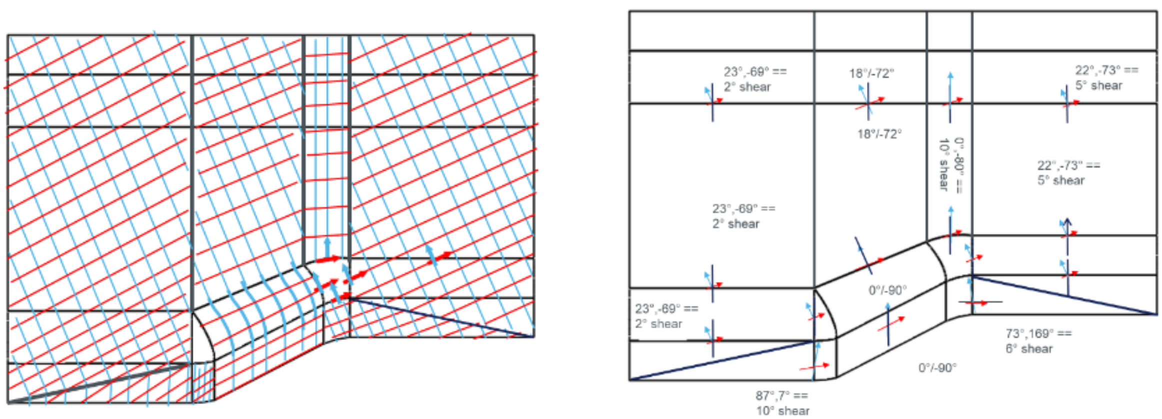

Figure E.1 – Strategy 1 summary

Table E.1 – Fabric 1 Single layer drape energies, strategy one (single curvature)

BS #	Radius (*cm*)	Length (*cm*)	Theta (°)	Yarn orientation (°)	**Bending energy (*Nmm*)**	**Spring back energy (*Nmm*)**	**Bending variability (*Nmm*)**	**Spring back variability (*Nmm*)**
2	2.5 cm	7 cm	60°	23°	**0.43**	**0.27**	**0.61**	**2.06**
4	2.5 cm	4 cm	60°	0°	**0.36**	**0.29**	**0.58**	**1.50**
6	2.5 cm	7 cm	60°	22°	**0.44**	**0.28**	**0.62**	**2.09**
7-1	2.5 cm	7 cm	60°	23°	**0.43**	**0.27**	**0.61**	**2.06**
7-2	2.5 cm	3.8 cm	60°	18°	**0.26**	**0.17**	**0.36**	**1.19**
7-3	2.5 cm	2.2 cm	60°	0°	**0.20**	**0.16**	**0.32**	**0.83**
7-4	2.5 cm	7 cm	60°	22°	**0.44**	**0.28**	**0.62**	**2.09**
9	2.75 cm	2.69 cm	18°	87°	**0.03**	**0.05**	**0.05**	**0.48**
11	3.00 cm	3.2 cm	22°	73°	**0.04**	**0.06**	**0.06**	**0.53**

Table E.2 – Fabric 1 single layer drape energy, strategy one (double curvature)

BS #	Shear Angle (°)	Total Surface Area (mm^2)	**Shear energy (*Nmm*)**	**Spring back energy (*Nmm*)**	**Shear energy variability (*Nmm*)**	**Spring back energy variability (*Nmm*)**
3	34.4	160 mm^2	**4.01**	**0.22**	**2.86**	**0.16**
5	15	284 mm^2	**0.82**	**0.05**	**3.8**	**0.21**

Table E.3 – Fabric 2 single layer drape energies, strategy one (single curvature)

BS #	Radius (*cm*)	Length (*cm*)	Theta (°)	Yarn orientation (°)	**Bending energy (*Nmm*)**	**Spring back energy (*Nmm*)**	**Bending variability (*Nmm*)**	**Spring back variability (*Nmm*)**
2	2.5 cm	7 cm	60°	23°	**0.68**	**1.16**	**1.07**	**2.86**
4	2.5 cm	4 cm	60°	0°	**0.43**	**0.77**	**0.84**	**1.73**
6	2.5 cm	7 cm	60°	22°	**0.68**	**1.17**	**1.07**	**2.86**
7-1	2.5 cm	7 cm	60°	23°	**0.68**	**1.16**	**1.07**	**2.86**
7-2	2.5 cm	3.8 cm	60°	18°	**0.38**	**0.65**	**0.59**	**1.56**
7-3	2.5 cm	2.2 cm	60°	0°	**0.24**	**0.42**	**0.46**	**0.95**
7-4	2.5 cm	7 cm	60°	22°	**0.68**	**1.17**	**1.07**	**2.86**
9	2.75 cm	2.69 cm	18°	87°	**0.02**	**0.10**	**0.09**	**0.62**
11	3.00 cm	3.2 cm	22°	73°	**0.05**	**0.19**	**0.15**	**1.03**

Table E.4 – – Fabric 2 single layer drape energy, strategy one (double curvature)

BS #	Shear Angle (°)	Total Surface Area (mm^2)	**Shear energy (*Nmm*)**	**Spring back energy (*Nmm*)**	**Shear energy variability (*Nmm*)**	**Spring back energy variability (*Nmm*)**
3	34.4	160 mm^2	**2.71**	**0.15**	**2.12**	**0.12**
5	15	284 mm^2	**1.27**	**0.07**	**2.83**	**0.16**

Table E.5 – Fabric 3 single layer drape energies, strategy one (single curvature)

BS #	Radius (*cm*)	Length (*cm*)	Theta (°)	Yarn orientation (°)	**Bending energy (*Nmm*)**	**Spring back energy (*Nmm*)**	**Bending variability (*Nmm*)**	**Spring back variability (*Nmm*)**
2	2.5 cm	7 cm	60°	23°	**0.68**	**1.60**	**1.28**	**2.82**
4	2.5 cm	4 cm	60°	0°	**0.66**	**1.57**	**1.29**	**2.23**
6	2.5 cm	7 cm	60°	22°	**0.70**	**1.65**	**1.30**	**2.87**
7-1	2.5 cm	7 cm	60°	23°	**0.68**	**1.60**	**1.28**	**2.82**
7-2	2.5 cm	3.8 cm	60°	18°	**0.43**	**1.00**	**0.77**	**1.67**
7-3	2.5 cm	2.2 cm	60°	0°	**0.36**	**0.86**	**0.71**	**1.23**
7-4	2.5 cm	7 cm	60°	22°	**0.70**	**1.65**	**1.30**	**2.87**
9	2.75 cm	2.69 cm	18°	87°	**0.24**	**2.18**	**0.40**	**2.10**
11	3.00 cm	3.2 cm	22°	73°	**0.22**	**1.82**	**0.39**	**1.99**

Table E.6 – Fabric 3 single layer drape energy, strategy one (double curvature)

BS #	Shear Angle (°)	Total Surface Area (mm^2)	**Shear energy (*Nmm*)**	**Spring back energy (*Nmm*)**	**Shear energy variability (*Nmm*)**	**Spring back energy variability (*Nmm*)**
3	34.4	160 mm^2	**1.44**	**0.08**	**0.73**	**0.04**
5	15	284 mm^2	**0.31**	**0.02**	**0.97**	**0.05**

Table E.7 – Fabric 1 multilayer drape energies, strategy one (single curvature)

BS #	Radius (*cm*)	Length (*cm*)	Theta (°)	Yarn orientation (°)	**Bending energy (*Nmm*)**	**Spring back energy (*Nmm*)**	**Bending variability (*Nmm*)**	**Spring back variability (*Nmm*)**
2	2.5 cm	7 cm	60°	23°	**1.75**	**1.70**	**2.21**	**7.20**
4	2.5 cm	4 cm	60°	0°	**1.33**	**1.49**	**1.94**	**4.89**
6	2.5 cm	7 cm	60°	22°	**1.78**	**1.73**	**2.23**	**7.26**
7-1	2.5 cm	7 cm	60°	23°	**1.75**	**1.70**	**2.21**	**7.20**
7-2	2.5 cm	3.8 cm	60°	18°	**1.02**	**1.02**	**1.27**	**4.07**
7-3	2.5 cm	2.2 cm	60°	0°	**0.73**	**0.82**	**1.07**	**2.69**
7-4	2.5 cm	7 cm	60°	22°	**1.78**	**1.73**	**2.23**	**7.26**
9	2.75 cm	2.69 cm	18°	87°	**0.12**	**0.35**	**0.17**	**1.60**
11	3.00 cm	3.2 cm	22°	73°	**0.16**	**0.43**	**0.21**	**1.89**

Table E.8 – Fabric 1 multilayer drape energy, strategy one (double curvature)

BS #	Shear Angle (°)	Total Surface Area (mm^2)	**Shear energy (*Nmm*)**	**Spring back energy (*Nmm*)**	**Shear energy variability (*Nmm*)**	**Spring back energy variability (*Nmm*)**
3	34.4	160 mm^2	**12.5**	**0.69**	**5.3**	**0.29**
5	15	284 mm^2	**1.17**	**0.06**	**7.06**	**0.39**

Table E.9 – Fabric 2 multilayer drape energies, strategy one (single curvature)

BS #	Radius (*cm*)	Length (*cm*)	Theta (°)	Yarn orientation (°)	**Bending energy (*Nmm*)**	**Spring back energy (*Nmm*)**	**Bending variability (*Nmm*)**	**Spring back variability (*Nmm*)**
2	2.5 cm	7 cm	60°	23°	**2.81**	**5.24**	**3.87**	**10.38**
4	2.5 cm	4 cm	60°	0°	**1.97**	**3.83**	**3.17**	**6.62**
6	2.5 cm	7 cm	60°	22°	**2.83**	**5.31**	**3.89**	**10.43**
7-1	2.5 cm	7 cm	60°	23°	**2.81**	**5.24**	**3.87**	**10.38**
7-2	2.5 cm	3.8 cm	60°	18°	**1.60**	**3.01**	**2.18**	**5.76**
7-3	2.5 cm	2.2 cm	60°	0°	**1.08**	**2.10**	**1.74**	**3.64**
7-4	2.5 cm	7 cm	60°	22°	**2.83**	**5.31**	**3.89**	**10.43**
9	2.75 cm	2.69 cm	18°	87°	**0.11**	**0.58**	**0.31**	**2.29**
11	3.00 cm	3.2 cm	22°	73°	**0.20**	**0.93**	**0.47**	**3.37**

Table E.10 – Fabric 2 multilayer drape energy, strategy one (double curvature)

BS #	Shear Angle (°)	Total Surface Area (mm^2)	**Shear energy (*Nmm*)**	**Spring back energy (*Nmm*)**	**Shear energy variability (*Nmm*)**	**Spring back energy variability (*Nmm*)**
3	34.4	160 mm^2	**5.36**	**0.29**	**3.01**	**0.17**
5	15	284 mm^2	**0.15**	**0.01**	**4.01**	**0.22**

Table E.11 – Fabric 3 multilayer drape energies, strategy one (single curvature)

BS #	Radius (*cm*)	Length (*cm*)	Theta (°)	Yarn orientation (°)	**Bending energy (*Nmm*)**	**Spring back energy (*Nmm*)**	**Bending variability (*Nmm*)**	**Spring back variability (*Nmm*)**
2	2.5 cm	7 cm	60°	23°	**2.53**	**6.09**	**4.23**	**9.34**
4	2.5 cm	4 cm	60°	0°	**2.43**	**5.94**	**4.15**	**7.27**
6	2.5 cm	7 cm	60°	22°	**2.60**	**6.27**	**4.31**	**9.50**
7-1	2.5 cm	7 cm	60°	23°	**2.53**	**6.09**	**4.23**	**9.34**
7-2	2.5 cm	3.8 cm	60°	18°	**1.58**	**3.81**	**2.52**	**5.51**
7-3	2.5 cm	2.2 cm	60°	0°	**1.34**	**3.27**	**2.28**	**4.00**
7-4	2.5 cm	7 cm	60°	22°	**2.60**	**6.27**	**4.31**	**9.50**
9	2.75 cm	2.69 cm	18°	87°	**0.80**	**7.43**	**1.06**	**5.87**
11	3.00 cm	3.2 cm	22°	73°	**0.75**	**6.23**	**1.08**	**5.73**

Table E.12 – Fabric 3 multilayer drape energy, strategy one (double curvature)

BS #	Shear Angle (°)	Total Surface Area (mm^2)	**Shear energy (*Nmm*)**	**Spring back energy (*Nmm*)**	**Shear energy variability (*Nmm*)**	**Spring back energy variability (*Nmm*)**
3	34.4	160 mm^2	**4.19**	**0.23**	**2.54**	**0.14**
5	15	284 mm^2	**0.54**	**0.03**	**3.38**	**0.19**

E.2. Strategy 2 drape energy and variability

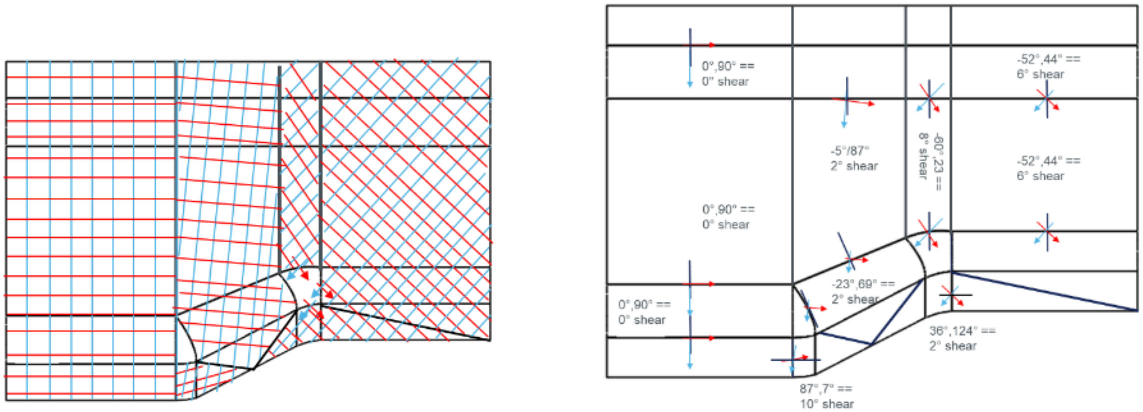

Figure E.2 – Strategy 2 summary

Table E.13 – Fabric 1 single layer drape energies, strategy two (single curvature)

BS #	Radius (*cm*)	Length (*cm*)	Theta (°)	Yarn orientation (°)	**Bending energy (*Nmm*)**	**Spring back energy (*Nmm*)**	**Bending variability (*Nmm*)**	**Spring back variability (*Nmm*)**
2	2.5 cm	7 cm	60°	0°	**0.63**	**0.51**	**1.02**	**2.63**
4	2.5 cm	4 cm	60°	23°	**0.25**	**0.16**	**0.35**	**1.18**
6	2.5 cm	7 cm	60°	52°	**0.25**	**0.11**	**0.35**	**1.09**
7-1	2.5 cm	7 cm	60°	0°	**0.63**	**0.51**	**1.02**	**2.63**
7-2	2.5 cm	3.8 cm	60°	5°	**0.32**	**0.25**	**0.48**	**1.36**
7-3	2.5 cm	2.2 cm	60°	60°	**0.08**	**0.04**	**0.10**	**0.35**
7-4	2.5 cm	7 cm	60°	52°	**0.25**	**0.11**	**0.35**	**1.09**
9	2.75 cm	2.69 cm	18°	87°	**0.03**	**0.05**	**0.05**	**0.48**
11	3.00 cm	3.2 cm	22°	36°	**0.04**	**0.08**	**0.10**	**0.78**

Table E.14 – Fabric 1 single layer drape energy, strategy two (double curvature)

BS #	Shear Angle (°)	Total Surface Area (*mm*^{2})	**Shear energy (*Nmm*)**	**Spring back energy (*Nmm*)**	**Shear energy variability (*Nmm*)**	**Spring back energy variability (*Nmm*)**
3	34.4°	160 mm^2	**4.01**	**0.22**	**2.86**	**0.16**
5	7.6°	284 mm^2	**0.13**	**0.01**	**3.80**	**0.21**

Table E.15 – Fabric 2 single layer drape energies, strategy two (single curvature)

BS #	Radius (*cm*)	Length (*cm*)	Theta (°)	Yarn orientation (°)	**Bending energy (*Nmm*)**	**Spring back energy (*Nmm*)**	**Bending variability (*Nmm*)**	**Spring back variability (*Nmm*)**
2	2.5 cm	7 cm	60°	0°	**0.75**	**1.35**	**1.47**	**3.03**
4	2.5 cm	4 cm	60°	23°	**0.39**	**0.66**	**0.61**	**1.63**
6	2.5 cm	7 cm	60°	52°	**0.55**	**0.63**	**1.30**	**3.11**
7-1	2.5 cm	7 cm	60°	0°	**0.75**	**1.35**	**1.47**	**3.03**
7-2	2.5 cm	3.8 cm	60°	5°	**0.40**	**0.71**	**0.72**	**1.62**
7-3	2.5 cm	2.2 cm	60°	60°	**0.15**	**0.17**	**0.33**	**0.87**
7-4	2.5 cm	7 cm	60°	52°	**0.55**	**0.63**	**1.30**	**6.95**
9	2.75 cm	2.69 cm	18°	87°	**0.02**	**0.10**	**0.09**	**0.62**
11	3.00 cm	3.2 cm	22°	36°	**0.09**	**0.48**	**0.21**	**1.30**

Table E.16 – – Fabric 2 single layer drape energy, strategy two (double curvature)

BS #	Shear Angle (°)	Total Surface Area (*mm*^{2})	**Shear energy (*Nmm*)**	**Spring back energy (*Nmm*)**	**Shear energy variability (*Nmm*)**	**Spring back energy variability (*Nmm*)**
3	34.4°	160 mm^2	**2.71**	**0.15**	**2.12**	**0.12**
5	7.6°	284 mm^2	**0.48**	**0.03**	**0.03**	**0.16**

Table E.17 – Fabric 3 single layer drape energies, strategy two (single curvature)

BS #	Radius (*cm*)	Length (*cm*)	Theta (°)	Yarn orientation (°)	**Bending energy (*Nmm*)**	**Spring back energy (*Nmm*)**	**Bending variability (*Nmm*)**	**Spring back variability (*Nmm*)**
2	2.5 cm	7 cm	60°	0°	**1.16**	**2.75**	**2.25**	**3.91**
4	2.5 cm	4 cm	60°	23°	**0.39**	**0.91**	**0.73**	**1.61**
6	2.5 cm	7 cm	60°	52°	**0.57**	**1.42**	**1.25**	**2.20**
7-1	2.5 cm	7 cm	60°	0°	**1.16**	**2.75**	**2.25**	**3.91**
7-2	2.5 cm	3.8 cm	60°	5°	**0.57**	**1.36**	**1.06**	**2.00**
7-3	2.5 cm	2.2 cm	60°	60°	**0.30**	**0.75**	**0.51**	**0.99**
7-4	2.5 cm	7 cm	60°	52°	**0.57**	**1.42**	**1.25**	**2.20**
9	2.75 cm	2.69 cm	18°	87°	**0.24**	**2.18**	**0.40**	**2.10**
11	3.00 cm	3.2 cm	22°	36°	**0.06**	**0.44**	**0.18**	**0.93**

Table E.18 – Fabric 3 single layer drape energy, strategy two (double curvature)

BS #	Shear Angle (°)	Total Surface Area (mm^2)	**Shear energy (*Nmm*)**	**Spring back energy (*Nmm*)**	**Shear energy variability (*Nmm*)**	**Spring back energy variability (*Nmm*)**
3	34.4°	160 mm^2	**1.44**	**0.08**	**0.73**	**0.04**
5	7.6°	284 mm^2	**0.01**	**0.00**	**0.97**	**0.05**

Table E.19 – Fabric 1 multilayer drape energies, strategy two (single curvature)

BS #	Radius (*cm*)	Length (*cm*)	Theta (°)	Yarn orientation (°)	**Bending energy (*Nmm*)**	**Spring back energy (*Nmm*)**	**Bending variability (*Nmm*)**	**Spring back variability (*Nmm*)**
2	2.5 cm	7 cm	60°	0°	**2.33**	**2.61**	**3.40**	**8.56**
4	2.5 cm	4 cm	60°	23°	**1.00**	**0.97**	**1.26**	**4.11**
6	2.5 cm	7 cm	60°	52°	**1.18**	**0.96**	**1.38**	**4.23**
7-1	2.5 cm	7 cm	60°	0°	**2.33**	**2.61**	**3.40**	**8.56**
7-2	2.5 cm	3.8 cm	60°	5°	**1.20**	**1.30**	**1.64**	**4.48**
7-3	2.5 cm	2.2 cm	60°	60°	**0.37**	**0.30**	**0.39**	**1.31**
7-4	2.5 cm	7 cm	60°	52°	**1.18**	**0.96**	**1.38**	**4.23**
9	2.75 cm	2.69 cm	18°	87°	**0.12**	**0.35**	**0.17**	**1.60**
11	3.00 cm	3.2 cm	22°	36°	**0.20**	**0.57**	**0.38**	**2.94**

Table E.20 – Fabric 1 multilayer drape energy, strategy two (double curvature)

BS #	Shear Angle (°)	Total Surface Area (mm^2)	**Shear energy (*Nmm*)**	**Spring back energy (*Nmm*)**	**Shear energy variability (*Nmm*)**	**Spring back energy variability (*Nmm*)**
3	34.4°	160 mm^2	**12.50**	**0.69**	**5.30**	**0.29**
5	7.6°	284 mm^2	**-0.55**	**-0.03**	**7.06**	**0.39**

Table E.21 – Fabric 2 multilayer drape energies, strategy two (single curvature)

BS #	Radius (*cm*)	Length (*cm*)	Theta (°)	Yarn orientation (°)	**Bending energy (*Nmm*)**	**Spring back energy (*Nmm*)**	**Bending variability (*Nmm*)**	**Spring back variability (*Nmm*)**
2	2.5 cm	7 cm	60°	0°	**3.45**	**6.69**	**5.54**	**11.59**
4	2.5 cm	4 cm	60°	23°	**1.60**	**3.00**	**2.21**	**5.93**
6	2.5 cm	7 cm	60°	52°	**2.01**	**2.82**	**3.80**	**9.44**
7-1	2.5 cm	7 cm	60°	0°	**3.45**	**6.69**	**5.54**	**11.59**
7-2	2.5 cm	3.8 cm	60°	5°	**1.80**	**3.46**	**2.70**	**6.13**
7-3	2.5 cm	2.2 cm	60°	60°	**0.56**	**0.79**	**1.00**	**2.71**
7-4	2.5 cm	7 cm	60°	52°	**2.01**	**2.82**	**3.80**	**7.10**
9	2.75 cm	2.69 cm	18°	87°	**0.11**	**0.58**	**0.31**	**2.29**
11	3.00 cm	3.2 cm	22°	36°	**0.34**	**2.04**	**0.71**	**4.49**

Table E.22 – Fabric 2 multilayer drape energy, strategy two (double curvature)

BS #	Shear Angle (°)	Total Surface Area (mm^2)	**Shear energy (*Nmm*)**	**Spring back energy (*Nmm*)**	**Shear energy variability (*Nmm*)**	**Spring back energy variability (*Nmm*)**
3	34.4°	160 mm^2	**5.36**	**0.29**	**3.01**	**0.17**
5	7.6°	284 mm^2	**-0.45**	**-0.02**	**4.01**	**0.22**

Table E.23 – Fabric 3 multilayer drape energies, strategy two (single curvature)

BS #	Radius (*cm*)	Length (*cm*)	Theta (°)	Yarn orientation (°)	**Bending energy (*Nmm*)**	**Spring back energy (*Nmm*)**	**Bending variability (*Nmm*)**	**Spring back variability (*Nmm*)**
2	2.5 cm	7 cm	60°	0°	**4.26**	**10.39**	**7.26**	**12.72**
4	2.5 cm	4 cm	60°	23°	**1.44**	**3.48**	**2.42**	**5.34**
6	2.5 cm	7 cm	60°	52°	**1.99**	**5.06**	**3.72**	**6.74**
7-1	2.5 cm	7 cm	60°	0°	**4.26**	**10.39**	**7.26**	**12.72**
7-2	2.5 cm	3.8 cm	60°	5°	**2.11**	**5.13**	**3.45**	**6.53**
7-3	2.5 cm	2.2 cm	60°	60°	**1.03**	**2.62**	**1.48**	**2.95**
7-4	2.5 cm	7 cm	60°	52°	**1.99**	**5.06**	**3.72**	**6.74**
9	2.75 cm	2.69 cm	18°	87°	**0.80**	**7.43**	**1.06**	**5.87**
11	3.00 cm	3.2 cm	22°	36°	**0.22**	**1.69**	**0.60**	**3.12**

Table E.24 – Fabric 3 multilayer drape energy, strategy two (double curvature)

BS #	Shear Angle (°)	Total Surface Area (mm^2)	**Shear energy (*Nmm*)**	**Spring back energy (*Nmm*)**	**Shear energy variability (*Nmm*)**	**Spring back energy variability (*Nmm*)**
3	34.4°	160 mm^2	**4.19**	**0.23**	**2.54**	**0.14**
5	7.6°	284 mm^2	**-0.22**	**-0.01**	**3.38**	**0.19**

E.3. Strategy 3 drape energy and variability

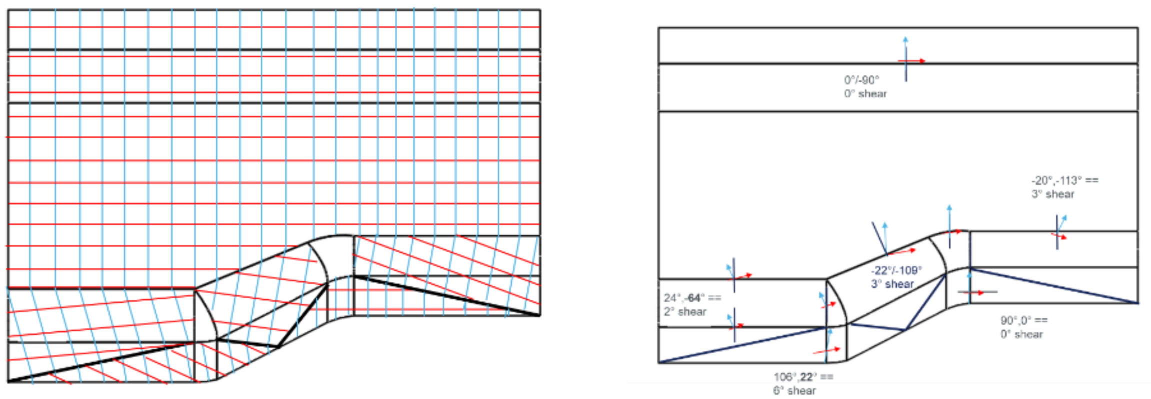

Figure E.3 – Strategy 3 summary

Table E.25 – Fabric 1 single layer drape energies, strategy three (single curvature)

BS #	Radius (*cm*)	Length (*cm*)	Theta (°)	Yarn orientation (°)	**Bending energy (*Nmm*)**	**Spring back energy (*Nmm*)**	**Bending variability (*Nmm*)**	**Spring back variability (*Nmm*)**
2	2.5 cm	7 cm	60°	24°	**0.42**	**0.26**	**0.60**	**2.04**
4	2.5 cm	4 cm	60°	22°	**0.25**	**0.16**	**0.35**	**1.19**
6	2.5 cm	7 cm	60°	20°	**0.46**	**0.30**	**0.64**	**2.14**
7-1	2.5 cm	20 cm	60°	0°	**1.79**	**1.46**	**2.91**	**7.51**
9	2.75 cm	2.69 cm	18°	16°	**0.05**	**0.13**	**0.08**	**0.86**
11	3.00 cm	3.2 cm	22°	90°	**0.04**	**0.13**	**0.08**	**0.95**

Table E.26 – Fabric 1 single layer drape energy, strategy two (double curvature)

BS #	Shear Angle (°)	Total Surface Area (mm^2)	**Shear energy (*Nmm*)**	**Spring back energy (*Nmm*)**	**Shear energy variability (*Nmm*)**	**Spring back energy variability (*Nmm*)**
3	9°	160 mm^2	**0.19**	**0.01**	**2.86**	**0.16**
5	3°	284 mm^2	**-0.15**	**-0.01**	**3.81**	**0.21**

Table E.27 – – Fabric 2 single layer drape energies, strategy three (single curvature)

BS #	Radius (*cm*)	Length (*cm*)	Theta (°)	Yarn orientation (°)	**Bending energy (*Nmm*)**	**Spring back energy (*Nmm*)**	**Bending variability (*Nmm*)**	**Spring back variability (*Nmm*)**
2	2.5 cm	7 cm	60°	24°	**0.68**	**1.15**	**1.06**	**2.86**
4	2.5 cm	4 cm	60°	22°	**0.39**	**0.67**	**0.61**	**1.64**
6	2.5 cm	7 cm	60°	20°	**0.69**	**1.18**	**1.08**	**2.87**
7-1	2.5 cm	20 cm	60°	0°	**2.14**	**3.85**	**4.21**	**8.65**
9	2.75 cm	2.69 cm	18°	16°	**0.07**	**0.47**	**0.13**	**1.11**
11	3.00 cm	3.2 cm	22°	90°	**0.03**	**0.53**	**0.12**	**1.31**

Table E.28 – Fabric 2 single layer drape energy, strategy two (double curvature)

BS #	Shear Angle (°)	Total Surface Area (mm^2)	**Shear energy (*Nmm*)**	**Spring back energy (*Nmm*)**	**Shear energy variability (*Nmm*)**	**Spring back energy variability (*Nmm*)**
3	9°	160 mm^2	**0.50**	**0.03**	**2.12**	**0.12**
5	3°	284 mm^2	**-0.10**	**-0.01**	**2.83**	**0.16**

Table E.29 – Fabric 3 single layer drape energies, strategy three (single curvature)

BS #	Radius (*cm*)	Length (*cm*)	Theta (°)	Yarn orientation (°)	**Bending energy (*Nmm*)**	**Spring back energy (*Nmm*)**	**Bending variability (*Nmm*)**	**Spring back variability (*Nmm*)**
2	2.5 cm	7 cm	60°	24°	**0.66**	**1.55**	**1.25**	**2.77**
4	2.5 cm	4 cm	60°	22°	**0.40**	**0.94**	**0.74**	**1.64**
6	2.5 cm	7 cm	60°	20°	**0.74**	**1.75**	**1.35**	**2.97**
7-1	2.5 cm	20 cm	60°	0°	**3.30**	**7.86**	**6.43**	**11.17**
9	2.75 cm	2.69 cm	18°	16°	**0.09**	**0.75**	**0.17**	**1.22**
11	3.00 cm	3.2 cm	22°	90°	**0.34**	**0.75**	**0.67**	**1.31**

Table E.30 – Fabric 3 single layer drape energy, strategy two (double curvature)

BS #	Shear Angle (°)	Total Surface Area (mm^2)	**Shear energy (*Nmm*)**	**Spring back energy (*Nmm*)**	**Shear energy variability (*Nmm*)**	**Spring back energy variability (*Nmm*)**
3	9°	160 mm^2	**0.05**	**0.00**	**0.73**	**0.04**
5	3°	284 mm^2	**-0.11**	**-0.01**	**0.97**	**0.05**

Table E.31 – Fabric 1 multilayer drape energies, strategy three (single curvature)

BS #	Radius (*cm*)	Length (*cm*)	Theta (°)	Yarn orientation (°)	**Bending energy (*Nmm*)**	**Spring back energy (*Nmm*)**	**Bending variability (*Nmm*)**	**Spring back variability (*Nmm*)**
2	2.5 cm	7 cm	60°	24°	**1.73**	**1.66**	**2.19**	**7.14**
4	2.5 cm	4 cm	60°	22°	**1.02**	**0.99**	**1.27**	**4.15**
6	2.5 cm	7 cm	60°	20°	**1.83**	**1.81**	**2.28**	**7.37**
7-1	2.5 cm	20 cm	60°	0°	**6.66**	**7.46**	**9.71**	**24.46**
9	2.75 cm	2.69 cm	18°	16°	**0.20**	**0.75**	**0.28**	**2.92**
11	3.00 cm	3.2 cm	22°	90°	**0.16**	**0.79**	**0.27**	**3.32**

Table E.32 – Fabric 1 multilayer drape energy, strategy two (double curvature)

BS #	Shear Angle (°)	Total Surface Area (mm^2)	**Shear energy (*Nmm*)**	**Spring back energy (*Nmm*)**	**Shear energy variability (*Nmm*)**	**Spring back energy variability (*Nmm*)**
3	9°	160 mm^2	**-0.22**	**-0.01**	**5.30**	**0.29**
5	3°	284 mm^2	**-0.98**	**-0.05**	**7.06**	**0.39**

Table E.33 – Fabric 2 multilayer drape energies, strategy three (single curvature)

BS #	Radius (*cm*)	Length (*cm*)	Theta (°)	Yarn orientation (°)	**Bending energy (*Nmm*)**	**Spring back energy (*Nmm*)**	**Bending variability (*Nmm*)**	**Spring back variability (*Nmm*)**
2	2.5 cm	7 cm	60°	24°	**2.78**	**5.18**	**3.86**	**10.34**
4	2.5 cm	4 cm	60°	22°	**1.62**	**3.03**	**2.22**	**5.96**
6	2.5 cm	7 cm	60°	20°	**2.89**	**5.43**	**3.95**	**10.52**
7-1	2.5 cm	20 cm	60°	0°	**9.85**	**19.13**	**15.84**	**33.12**
9	2.75 cm	2.69 cm	18°	16°	**0.31**	**2.18**	**0.9**	**4.12**
11	3.00 cm	3.2 cm	22°	90°	**0.14**	**2.43**	**0.46**	**4.77**

Table E.34 – Fabric 2 multilayer drape energy, strategy two (double curvature)

BS #	Shear Angle (°)	Total Surface Area (mm^2)	**Shear energy (*Nmm*)**	**Spring back energy (*Nmm*)**	**Shear energy variability (*Nmm*)**	**Spring back energy variability (*Nmm*)**
3	9°	160 mm^2	**-0.23**	**-0.01**	**3.01**	**0.17**
5	3°	284 mm^2	**-0.89**	**-0.05**	**4.01**	**0.22**

Table E.35 – Fabric 3 multilayer drape energies, strategy three (single curvature)

BS #	Radius (*cm*)	Length (*cm*)	Theta (°)	Yarn orientation (°)	**Bending energy (*Nmm*)**	**Spring back energy (*Nmm*)**	**Bending variability (*Nmm*)**	**Spring back variability (*Nmm*)**
2	2.5 cm	7 cm	60°	24°	**2.45**	**5.90**	**4.16**	**9.17**
4	2.5 cm	4 cm	60°	22°	**1.49**	**3.85**	**2.46**	**5.43**
6	2.5 cm	7 cm	60°	20°	**2.75**	**6.64**	**4.47**	**9.83**
7-1	2.5 cm	20 cm	60°	0°	**12.16**	**29.70**	**20.74**	**36.34**
9	2.75 cm	2.69 cm	18°	16°	**0.32**	**2.84**	**0.57**	**4.02**
11	3.00 cm	3.2 cm	22°	90°	**1.13**	**2.87**	**1.74**	**4.34**

Table E.36 – Fabric 3 multilayer drape energy, strategy two (double curvature)

BS #	Shear Angle (°)	Total Surface Area (mm^2)	**Shear energy (*Nmm*)**	**Spring back energy (*Nmm*)**	**Shear energy variability (*Nmm*)**	**Spring back energy variability (*Nmm*)**
3	9°	160 mm^2	**-0.10**	**-0.01**	**2.54**	**0.14**
5	3°	284 mm^2	**-0.34**	**-0.02**	**3.38**	**0.19**